

# Relaxation behavior of pure and binary glass formers

– studied by Dielectric and NMR spectroscopy

Von der Universität Bayreuth  
zur Erlangung des Grades eines  
Doktors der Naturwissenschaften (Dr. rer. nat.)  
genehmigte Abhandlung

von

**Thomas Körber**

aus Forchheim

1. Gutachter: Prof. Dr. Werner Köhler
2. Gutachter: Prof. Dr. Ernst Rößler
3. Gutachter: Prof. Dr. Kay Saalwächter

Tag der Einreichung: 27. Juli 2021

Tag des Kolloquiums: 01. Dezember 2021



## Table of Contents

<b>I</b>	<b>Abstract</b>	<b>1</b>
<b>II</b>	<b>Kurzfassung</b>	<b>3</b>
<b>III</b>	<b>Extended Abstract</b>	<b>5</b>
	1 Relaxation Behaviour of Pure Glass Formers .....	7
	1.1 The Glass Transition Phenomenon .....	7
	1.2 Results & Discussion .....	15
	1.2.1 High- $T_g$ Glass Formers (Publication 1) .....	15
	1.2.2 Relaxation Stretching of Molecular Liquids (Publication 2) .....	19
	2 Relaxation Behaviour of Binary Glass Formers.....	24
	2.1 State of the Art .....	24
	2.2 Results & Discussion .....	31
	2.2.1 Moderate $T_g$ -contrast (Publication 3).....	31
	2.2.2 High $T_g$ -contrast (Publication 4 and 5) .....	35
	2.2.3 Discussion & Conclusion .....	43
<b>IV</b>	<b>Publications</b>	<b>51</b>
	1 List of Publications .....	51
	2 Further Publications.....	53
<b>V</b>	<b>References</b>	<b>143</b>



---

# I Abstract

Dielectric (DS) and nuclear magnetic resonance (NMR) spectroscopy are applied to investigate the component-specific relaxation behaviour of binary low-molecular glass formers. The systems are characterized by a more or less high  $T_g$ -contrast, i.e. a more or less high glass transition temperature ( $T_g$ ) difference of the neat components.

In cooperation with the department of Macromolecular Chemistry I (group of H.-W. Schmidt), several high- $T_g$  systems are synthesized and characterized by DS regarding the interplay of main ( $\alpha$ ) and secondary ( $\beta$ ) relaxation (Publication 1). Re-addressing relaxation features of neat glass formers, systematic differences in the relaxation stretching probed by DS vs. NMR and photon correlation spectroscopy (PCS) are discovered (Publication 2). Frequency-temperature-superposition (FTS) appears to be valid and a generic stretching ( $\beta_K \approx 0.58 \pm 0.06$ ) is found in the case of PCS, NMR, and DS provided the systems are not polar. For highly polar systems, deviations of FTS and the stretching are found for DS in contrast to PCS and NMR. This difference is explained by assuming collective (coherent) dynamics measured by DS vs. incoherent dynamics probed by  $^2\text{H}$  and  $^{31}\text{P}$  NMR and PCS in accordance with recent studies. Thereby, a method analysing the NMR spin-lattice relaxation rate as function of the spin-spin relaxation rate is proposed, which directly provides a kind of susceptibility function (and thus the relaxation stretching) in addition to the NMR coupling constant. Starting with two binary mixtures with a moderate  $T_g$  difference ( $\Delta T_g = 63$  K and 89 K), especially the distribution of correlation times  $G(\ln \tau_{\alpha_1})$ , specifying the dynamics of the polar high- $T_g$  component, is addressed by DS (Publication 3). In contrast to neat glass formers, the spectra show a broadening and failure of FTS with increasing additive (low- $T_g$  component) concentration. This is confirmed by stimulated echo NMR experiments probing directly the orientational correlation function. Considering isodynamic points in the *ns* regime, a dynamical decoupling of the two components as well as strong dynamic heterogeneities are found concerning the low- $T_g$  component.

Choosing the most suitable high- $T_g$  glass former *m*-TPTS ( $T_g = 350$  K) from the series of newly synthesized systems concerning the glass stability in the mixture with tripropyl phosphate (TPP,  $T_g = 134$  K), DS and DSC investigations are performed in the concentration range  $w_{\text{TPP}} = 4\%$  up to 90% at first (Publication 4). Anticipating the NMR results, which yield two isotropic processes, two main relaxations  $\alpha_1$  (high- $T_g$  component) and  $\alpha_2$  (low- $T_g$  component) with two  $T_g$  values  $T_{g_1}(w_{\text{TPP}})$  and  $T_{g_2}(w_{\text{TPP}})$  are found up to highest concentrations. For  $T_{g_2}(w_{\text{TPP}})$ , a maximum is found at intermediate concentrations. To cope with the extraordinary spectral broadening, a spectral model consisting of a generalized Cole–Davidson ( $\alpha_1$ ) and a Havriliak–Negami function

---

with a low frequency truncation ( $\alpha_2$ ) is introduced. The total relaxation strength  $\Delta\epsilon$  strongly deviates from the expected behaviour for ideal mixing. Therefore, care must be taken interpreting the corresponding  $\Delta\epsilon_{\alpha_i}$  as representation of component populations.

The actual populations are accessed via component-selective NMR experiments (Publication 5). Spectra and stimulated echo decays of deuterated *m*-TPPTS-d<sub>4</sub> (<sup>2</sup>H) and TPP (<sup>31</sup>P) are analysed to quantitatively understand the dielectric spectra. The high- $T_g$  component shows relaxation like that of neat systems, yet with some broadening upon mixing. This correlates with a high-frequency broadening found in the dielectric spectra. The low- $T_g$  component exhibits highly stretched relaxations and strong dynamic heterogeneities indicated by “two-phase” NMR spectra, reflecting varying fractions of fast and slow liquid-like reorienting molecules down to lowest concentrations (4%). This indicates, that isotropic reorientation prevails in the rigid high- $T_g$  matrix stretching from close to  $T_g^{TPP}$  to  $T_{g_1}(w_{TPP})$ , correlating with a low-frequency broadening of the dielectric spectra. The maximum behaviour of  $T_{g_2}(w_{TPP})$  is recovered also in the NMR experiments, signaling extreme separation of the component dynamics at low  $w_{TPP}$ . Scrutinizing NMR relaxation data of several (polymeric) mixtures investigated previously and in this work as a function of concentration, a generic scenario is found for systems with high  $T_g$ -contrast ( $\Delta T_g \geq 170$  K). Differences are recognized for systems with lower  $\Delta T_g$ .

To understand the observed maximum in  $T_{g_2}(w_{add})$ , a crossover from “single glass” to “double glass” scenario is suggested, which is revealed by recent molecular dynamics simulations of hard spheres. Furthermore, a second population of TPP molecules is revealed in the analysis, which is associated with the dynamics of the high- $T_g$  component. However, the fractions are lower than suggested by the dielectric spectra, which is discussed by the role of collective dynamics probed by dielectric but not by NMR spectroscopy.

---

## II Kurzfassung

Dielektrische (DS) und kernmagnetische Resonanzspektroskopie (NMR) werden eingesetzt, um das Relaxationsverhalten in binären niedermolekularen Glasbildnern komponentenspezifisch zu untersuchen. Die Systeme sind durch einen vergleichsweise hohen  $T_g$ -Kontrast, d.h. eine mehr oder weniger große Differenz der Glasübergangstemperatur ( $T_g$ ) der reinen Komponenten gekennzeichnet.

In Zusammenarbeit mit der Makromolekularen Chemie I (Arbeitsgruppe von H.-W. Schmidt) werden mehrere Hoch- $T_g$ -Systeme synthetisiert und mittels der DS hinsichtlich des Zusammenspiels von Haupt- ( $\alpha$ ) und Sekundärrelaxation ( $\beta$ ) charakterisiert (Publikation 1). Unter Einbeziehung der Relaxationseigenschaften weiterer reiner Glasbildner werden systematische Unterschiede in der Streckung der Relaxationsfunktion, die mittels DS, NMR und Photonenkorrelationsspektroskopie (PCS) untersucht werden, entdeckt (Publikation 2). Das Frequenz-Temperatur-Superposition (FTS) Prinzip scheint gültig zu sein und ein generischer Streckungsparameter ( $\beta_K \approx 0.58 \pm 0.06$ ) wird bei PCS, NMR und DS gefunden, sofern die Systeme nicht polar sind. Für hochpolare Systeme werden für DS, im Gegensatz zu PCS und NMR, Abweichungen von FTS und dem Streckungsparameter gefunden. Dieser Unterschied wird dadurch erklärt, dass in Anlehnung an jüngste Arbeiten in der DS kollektive (kohärente) Dynamik gemessen wird, wohin gegen die  $^2\text{H}$ - und  $^{31}\text{P}$ -NMR sowie die PCS inkohärente Dynamik erfassen. Bei diesen Untersuchungen wird eine Methode zur Analyse der NMR-Spin-Gitter-Relaxationsrate als Funktion der Spin-Spin-Relaxationsrate vorgestellt, die zusätzlich zur NMR-Kopplungskonstante direkt eine Art Suszeptibilitätsfunktion (und damit die Relaxationsstreckung) liefert.

Ausgehend von zwei binären Mischungen mit moderatem  $T_g$ -Unterschied ( $\Delta T_g = 63$  K und 89 K) wird die Verteilung der Korrelationszeiten  $G(\ln \tau_{\alpha_1})$ , die die Dynamik der polaren Hoch- $T_g$ -Komponente beschreibt, mit Hilfe der DS untersucht (Publikation 3). Im Gegensatz zu reinen Glasbildnern zeigen die Spektren mit zunehmender Konzentration der Nieder- $T_g$ -Komponente eine Verbreiterung und ein Versagen von FTS. Dies wird durch stimulierte Echo NMR-Experimente, die direkt die Orientierungskorrelationsfunktion widerspiegeln, bestätigt. Betrachtet man isodynamische Punkte im  $ns$ -Bereich, so findet man eine dynamische Entkopplung der beiden Komponenten sowie starke dynamische Heterogenitäten bezüglich der Nieder- $T_g$ -Komponente.

Aus der Reihe der neu synthetisierten Systeme wird der am besten geeignete Hoch- $T_g$ -Glasbildner  $m$ -TPTS ( $T_g = 350$  K) hinsichtlich der Glasstabilität in der Mischung mit Tripropyl-phosphat ( $TPP$ ,  $T_g = 134$  K) ausgewählt, um zunächst DS- und DSC-Untersuchungen im Konzentrationsbereich  $w_{TPP} = 4\%$  bis 90% durchzuführen (Publikation

---

4). Es werden zwei Hauptrelaxationen  $\alpha_1$  (Hoch- $T_g$ -Komponente) und  $\alpha_2$  (Nieder- $T_g$ -Komponente) bis zu höchsten Konzentrationen gefunden, die zu zwei  $T_g$ -Werten,  $T_{g_1}(w_{TPP})$  und  $T_{g_2}(w_{TPP})$ , führen (zwei isotrope Prozesse werden auch in der NMR gefunden). Für  $T_{g_2}(w_{TPP})$  wird ein Maximum bei mittleren Konzentrationen  $w_{TPP}$  gefunden. Um die außergewöhnliche spektrale Verbreiterung zu bewältigen, wird ein Modell eingeführt, das aus einer verallgemeinerten Cole-Davidson ( $\alpha_1$ ) und einer Havriliak-Negami-Funktion mit einem Niederfrequenzabbruch ( $\alpha_2$ ) besteht. Die Gesamt-Relaxationsstärke  $\Delta\varepsilon$  weicht stark von dem erwarteten Verhalten einer idealen Mischung ab. Daher ist bei der Interpretation der entsprechenden  $\Delta\varepsilon_{\alpha_i}$  als Populationen der Komponenten Vorsicht geboten.

Aussagen über die tatsächlichen Populationen erfolgen über die komponentenselektiven NMR-Experimente (Publikation 5). NMR Spektren und stimulierte Echoabfälle von deuteriertem *m*-TPTS- $d_4$  ( $^2\text{H}$ ) und TPP ( $^{31}\text{P}$ ) werden analysiert, um die dielektrischen Spektren quantitativ zu verstehen. Die Hoch- $T_g$ -Komponente zeigt ein Relaxationsverhalten vergleichbar mit reinen Systemen, jedoch mit einer gewissen Verbreiterung in der Mischung. Dies korreliert mit der Hochfrequenz-Verbreiterung der dielektrischen Spektren. Die Nieder- $T_g$ -Komponente zeigt stark gestreckte Relaxationen und starke dynamische Heterogenitäten, die sich in der NMR in sogenannten Zweiphasen-Spektren zeigen. Diese spiegeln unterschiedliche Anteile von schnellen und langsamen flüssigkeitsähnlich reorientierenden Molekülen bis hinunter zu niedrigsten Konzentrationen (4%) wider. Dies deutet darauf hin, dass in der festen Hoch- $T_g$ -Matrix eine isotrope Reorientierung stattfindet, die sich nahezu von  $T_g^{TPP}$  bis  $T_{g_1}(w_{TPP})$  erstreckt, was mit einer niederfrequenten Verbreiterung der dielektrischen Spektren korreliert. Das Maximum von  $T_{g_2}(w_{TPP})$  wird auch in den NMR-Experimenten wiedergefunden und signalisiert eine extreme Trennung der Komponentendynamik bei niedrigem  $w_{TPP}$ . Betrachtet man die NMR-Relaxationsdaten mehrerer zuvor und in dieser Arbeit untersuchter Mischungen als Funktion der Konzentration, so findet man ein generisches Verhalten für Systeme mit hohem  $T_g$ -Kontrast ( $\Delta T_g \geq 170$  K). Bei kleinerem  $\Delta T_g$  finden sich davon Abweichungen.

Das beobachtete Maximum von  $T_{g_2}(w_{TPP})$  sollte in einem "Einfach-Glas"- zu "Doppel-Glas"-Szenario verstanden werden, wie es durch jüngste Molekulardynamik-Simulationen von harten Kugeln aufgedeckt wurde. Darüber hinaus zeigt unsere Analyse, dass eine zweite Population von TPP-Molekülen existiert, die mit der Dynamik der Hoch- $T_g$ -Komponente verbunden ist. Die Anteile sind jedoch geringer als die dielektrischen Spektren nahelegen, was durch die Rolle der kollektiven Dynamik, die bei der dielektrischen, aber nicht der NMR-Spektroskopie gemessen wird, erklärt wird.

---

### III Extended Abstract

Condensed matter physics provides one of the richest fields of physical research, dealing with the complex many-body interaction on all kind of levels. One part of this field addresses structural glasses, i.e. amorphous solids lacking long-range order compared to crystals. Common window glasses, consisting mostly of inorganic silica and other metal or metalloid oxides over to certain ceramics and metallic glasses, used in the aerospace industry or consumer electronics, up to the polymeric and organic glasses are ubiquitous and indispensable. Due to the enormous range of different systems and applications of glasses, scientists have been striving for several decades to understand the nature of a glass, but:

”The nature of glass remains anything but clear“.<sup>1</sup>

Although this quote was stated some time ago (2008) and large effort was put into studying the nature of glass and especially the transition from a fluid to a glass ever since, it is still valid. To be more precise, the glass transition phenomenon was investigated experimentally very well in the last decades for an enormous amount of different systems. But no generally accepted theoretical description was developed yet, explaining the underlying physics and the richness of experimental observations. Philip W. Anderson remarked already in 1995: “The deepest and most interesting unsolved problem in solid state theory is probably the theory of the nature of glass and the glass transition.”<sup>2</sup> Experimentally, one has moved to more complex systems, like binary mixtures, providing a large amount of different applications, as well as new experimental findings and insights.

In this thesis, low-molecular (highly) asymmetric binary mixtures are investigated with dielectric and nuclear magnetic resonance (NMR) spectroscopy, to grasp the component specific dynamics. Asymmetry defines in this sense, that the two components have strongly different glass transition temperatures. While characterizing pure low-molecular high- $T_g$  glass formers, which are suitable for the binary mixtures, several questions in the field of pure glass formers are found unanswered and are re-investigated. Therefore, an overview of the challenges of pure glass formers along with the new insights is presented in section 1. Subsequently, the dynamics in binary mixtures with varying  $T_g$ -contrasts are addressed in section 2.



# 1 Relaxation Behaviour of Pure Glass Formers

In this chapter, a brief overview of the experimental and theoretical effort studying the phenomenon of the glass transition is provided. Subsequently, the results obtained in the course of this work on the relaxation behaviour of pure glass formers are presented.

## 1.1 The Glass Transition Phenomenon

Starting with the experimental observations obtained for an enormous amount of different systems, ranging from silicate to metallic glasses over to spin glasses up to polymers and proteins, the basic physical properties and relaxation features will be explained for simple molecular glass formers.

The most vivid property describing the dynamics of a liquid is the viscosity  $\eta(T)$ , which depicts the macroscopic flow behaviour. A glass can be obtained by cooling down the liquid while avoiding the crystallisation crossing the melting point  $T_m$ .<sup>6</sup> Therefore, the glass transition phenomenon is characterized by the three temperature regions, shown for *o*-terphenyl in Figure 1.1: liquid, supercooled liquid and glass. Thereby, the viscosity drastically increases from  $\eta \approx 10^{-2}$  Pas at the melting point  $T_m$  by more than 14 orders of magnitude to solid-state typical values of  $\eta \approx 10^{12}$  Pas around the glass transition temperature  $T_g$  in a comparable small temperature range. Speaking in terms of relaxation times  $\tau$ , which can be approximated via the shear modulus ( $\tau = \eta/G_S$ ), the glass transition temperature is conventionally defined as the temperature, when  $\tau = 100$  s. The relaxation time gives the time scale of a (linear response) experiment, which is

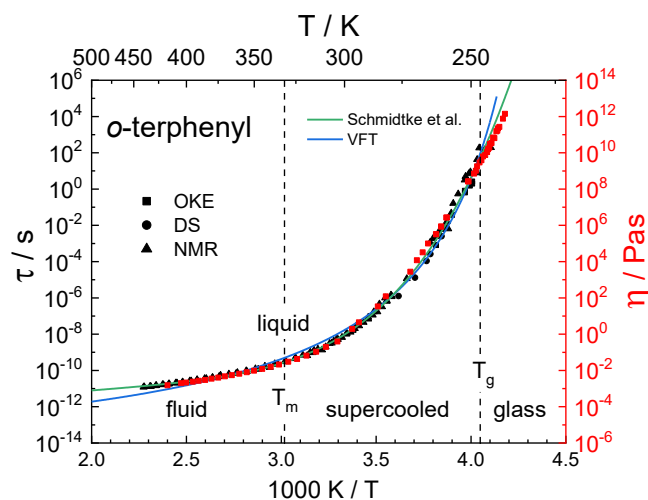


**Figure 1.1:** Viscosity  $\eta$  as function of the inverse temperature for the simple liquid *o*-terphenyl (red squares, right scale).<sup>3</sup> Reorientational correlation time  $\tau$  from various methods (black symbols, left scale).<sup>4</sup> Blue line: VFT interpolation. Green line: interpolation via Schmidtke et al.<sup>5</sup>

needed to equilibrate the system after perturbation (e.g. shear stress, temperature step, voltage). This structural (main) relaxation is called  $\alpha$ -relaxation. The glass ( $T < T_g$ ) can thus be depicted as liquid with extremely high viscosity, no more relaxing on experimental time scales.

On a microscopic scale, the structural relaxation can be investigated for example with neutron scattering (NS), measuring the density and tagged-particle correlation function on the order of *ps* to *ns*.<sup>7</sup> To cover the glass transition over the full dynamical range of more than 12 decades, additional broadband techniques are required. Thus, methods like dielectric spectroscopy (DS),<sup>8</sup> depolarized light scattering (DLS)<sup>9</sup> or nuclear magnetic resonance (NMR)<sup>10</sup> spectroscopy are employed - as in this thesis. They probe the reorientational correlation function of the corresponding Legendre polynomial  $P_l(\cos(\theta))$ :

$$C_l(t) = \frac{\langle P_l(\cos(\theta(t))) P_l(\cos(\theta(0))) \rangle}{\langle P_l(\cos(\theta(0)))^2 \rangle} \quad (1)$$

Whereas DS probes the rank  $l = 1$  correlation function, DLS and NMR measure  $C_2(t)$ . The average correlation time  $\tau$  is given by the integral over the correlation function. Because some of the methods work in the frequency domain, the correlation function is indirectly probed via the dynamic susceptibility  $\chi(\omega)$ . The dissipative part is connected to the Fourier transform of the correlation function (the spectral density  $J(\omega)$ ) by the fluctuation-dissipation theorem ( $\chi''(\omega) \propto \omega \cdot J(\omega)$ ).<sup>11</sup>

With an extensive amount of different glass forming systems being investigated - although quite different correlation functions are probed - common experimental fingerprints of “glassy dynamics” are found.<sup>8,12-15</sup> The measured correlation function shows always a two-step decay – one in the picosecond range and another final slow decay ( $\alpha$ -process). The main relaxation is always stretched and the corresponding correlation times  $\tau_\alpha$  follow a non-Arrhenius temperature dependence which resembles closely that of the viscosity in most cases (cf. Figure 1.1). In the supercooled regime,  $\tau_\alpha(T)$  is often described by the empirical Vogel-Fulcher-Tammann (VFT) equation (blue line in Figure 1.1):<sup>16-18</sup>

$$\tau_\alpha = \tau_{\alpha_0} \exp\left(\frac{A}{T - T_0}\right) \quad (2)$$

$\tau_{\alpha_0}$ ,  $A$  and  $T_0$  are empiric constants. To cover also the high temperature regime of  $\tau_\alpha(T)$ , several other equations are proven useful.<sup>5,19,20</sup> Schmidtke et al.<sup>5</sup> for instance, proposed an Arrhenius-like temperature dependence with an additional exponential temperature dependant part of the activation energy, providing superior interpolations

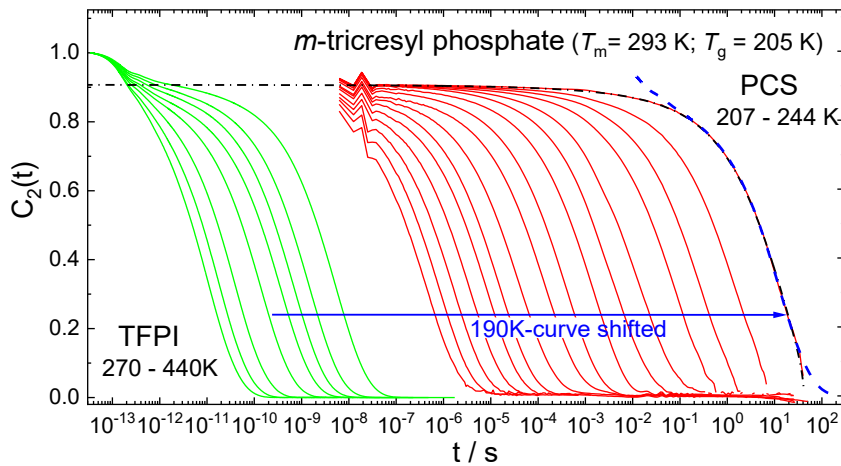


**Figure 1.2:** Correlation function  $C_2(t)$  of  $m$ -TCP, obtained from different LS setups (photon correlation spectroscopy (PCS) and Tandem-Fabry-Perot interferometry (TFPI)). Dash-dotted line: Kohlrausch interpolation. Dashed blue line: Data at  $T = 290$  K shifted to coincide with that at  $T = 207$  K. Figure adapted from ref.<sup>15</sup>

even up to the boiling point (green line in Figure 1.1). All these equations demonstrate the tremendous slowing down of the molecules during the glass transition.

Regarding the reorientational correlation function of the molecular liquid  $m$ -tricresyl phosphate ( $m$ -TCP), the fingerprints of glassy dynamics are shown in Figure 1.2. With different DLS setups (Tandem Fabry-Perot-interferometry (TFPI) and Photon correlation spectroscopy (PCS)),  $C_2(t)$  was measured, starting almost at the boiling point down to  $T_g$ .<sup>15</sup> The shape of the long-time behaviour of  $C_2(t)$  appears unchanged over the whole  $T$ -range, which is known as time-temperature superposition (TTS). To what extent TTS or frequency-temperature superposition (FTS) for frequency dependent experiments (e.g. DS, NMR) is valid and characteristic for glass forming systems is still debated.<sup>21</sup> The non-exponentiality (stretching) of the main relaxation is commonly determined via a stretched exponential (Kohlrausch) function:<sup>22,23</sup>

$$f(t) = \exp\left(-\left(\frac{t}{\tau_K}\right)^{\beta_K}\right), \quad 0 < \beta_K < 1 \quad (3)$$

The value  $\beta_K$  ranges from 0.3 up to 0.8.<sup>24,25</sup> Other functions like Cole-Davidson (CD)<sup>26,27</sup> or Havriliak-Negami (HN)<sup>27,28</sup> are also used in particular in the frequency domain in their analytical form, to account for the non-Debye relaxation. Speaking of the frequency domain, the apparently simple two-step time correlation function reveals several additional features due to the superior spectral resolution, especially at higher frequencies compared to the main relaxation.

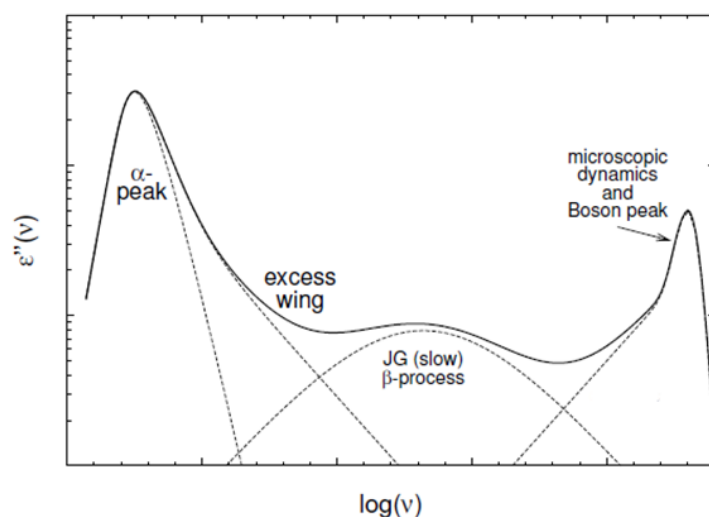


**Figure 1.3:** Schematic representation of the dielectric loss  $\varepsilon''(\nu)$  of the various relaxation processes in supercooled liquids, that can be observed in principle. Reprinted with permission ref.<sup>29</sup> Copyright (2003) by AIP Publishing.

An overview of the most common processes found in the susceptibility representation is provided in Figure 1.3 for the dielectric loss ( $\varepsilon''(\nu) = \Delta\varepsilon \cdot \chi''(\omega)$ , relaxation strength  $\Delta\varepsilon$ ). The  $\alpha$ -relaxation is found at lowest frequencies (longest times), accompanied by the so called “excess-wing”,<sup>30</sup> a (slow) secondary ( $\beta$ -) relaxation<sup>31</sup> and the microscopic dynamics/boson peak<sup>12</sup> at highest frequencies. The latter processes correspond to the first fast step found in the time correlation function, including a kind of intermolecular attempt frequency (Einstein frequency).<sup>32</sup>

Normally, the excess wing is only resolvable in so called type A glass formers,<sup>33</sup> which lack any spectrally separated secondary relaxations. The origin of the excess wing as well as the secondary relaxation is still controversially discussed. One possibility is, that the excess wing is a hidden secondary relaxation,<sup>30,34–36</sup> whereas others reckon it as intrinsic to the main relaxation as some kind of precursor.<sup>37,38</sup> For the secondary relaxations, one distinguished between the intrinsic (Johari-Goldstein) process,<sup>31,39</sup> even found for simple rigid molecules like toluene, exhibiting certain common properties (Arrhenius temperature dependence, change of relaxation strength above and below  $T_g$ , etc.),<sup>33</sup> and those due to intramolecular degrees of freedom, like side-group relaxations in polymers.<sup>40</sup> All these processes were also found in NS,<sup>41–44</sup> mechanical relaxation,<sup>45,46</sup> DLS<sup>47–50</sup> and NMR spectroscopy<sup>10,51</sup> for instance.

Several attempts were made to find correlations between experimental parameters of glassy dynamics. Böhmer et al.<sup>52</sup> found a correlation between the stretching parameter and the fragility, giving a characteristic measure of the change of the correlation times at  $T_g$ . Or more recently, Paluch et al.<sup>25</sup> proposed an anticorrelation between the polar-

ity ( $\Delta\varepsilon$ ) and the stretching parameter  $\beta_K$ , explained by the interaction potential contribution of the dipole-dipole interaction. Nielsen et al.<sup>53</sup> on the other hand found a prevalence of approximately  $-0.5$  as minimum high frequency slope in the dielectric spectra. From viscoelastic measurements, even a generic main relaxation pattern is proposed on the basis of a common fast relaxation (excess wing) by Gainaru and co-workers.<sup>54,55</sup> Thus, several experimental questions remain unsolved.

Comparing the glass “transition” in terms of theoretical considerations to a classical phase transition, one must consider thermodynamic properties changing upon supercooling like the volume  $V$  or enthalpy  $H$  and their corresponding derivatives, e.g. the expansion coefficient  $\alpha_p = \left(\frac{\partial V}{\partial T}\right)_p$  and the heat capacity  $c_p = \left(\frac{\partial H}{\partial T}\right)_p$ , which is depicted in Figure 1.4. At first glance, a second-order phase transition with a single order parameter might be identified,<sup>56</sup> which was discussed in the early glass research,<sup>57–59</sup> but proven insufficient to describe for instance the entropy and volume relaxation in general.<sup>60–62</sup> Nevertheless, the conventionally defined glass transition temperature  $T_g$  is clearly determined by a change in the thermodynamic properties or step in their derivatives using a distinct cooling rate (10 K/min). Due to the cooling rate dependence of  $T_g$ ,<sup>63</sup> it is rather seen as a kinetic phenomenon than a phase transition.<sup>64,65</sup> Still, the idea of an underlying hidden real phase transition ( $T < T_g$ ) drove a series of theories, starting with the work of Kauzmann,<sup>66</sup> and Adam and Gibbs.<sup>67</sup> Alternatively, considering the glass transition as a mere kinetic phenomenon, the first-principles approach of Mode Coupling Theory (MCT) was developed.<sup>68–70</sup> Herein, the time dependence of the density fluctuations is described via a set of non-linear differential equations

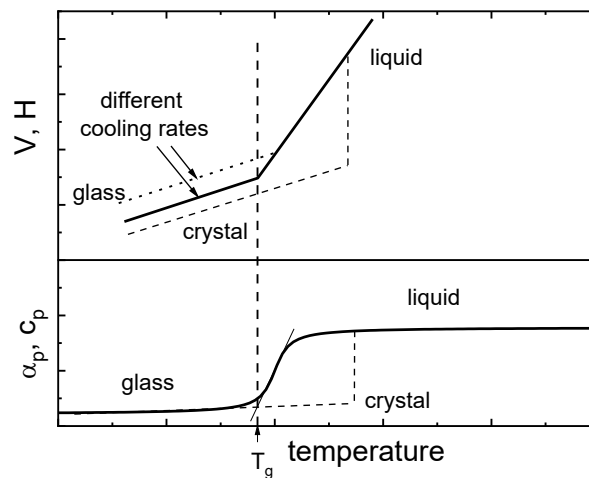


**Figure 1.4:** Volume / enthalpy (upper) and the corresponding temperature derivatives (lower) sketched as function of temperature. Dashed line: behaviour of a crystal for comparison.

including a retardation term, reproducing the slowing down of the dynamics via the cage effect.<sup>71</sup> Nowadays, the most sophisticated theoretical concept is the random first order transition theory (RFOT).<sup>72–74</sup> It generalizes the theory of a first-order crystallization transition to an amorphous state via the density fluctuations as order parameter in combination with a large number of metastable glassy states with distinct energy barriers. In addition, a large variety of other models exist such as potential energy landscape models,<sup>75–77</sup> elastic models,<sup>65</sup> kinetically constrained models,<sup>78,79</sup> Gaussian trap models<sup>80</sup> or other microscopic theories.<sup>81,82</sup> The sheer amount of different theories trying to explain the glass transition phenomenon (with varying transition temperatures) shows its complexity and the long way to go.

Besides experimental methods, molecular dynamic (MD) simulations provide the possibility to test (falsify) these theories. The trajectory of each individual particle is calculated and observables like the intermediate scattering function  $F_S(\mathbf{q}, t)$  or the mean-squared displacement (experimentally often hardly accessible) can be determined.

The Kob-Andersen model of a Lennard-Jones mixture,<sup>83,84</sup> consisting of two slightly mismatched particles in size to avoid crystallization, was pioneering the way of glassy MD simulations until now.<sup>85,86</sup> But also fully atomistic models with a variety of internal degrees of freedom of simple molecular liquids up to polymers are feasible nowadays.<sup>87</sup> In Figure 1.5 (a), the simulated mean-squared displacement of particles during supercooling is depicted, showing the ballistic, localized, and diffusive regimes.<sup>88</sup> The particles are trapped for a certain time by their nearest neighbours, which prolongs in time with decreasing temperature (the cage effect described by MCT).

Not only ensemble averaged values can be determined but also single particle motion can be investigated, resolving “dynamic heterogeneities” in supercooled liquids (cf. Figure 1.5 (b)).<sup>88–92</sup> There exist particles that move either much faster or much slower than expected assuming a Gaussian distribution of particles’ displacements.<sup>92</sup> Mobility clusters are formed, increasing in size upon supercooling. Dynamic heterogeneities correspond to different mobilities and thus a distribution of correlation times  $G(\ln \tau_\alpha)$  is present in supercooled liquids, giving a possible explanation of the measured stretching of the correlation function. Also various experiments investigating higher order susceptibilities, like multidimensional NMR,<sup>93–95</sup> and non-resonant hole burning experiments,<sup>96–98</sup> were performed to characterize these dynamic heterogeneities. The lifetime was found on the order of the main relaxation time  $\tau_\alpha$ ,<sup>94</sup> whereas a characteristic length scale increasing with supercooling on the order of some nanometres was detected.<sup>95,99–101</sup> Dynamic heterogeneities are also the key elements in RFOT theory, to explain the glass transition phenomenon and experimental observation so far.

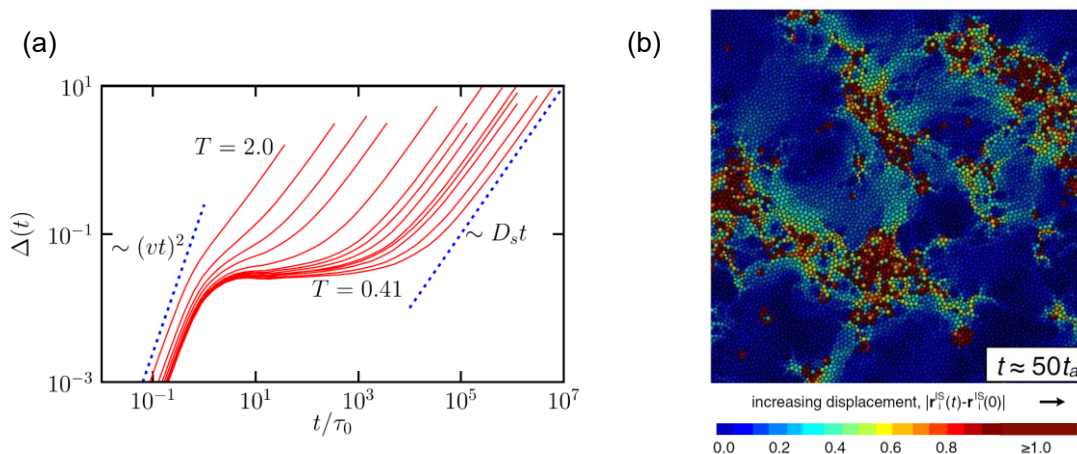


**Figure 1.5:** (a) Mean-squared displacements  $\Delta(t)$  of particles of a simple Lennard-Jones glass-forming liquid. With decreasing temperature, the particle displacements become increasingly slow with several distinct regimes: ballistic, localized (MCT: cage effect), and diffusive. Reprinted with permission from ref.<sup>88</sup> Copyright (2011) by the American Physical Society. (b) Dynamical heterogeneity: projection in space of a two-dimensional supercooled mixture with particles coloured according to overlap with initial positions. Trajectory length is about a tenth of a relaxation time at these conditions; spatial segregation of dynamics is evident. Reprinted with permission from ref.<sup>102</sup> Copyright (2011) by the American Physical Society.

Although MD simulations provide an enormous potential for further investigations - special computational setups and algorithms are developed<sup>103–105</sup> - the full dynamic range cannot be reached by simulations yet and further experiments are mandatory.

To account for the massive time window of more than 12 decades necessary to investigate glassy (rotational) dynamics, a large variety of experimental methods can be applied, which is sketched in Figure 1.6 with the corresponding time windows. In this work, DS and especially NMR spectroscopy is used to cover a large range of correlation times. The theoretical background of these methods is given in the standard literature<sup>27,106–108</sup> and is described in detail for every experiment in the corresponding publication.

Nevertheless, some important points should be mentioned. DS measures the reorientational correlation function  $C_1(t)$  via the dipole-dipole interaction, only if intermolecular correlation effects can be neglected, which is generally assumed to be valid.<sup>27,109</sup> But recently, Pabst et al.<sup>110</sup> for instance found in a polar van der Waals liquid an additional slow contribution to the main relaxation, vanishing when diluted with a non-polar solvent. This finding is in line with a recent theory by Déjardin et al.,<sup>111</sup> strongly questioning this assumption. Thus, effects from coherent (multiparticle) dynamics must be considered in DS in contrast to PCS, <sup>2</sup>H and <sup>31</sup>P NMR. The latter NMR methods probe the reorientational correlation function  $C_2(t)$  via the quadrupolar interaction with the electric field gradient or the chemical shift anisotropy (neglecting the weak

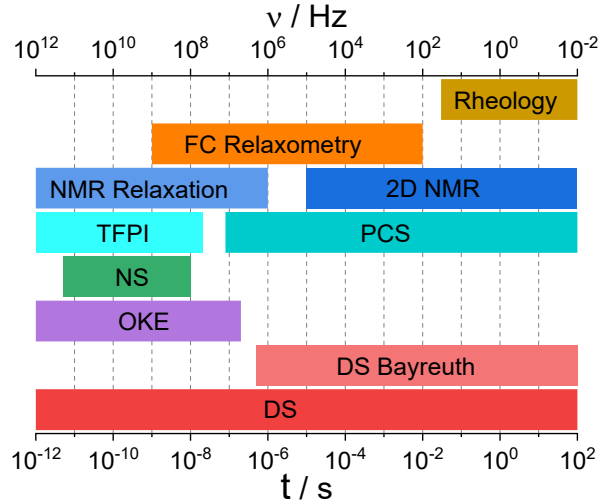


**Figure 1.6:** Overview of the most applied experimental techniques used to study glassy dynamics with their corresponding time/frequency range. Dielectric Spectroscopy (DS), Optical Kerr effect (OKE), Neutron scattering (NS), Light scattering (Tandem Fabry-Perot-interferometry (TFPI), photon correlation spectroscopy (PCS)), Field Cycling (FC) relaxometry and conventional NMR relaxation and 2D NMR as well as Rheology.

dipolar interaction), which probes purely single particle (incoherent) dynamics. The measured spin-lattice ( $R_1$ ) and spin-spin relaxation times ( $R_2$ ) are connected to the spectral density  $J(\omega)$ :<sup>106</sup>

$$^2\text{H:} \quad R_1 = K_Q [J(\omega) + 4J(2\omega)] \quad R_2 = \frac{K_Q}{2} [3J(0) + 5J(\omega) + 2J(2\omega)] \quad (4)$$

$$^{31}\text{P:} \quad R_1 = K_{CSA} J(\omega) \quad R_2 = \frac{K_{CSA}}{6} [4J(0) + 3J(\omega)] \quad (5)$$

$K_Q/K_{CSA}$  gives the corresponding coupling constant. The stimulated echo technique provides under certain experimental parameter restriction directly access to  $C_2(t)$ .<sup>10,112</sup> For PCS, single particle dynamics is assumed to be probed at low frequencies/temperatures.<sup>113</sup> Yet, coherent influence at high temperatures and high frequencies far from the main relaxation cannot be ruled out.<sup>113</sup>

## 1.2 Results & Discussion

On the way to the dynamics of binary non-polymeric (highly) asymmetric mixtures, the first task was to find a suitable system, to overcome problems like de-mixing, crystallization and other interfering effects, found in previous investigations in the group of E. Rössler (Bayreuth).<sup>114,115</sup> Therefore, neat low-molecular high- $T_g$  glass formers had to be developed (cf. also thesis of Felix Krohn, Makromolekulare Chemie I, group of H.-W. Schmidt) overcoming these problems in the mixture. While characterizing these newly synthesized systems (Publication 1), we encountered old unsolved problems of the glass transition phenomenon which were tackled during this thesis among others by a systematic comparison of the data collected in recent years in the Bayreuth group mainly for low- $T_g$  glass formers (Publication 2).

### 1.2.1 High- $T_g$ Glass Formers (Publication 1)

The specially synthesized high- $T_g$  glass formers consist of a rather large, non-polar spirobifluorene core and differently polar side groups leading to varying high  $T_g$  values. Their molecular structure and glass transition temperatures are shown in 1.7. Especially the steric frustration introduced via the variety of side groups as well as the high mass of the rigid core lead to a good glass stability and the high  $T_g$  values. Additionally, the rigid core can be deuterated and thus no additional degrees of freedom interfere when investigating the main relaxation later on via  $^2\text{H}$  NMR spectroscopy. The dielectric relaxation strength changes strongly for the different compounds, depending on the polarity of the side group.

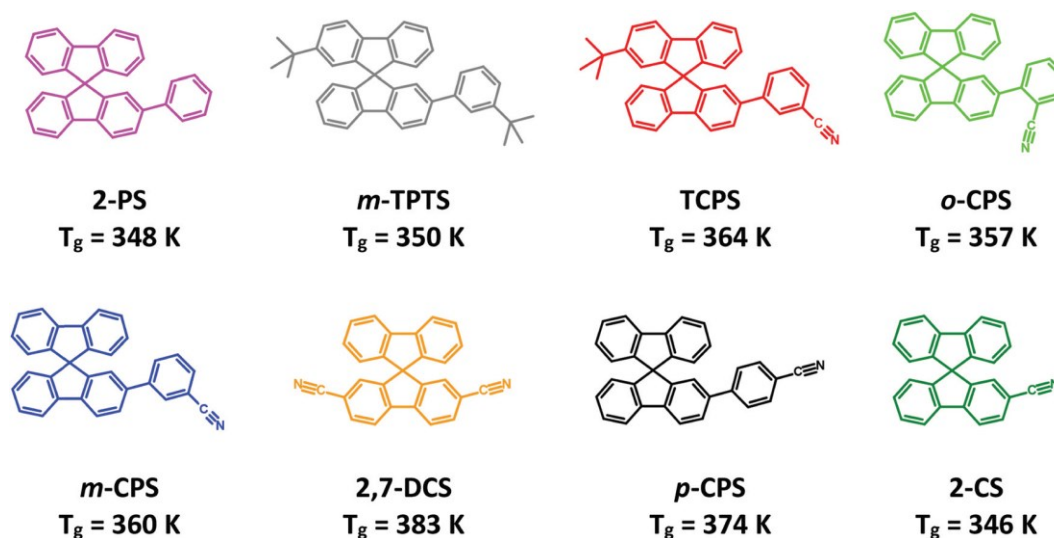


**Figure 1.7:** Structure and glass transition temperature  $T_g$  of the investigated glass formers. Figure from Publication 1.

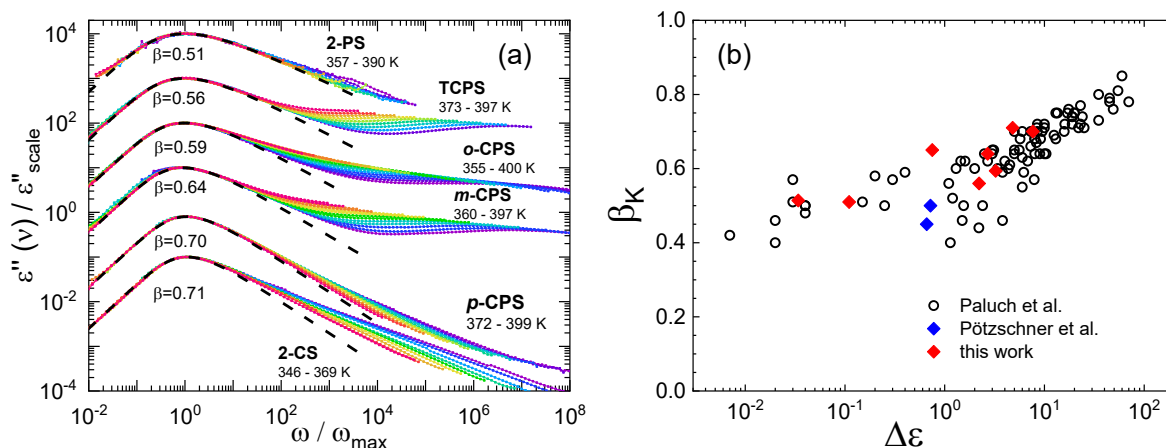


**Figure 1.8:** (a) Master curves (coloured symbols) and respective Kohlrausch fits (dashed black lines, stretching parameter  $\beta_K$  indicated) for the systems indicated (cf. 1.7). Master curves constructed by scaling axes by peak amplitude and frequency, respectively; they are shifted to an arbitrary height. Temperature corresponding to the curves increases from violet to red. (b) Stretching parameter  $\beta_K$  as function of the dielectric relaxation strength  $\Delta\varepsilon$  for a large collection of systems from Paluch et al.<sup>25</sup> (open black circles), the two high- $T_g$  glass formers SBC and DH 379 from Pötzschner et al.<sup>114,115</sup> (blue diamonds), and the herein investigated systems (red diamonds). Figures from Publication 1.

All these organic high- $T_g$  glass formers were characterized by DS. An excerpt of the dielectric spectra is shown as master curve (scaled on the main relaxation peak) in Figure 1.8 (a), together with the corresponding Kohlrausch fits to determine the stretching of the  $\alpha$ -relaxation. Typical relaxation features of molecular low- $T_g$  systems are discovered and compared in the publication to those of several reference systems (polybutadiene (PB), toluene (Tol), tripropyl phosphate (TPP), decahydro isoquinoline (DHIQ), 3,3',4,4'-benzophenonetetracarboxylic dianhydride (2-PC) and felodipine (FD)). The relaxation stretching  $\beta_K$  varies for the different high- $T_g$  systems between 0.51 and 0.71 whereas the fragility index resembles that of other molecular low- $T_g$  glass formers, showing no clear dependence on the stretching  $\beta_K$  as proposed e.g. by Böhmer et al.<sup>52</sup> Frequency-temperature superposition seems to apply around the peak, but the occurrence of some kind of  $\beta$ -relaxation hampers the identification of a possible generic relaxation pattern including  $\alpha$ -peak and excess wing.<sup>55</sup>

Nevertheless, the stretching  $\beta_K$  shows a trend to be lower the lower the relaxation strength  $\Delta\varepsilon$  is, which was first recognized by Nielsen et al.<sup>53</sup> and recently considered by Paluch et al.<sup>25</sup> as explained above. Figure 1.8 (b) shows the stretching parameter  $\beta_K$  found by Paluch et al.<sup>25</sup> (open black circles) as function of the relaxation strength  $\Delta\varepsilon$  on a semi-logarithmic scale as well as the data of our high- $T_g$  components (red diamonds) and those from previous projects (blue diamonds).<sup>114,115</sup> The overall trend is nicely confirmed. Yet, we do not find any outlier when the direction of the dipole moment introduced by the nitrile group is changed with respect to some molecular axis,

which was recently reported.<sup>116</sup> Also, the local positioning of the polar nitrile group at the rather large core interacting only via van-der-Waals forces - potentially having an effect on the stretching<sup>116</sup> - does not change the trend  $\beta_K$  vs.  $\Delta\varepsilon_\alpha$ .

Overall, one must keep in mind, that the determination of the stretching parameter  $\beta_K$  depends strongly on the applied analysis and should only be compared for different systems analyzed the same way (cf. section 1.2.2). The secondary relaxation of TCPS for example, was considered within the Williams-Watts approach (the correlation function is taken as product of individual correlation functions of the  $\alpha$ - and  $\beta$ -relaxation, instead of the sum as mostly done),<sup>33,117,118</sup> leading to a 10% smaller stretching parameter compared to a pure Kohlrausch analysis of the peak at  $T_g$ .

Taking a closer look at the secondary relaxations in all our high- $T_g$  glass formers, one recognizes several differences. Well resolved  $\beta$ -relaxations are only found for those glass formers with a nitrile group attached in *o*- or *m*-position of the phenyl ring linked to the rigid spiro core. In the *p*-position as well as when one or two nitrile groups are directly attached to the spiro core as in 2-CS and 2,7-DCS, no clearly resolved  $\beta$ -relaxation is observed. Absence of any nitrile group lowers the relaxation strength  $\Delta\varepsilon_\alpha$  significantly, and no typical  $\beta$ -relaxation pattern is recognized either.

In addition, the separation of  $\alpha$ - and  $\beta$ -process ( $T \leq T_g$ ) varies significantly because the average activation energy  $E_\beta$  varies between 12 and 32  $RT_g$  whereas fragility remains essentially the same. This can be clearly seen in Figure 1.9 (a), where the time constant  $\tau_\beta$  as a function of reduced temperature  $T_g/T$  with an “average”  $\alpha$ -process (black line) of the herein investigated glass formers is shown. The detailed spectral analysis in the frame of the Williams-Watts approach of TCPS and 2-PC provides

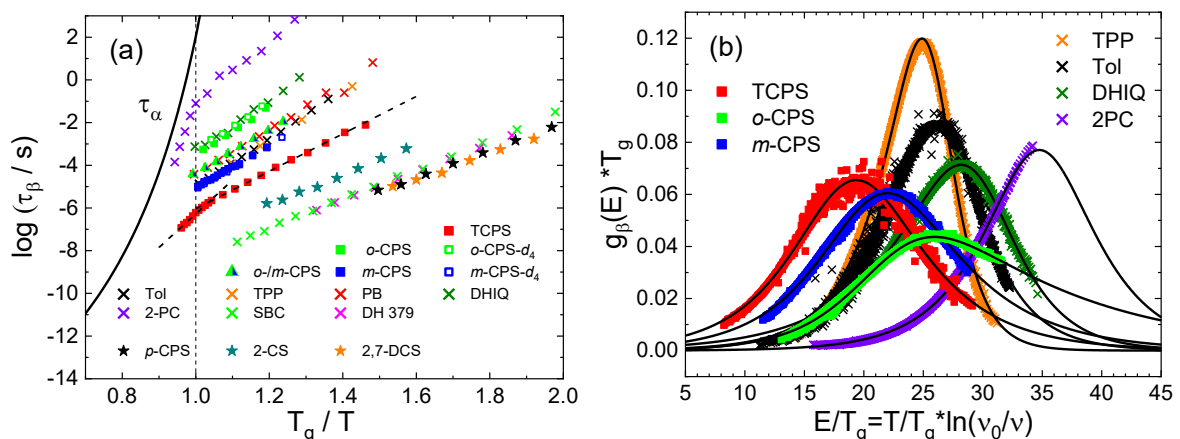


**Figure 1.9:** (a) Time constant  $\tau_\beta$  as a function of reduced temperature  $T_g/T$  with “average”  $\alpha$ -process (black line) of the investigated glass formers.  $\tau_\beta$  was determined with a Williams-Watts approach for TCPS (red squares) and 2-PC (purple crosses) also above  $T_g$ . (b) Normalised distribution  $g_\beta(E)$  scaled by  $T_g$  for several analysed systems (colour and symbol). Black lines: fits along a distribution function proposed in ref.<sup>29</sup> Figures from Publication 1.

quantitative relaxation strengths and time constants. In particular, the temperature dependence of  $\tau_\beta(T)$  shows a crossover to a stronger temperature dependence above  $T_g$ , a phenomenon well known,<sup>8,33,119,120</sup> and its relaxation strength strongly increases above  $T_g$ , whereas it remains virtually constant below.

$E_\beta$  increases somewhat systematically with  $T_g$ , as well as the width of the underlying temperature independent distribution  $g_\beta(E)$ , shown by the corresponding scaling of the DS data (symbols) in Figure 1.9 (b) on a reduced energy scale  $E/T_g$ . The master curves  $g_\beta(E)$  were obtained by rescaling the DS spectra below  $T_g$  assuming a distribution of individual, thermally activated processes.<sup>121</sup> Similar distributions  $g_\beta(E/T_g)$  are found with widths changing about a factor 2. Thus, the previously established relationship  $E_\beta \approx 24 RT_g$ <sup>33</sup> is only followed approximately, if at all. Furthermore, an estimate of the relative relaxation strength of the  $\beta$ -relaxation compared to the  $\alpha$ -relaxations  $\Delta\epsilon_\beta/\Delta\epsilon_\alpha$  was proposed, resulting in a broad range of 0.03 (TPP) up to 0.32 (DHIQ).

Thus, this is quite difficult to reconcile with the universal relaxation pattern revealed by NMR, interpreting the  $\beta$ -process as a generic cooperative phenomenon.<sup>122–124</sup> Independent of molecular details, the  $\beta$ -process involves an essentially spatially isotropic reorientation of the molecules, though highly hindered. Yet, a possible anisotropic character was discussed,<sup>125</sup> which could not be found for toluene deuterated at different positions.<sup>126</sup> In the case of the present glass formers, the  $\beta$ -relaxation depends on the actual position of the nitrile group. Whether this is an indication of an anisotropic character or a “localized”  $\beta$ -relaxation restricted to the motion of the phenyl ring alone, can be checked, e.g. by investigating a deuterated core by <sup>2</sup>H NMR – a future task beyond this thesis.

## 1.2.2 Relaxation Stretching of Molecular Liquids (Publication 2)

Given the insights of Publication 1 about a possible relationship between the relaxation stretching and the dielectric relaxation strength,<sup>25,53,127</sup> as well as a recent rheological survey of viscous liquids pointing towards a generic viscoelastic compliance signature of the  $\alpha$ -relaxation,<sup>54,55</sup> the question arises whether these findings are method specific or more of general nature. Therefore, a systematic evaluation of the spectral shape of the  $\alpha$ -relaxation of type A glass formers, lacking a discernible secondary relaxation, was attempted.

The reorientational dynamics was probed by the three techniques DS, PCS and NMR with a common model, interpolating the susceptibility by a sum of a Kohlrausch (main relaxation) and a Cole-Davidson (excess wing) susceptibility function. As already mentioned, any analysis of the main relaxation without considering the excess wing contribution (in type A glass formers) is obsolete.

The 14 analysed literature systems measured previously in our group with DS (symbols) are shown in Figure 1.10 (a) together with the model interpolations (lines). The main relaxation peak broadens with decreasing relaxation strength as expected. For the three glass formers glycerol, *m*-TCP and OTP, a direct comparison between Field Cycling

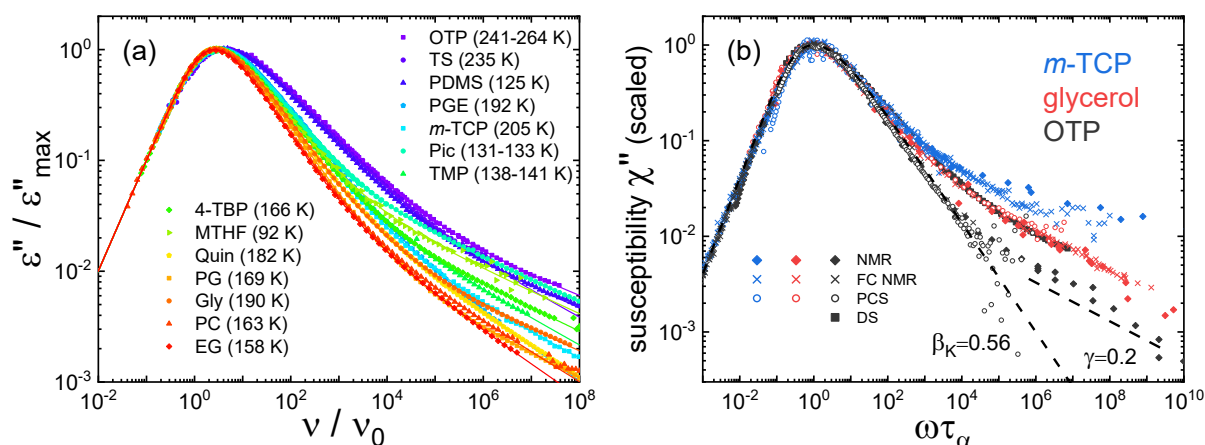


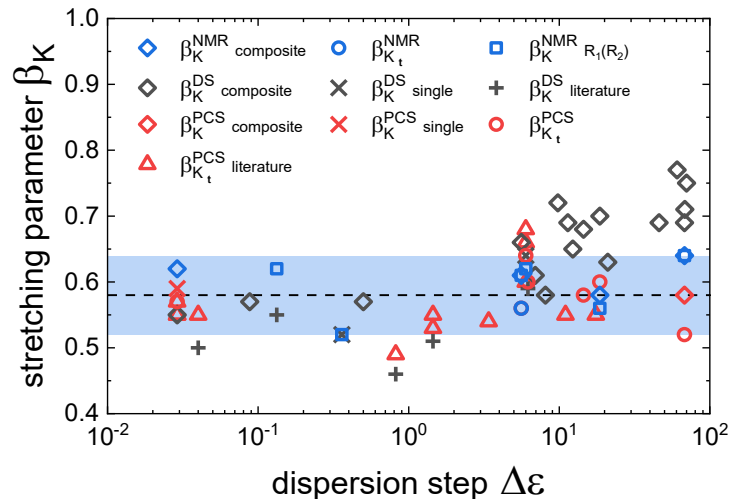
**Figure 1.10:** (a) Dielectric spectra of type A glass formers (symbols) measured close to  $T_g$  interpolated by a sum of a Kohlrausch (main relaxation) and a Cole-Davidson (excess wing) susceptibility (lines). Measurement temperatures are given (temperature range: master curve). (b) Rotational susceptibility of *m*-TCP (blue symbols),<sup>15,128,129</sup> glycerol (red symbols)<sup>51,110,130</sup> and *o*-terphenyl (black symbols),<sup>131-133</sup> as obtained from PCS (open circles), FC  $^1\text{H}$  NMR relaxometry (pluses),  $^{31}\text{P}/^{2}\text{H}$  NMR single-frequency spin relaxation (diamonds) and DS (squares). Dashed line: low-relaxation-strength limit of the  $\alpha$ -process from DS ( $\beta_K = 0.56$ ). Figures adapted from Publication 2.

(FC) NMR, conventional single-frequency NMR (assuming FTS) and PCS in the susceptibility representation is given in Figure 1.10 (b). One recognizes that among these materials the width of the  $\alpha$ -relaxation peak varies much less than the corresponding dielectric spectra in Figure 1.10 (a). Yet, the relative amplitude of the (weak) excess wing appears to be method and system dependent with a high-frequency exponent close to 0.2 for all systems and methods. Since the relation  $\chi''_{l=2}(\omega) \approx 3\chi''_{l=1}(\omega)$  does not always apply, in contrast to what was previously thought,<sup>15</sup> the relative contribution of the excess wing with respect to that of the  $\alpha$ -relaxation peak cannot generally be explained by assuming small angular displacements.

Furthermore, FTS seems to be valid for these systems measured by PCS and NMR, which could be shown by the equivalence of the susceptibilities:  $\chi''_{PCS}(\omega\tau) \propto \chi''_{NMR}(\tau) \propto \chi''_{NMR}(\omega)$ . Explicitly, no difference was found, whether the susceptibility was analysed as function of  $\tau$  or  $\omega$  or as master curve  $\omega\tau$ . Various results from neutron scattering,<sup>7,43,134</sup> as well as from molecular simulations<sup>135,136</sup> hint also at the applicability of FTS. For DS a systematic narrowing of the dielectric relaxation with increasing temperature was found. Thereby, the effect is stronger for more polar systems. For the systems with lowest polarities, the DS main relaxation seems to find a limit with a stretching parameter of  $\beta_K \approx 0.56$  (black squares in Figure 1.10 (b)), which fits to the average behaviour found for PCS and NMR (dashed line in Figure 1.10 (b)), whereas for higher polarities higher stretching parameters are found in DS.

Summarizing and tentatively generalizing our findings for the reorientational dynamics of molecular liquids, the stretching parameter  $\beta_K$  is shown in Figure 1.11 as function of the dielectric relaxation strength  $\Delta\epsilon$  for all systems analyzed together with some literature values from PCS (red symbols), NMR (blue symbols) and DS (grey symbols). A “genuine” stretching parameter  $\beta_K$  of  $0.58 \pm 0.06$  (blue area) is probed by PCS and NMR, and by DS provided  $\Delta\epsilon \leq 6$ . Polar probe molecules in nonpolar solvents show similar values.<sup>137</sup> Larger  $\beta_K$  values are revealed in DS for liquids with higher relaxation strengths. These results show, that the dipole-dipole interactions does not generally trigger a narrowing of the underlying distribution of molecular reorientation times proposed by Paluch et al.<sup>25</sup>

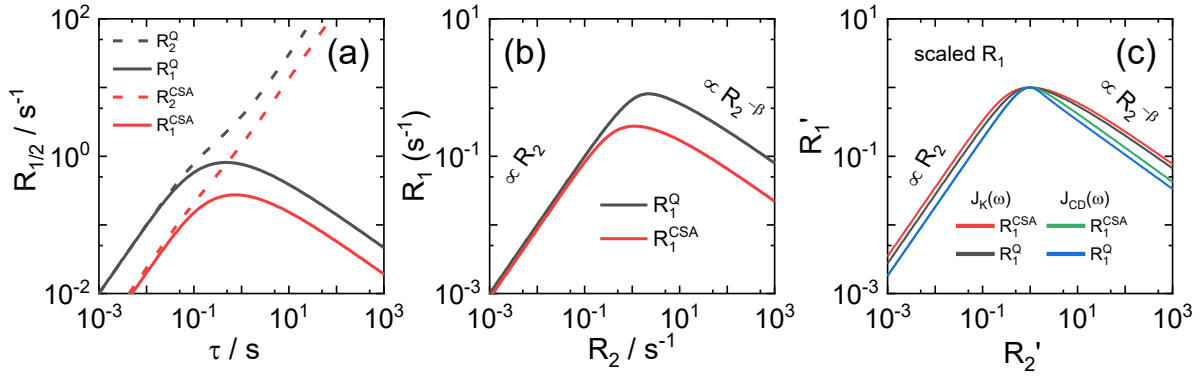
It is a future task to resolve these differences which could find its possible explanation in the differences between collective dynamics (cross-correlation effects<sup>138</sup>) probed by DS vs. single particle dynamics probed mainly via PCS,<sup>113</sup> and purely via <sup>2</sup>H and CSA dominated NMR spin relaxations. A suggested connection,<sup>110,139</sup> that the differences of the stretching parameters found for polar liquids between the different experimental methods could be connected to the spectral enhancement via the Kirkwood factor could not be confirmed in our data. In a very recent paper (becoming available after our



**Figure 1.11:** Stretching parameters  $\beta_K^{DS}$  (black),  $\beta_K^{PCS}$  (red), and  $\beta_K^{NMR}$  (blue) as a function of  $\Delta\varepsilon$ . Analysis in the frequency domain ( $\omega$ ): composite fits (diamonds) and single Kohlrausch fits (crosses) if no composite fit possible; Analysis in the time domain ( $t$ ): single fits (circles);  $R_1$  vs.  $R_2$  analysis (squares). Literature data: triangles (PCS) and plusses (DS). Figure adapted from Publication 2.

paper was submitted),<sup>140</sup> the authors propose a generic structural relaxation in supercooled liquids measured via PCS. Still, it is of interest to resolve, whether the weak “scatter” in the PCS and NMR database is due to experimental uncertainties or whether it reflects peculiarities of the liquids.

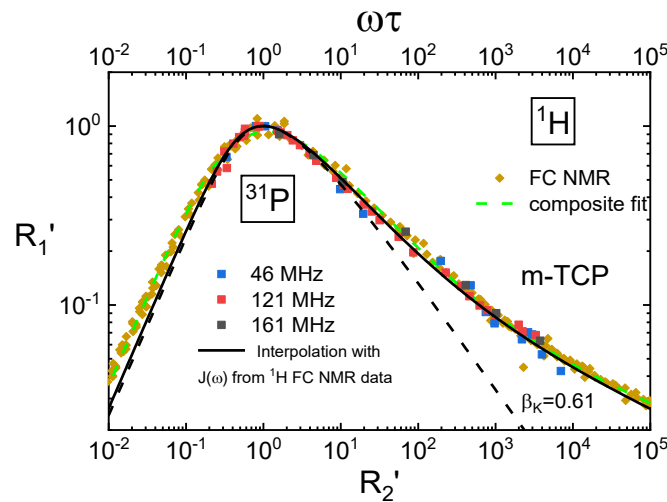
During the analysis of the NMR data of this study (Publication 2), we demonstrated that a new simple single-frequency analysis of the spin-lattice relaxation rate  $R_1(T)$  as a function of the spin-spin relaxation rate  $R_2(T)$  yields the stretching parameter, given that FTS works for the NMR response. This is demonstrated in Figure 1.12. The rates  $R_1(\tau)$  and  $R_2(\tau)$  are calculated for a Kohlrausch spectral density in Figure 1.12 (a) via the BPP equation (cf. eqs. (4), (5)).<sup>141</sup> Plotting  $R_1$  as function of  $R_2$  at the same correlation time (temperature) is shown in Figure 1.12 (b). In the limit of extreme narrowing conditions ( $\omega\tau_\alpha \ll 1$ ),  $R_1$  is directly proportional to  $R_2$ , whereas in the slow-motion limit ( $\omega\tau_\alpha \gg 1$ ),  $R_1$  is proportional to  $R_2^{-\beta}$  (stretching parameter  $\beta$ ). This is a general finding independent of the underlying spectral density, which can be seen in Figure 1.12 (c), where the normalized relaxation rate  $R'_1(R'_2)$  is depicted for a Kohlrausch and a Cole-Davidson spectral density. The details of the  $R_1 = f(R_2)$  curve around the maximum ( $\omega_L\tau \cong 1$ ) depend on the relaxation mechanism and allow to determine the kind of underlying spectral density. Good agreement between the  $R_1(R_2)$  results and the relaxation spectrum obtained using FC  $^1\text{H}$  NMR relaxometry or PCS are found. In



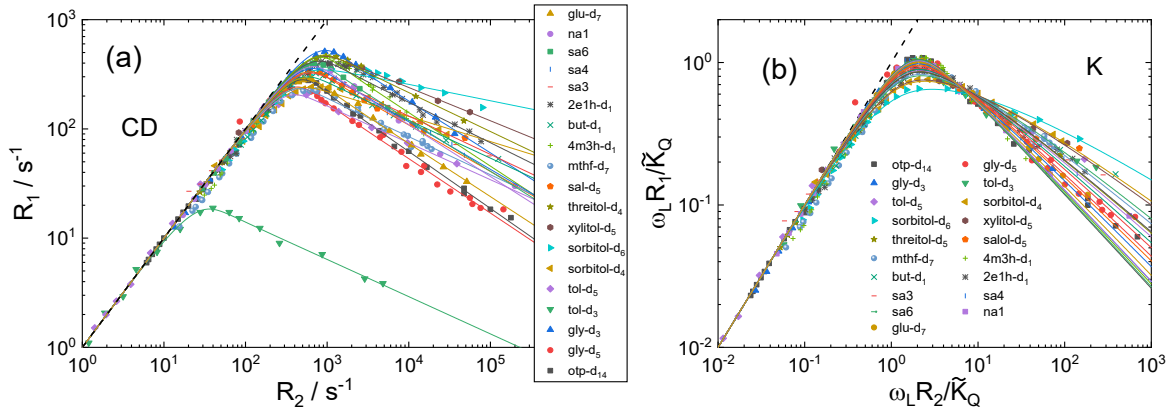
**Figure 1.12:** (a) Spin-lattice relaxation rate  $R_1(\tau)$  (lines) and spin-spin relaxation rate  $R_2(\tau)$  (dashed lines) calculated according to the BPP equation<sup>141</sup> for the quadrupolar ( $^2\text{H}$ , grey) and CSA dominated relaxation ( $^{31}\text{P}$ , red) ( $K_Q = K_{CSA} = 1$ ,  $\omega = 1$ ,  $\beta_K = 0.5$ ). (b)  $R_1$  as function of  $R_2$ . (c) Quadrupolar and CSA relaxations assuming a Kohlrausch and a CD spectral density, both with  $\beta = 0.5$ . The variables  $R'_1 = R_1/R_1^{\max}$  and  $R'_2 = R_2/R_2(R_1^{\max})$  are used to be insensitive to variations in coupling constants and Larmor frequencies. Figures adapted from Publication 2.

Figure 1.13, a direct comparison to the FC  $^1\text{H}$  master curve is shown for  $m\text{-TCP}$  analysed with the same underlying spectral density parameters (green-dashed line vs. black line).

Previously, the stretching parameters and correlation times  $\tau_\alpha(T)$  were determined directly via the BPP equation with a CD spectral density from combined measurements of  $R_1(T)$  and  $R_2(T)$ .<sup>128,130,131,142</sup> This new method complements the previous approaches with the big advantage, that an exact knowledge of the temperature/correlation time



**Figure 1.13:**  $^{31}\text{P}$  NMR relaxation rate  $R'_1 = R_1/R_1^{\max}$  as a function of  $R'_2 = R_2/R_2(R_1^{\max})$  (squares, bottom x-axis)<sup>128</sup> and FC  $^1\text{H}$  NMR relaxation rate  $R'_1$  as a function of  $\omega\tau$  (yellow diamonds, top x-axis)<sup>129</sup> of  $m\text{-TCP}$  on the same scale. Solid black line ( $^{31}\text{P}$  NMR): Interpolation according to the spectral density of the  $^1\text{H}$  FC NMR data (green dashed line; composite fit). Dashed black line: Kohlrausch ( $\alpha$ ) contribution. Figure from Publication 2.



**Figure 1.14:** (a)  $^2\text{H}$  spin-lattice relaxation rate  $R_1$  plotted against the spin-spin-relaxation rate  $R_2$  for several glass forming liquids (see Table 1 in ref.<sup>143</sup> for abbreviations and references). The lines are interpolations of  $R_1(R_2)$  with an inserted CD spectral density. Dashed line:  $R_1 = R_2$ . (b) Rescaled  $^2\text{H}$  spin-lattice relaxation rate  $R_1$  plotted against the rescaled spin-spin-relaxation rate  $R_2$  in a way to remove the effect of differences in the effective coupling constants  $\tilde{K}_Q$  and Larmor frequencies  $\omega_L$ . Solid lines: Fits using a Kohlrausch spectral density to calculate  $R_1(R_2)$ . Figure adapted from ref.<sup>143</sup>

is not necessary to determine the stretching and the coupling constant with the internal reference of  $R_2$ .

This approach was applied in a further publication to a large variety of  $^2\text{H}$  NMR systems,<sup>143</sup> measured at different Larmor frequencies ( $\omega_L$ ) for a CD spectral density in Figure 1.14 (a). The Kohlrausch ansatz, which seems superior for these systems, is shown in Figure 1.14 (b), where the relaxation rate is plotted normalized via the Larmor frequency and the determined coupling constant  $\tilde{K}_Q$ , to remove their influence on the relaxation rates. Thus, also the effective coupling constant and the type of underlying spectral density can be estimated with this method. For this large variety of different systems, the analysis reveals a stretching variation of  $0.39 \leq \beta_K \leq 0.67$ , which is larger than the one extracted in Publication 3. These parameters are determined under the assumption of FTS, which should be further tested, especially for flexible molecules like sorbitol. Thus, one has to disentangle conformational from structural relaxations. In particular, in the fluid regime the correlation functions of sorbitol, probed at the end groups ( $-\text{d}_4$ ) and at the OH groups ( $-\text{d}_6$ ), turned out to be rather different. However, the site individuality tends to vanish in the highly viscous regime.<sup>143</sup> Care must be taken when analysing the relaxation in flexible molecules and at special sites with NMR spectroscopy.

## 2 Relaxation Behaviour of Binary Glass Formers

After the preparatory work about high- $T_g$  glass formers and the consequential digression about the relaxation in neat glass formers, an overview of the experimental and theoretical considerations provided so far for binary glass formers will be given in the State of the Art. Following, the results within the framework of this thesis regarding the relaxation in molecular binary glass formers with moderate  $T_g$ -contrast as well as high  $T_g$ -contrast are discussed.

### 2.1 State of the Art

The investigations of the dynamics of binary mixtures started with technological relevant polymer blends<sup>144,145</sup> and polymer-plasticizer systems.<sup>146–150</sup> Especially dynamically highly asymmetric systems with a larger difference of their components  $T_g$ 's ( $T_g$ -contrast  $\Delta T_g$ ) and non-polymeric (molecular) systems<sup>114,151–155</sup> are of relevance as potential model systems with significant molecular size disparity. Such systems created a large interest of theoretical studies and molecular dynamics simulations.<sup>156–164</sup>

The relaxation behaviour of binary glass formers is more complex than that of neat glasses. Starting with the main experimental results provided so far, differential scanning calorimetry (DSC) is the method of choice to determine the glass transition temperatures. Whereas at first, a single DSC step was observed for such kind of systems and interpreted as requirement for the miscibility of a system,<sup>145,165</sup> it is now known for a variety of systems, that the component dynamics is decoupled with two distinct  $T_g$ 's.<sup>114,115,150,154,166–170</sup> Most of the studies discovered the two  $T_g$ 's especially at intermediate concentrations, whereas for low and high additive concentrations only one  $T_g$  was recognized, e.g. depicted in Figure 2.1 (a) for polystyrene (PS) blended with three different molecular low- $T_g$  additives.<sup>167</sup>

One of the first studies, showing two  $T_g$ 's even for lowest additive concentrations was conducted by Blochowicz et al.,<sup>154</sup> followed by the work of Kahlau et al.<sup>150</sup> on the low- $T_g$  component tripropyl phosphate (TPP) mixed with the high- $T_g$  component PS, which results in a contrast of  $\Delta T_g = 200$  K. The corresponding DSC curves of the latter system are shown in Figure 2.1 (b), with clearly two steps for several concentrations. This particular system will serve as example demonstrating the main aspects of highly asymmetric binary glass formers, because it is one of the experimentally best investigated systems. DS and component selective NMR experiments ( $^{31}\text{P}/^2\text{H}$ ) were performed.<sup>150,171</sup> The DS spectra at low concentrations ( $w_{TPP} = 0.18$ ) in Figure 2.1 (c)

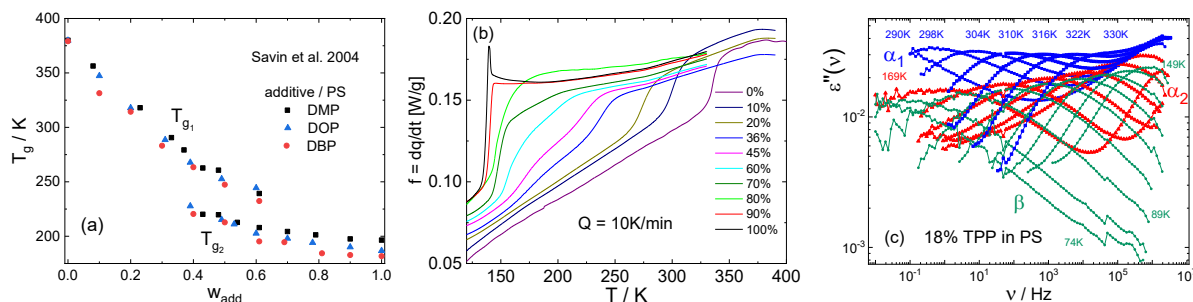


**Figure 2.1:** (a) Concentration dependence of  $T_{g_{1/2}}$  for PS mixtures with DMP, DBP, and DOP. Data from Savin et al.<sup>167</sup> (b) DSC traces (heat flow per sample mass  $f = dq/dt$ ) for mixtures TPP/PS and neat systems ( $w_{\text{TPP}} = 0\%$  and  $100\%$ ) at the heating rate  $Q = 10$  K/min. Reprinted with permission from ref.<sup>150</sup> Copyright (2014) by AIP Publishing. (c) Dielectric spectra of the TPP/PS mixture with  $w_{\text{TPP}} = 0.18$ . Three different processes are marked by color. Figure adapted from ref.<sup>126</sup>

show even three processes. At highest temperatures the  $\alpha_1$ -process (blue squares), attributed to the PS dynamics, is found, whereas at intermediate temperatures the  $\alpha_2$ -process (red triangles), connected to the TPP dynamics, is encountered. At lowest temperatures a secondary process (green circles) is present, typical of the neat low- $T_g$  component TPP.<sup>172</sup> The assignment was ratified by the component selective  $^2\text{H}$  and  $^{31}\text{P}$  NMR experiments.<sup>171</sup>

The two main relaxations were discovered for the whole concentration range, shown via the reorientational correlation times  $\tau(w_{\text{TPP}}, T)$  from the DS and NMR experiments in Figure 2.2 (a). For high concentrations, a VFT-like temperature dependence was found for both main relaxations, whereas for lower  $w_{\text{TPP}}$  a fragile-to-strong transition for  $\tau_{\alpha_2}(T)$  sets in at the glass transition temperature  $T_{g_1}$ . Such a temperature dependence was also found for polymer-blends<sup>145</sup> and for supercooled liquids in nano-confinements.<sup>173–178</sup> Extrapolating this Arrhenius-like temperature dependence to  $\tau = 100\text{s}$  leads to  $T_{g_2}$  decreasing with decreasing  $w_{\text{TPP}}$ . Although an Arrhenius-like temperature dependence is found, this second process is no secondary relaxation, because it was proven via the NMR experiments, that isotropic reorientation is involved which characterizes a main relaxation.<sup>171</sup>

Thus, the DS and NMR investigations confirm the two  $T_g$ 's from DSC and even suggest two  $T_g$ 's up to highest concentrations (Figure 2.2 (b)). The strong dynamic decoupling of the two components at low  $w_{\text{TPP}}$  is evident in Figure 2.2 (b). The glass transition temperature  $T_{g_1}$ , attributed to the dynamics of the high- $T_g$  component PS, shows the well-known plasticizer effect, decreasing with increasing additive concentration.<sup>179</sup> On the other side, the dynamics attributed to the low- $T_g$  component TPP ( $T_{g_2}$ ) shows at highest concentration the expected anti-plasticizer effect, rising with decreasing  $w_{\text{TPP}}$ . At intermediate concentrations,  $T_{g_2}$  saturates and decreases again at lowest  $w_{\text{TPP}}$ , lead-

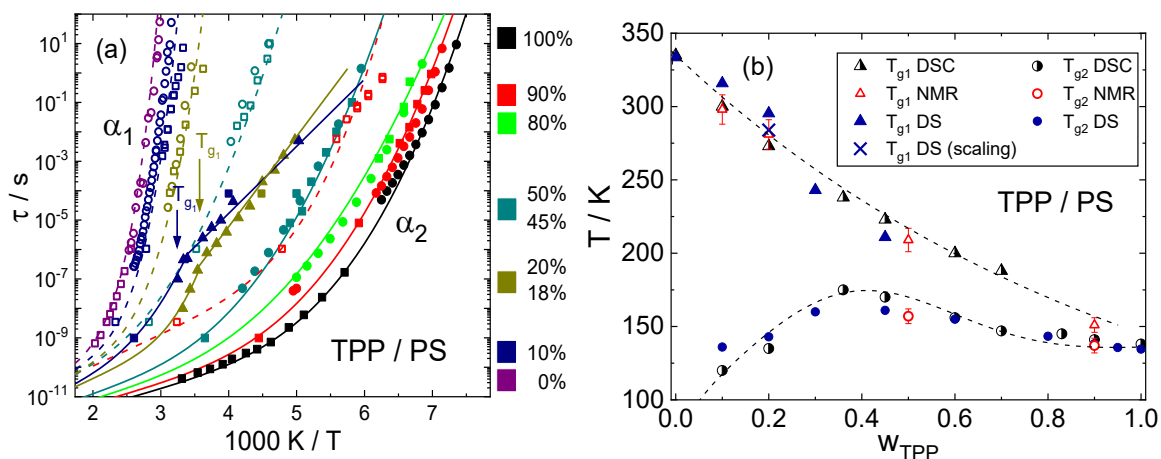


**Figure 2.2:** (a) Time constants of the mixture TPP/PS. Colour code defines mass concentration. Open symbols and dashed lines depict the  $\alpha_1$ -relaxation, filled symbols and solid lines the  $\alpha_2$ -relaxation (circles from DS, squares from NMR, triangles from combined NMR/DS). Arrows mark  $T_{g1}$ . Figure adapted from ref.<sup>126</sup> (b) Glass transition temperatures  $T_{g1/2}$  as a function of TPP concentration by DSC, NMR, and DS for all investigated mixtures. Dashed lines: guides for the eye. Reprinted with permission from ref.<sup>150</sup> Copyright (2014) by AIP Publishing.

ing to a maximum of  $T_{g2}(w_{TPP})$ , which was found for several other non-polymeric systems as well.<sup>114,115,154</sup> In total,  $T_{g2}$  changes rather marginal with  $w_{TPP}$  compared to  $T_{g1}$ . This unexpected behaviour of  $T_{g2}$  is still in debate<sup>180,181</sup> and will be addressed in this thesis.

The DS evolution of the  $\alpha_2$ -process with concentration  $w_{TPP}$  is summarized in Figure 2.3 (a). The dielectric  $\alpha_2$ -spectra strongly broaden with decreasing  $w_{TPP}$  especially on

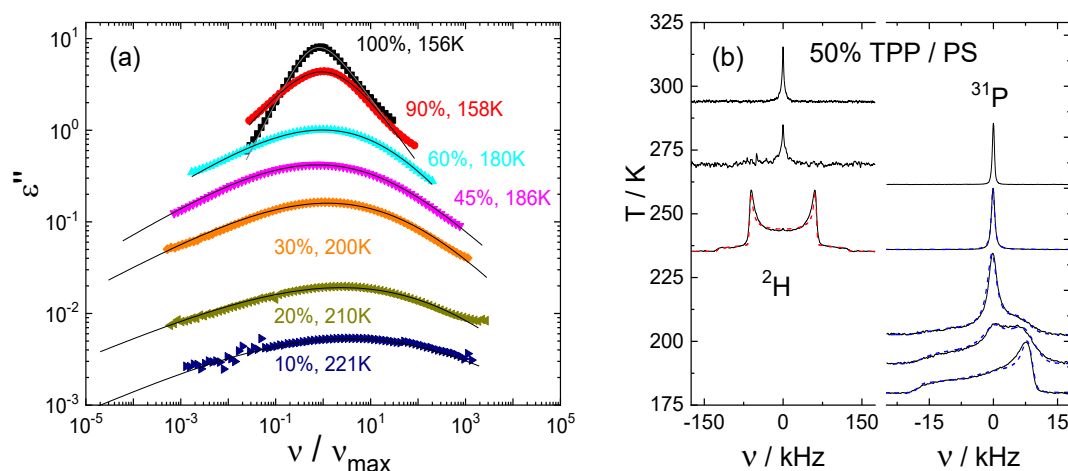


**Figure 2.3:** (a) Evolution of the dielectric spectra of the  $\alpha_2$ -relaxation with concentration  $w_{TPP}$ . Figure from ref.<sup>171</sup> (b)  $^2H$  and  $^{31}P$  NMR 1D spectra of a 50% TPP/PS mixture, baseline of spectra marks temperature on vertical axis. Blue dashed lines: fits by superposition of solid-state spectrum and liquid like Lorentzian line (two-phase spectra). Red dashed line: solid state (Pake) spectrum. Figure adapted from ref.<sup>126</sup>

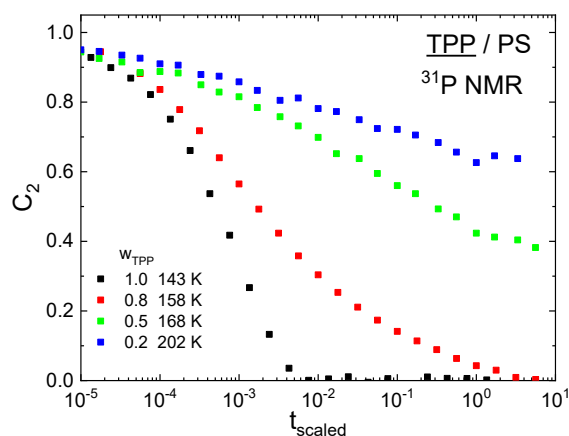


**Figure 2.4:** Reorientational correlation function  $C_2$  of TPP in the mixture TPP/PS for different concentrations  $w_{TPP}$  starting with the same initial correlation measured via the  $^{31}\text{P}$  stimulated echo technique. For comparison:  $C_2$  of pure TPP (black squares) shifted to match the initial correlation. Data from refs.<sup>171,185</sup>

the low-frequency side. In contrast, the high- $T_g$  component shows only a slight broadening compared to the neat system. For the dielectric spectra, a strong temperature dependence is found reflecting the failure of FTS. The difference of the underlying distribution of correlation times  $G(\ln \tau_{\alpha_{1/2}})$  can be seen directly in the NMR spectra shown for  $w_{TPP} = 0.50$  in Figure 2.3 (b). Whereas for the  $^{31}\text{P}$  spectra of TPP, so called “two-phase spectra” are found for a large temperature range, no such indications are found for PS in the  $^2\text{H}$  spectra. Two-phase spectra are characterized by a superposition of a liquid (Lorentzian) line and a solid-state spectrum with different weighting factors changing with temperature,<sup>10,182</sup> reflecting slow and fast isotropic reorientation at the same time. Thus, a very broad distribution of correlation times  $G(\ln \tau_{\alpha_2})$  is present. Also, the dynamic decoupling is directly seen with a solid-state (Pake) spectrum for PS at 235 K and an isotropic liquid-like line for TPP. The final solid-state spectrum of TPP is reached at around 175 K.

Additional information about the kind of motion were obtained from 2D NMR experiments in the time and frequency domain. The strong dynamic heterogeneities found as almost logarithmic decays of the correlation function  $C_2$  at low  $w_{TPP}$  (Figure 2.4) are clearly of transient nature. This was demonstrated for TPP/PS in Figure 2.5 below  $T_{g_1}$  (isotropic exchange spectra), as well as in the temperature range of the two-phase spectra, showing exchange between the fast (Lorentzian line) and slow (solid-state spectrum) TPP molecules. This behaviour was found for a variety of different systems.<sup>115,183,184</sup>

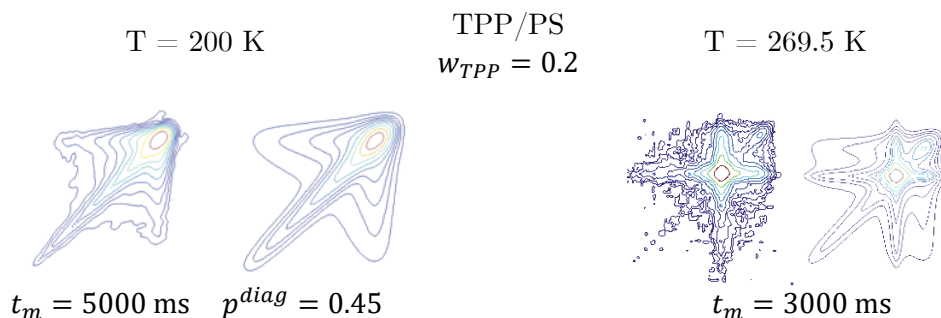


**Figure 2.5:** Experimental 2D  $^{31}\text{P}$  NMR exchange spectrum of a TPP/PS mixture ( $w_{\text{TPP}} = 0.2$ ) at  $T = 200$  K (left, below  $T_{g_1}$ ) and at  $T = 269.5$  K (right, above  $T_{g_1}$ ) with a long mixing time  $t_m$  as indicated. Next to the measured spectrum: calculated spectrum assuming a broad distribution of isotropic reorientation. At  $T = 269.5$  K exchange among liquid-like and solid-like TPP molecules is demonstrated. Figure adapted from ref.<sup>171</sup>

One of the issues not yet understood, is the dielectric relaxation strength  $\Delta\varepsilon_{\alpha_1}$  of the  $\alpha_1$ -process, which increases strongly at low temperatures and is even larger than  $\Delta\varepsilon_{\alpha_2}$  at low  $w_{\text{TPP}}$  (cf. Figure 2.1 (c)) although pure TPP has a two orders of magnitude higher  $\Delta\varepsilon$  than pure PS. One possible explanation for this behaviour, found for several other systems as well, was first proposed by Blochowicz et al.,<sup>149,154</sup> assuming a “fast” and “slow” fraction of additive molecules, whereby the slow fraction participates in the  $\alpha_1$ -relaxation of the high- $T_g$  component leading to the enhanced  $\Delta\varepsilon_{\alpha_1}$ . Above a critical temperature  $T_C$ , the slow fraction of additive molecules appears to vanish. As suggested by Blochowicz, this would correspond to a type A glass transition proposed by MCT and simulations in contrast to the type B transition predicted by MCT for neat glasses. Indications of this slow fraction are found by Bock et al. in the stimulated echoes, assuming a temperature dependent fraction of slowly relaxing TPP molecules.<sup>171</sup> However, no further hints are found in other NMR observables and other systems so far.<sup>114,115,171</sup>

MD simulations of binary mixtures consisting of particles (lacking orientational degrees of freedom),<sup>158–160,162,186</sup> reported a dynamical decoupling of both particle species. The large particles exhibit a standard glass transition controlled by the cage effect, while the small particles show a sub-diffusive behaviour remaining mobile within the arrested matrix of the large particles. This can be seen via the self-diffusion coefficient as function of density (or temperature) in Figure 2.6,<sup>160</sup> showing the increasing decoupling of the large and small diffusion coefficients at higher densities. Meanwhile, the structure shows no essential change superior to the expected compression (inset of Figure 2.6).<sup>160</sup> In particular, for larger size disparities quasi-logarithmic decays are observed in the density-density correlator, but less pronounced in the self-correlation function.<sup>158,159,162</sup>

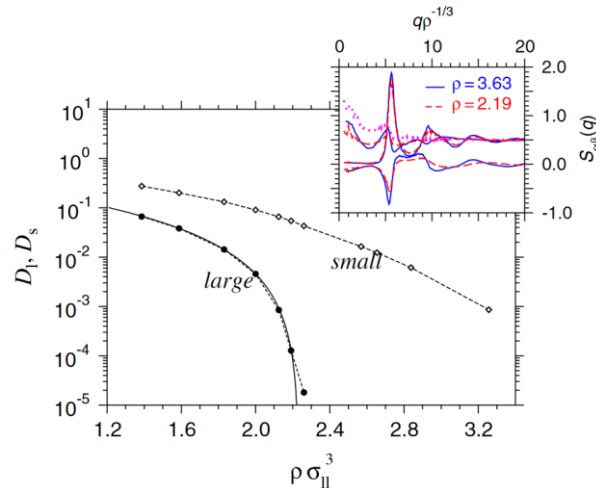


**Figure 2.6:** MD-simulated self-diffusion coefficients for small ( $D_s$ ) and large (soft sphere) particles ( $D_l$ ) in a disparate-sized binary mixture. Inset: partial static structure factors  $S_{\alpha\beta}(q)$  at two densities as functions of  $q\rho^{-1/3}$ , showing little change. Reprinted with permission from ref.<sup>160</sup> Copyright (2009) by the American Physical Society.

Another MD simulation is of interest, investigating the mixture of two water-like model molecules with different polarities, providing a large dynamical contrast while the mixture still remains miscible.<sup>163</sup> The authors showed, that the spatially heterogeneous dynamics is controlled by growing concentration fluctuations upon cooling, typical of approaching spinodal decomposition. The probability of finding a certain concentration fluctuation, however, is narrow in the case of the slow component whereas it is broadly distributed for the fast component. One has to keep in mind though, that the system was designed to mimic water-specific interactions. Clearly, concentration fluctuations are of relevance, and are used to explain the strong dynamic heterogeneities especially in polymer-blends,<sup>187–189</sup> whereby also self-concentration effects<sup>190,191</sup> or a combination of both<sup>192,193</sup> are discussed.

The dynamics of binary systems were also investigated in terms of the MCT,<sup>157,158,161,194</sup> drawing similar conclusions. Again, coherent dynamics of the small particles leads to an additional peak at frequencies connected with that of the slow dynamics of the large particles.<sup>156</sup> In that case the smaller particles retain mobility below  $T_g$  of the larger ones and undergo a localization transition in the confinement of a frozen matrix. In this respect, work on MCT in so-called quenched-annealed systems<sup>195,196</sup> and simulations for a Lorentz-gas model<sup>197</sup> may be relevant. In such systems, MCT predicts higher order singularities<sup>186,198,199</sup> in the vicinity of which the correlation functions of the smaller molecules become extremely broad and quasi-logarithmic decay curves are expected as observed in simulations and experiments.

Although usually not explicitly discussed in experimental studies, it is important to distinguish between incoherent (single particle) and coherent (collective) dynamics. As

### III.2 Relaxation Behaviour of Binary Glass Formers

---

it turned out in the case of binary glass formers, severe differences are reported by theoretical studies as well as MD simulations mentioned above.

All the experiments, theories and simulations explained above apply especially to highly asymmetric mixtures with a large size disparity ( $T_g$ -contrast). But binary mixtures were also investigated as function of size disparity,<sup>159,200-202</sup> showing a strong variation in the dynamic decoupling. For smaller size disparity of the particles, only a simultaneous arrest of both particle species is found which passes over to the above explained behaviour for larger size disparity.

## 2.2 Results & Discussion

At first, two systems with rather moderate  $T_g$ -contrasts were studied (Publication 3), before turning to the relaxation behaviour in a highly asymmetric low-molecular systems (Publication 4 and 5). These systems were investigated by dielectric and NMR spectroscopy. In particular,  $^2\text{H}$  and  $^{31}\text{P}$  relaxation rates, NMR spectra and stimulated echo decays were analyzed attempting to understand the dielectric spectra in terms of component specific dynamics. A common scenario is proposed discussing the results determined in thesis as well as in previous works.

### 2.2.1 Moderate $T_g$ -contrast (Publication 3)

Several highly asymmetric binary mixtures were investigated so far by our group,<sup>114,115,150,184</sup> whereby the low- $T_g$  component always dominated the dielectric response, reflecting the additive dynamics. Therefore, two decisive things were changed. (I) Systems with smaller  $T_g$ -contrast, specifically toluene (tol)/quinaldine (quin) ( $\Delta T_g = 63$  K) and toluene/*m*-tricreysl phosphate (*m*-TCP) ( $\Delta T_g = 89$  K) were chosen. (II) The high- $T_g$  components have a significantly higher dipole moment (1.5 orders of magnitude) compared to that of the low- $T_g$  component. Thus, they dominate the dielectric spectra. Exemplarily, the results on the mixture tol/*m*-TCP are discussed; the system tol/quin shows very similar results.<sup>203</sup>

The dielectric spectra of the system tol/*m*-TCP are shown in Figure 2.7 as master curves. Therefore, the individual dielectric loss spectra  $\varepsilon''(\omega)$  are normalised by the dielectric relaxation strength  $\Delta\varepsilon$  determined from the real part  $\varepsilon'(\omega)$  and shifted along the  $\omega$  axis onto the straight line  $\varepsilon''(\omega)/\Delta\varepsilon = \omega$ . In this representation, the shift factors directly provide the correlation time  $\tau$  in a model independent manner. Starting with pure *m*-TCP up to the  $w_2 = 0.21$  mixture, FTS applies, yet, the overall peak becomes somewhat broader with respect to that of neat *m*-TCP (black dashed line). For the concentrations  $w_2 = 0.45$  and higher, FTS fails and the relaxation broadens further up to highest concentrations, whereas the high-frequency flank remains essentially the same until spectral contributions from toluene are observed; a  $\beta$ -relaxation typical of toluene is found. A simple Kohlrausch or CD function is not able to reproduce the broadening of the spectra. Therefore, the spectra had to be described with a Generalized Cole Davidson function (GCD)<sup>204</sup> for the main relaxation peak, providing an additional width parameter independent of the high-frequency slope. The width of the dielectric spectra corresponds well to the measured  $^{31}\text{P}$  NMR stimulated echo decays (cf. Figure 8 in Publication 3).

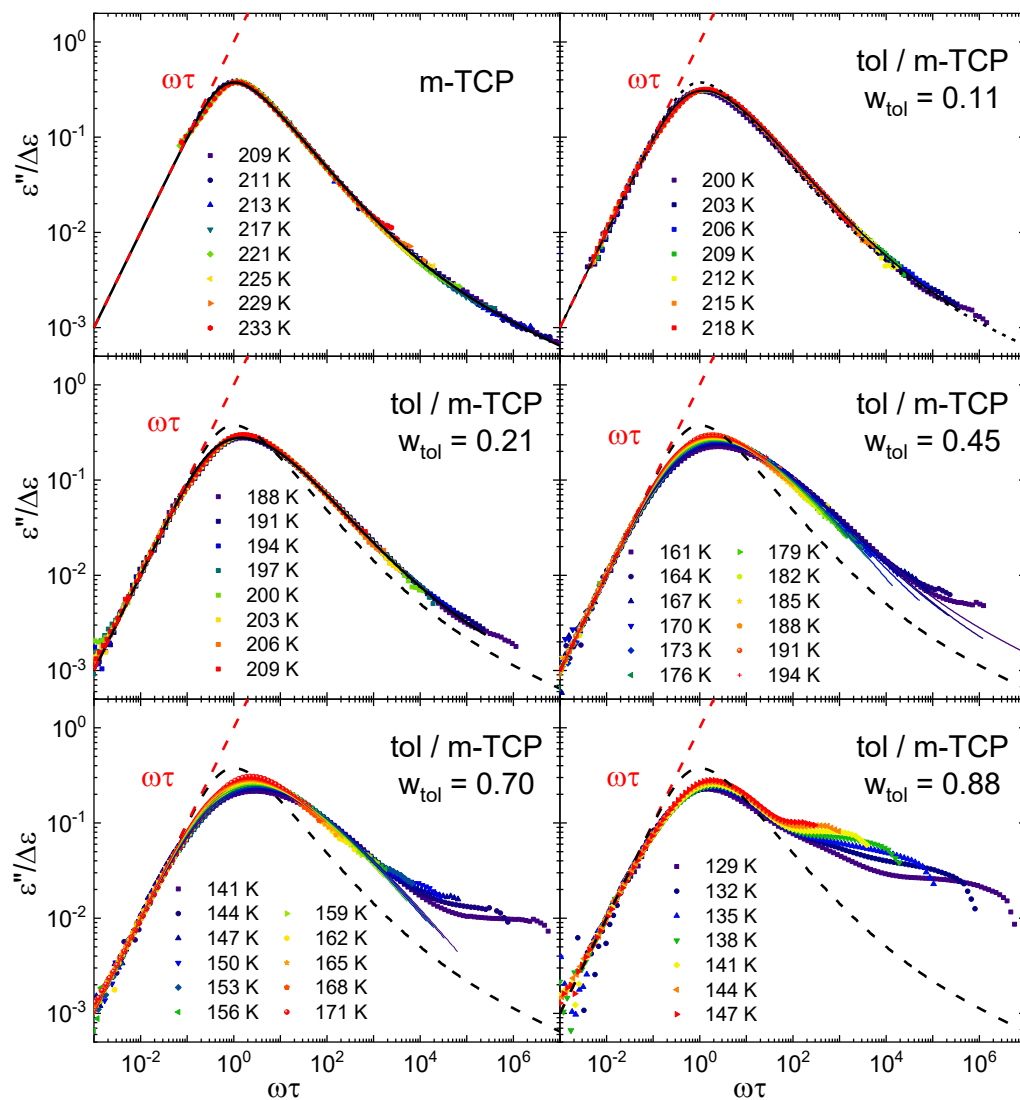


**Figure 2.7:** Master curves of the dielectric spectra of the mixture toluene/*m*-TCP at different temperatures and different mass concentrations of toluene. Straight dashed line represents low-frequency limit  $\omega\tau$ . For comparison, the fit of the master curve of neat *m*-TCP is added in each case (black dashed line). The fits, a superposition of the GCD (main peak) and CD function (excess wing), are shown as solid lines. Figure from Publication 3.

Furthermore, spin-lattice relaxation rates  $R_1(T)$  were measured for both components (Figure 2.8), which probe the spectral density at the Larmor frequency as function of temperature (cf. eqs. (4), (5)). For the additive toluene (Figure 2.8 (a)), the  $^2\text{H}$  relaxation rates  $R_1(T)$  shift to higher temperatures, the shape broadens and the peak maximum lowers successively upon adding *m*-TCP. This directly reflects the broadening of the relaxation function of the low- $T_g$  component. Even indications of a separate peak (secondary process known from pure toluene) are more and more visible. The  $^{31}\text{P}$  relaxation rates of the high- $T_g$  component *m*-TCP (Figure 2.8 (b)) shift upon dilution with

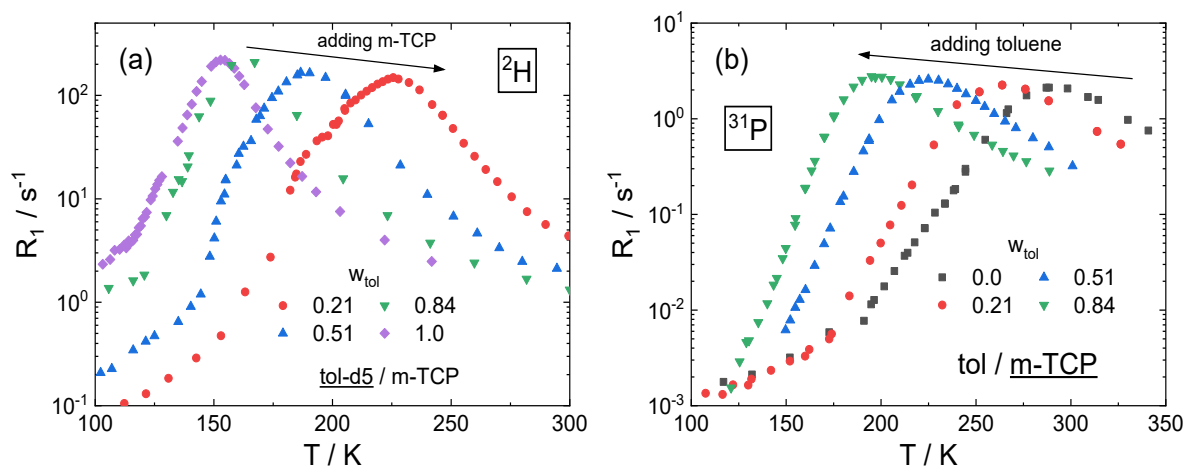


**Figure 2.8:** Spin-lattice relaxation rate  $R_1 = 1/T_1$  as a function of temperature for different concentrations  $w_{tol}$ : (a) Toluene in the mixture toluene/*m*-TCP probed by  $^2H$  NMR. Pure toluene data adapted from refs.<sup>205,206</sup> (b) *m*-TCP in the same mixture with toluene probed by  $^{31}P$  NMR. Figures from Publication 3.

toluene to lower temperatures (plasticizer effect), whereas the overall shape stays fairly the same.

In contrast to systems with larger  $T_g$ -contrast, the dynamic decoupling observed in the NMR spectra (Figure 2.9) is not that strong and therefore the lineshape changes of the high- $T_g$  and low- $T_g$  component take place at comparable temperatures. Still, the changes set in at slightly higher temperatures for *m*-TCP. One finds “two-phase” spectra for toluene, yet, in a rather small temperature interval. Furthermore, two-phase spectra are recognized for *m*-TCP as well. This means, that not only  $G(\ln \tau_{\alpha_2})$  is broadened in the mixture but also  $G(\ln \tau_{\alpha_1})$ , which was not observable in our previous investigations with higher  $T_g$ -contrast (see also section below). The strong plasticizer effect of toluene is seen comparing the NMR spectra for pure *m*-TCP with those in the mixture.

The overall dynamic picture is provided in Figure 2.9 (b), showing the correlation times for the different concentrations obtained from the DS and NMR experiments, including stimulated echo, spin-lattice relaxation rate  $R_1(w_{TTPP}, T)$  and the spin-spin relaxation rates  $R_2(w_{TTPP}, T)$  measurements (cf. eqs. (4), (5)), determined at highest temperatures. At least in the low viscous regime, two separate relaxation processes (open vs. closed symbols) are found for the whole concentration range. The conventional glass transition temperature  $T_g = T(\tau = 100s)$  is experimentally not reached for both components in this system, because the quadrupolar relaxation rate strongly interfered the  $^2H$  stimulated echo decays.

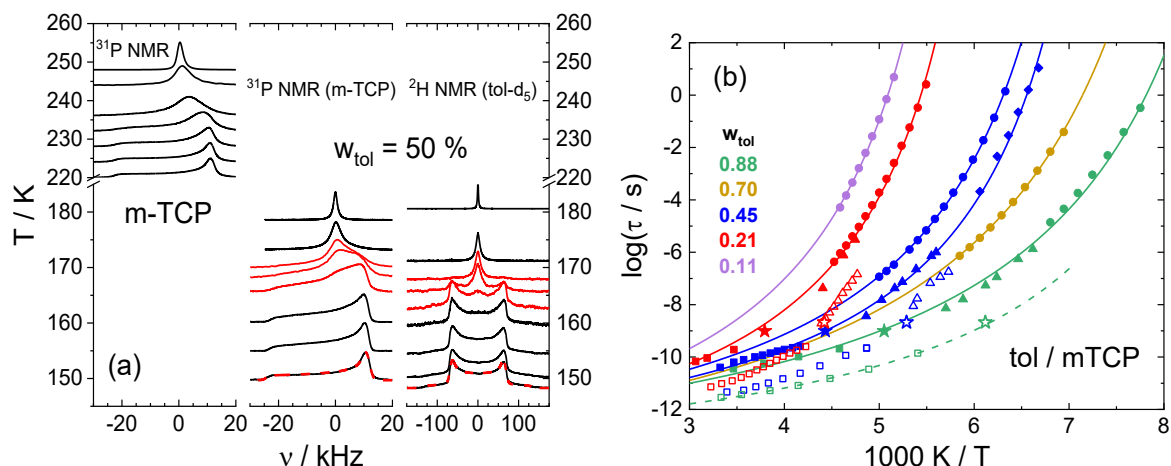


**Figure 2.9:** (a)  $^2\text{H}$  and  $^{31}\text{P}$  NMR spectra of the mixture toluene/*m*-TCP with  $w_{\text{tol}} = 0.50$ . Their baseline defines the temperature. The temperature range with two-phase spectra is marked. At lowest temperatures, the dashed lines show the fits of the solid-state spectra to determine the corresponding coupling constant  $\delta_{Q/CSA}$ . On the left side, the  $^{31}\text{P}$  NMR spectra of pure *m*-TCP for comparison. (b) Time constants of *m*-TCP and toluene in their mixture by DS (circles), by  $^{31}\text{P}$  NMR ( $\alpha_1$ : filled symbols) and by  $^2\text{H}$  NMR ( $\alpha_2$ : open symbols).  $\tau$  determined from  $T_1$ -minima (stars), from high temperature  $R_1$  relaxation data (squares), from  $R_2$  relaxation times (triangles) and from  $^{31}\text{P}$  stimulated echo data (diamonds). NMR concentrations differ slightly from those shown for DS ( $w_{\text{tol}}^{\text{NMR}} = 0.51, 0.84$ ). Figures from Publication 3.

### 2.2.2 High $T_g$ -contrast (Publication 4 and 5)

A highly asymmetric low-molecular binary glass former was developed with the high- $T_g$  component 2-(*m*-*tert*butylphenyl)-2'-*tert*butyl-9,9'-spirobi[9H]fluorene (*m*-TPTS,  $T_g = 350$  K) and the low- $T_g$  component tripropyl phosphate (TPP,  $T_g = 134$  K). Thus, a difference of their  $T_g$ 's of  $\Delta T_g = 216$  K could be reached. No indications of de-mixing or crystallisation were found in the whole concentration range. The corresponding chemical structures are shown in Figure 2.10. For the component selective NMR measurements, *m*-TPTS was deuterated at one of the phenyl rings of the rigid spirobifluorene core - another advantage of this system.

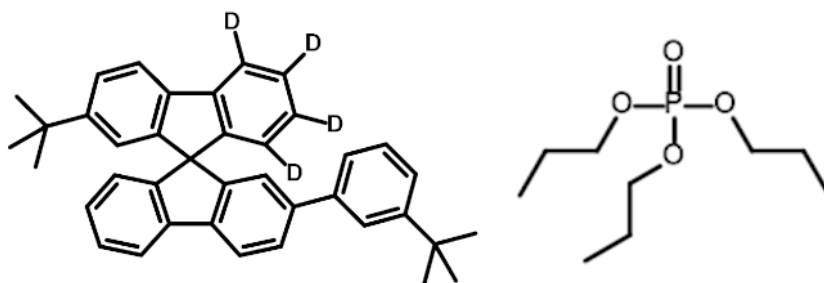


**Figure 2.10:** Chemical structures of the high- $T_g$  component *m*-TPTS-d4 (left,  $^2\text{H}$ ) and the low- $T_g$  component TPP (right,  $^{31}\text{P}$ ) used for the binary mixtures. Figure from Publication 4.

For the neat components, dielectric spectra were measured showing the typical behaviour of neat glass formers discussed in section 1.2.2. The dielectric relaxation strength  $\Delta\varepsilon$  of TPP was found to be 240 times larger than that of *m*-TPTS at their respective  $T_g$ 's. Thus, one expects to measure only the dynamics of TPP in the DS experiments. Starting in the limit of high additive concentration  $w_{\text{TPP}} = 0.90$ , the dielectric spectra are shown in Figure 2.11 (a) as black symbols. One peak is found which is attributed to the dynamics of the low- $T_g$  component ( $\alpha_2$ -process). Compared to neat TPP (green diamonds), the spectra in the mixture are strongly broadened on the low frequency side changing with temperature and significantly reduced in their relaxation strength. The spectra are interpolated by the Havriliak-Negami (HN) function (red lines), which provides the two parameters  $a_{\text{HN}}$  and  $c_{\text{HN}}$ , describing the low- and high-frequency slope independently.<sup>207</sup> Due to the strong DC contribution in the dielectric loss spectra, possibly hiding additional (small) relaxation features, we also applied a method developed by Wübbenhorst et al.,<sup>208</sup> providing an Ohmic-conduction-free dielectric loss representation  $\partial\varepsilon' \equiv \frac{\pi}{2} \frac{\partial\varepsilon'(\omega)}{\partial \ln \omega}$  (blue crosses), calculated of the real part of the dielectric susceptibility  $\varepsilon'$ . Thus, we could detect for the first time an additional low-frequency peak at

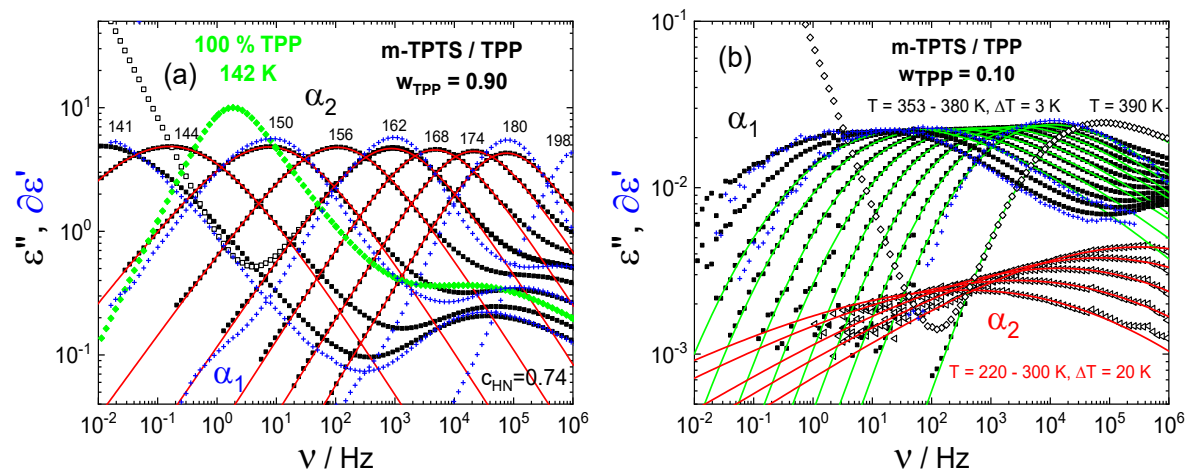


**Figure 2.11:** (a) Dielectric spectra  $\varepsilon''$  of the mixture  $w_{TPP} = 0.90$  (black squares, HN fits as red lines) and for comparison a spectrum of neat TPP (green diamonds). DC conductivity contribution is subtracted. For selected temperatures, derivative data  $\partial\varepsilon'$  (blue crosses) are shown. An additional relaxation contribution is recognized at lowest intensities ( $\alpha_1$ ), which cannot be resolved in  $\varepsilon''$ . (b)  $\varepsilon''$  of the mixture  $w_{TPP} = 0.10$  with two relaxations  $\alpha_1$  (squares) and  $\alpha_2$  (open triangles). DC conductivity contribution is subtracted; original data is shown for  $T = 390$  K (open diamonds). Temperatures (K) are indicated. Green lines are GCD fits, red lines are HN fits. For selected temperatures, the derivative data  $\partial\varepsilon'$  is shown (blue crosses). Figures from Publication 4.

the highest concentrations, presumably reflecting the dynamics of the high- $T_g$  component ( $\alpha_1$ -process). In the limit of low additive concentration ( $w_{TPP} = 0.10$ ) as depicted in Figure 2.11 (b), two strongly separated relaxations  $\alpha_1$  (squares) and  $\alpha_2$  (open triangles) are found. The dominating peak is hereby the  $\alpha_1$ -relaxation (despite the very low polarity of *m*-TPTS), which is significantly broadened especially on the high frequency side. Even the GCD function (green line) is no more sufficient at lowest temperatures to account for the full peak shape. Regarding the  $\alpha_2$ -relaxation, it is extremely broad as well and low in amplitude. At even lower additive concentrations, the  $\alpha_2$  spectra become such broad, that they almost disappear in the noise of the instrument (cf. Figure 18 in Publication 4).

For intermediate concentrations, the dielectric spectra of  $w_{TPP} = 0.40$  are exemplarily shown in Figure 2.12 (a) with two main relaxations present in the given frequency window. The ratio of the amplitudes  $\alpha_1/\alpha_2$  strongly depends on the temperature, increasing with decreasing temperature. Quantitatively, the  $\alpha_1$ -relaxation is described by a GCD function and regarding the  $\alpha_2$ -relaxation, accounting for its low-frequency broadening, a truncated HN was introduced. Therefore, the analytical HN susceptibility function  $\chi''_{HN}(\omega)$  was numerically Fourier transformed<sup>209</sup> ( $\phi_{HN}(t)$ ) and derivated to obtain the corresponding pulse response function  $\varphi_{HN} = -d\phi_{HN}(t)/dt$ . Then, an exponential cut-off ( $\tau_C$ ) was multiplied to  $\varphi_{HN}$ , whereas  $\tau_C$  was set to the longest time constant in our system, the average time constant of the  $\alpha_1$ -relaxation ( $\tau_C = \langle\tau_{\alpha_1}\rangle$ ).

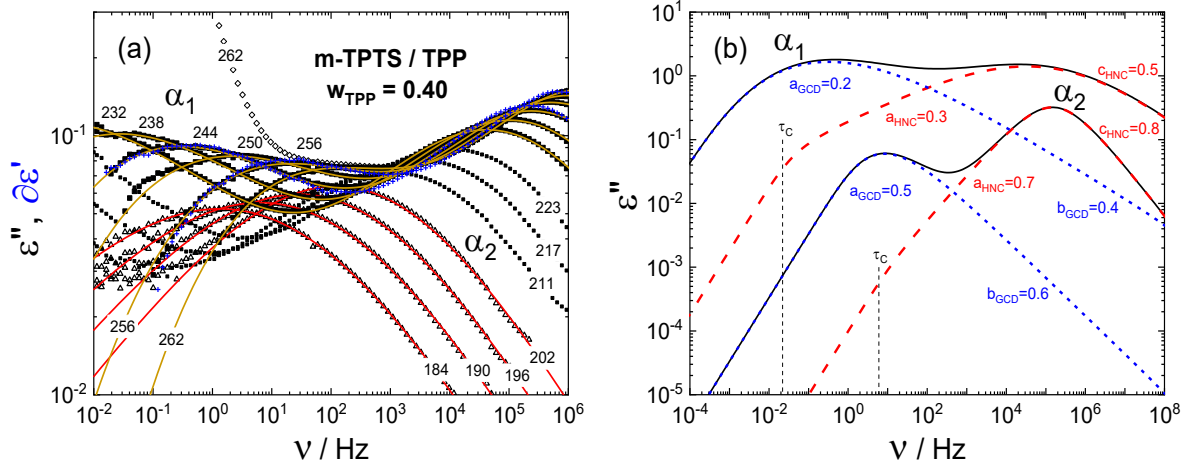


**Figure 2.12:** (a) Dielectric spectra  $\varepsilon''$  of  $w_{TPP} = 0.40$  (squares). DC conductivity contribution is subtracted. Original data is shown for one temperature (open diamonds). Temperatures (K) are given. Yellow lines denote composite fits, red lines are HN fits to  $\alpha_2$  (open triangles). For selected temperatures, the derivative data  $\partial\varepsilon'$  is shown (blue crosses). (b) Calculated dielectric loss spectra for two sets of parameters ( $\Delta\varepsilon_{GCD} = \Delta\varepsilon_{HNC}$  and  $\Delta\varepsilon_{GCD} = 0.5 \cdot \Delta\varepsilon_{HNC}$ ,  $\tau_{GCD} = 0.01s$ ,  $\tau_{HNC} = 1 \cdot 10^{-6}s$ ). Blue dashed lines are GCD functions, red dashed lines are HNC functions with cut-off  $\tau_c = \langle\tau_{GCD}\rangle$ , and the black lines are the corresponding composite functions. Figures from Publication 4.

$$\varphi_{HNC}(t) = \varphi_{HN}(t) \cdot \exp\left(-\frac{t}{\tau_c}\right) \quad (5)$$

$\varphi_{HNC}(t)$  leads in the susceptibility representation to the HN relaxation function with cut-off (HNC), showing a low-frequency power law with exponent  $a_{HNC}$  and a  $\omega^1$  behaviour at lowest frequencies, which is required for the slowest relaxation process in a liquid. A superposition of a GCD and a HNC function is used whenever both relaxations  $\alpha_1$  and  $\alpha_2$  are observed in the dielectric spectra:

$$\varepsilon''(\omega) = \Delta\varepsilon_{GCD} \cdot \chi''_{GCD}(\omega) + \Delta\varepsilon_{HNC} \cdot \chi''_{HNC}(\omega) = \varepsilon''_{\alpha_1}(\omega) + \varepsilon''_{\alpha_2}(\omega) \quad (6)$$

which is called ‘‘composite fit’’. This approach is sketched in Figure 2.12 (b).

Starting with the relaxation strength corrected for the Curie law  $\Delta\varepsilon(w_{TPP}) \cdot T$  in Figure 2.13 (a), the total relaxation strength  $\Delta\varepsilon$  is purely determined by that of TPP ( $\Delta\varepsilon_{\alpha_2}$ , open circles) for highest concentrations with a slight deviation from the Curie law. For lower concentrations  $w_{TPP} \leq 0.5$ , the Curie law applies for  $\Delta\varepsilon$  (squares) composed of the two contributions  $\Delta\varepsilon_{\alpha_1}$  (pluses) and  $\Delta\varepsilon_{\alpha_2}$  (open circles) with distinct temperature dependences. Whereas  $\Delta\varepsilon_{\alpha_2}$  decreases with supercooling,  $\Delta\varepsilon_{\alpha_1}$  increases in a similar amount. Already for  $w_{TPP} \leq 0.4$ ,  $\Delta\varepsilon_{\alpha_1}$  is comparable or even larger than  $\Delta\varepsilon_{\alpha_2}$ . Averaging over the measured temperature range  $\langle\Delta\varepsilon(w_{TPP}, T) \cdot T\rangle/\langle T\rangle$ , a strongly non-linear behaviour was found in contrast to the linear concentration dependence expected in the case of ideal mixing (cf. Figure 11 (b) in Publication 4). The most probable time constants  $\tau(w_{TPP}, T)$  are depicted in Figure 2.13 (b) for the  $\alpha_1$ - (circles) and  $\alpha_2$ -process

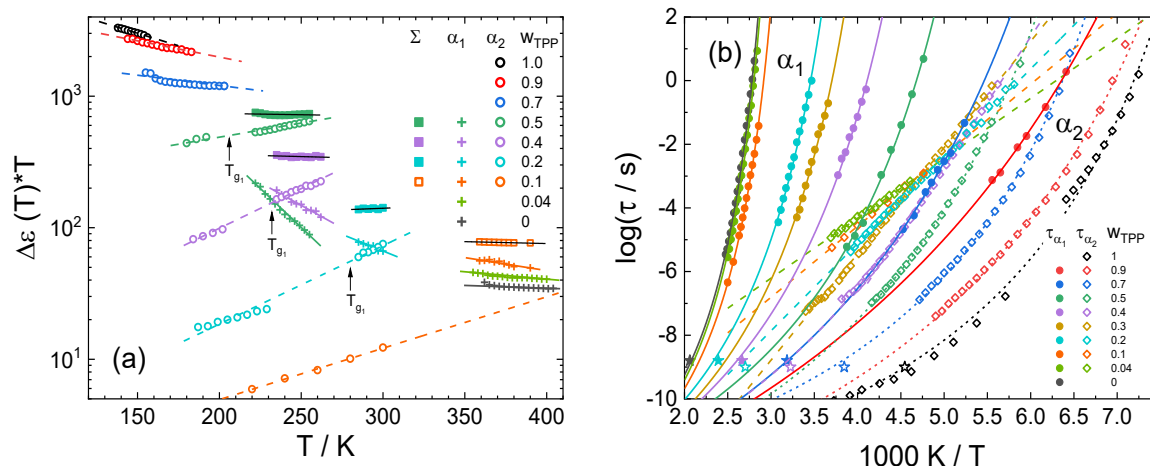


**Figure 2.13:** (a) Curie corrected relaxation strength  $\Delta\varepsilon(w_{TPP}) \cdot T$  for  $\alpha_1$  (plusses),  $\alpha_2$  (circles) and the sum of both (squares) on a logarithmic scale. The gap in between  $\alpha_2$  data of one concentration is due to the used composite fit at high  $T$  and HN fit at low  $T$ . In between, no appropriate fit was possible. Lines are guides for the eye. For  $w_{TPP} = 0.10$ ,  $\Delta\varepsilon_{\alpha_2}$  was linearly approximated (dashed orange line) and used to calculate the total  $\Delta\varepsilon$  (orange open squares). (b) Time constants  $\tau$  from peak picking for the  $\alpha_1$ - (circles, stars) and the  $\alpha_2$ -process (open diamonds, open stars). Concentration is colour coded. Stars are from NMR relaxation. VFT (lines,  $\alpha_1$ ) and VFT/Arrhenius temperature dependence (dashed lines,  $\alpha_2$ ) is shown. Figures from Publication 4.

(open diamonds). The  $\alpha_1$ -process shows a VFT like temperature behaviour (lines) for the whole concentration range. For the  $\alpha_2$ -process (attributed to the low- $T_g$  component), one recognises a crossover from a non-Arrhenius temperature dependence (VFT) at high  $w_{TPP}$  to an Arrhenius at low  $w_{TPP}$ .

Anticipating our NMR results, that the reorientational dynamics of the TPP molecules in the slow high- $T_g$  matrix is an isotropic, liquid-like reorientation, we define a second isodynamic point  $T_{g2} = T_{g2}(w_{TPP})$ . The latter exhibits a maximum at intermediate  $w_{TPP}$ , whereas  $T_{g1}$  (high- $T_g$  component) displays the expected plasticizer effect (Figure 2.14 (a)). Both glass transition temperatures are recognized in the DSC measurements, too (Figure 2.14 (b)). The maximum of  $T_{g2}$  indicates extreme separation of the component dynamics at low  $w_{TPP}$ , characterizing the virtually concentration-independent slow-down of the TPP molecules in an essentially arrested matrix of  $m$ -TPTS.

The component selective NMR experiments were performed on the deuterated  $m$ -TPTS- $d_4$ , having a slightly higher  $T_g$  (356 K) than  $m$ -TPTS, mixed with TPP. For the  $^2\text{H}$  spectra of neat  $m$ -TPTS- $d_4$ , a typical transition for supercooled liquids<sup>10</sup> is observed in Figure 2.15 (a), providing a solid-state (Pake) spectrum at lowest temperatures, which collapses within a small temperature range above  $T_g$  to yield a Lorentzian line quickly decreasing in width. In between, a gap is present, where no spectra can be taken because the FID is too short. In the mixtures, the plasticizer effect is clearly seen

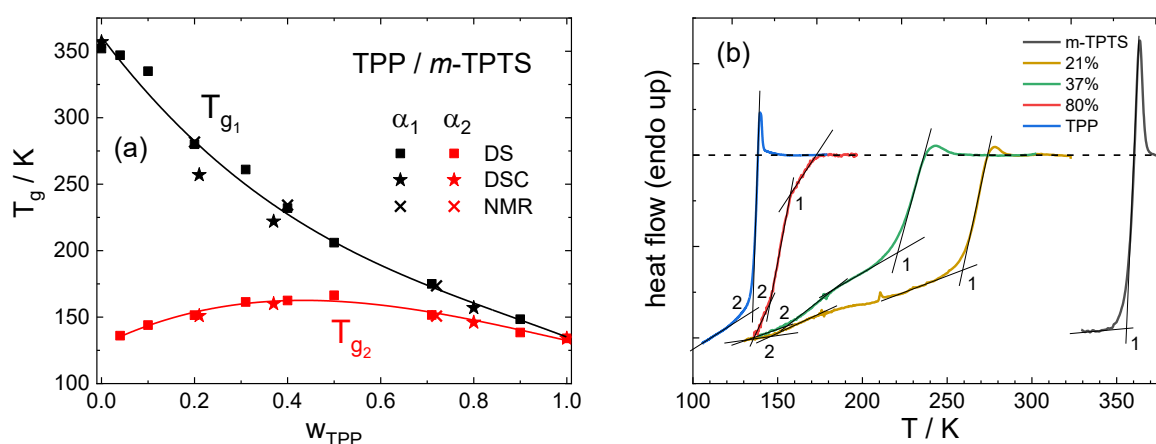


**Figure 2.14:** (a) Glass transition temperatures  $T_{g_{1,2}}(w_{TPP})$  from DS (squares), DSC (stars) and NMR measurements (crosses).  $T_{g_1}$  ( $\alpha_1$ -process,  $m$ -TPTS dynamics) is shown in black and  $T_{g_2}$  ( $\alpha_2$ -process, TPP dynamics) in red. Figure adapted from Publication 5. (b) DSC measurements (coloured lines) for the neat compounds  $m$ -TPTS (grey) and TPP (blue), as well as in the mixture with  $w_{TPP} = 0.21$  (yellow), 0.37 (green) and 0.80 (red). All DSC measurements are scaled to a common baseline (dashed line) and comparable total heights. Lines indicate the crossing points determining the  $T_g$ 's and the numbers denote the corresponding process. Figure from Publication 4.

by the onset of the transition shifting to much lower temperatures with increasing  $w_{TPP}$ , but no qualitative difference is found.

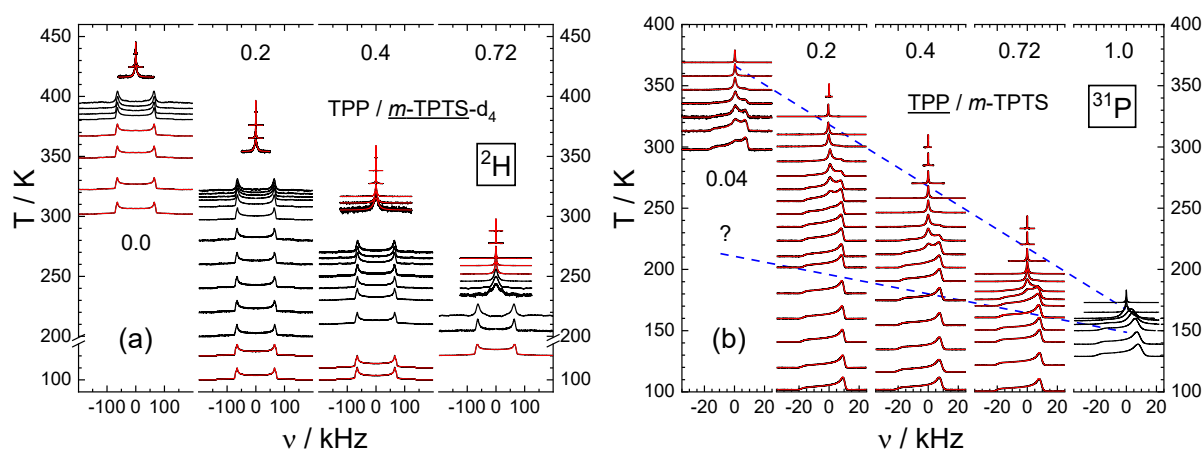


**Figure 2.15:** (a)  $^2\text{H}$  NMR spectra (black lines) of neat  $m$ -TPTS- $d_4$  ( $w_{TPP} = 0.0$ ) and the mixture TPP/ $m$ -TPTS- $d_4$  for the concentrations  $w_{TPP}$  (mass percentage) as indicated. Baseline of the spectrum gives the measurement temperature. Red lines: fits by a Lorentzian line at high temperatures and a Pake spectrum at low temperatures. (b)  $^{31}\text{P}$  NMR spectra (black lines) of neat TPP ( $w_{TPP} = 1.0$ ) and of the mixture TPP/ $m$ -TPTS- $d_4$  for additive concentrations  $w_{TPP}$  as indicated. The baseline of the spectra gives the measurement temperature. Red lines: fits by a Lorentzian line at high temperatures and a solid-state powder spectrum at low temperatures. Weighted superposition (two-phase spectra) at intermediate temperatures; temperature range marked by the blue dashed lines. Figures from Publication 5.

Reflecting the dynamics of the TPP molecules, the  $^{31}\text{P}$  NMR spectra reveal a completely different behaviour in Figure 2.15 (b). Whereas a smooth transition from an asymmetric powder spectrum to a Lorentzian line in a very small temperature range (150 K to 165 K) is observed for neat TPP, a broad intermediate temperature range is found in the mixtures showing two-phase spectra. The temperature range of the two-phase spectra is marked via the dashed blue lines, increasing continuously with decreasing  $w_{\text{TPP}}$ . Thus, strong dynamic heterogeneities cover the dynamics of the low- $T_g$  component in contrast to the high- $T_g$  component, for which such two-phase spectra are missing. The  $^{31}\text{P}$  two-phase spectra are analysed (red lines in Figure 2.15 (b)) by a weighted superposition of a Lorentzian line  $L(\omega)$  and a solid-state powder spectrum  $P_{\text{CSA}}(\omega)$ :

$$S(\omega, T) = W(T)L(\omega) + (1 - W(T))P_{\text{CSA}}(\omega) \quad (6)$$

providing the concentration dependent weighting factor  $W(w_{\text{TPP}}, T)$  (cf. Figure 2.17 (b)). Clearly, the lower the additive concentration the wider is the two-phase temperature regime (cf. also inset Figure 2.22 (b)).

Furthermore, stimulated echo experiments, directly measuring the correlation function  $C_2(t)$ , were conducted for TPP as well as  $m$ -TPPTS- $d_4$ . Starting with the  $^2\text{H}$  stimulated echoes of neat  $m$ -TPPTS- $d_4$ , a typical correlation function of Kohlrausch like type with  $\beta_K \approx 0.5$  was found. In the mixtures, the stretching increases continuously with increasing  $w_{\text{TPP}}$ , leading to  $\beta_K \approx 0.2$  at  $w_{\text{TPP}} = 0.72$ . The time constants and temperature/concentration evolution correspond well to the dielectric  $\alpha_1$ -relaxation.

The dynamics of the additive TPP probed by the  $^{31}\text{P}$  stimulated echo experiments show a more complex behaviour (Figure 2.16). Very broad correlation decays are found, whereas for the lower concentrations even a plateau is detected. In order to compare the NMR experiments to the DS spectra, the FT of a HN function ( $\phi_{\text{HN}}$ ) was used to analyse the echo decays. Whereas for  $w_{\text{TPP}} = 0.72$  (Figure 2.16 (a)), almost identical time constants and HN parameters are found compared to DS, a simple HN function

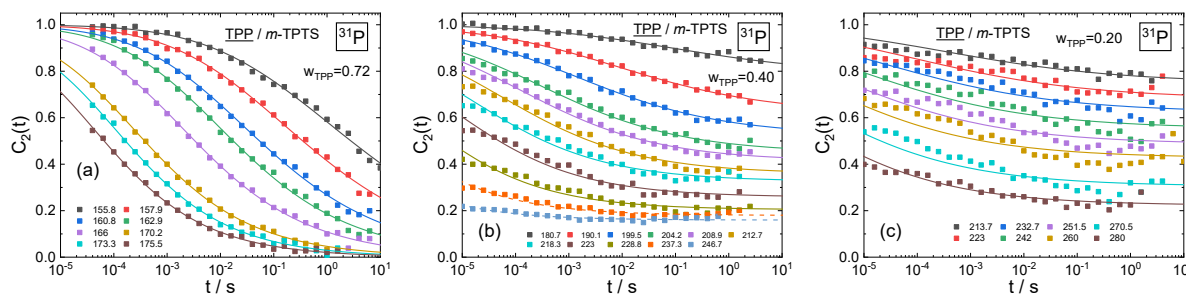


**Figure 2.16:**  $^{31}\text{P}$  NMR correlation function  $C_2(t)$  (squares) of the low- $T_g$  component in the mixtures  $w_{\text{TPP}} = 0.72$  (a),  $0.4$  (b) and  $0.2$  (c). The measured decays are  $T_1$  and spin-diffusion corrected. Temperature in K is color-coded. Lines: (a) HN fits; (b), (c) HN fits with a residual plateau value ( $\phi_{\text{HN}} + f_{\alpha_1}$ ). Dashed lines in (b): Guide for the eye. Figures from Publication 5.

is no more sufficient for lower concentrations and the a residual plateau value has to be accounted for (Figure 2.16 (b), (c)). This plateau value can be interpreted as sub-ensemble of TPP molecules, not relaxing on the experimental time scale, probably until the  $\alpha_1$ -relaxation, provided that some kind of anisotropic motion can be excluded. Isotropic-like motion was found for a variety of highly asymmetric binary glasses via 2D NMR experiments and explained in the State of the Art (Figure 2.5). Therefore, we also assumed isotropic reorientation for the mixture TPP/*m*-TPTS and the correlation function of the additive was analysed as superposition of a HN decay and a plateau value ( $C_2 = \phi_{HN} + f_{\alpha_1}$ ). To overcome the ambiguity of a free fit of the extremely stretched decays, the HN parameters determined by DS for the corresponding concentration were used to extract information about the time constants and the plateau value  $f_{\alpha_1}(w_{TPP}, T)$ .

In Figure 2.17 (a),  $f_{\alpha_1}(w_{TPP}, T)$  (squares) is collated to the comparable information from DS, the relative relaxation strength of the  $\alpha_1$ -relaxation  $\Delta\varepsilon_{\alpha_1}/\Delta\varepsilon$  (open circles). One clearly recognizes, that  $\Delta\varepsilon_{\alpha_1}/\Delta\varepsilon(T)$  is significantly larger than  $f_{\alpha_1}(T)$  indicating that the dielectric relaxation strength  $\Delta\varepsilon_{\alpha_1}$  should not be interpreted as a measure of the molecular TPP population participating in the  $\alpha_1$ -process. With all this collected information from DS and NMR, we attempted for the first time a quantitative explanation of our NMR weighting factors  $W(w_{TPP}, T)$  in the sense of molecular populations. At first, the distribution of correlation times  $G(\ln \tau_{\alpha_2})$  considering only the dielectric

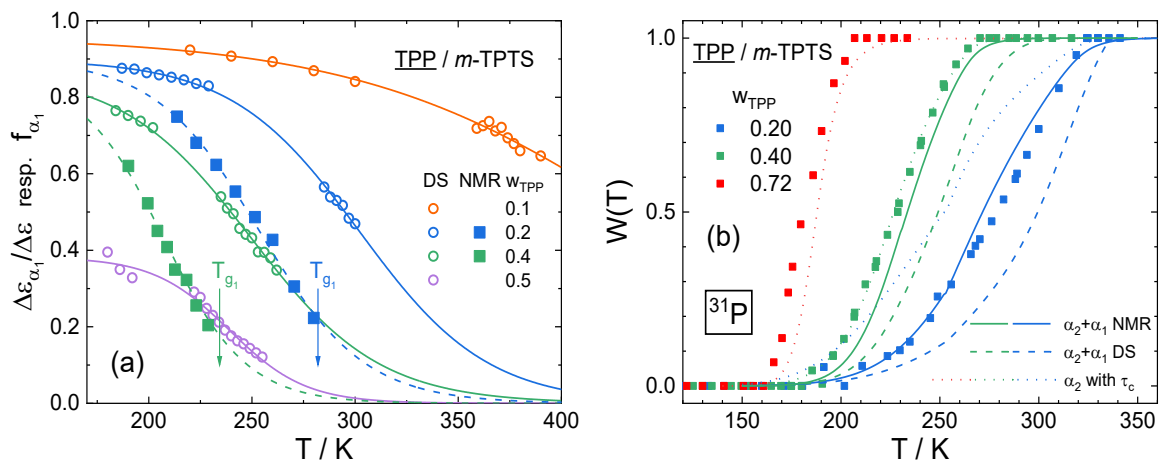


**Figure 2.17:** (a) Relative relaxation strength of the  $\alpha_1$ -process  $\Delta\varepsilon_{\alpha_1}/\Delta\varepsilon$  (open circles) for several concentrations as function of temperature from DS. Residual plateau value  $f_{\alpha_1}(T)$  (squares) from  $^{31}\text{P}$  NMR stimulated echos for  $w_{TPP} = 0.2$  and  $0.4$ . Lines: Logistic interpolations. (b) Weighting factor  $W(T)$  representing the Lorentzian part of the  $^{31}\text{P}$  spectra for the different concentrations (squares). Dotted lines:  $W(T)$  calculated according to  $G(\ln \tau_{\alpha_2})$  with a cut-off  $\tau_c$  from DS. Dashed lines: DS  $\alpha_2$ - and  $\alpha_1$ -relaxation with relative DS strength from (a). Solid lines: Reduced fraction of the  $\alpha_1$ -relaxation based on the NMR analysis ( $f_{\alpha_1}(T)$ ). Figures adapted from Publication 5.

$\alpha_2$ -relaxation, was calculated within the model of a truncated HN susceptibility from the dielectric time constants and HN parameters, to clarify whether the slow sub-ensemble of TPP molecules is also visible in the NMR spectra. The weighting factor is then given by  $W(T) = \int_0^{\tau_\delta} G(\ln \tau(T)) d \ln \tau$ , integrating up to the time constant given by the inverse coupling constant ( $\tau_\delta \approx 1/\delta_{CSA}$ ). The resulting dotted lines (Figure 2.17 (b)) show strong deviations for the lowest concentration, whereas good predictions within our model are possible for higher concentrations. Taking the dielectric  $\alpha_1$ -process into account, by using the DS fractions given in Figure 2.17 (a) (logistic interpolation of open circles), the dashed lines in Figure 2.17 (b) are obtained, which overrate the fraction of slow TPP molecules by far. The solution is given by using the interpolation of the slow NMR fraction  $f_{\alpha_1}(w_{TPP}, T)$  (dashed line in Figure 2.17 (a)) shown as solid lines in Figure 2.17 (b), providing quite good agreement especially for the lowest concentration.

The final dynamic picture is depicted in Figure 2.18, where the time constants for the different NMR concentrations of the  $\alpha_1$ - (full symbols) and the  $\alpha_2$ -relaxation (open symbols) are shown from DS (circles) and NMR. In addition to the stimulated echo experiments (triangles), time constants were determined from spin-spin-relaxation rates  $R_2$  (diamonds) and spin-lattice relaxation rates  $R_1$  (stars, oblique triangles) as well. The NMR experiments nicely confirm the two main-relaxations known from DS and show the fragile-to-strong transition found for  $\tau_{\alpha_2}(T)$  at intermediate  $w_{TPP}$ . Thus, the assignment of the dielectric relaxation processes to the corresponding components seems correct. Still, the unconventional maximum in  $T_{g_2}(w_{TPP})$  (Figure 2.14 (a)) remains to be explained.

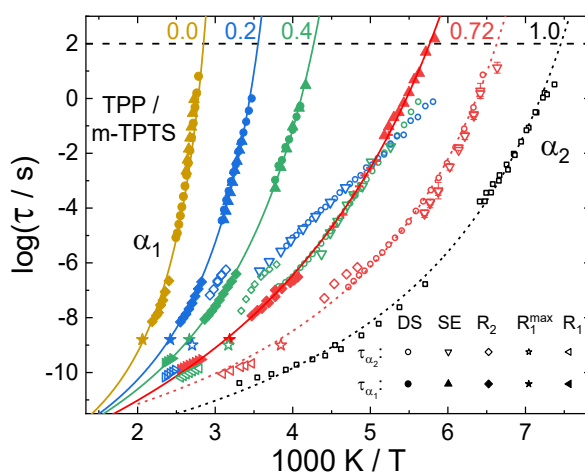


**Figure 2.18:** Time constants  $\tau_{\alpha_1}(w_{TPP}, T)$  (closed symbols) and  $\tau_{\alpha_2}(w_{TPP}, T)$  (open symbols) from NMR experiments (stimulated echo (SE, triangles), spin-spin relaxation rates ( $R_2$ , diamonds), spin-lattice relaxation rate maxima ( $R_1^{\max}$ , stars) and spin-lattice relaxation rates in the fast motion limit ( $R_1$ , oblique triangles)), DS (circles,  $w_{TPP} = 0.70$ ), and literature (TPP, open squares).<sup>185</sup> Colour coded concentration  $w_{TPP}$  is indicated. Figure from Publication 5.

## 2.2.3 Discussion & Conclusion

### *A generic scenario for highly asymmetric binary glass formers*

Summarizing the component dynamics revealed by our NMR and dielectric studies including those of previous works as well as data not fully analysed in the papers published so far, a generic scenario in highly asymmetric binary mixtures is outlined. The most prominent feature is the observation of a highly decoupled liquid-like additive dynamics in the virtually rigid matrix of the high- $T_g$  component, displaying pronounced dynamic heterogeneities not observed as such in neat systems.

In the  $ns$  correlation time regime, i.e. high temperatures, first insights about the concentration dependent evolution of the dynamics are obtained from spin-lattice relaxation rates  $R_1(T)$ . For the mixture TPP/ $m$ -TPTS- $d_4$ , the corresponding rates are shown for TPP (full squares) and  $m$ -TPTS- $d_4$  (open circles) in Figure 2.19. Clearly, the plasticizer effect for the high- $T_g$  component ( $^2\text{H}$ ), the anti-plasticizer effect for the low- $T_g$  component ( $^{31}\text{P}$ ), as well as the dynamic decoupling is observed. Additionally, the partly hidden secondary relaxation of neat TPP is developing an own relaxation peak due to the larger separation of main and secondary relaxations, which is also found in the other mixtures.<sup>124,203,207,211</sup> The secondary relaxation changes only minor or not at all (e.g. Figure 2.19 (b) and see also Figure 14 in Publication 4), which makes these mixtures predestined to study the secondary relaxation as the main relaxation does not interfere.<sup>212</sup>

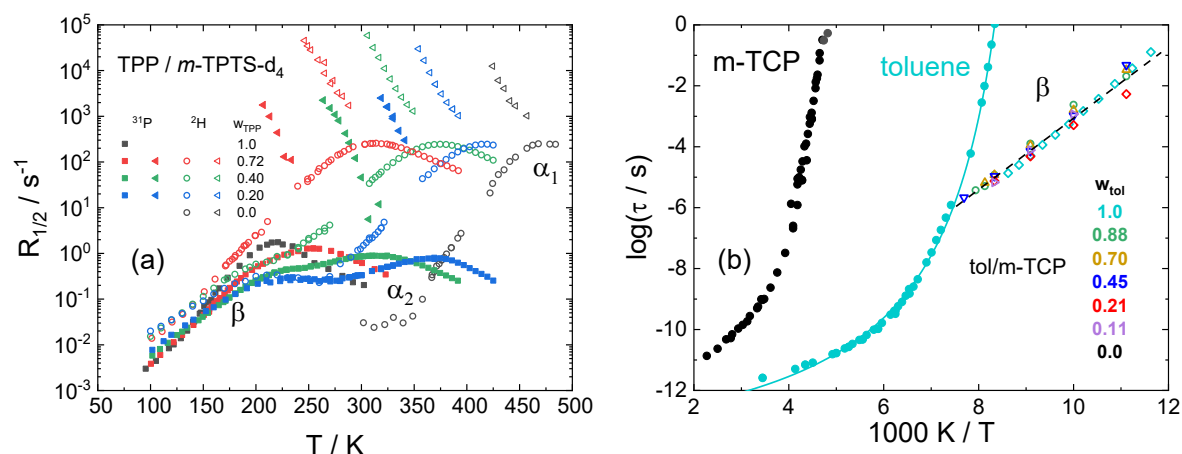


**Figure 2.19:** (a) Spin-lattice relaxation rates  $R_1(w_{\text{TPP}})$  ( $^2\text{H}$ : open circles;  $^{31}\text{P}$ : filled squares) and spin-spin relaxation rates  $R_2(w_{\text{TPP}})$  ( $^2\text{H}$ : open triangles;  $^{31}\text{P}$ : filled triangles) in the mixture TPP/ $m$ -TPTS- $d_4$ . Concentration  $w_{\text{TPP}}$  is colour-coded. Figure from Publication 5, Supporting Information. (b) Time constants of neat  $m$ -TCP and neat toluene from literature.<sup>185,210</sup> In addition, the relaxation times of the  $\beta$ -process of the mixture toluene/ $m$ -TCP as determined by DS (open symbols). Figure from Publication 3.

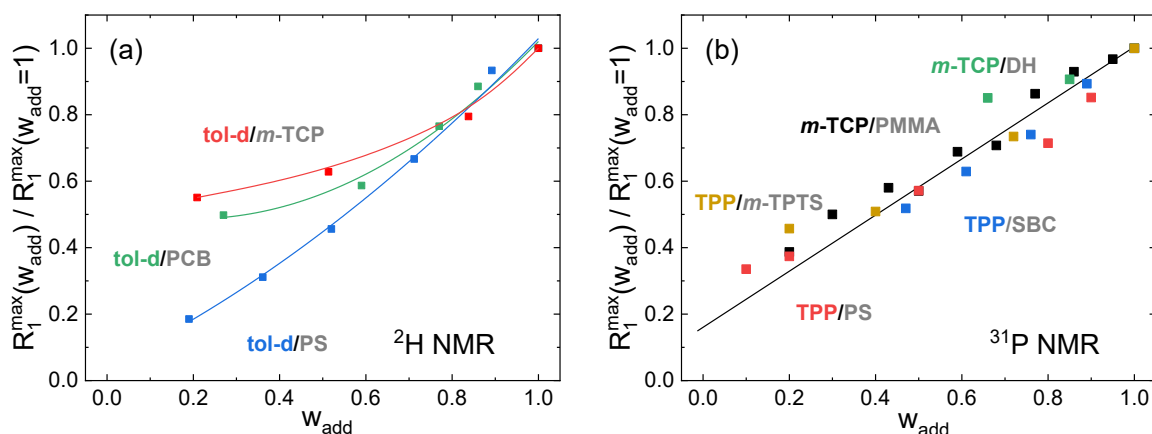


**Figure 2.20:** (a) Normalized relaxation rate maxima  $R_1^{\max}(w_{\text{add}})/R_1^{\max}(w_{\text{add}}=1)$  in the case of the low- $T_g$  (additive) component toluene for various high- $T_g$  components, as revealed by  $^2\text{H}$  NMR.<sup>212,213</sup> (b) Corresponding normalized relaxation rate maxima as obtained by  $^{31}\text{P}$  NMR of the phosphorus containing components.<sup>114,115,177</sup> Colour gives the measured component of the mixtures. The  $T_g$ -contrast is 89 K for the system toluene (tol)/*m*-TCP, 129 K for tol/PCB and at least 170 K up to 250 K for all other analyzed systems. Figures adapted from Publication 3.

An important feature is given by the analysis of the relaxation maxima (model independent). Plotting the relaxation rate at the relaxation maximum normalized to its value of the neat component against the mass fraction  $w_2$  of the low- $T_g$  component, a common scenario is revealed for a variety of different systems in Figure 2.20: The evolution of the relaxation spectrum with concentration is apparently controlled only by the  $T_g$ -contrast. For large contrasts ( $\Delta T_g \gtrsim 170$  K), a universal pattern is observed regardless of which component is considered and which NMR probe is employed ( $^2\text{H}$  or  $^{31}\text{P}$  NMR). The lower the additive concentration, the larger is the width of the underlying relaxation process of the additive. Deviations from this behaviour set in earlier the lower the  $T_g$ -contrast. Thus, this representation gives a measure of the underlying distribution of correlation times, provided the relaxation rates are measured at the same Larmor frequency and the coupling constant does not change in the mixture.

Under these conditions, the temperature of the relaxation maxima gives an isodynamic point  $T_g^{\text{NMR}}(w_{\text{add}})$ , which reflects the dynamics of the two components in the *ns* regime. The reciprocal temperature  $1000/T_g^{\text{NMR}}(w_{\text{TPP}})$  is given as function of the additive concentration in Figure 2.21 for moderate and high  $T_g$ -contrast systems. The systems show approximately a Gordon-Taylor-like<sup>214</sup> linear relationship for each component separately. This elucidates that the dynamics of both components are separated over the entire concentration range already in the low viscous regime. No indications of the behaviour leading to a maximum in  $T_{g_2}(w_2)$  can be discovered in the *ns* regime in these data.

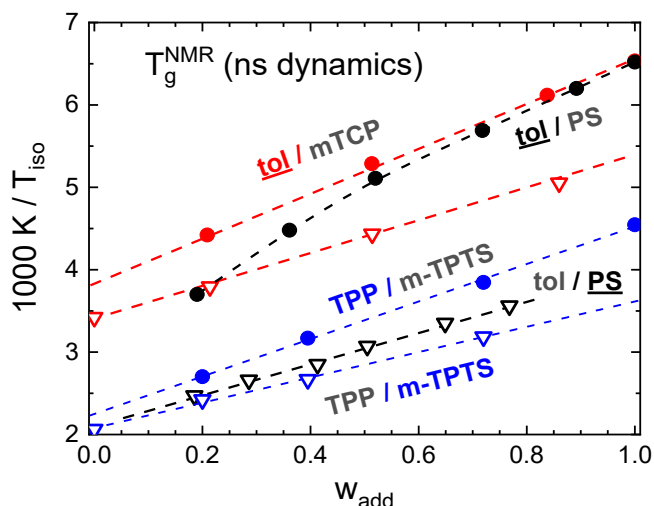


**Figure 2.21:** Isodynamic points  $T_g^{\text{NMR}}$  ( $^2\text{H}$  ( $\tau = 0.61/\omega_L$ ) and  $^{31}\text{P}$  NMR ( $\tau = 1/\omega_L$ ), ns dynamics) in terms of reciprocal temperatures  $1000/T_g^{\text{NMR}}$  plotted versus additive mass fraction  $w_{\text{add}}$  of the systems toluene(tol)/*m*-TCP, toluene/polystyrene (PS), and TPP/*m*-TPTS respectively. System is given by color and component by symbol. Lines are guides for the eye. Figure adapted from Publication 3.

The broadening of  $G(\ln \tau_{\alpha_2})$  manifests in the strongly temperature dependent dielectric  $\alpha_2$ -spectra as pronounced low-frequency broadening. Thus, FTS is violated. The corresponding NMR spectra are characterized by the appearance of two-phase spectra extending over a very large temperature range, reflecting strong dynamic heterogeneities, i.e., slow and fast liquid-like molecules are present. The temperature of the weighting factors  $W(T) = 0.5$  thereby shifts to lower temperatures with increasing additive concentration, whereas the width of the two-phase spectra regime  $\Delta T_W$  increases with decreasing additive concentration, as shown for several mixtures in Figure 2.22.<sup>115,171,182</sup> These motional heterogeneities are actually dynamical in the sense that slow and fast molecules mutually exchange their time constants proven by 2D exchange NMR in several systems.<sup>115,171,183,184</sup> Thus, one expects, that the additive dynamics involve rotation as well as translation.<sup>183</sup>

The dielectric relaxation attributed to the  $\alpha_2$ -relaxation becomes extremely wide at lowest concentrations, whereas quasi-logarithmic decays or, at least, peculiarly stretched decays of the corresponding time correlation function are probed via the stimulated echo technique.<sup>114,115,171,184</sup> Moreover, it yields a plateau which indicates that a fraction of TPP molecules decays at much longer times, a feature not so clearly recognizable in our previous experiments.<sup>114,115,171</sup> In the case of TPP/*m*-TPTS- $d_4$ , the slow fraction of molecules could even be quantitatively probed in the evolution of  $W(T)$ , suggesting, that these slow additive molecules are associated with the matrix dynamics ( $\alpha_1$ ) whereas the fraction depends strongly on the temperature.

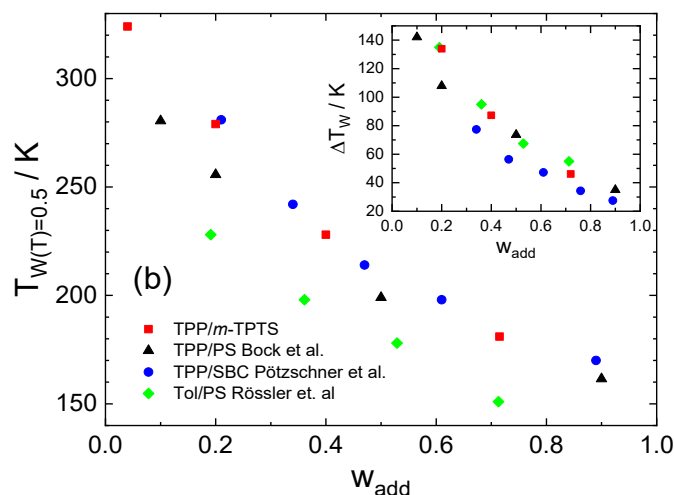


**Figure 2.22:** Temperature of  $W(T) = 0.5$  as function of the additive concentration  $w_{add}$  for the systems TPP/*m*-TPTS- $d_4$  (red symbols,  $\Delta T_g = 222$  K), TPP/polystyrene (grey triangles,  $\Delta T_g = 200$  K),<sup>171</sup> TPP/SBC (grey circles,  $\Delta T_g = 222$  K),<sup>115</sup> and toluene/polystyrene ( $\Delta T_g = 256$  K)<sup>182</sup>. Note: Components have slightly different  $T_g$ 's. Inset: Width of the two-phase temperature region  $\Delta T_W$  for the different systems and concentrations. Figure from Publication 5.

In contrast to the dynamics of the additive, the high- $T_g$  component in highly asymmetric mixtures displays no two-phase spectra and the corresponding NMR stimulated echo decays exhibit a progressively stronger stretching compared to that of the neat system, yet, it remains of Kohlrausch-type. Thus, the broadening of the dielectric  $\alpha_1$ -spectra should not be interpreted as a consequence of a particular distribution of isotropic reorientations but rather a feature similar to the excess wing phenomenon reported for pure glass formers.<sup>15,30</sup>

For the overall temperature dependence, a VFT-like behaviour is found for the  $\alpha_1$ -relaxation for all additive concentrations  $w_{add}$ , whereas a crossover from a VFT-like temperature dependence at high  $w_{add}$  to an Arrhenius-like temperature dependence for low  $w_{add}$  is found for a variety of different systems.<sup>114,115,171</sup> The crossover of  $\tau_{\alpha_2}(T)$  seems to take place around  $T_{g_1}$ . Thus, the well-known plasticizer effect for the corresponding  $T_{g_1}(w_{add})$  is found (Figure 2.23) as well as a maximum in  $T_{g_2}(w_{add})$  because the apparent activation energy of  $\tau_{\alpha_2}(T)$  decreases with decreasing  $w_{add}$ .

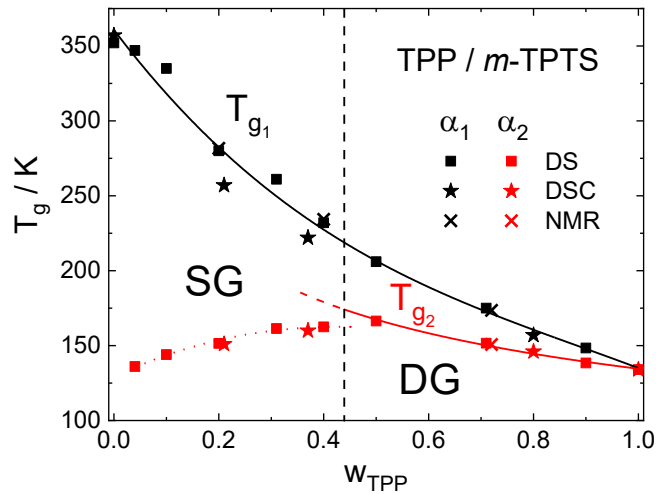


**Figure 2.23:** Glass transition temperatures  $T_{g_{1,2}}(w_{TPP})$  from DS (squares), DSC (stars) and NMR measurements (crosses). Transition from fluid to single glass (SG) respectively double glass (DG) scenario suggested by recent MD simulations.<sup>164</sup> Figure from Publication 5.

Looking in detail to a recent MD simulation of highly asymmetric hard spheres (HS) by Lázaro-Lázaro et al. (2019),<sup>164</sup> a possible explanation is proposed. Quite severe differences of the self- (SISF) and collective-intermediate-scattering function are found for distinct paths in the state space analysed in terms of volume fraction. Two transition scenarios are observed: At high volume fractions of the small particles, a transition from the fluid to a “double glass” (DG) is observed, which is characterized by the simultaneous arrest of self and collective dynamics of the small and large particles (Figure 2.24 (a)). At low volume fractions, the fluid to “single glass” (SG) transition is found, where only the large particles show a dynamic arrest in the SISF and the small

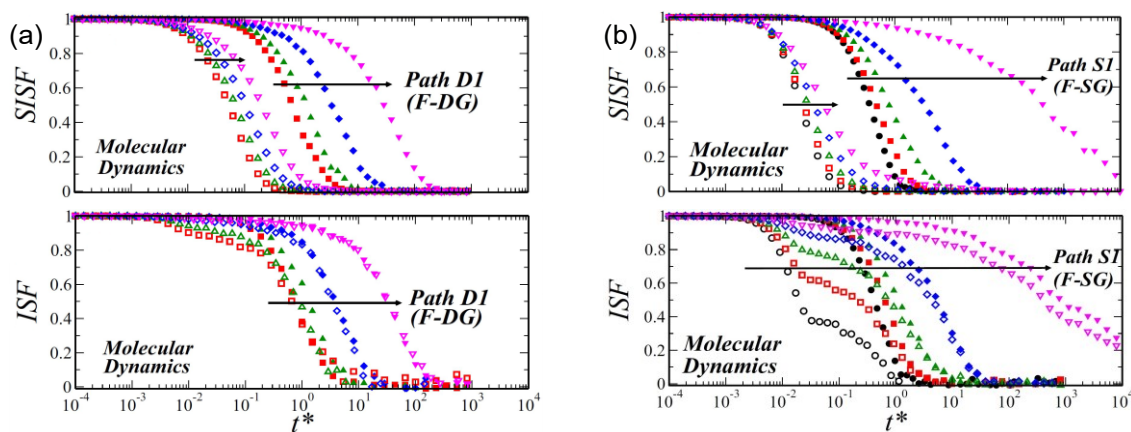


**Figure 2.24:** (a) Self- and collective-intermediate-scattering functions (SISF and ISF) of the large (closed symbols) and small particles (open symbols), calculated along the state points of the fluid to double glass path (F-DG), at fixed  $q^* = 7.18$ , as a function of the reduced time  $t^* \equiv t/t_b^0$ . (b) SISF and ISF along the state points of the fluid to single glass path (F-SG). Results obtained with event-driven MD simulations. Reprinted with permission from ref.<sup>164</sup> Copyright (2019) by the American Physical Society.

particles remain mobile (Figure 2.24 (b)). Thereby, a large difference between self-(incoherent) and collective (coherent) dynamics is noticed for the small particles. The coherent correlations are frozen along the arrest of the large particles whereas the self-correlators show a decay to zero. Thereby, the relaxation pattern of the SISF is similar to that seen in crowded environments like diffusion in heterogeneous porous media<sup>164</sup> and one may speak of confinement effects.<sup>196</sup>

Assuming, that the explained scenario for HS can be employed for our highly asymmetric mixtures, the experiments suggest the following to resolve the maximum in  $T_{g_2}(w_{TPP})$ . In the case of high  $w_{TPP}$ , a transition from the liquid state to a “double glass” is observed also in the reorientational dynamics, which is characterized by an almost simultaneous arrest of the small (low- $T_g$ ) and large (high- $T_g$  component) particle dynamics with two distinct  $T_g$ 's. For lower concentrations  $w_{TPP}$ , a “single glass” is induced upon supercooling providing only one real  $T_g$ . The experimentally observed very low  $T_{g_2}(w_{TPP})$  (experimentally defined as an isodynamical point) only signals that (part of) the additive molecules reflect a trend not to arrest. A certain fraction of small-size particles will - as shown via the stimulated echo decays as well as the dielectric distribution  $G(\ln \tau_{\alpha_2})$  with a pronounced long-time tail reaching more or less times on the order of  $\tau_{\alpha_1}$  - undergo a similar transition as the high- $T_g$  component, a feature not so clearly recognized in the simulation.<sup>164</sup> Of course, these temperatures are hard to simulate and taking orientational degrees of freedom into account may change the picture even more significantly.<sup>215-218</sup> The crossover from the DG to SG mechanism is given by the demarcation line at the previous maximum of  $T_{g_2}(w_{TPP})$ .

However, it is not clear what happens in the limit of very low concentrations, although DS and NMR results show no indications of change even at lowest concentrations ( $w_{TPP} = 0.04$ ). For example, many optical experiments are done by adding some dye molecules at very low concentration to probe the main dynamics of a glassy matrix.<sup>219,220</sup> We note, however, that two-phase spectra were also reported for deuterated 3.4% hexamethyl benzene and even for 0.5% benzene in oligo styrene.<sup>183</sup> Hence, such spectra may be just the finger print of molecules diffusing translationally in a random potential created by the amorphous matrix. Quantitative cross polarization may help to push NMR studies towards this limit of infinite dilution.<sup>221</sup>

The strong difference between coherent and incoherent dynamics, found in MD simulations as well as in theories (cf. State of the Art), could also explain the significant difference in terms of relaxation strength by DS and molecular population provided by NMR. A simple picture is proposed by a very recently submitted work of Böhmer et al.<sup>222</sup>, investigating the rotational dynamics in a binary mixture with DS, DLS and atomistic MD simulations. A single additive molecule leaves the matrix sites on the

time scale  $\tau_{\alpha_2}$  but other molecules visit an identical site, thus keeping some correlations up to the time scale  $\tau_{\alpha_1}$  at which the high- $T_g$  matrix relaxes. Due to cross correlation effects being relevant in DS, the enhanced amplitude of the dielectric  $\alpha_1$ -relaxation may reflect contributions of coherent dynamics, whereas the NMR experiments probe purely incoherent dynamics. Possibly, the non-ideal behaviour of  $\Delta\epsilon(w_{TPP})$  may also find its explanation via the cross-correlation effects found in neat systems as discussed before. Clearly, DS reflects coherent contributions in the relaxation of pure and binary glass formers, which are so far mostly not considered in literature<sup>25,181</sup> but need to be considered in the future.

In case of a large contrast, as given in this thesis in a low-molecular system - over the whole concentration range - and usually in polymer-plasticizer systems, the above-described generic relaxation pattern is observed. The scenario depends therefore not on the specific molecular properties, but on the dynamic contrast  $\Delta T_g$ . Reducing  $\Delta T_g$  as done with the mixture tol/*m*-TCP and tol/quin, qualitatively similar results are reported. Naturally, the extent of decoupling of the component dynamics shrinks as well as the width of the temperature interval displaying two-phase spectra. Importantly, however, two-phase spectra are now also observed for the high- $T_g$  component. It appears that the extent of dynamic heterogeneities becomes more symmetric as expected when concentration fluctuations play a major role.<sup>223</sup>

Dynamically decoupled component dynamics, spectral broadening with failure of FTS, and a fragile-to-strong transition of the low- $T_g$  component around  $T_{g1}$  are also observed in asymmetric polymer blends.<sup>145</sup> Very recently it was even argued that “the dynamics of hydrated proteins are the same as the dynamics of highly asymmetric mixtures of glass-formers.”<sup>224</sup> Thus, the generic scenario sketched in this thesis is highly relevant for a large amount of different systems with pronounced dynamic contrast.



---

## IV Publications

### 1 List of Publications

- Pub. 1**      **Main and secondary relaxations of non-polymeric high- $T_g$  glass formers as revealed by dielectric spectroscopy**  
T. Körber, F. Krohn, C. Neuber, H.-W. Schmidt and E. A. Rössler  
*Physical Chemistry Chemical Physics* 22, 9086-9097 (2020).
- Pub. 2**      **Systematic differences in the relaxation stretching of polar molecular liquids probed by dielectric vs magnetic resonance and photon correlation spectroscopy**  
T. Körber, R. Stäglich, C. Gainaru, R. Böhmer and E. A. Rössler  
*The Journal of Chemical Physics* 153, 124510 (2020).
- Pub. 3**      **Dynamically asymmetric binary glass formers studied by dielectric and NMR spectroscopy**  
T. Körber, R. Minikejew, B. Pötzschner, D. Bock and E. A. Rössler  
*The European Physical Journal E* 42, 143 (2019).
- Pub. 4**      **Reorientational dynamics of highly asymmetric binary non-polymeric mixtures – a dielectric spectroscopy study**  
T. Körber, F. Krohn, C. Neuber, H.-W. Schmidt and E. A. Rössler  
*Physical Chemistry Chemical Physics* 23, 7200-7212 (2021).
- Pub. 5**      **Reorientational dynamics in highly asymmetric binary low-molecular mixtures – a quantitative comparison of dielectric and NMR spectroscopy results**  
T. Körber, B. Pötzschner, F. Krohn and E. A. Rössler  
*The Journal of Chemical Physics* 155, 024504 (2021).

**Individual contribution to collaborated publications**

- Pub. 1** I conducted the quantitative analysis of the DS measurements with special attention to the secondary relaxations. The manuscript was mainly written in cooperation with F. Krohn and E. Rößler.
- Pub. 2** I reanalysed the susceptibilities of more than 20 systems with a new model for different measurement methods and developed the method of analysing  $R_1$  as function of  $R_2$ . The compilation of the paper was done mainly in cooperation with E. Rößler and in fruitful discussions with the other authors.
- Pub. 3** I measured all NMR experiments in the mixtures during this thesis and executed the analysis of the NMR experiments as well as DS spectra. The manuscript was written in cooperation with E. Rößler.
- Pub. 4** I developed the truncated HN function for the  $a_2$ -relaxation and performed the quantitative analysis of all DSC and DS measurements. The manuscript was mainly composed in cooperation with E. Rößler.
- Pub. 5** I measured all NMR experiments except for pure TPP and the 0.04 mixture and analysed all of them. I matched the DS spectra from Publication 4 to the NMR results quantitatively. The manuscript was prepared in cooperation with E. Rößler.

---

## 2 Further Publications

- **The Nature of Secondary Relaxations: The Case of Poly(ethylene-altpropylene) Studied by Dielectric and Deuteron NMR Spectroscopy**  
T. Körber, F. Mohamed, M. Hofmann, A. Lichtinger, L. Willner and E. A. Rössler, *Macromolecules* 50, 1554–1568 (2017)
- **Dynamic Heterogeneities in Binary Glass-Forming Systems**  
D. Bock, T. Körber, F. Mohamed, B. Pötzschner, and E. A. Rössler  
In: *The Scaling of Relaxation Processes*, Springer, Cham, 173-201 (2018).
- **NMR at pressures up to 90 GPa**  
T. Meier, S. Khandarkhaeva, S. Petitgirard, T. Körber, A. Lauerer, E. Rössler and L. Dubrovinskya, *Journal of Magnetic Resonance* 292, 44–47 (2018).
- **Signature of reptation in the long-time behavior of the deuteron NMR Free Induction Decay in high molecular mass polymer melts**  
N.F. Fatkullin, T. Körber and E. A. Rössler, *Polymer* 142, 310-315 (2018).
- **On the theory of deuteron NMR free induction decay of reptating polymer chains: Effect of end segment dynamics**  
I. K. Ostrovskaya, N. F. Fatkullin, T. Körber, E. A. Rössler, A. Lozovoi, C. Mattea and S. Stapf, *The Journal of Chemical Physics*. 152, 184904 (2020).
- **Nuclear spin relaxation in viscous liquids: relaxation stretching of single-particle probes**  
M. Becher, T. Körber, A. Döß, G. Hinze, C. Gainaru, R. Böhmer, M. Vogel and E. A. Rössler, *The Journal of Physical Chemistry B*, 125, 13519-13532 (2021).



---

## Publication 1

**Main and secondary relaxations of  
non-polymeric high- $T_g$  glass formers as  
revealed by dielectric spectroscopy**

**T. Körber, F. Krohn, C. Neuber,  
H.-W. Schmidt and E. A. Rössler**

*Physical Chemistry Chemical Physics*

**22**, 9086-9097 (2020).

DOI: 10.1039/d0cp00930j

© Royal Society of Chemistry 2020



Cite this: DOI: 10.1039/d0cp00930j

# Main and secondary relaxations of non-polymeric high- $T_g$ glass formers as revealed by dielectric spectroscopy†

 Thomas Körber,<sup>‡a</sup> Felix Krohn,<sup>‡b</sup> Christian Neuber,<sup>id b</sup> Hans-Werner Schmidt<sup>id b</sup> and Ernst A. Rössler<sup>id \*a</sup>

A series of high- $T_g$  glass formers with  $T_g$  values varying between 347 and 390 K and molar masses in the range of 341 and 504 g mol<sup>-1</sup> are investigated by dielectric spectroscopy. They are compared to paradigmatic reference systems. Differently polar side groups are attached to a rigid non-polar core unit at different positions. Thereby, the dielectric relaxation strength varies over more than two decades. All the relaxation features typical of molecular glass formers are rediscovered, *i.e.* stretching of the main ( $\alpha$ -) relaxation, a more or less pronounced secondary ( $\beta$ -) process, and a fragility index quite similar to that of other molecular systems. The position of the polar nitrile side group influences the manifestation of the  $\beta$ -relaxation. The  $\alpha$ -relaxation stretching displays the trend to become less with higher relaxation strength  $\Delta\epsilon_\alpha$ , confirming recent reports. Typical for a generic  $\beta$ -process is the increase of its amplitude above  $T_g$ , which is found to follow a power-law behaviour as a function of the ratio  $\tau_\alpha/\tau_\beta$  with a universal exponent; yet, its relative amplitude to that of the  $\alpha$ -relaxation varies as does the temporal separation of both processes. The mean activation energy of the  $\beta$ -process as well as the width of the energy distribution  $g_\beta(E)$  increases more or less systematically with  $T_g$ . The latter is determined from the dielectric spectra subjected to a scaling procedure assuming a thermally activated process. Plotting  $g_\beta(E)$  as a function of the reduced energy scale  $E/T_g$ , the distributions are centred between 19–35 and their widths differ by a factor 2–3.

 Received 19th February 2020,  
Accepted 1st April 2020

DOI: 10.1039/d0cp00930j

[rsc.li/pccp](http://rsc.li/pccp)

## 1. Introduction

Investigating the dynamics in super-cooled molecular liquids, most studies have focused on systems with their glass transition temperature  $T_g$  below ambient temperatures.<sup>1–5</sup> Most prominently, covering a wide frequency range of up to 16 decades, dielectric spectroscopy (DS) has revealed the spectral evolution of the dynamic susceptibility regarding molecular reorientation. Likewise, depolarized light scattering (DLS)<sup>6–9</sup> and optical Kerr effect (OKE)<sup>10,11</sup> have provided information on molecular reorientation, however over a smaller time or frequency range. Clearly, a non-exponential (stretched) correlation function or equivalently a non-Lorentzian spectral density underlies the main ( $\alpha$ -) relaxation. Yet, there is no full agreement on the details or generic features of its spectral shape due to the interference of additional spectral

contributions on the high-frequency flank of the relaxation peak. Typically, secondary relaxations like the Johari  $\beta$ -relaxation<sup>1,12–15</sup> and the excess wing<sup>1,2,16–18</sup> show up close to  $T_g$ , or contributions of microscopic dynamics occur, the latter hampering an analysis of the susceptibility spectra collected in the GHz range by DLS or OKE.

Attempts were made to correlate some spectral parameters with other quantities characterizing “glassy dynamics”. For example, scrutinizing organic and inorganic glass formers, the stretching parameter was found to be correlated with the extent of fragility, the latter describing the steepness of the logarithm of the time constant  $\tau_\alpha$  at  $T_g$  on the reduced temperature scale  $T_g/T$ .<sup>19</sup> The more fragile the glass former, the larger the stretching. However, a study on molecular systems as well as ionic liquids did not find any correlations.<sup>20</sup> Recently, collecting data on “almost all” molecular glass formers studied so far, the authors established a trend between the dielectric relaxation strength  $\Delta\epsilon_\alpha$  and the stretching parameter  $\beta_K$  of the  $\alpha$ -process.<sup>21</sup> The higher  $\Delta\epsilon_\alpha$ , the weaker is the stretching, *i.e.* the higher is the Kohlrausch stretching parameter  $\beta_K$ . Actually, this connection was already reported before.<sup>22</sup> Regarding the more or less ubiquitous presence of a secondary ( $\beta$ -) process emerging close to  $T_g$  and persisting below  $T_g$ ,<sup>1,12–15</sup> the corresponding activation energy follows in many cases a

<sup>a</sup> Department of Inorganic Chemistry III and Northern Bavarian NMR Centre, University of Bayreuth, 95440 Bayreuth, Germany. E-mail: ernst.roessler@uni-bayreuth.de

<sup>b</sup> Department of Macromolecular Chemistry and Bavarian Polymer Institute, University of Bayreuth, 95440 Bayreuth, Germany

† Electronic supplementary information (ESI) available. See DOI: 10.1039/d0cp00930j

‡ Both authors contributed equally to this manuscript.

relation  $E_{\beta} = 24T_g$  (in K).<sup>1</sup> Although several exceptions were found,<sup>1,23,24</sup> it is still a non-trivial fact that quite different systems, like for instance polybutadiene and toluene, display this relation.

Polymeric glass formers with  $T_g$  values well above ambient temperatures are well studied and widely employed in innumerable technical applications. In recent years, interest in non-polymeric high- $T_g$  glass formers, *i.e.*, molecular glasses, has grown. Their applications range from the use in electronic devices,<sup>25–28</sup> resist materials for lithography,<sup>29–31</sup> to pharmaceutical formulations.<sup>32,33</sup> It is the combination of properties usually observed in polymers with the benefits of a low molecular nature that makes these glasses ideal materials for specific applications. Just as polymers, molecular glasses allow the formation of stable thin films. In contrast to polymers, however, they possess a well-defined molecular structure and purification can be done using standard chromatographic techniques. Solvent-free vapour processing has been demonstrated for a variety of molecular glasses.<sup>34,35</sup> Their application, however, is limited due to their high tendency to crystallize as compared to polymeric glass former.<sup>32,36</sup>

In the present contribution, we characterized a series of high- $T_g$  systems in terms of their dielectric response above as well as below  $T_g$ . The systems are based on a non-polar 9,9'-spirobi[9H]fluorene core unit and by introducing more or less polar substituents, a variety of high- $T_g$  materials were synthesized.<sup>37</sup> This “spiro core” consists of two planar fluorene units linked at the bridging C<sub>9</sub> atom with a 90° twist angle. This results in a rigid structure yielding molecular glasses with high  $T_g$  values. The systems considered here are part of a long-running research project specially synthesising non-polymeric high- $T_g$  glass formers.<sup>38,39</sup> Regarding the possibility to enhance  $T_g$  by introducing polar side groups, a first study was recently published.<sup>37</sup>

It is of fundamental interest to examine the influence of substituents on the dynamics of the molecules. The present substituents include *tert*-butyl groups, phenyl rings, and nitrile groups. Absence or presence and position of a nitrile group control

the relaxation strength  $\Delta\epsilon_{\alpha}$  as well as the manifestation of the  $\beta$ -relaxation. The  $T_g$  values lie in the range of 347–390 K. Usually, a  $T_g$  increase is caused by a higher molar mass. Averaging over  $T_g$  data of many systems, a relation  $T_g \propto M^{0.5}$  was found,<sup>40</sup> yet, the exponent can be increased by introducing highly polar side moieties.<sup>37</sup>

Here, we analyse in detail the spectral shapes of  $\alpha$ - and  $\beta$ -relaxation, corresponding time constants, and fragility. We check the above-mentioned correlation between stretching parameter and relaxation strength. As high  $T_g$  values are involved, we also investigate the relation for the (mean) activation energy of the  $\beta$ -process  $E_{\beta} = f(T_g)$ . Furthermore, a comparison with typical low- $T_g$  glass formers as reference systems is performed. As will be demonstrated, beyond the more or less systematic growth of the activation energy  $E_{\beta}$  and the width of energy distribution  $g_{\beta}(E)$  with  $T_g$ , we analyse the increase of the relaxation strength above  $T_g$  as a characteristic feature of the generic  $\beta$ -process. It turns out, that the relative amplitude of the  $\beta$ -relaxation increases along a power-law behaviour with the separation of the two processes becoming smaller. The increase appears to be universal though the amplitude is different.

## 2. Experimental

### 2.1. Systems studied

In Fig. 1, the chemical formulae of the investigated glass formers are shown together with their abbreviations used throughout the text. In general, “S” is used for the core unit spirobifluorene, “C” stands for an attached cyano group, “P” for an attached phenyl group, and “T” for an attached *tert*-butyl group. The combination “CP” is used for an attached cyanophenyl group. In detail, the abbreviations of the compounds are derived from their structure as follows: *o*-CPS, *m*-CPS, and *p*-CPS are all 2-(cyanophenyl)-spirobifluorenes, with the cyano group being in *ortho*, *meta*, or *para*-position, respectively. 2-CS

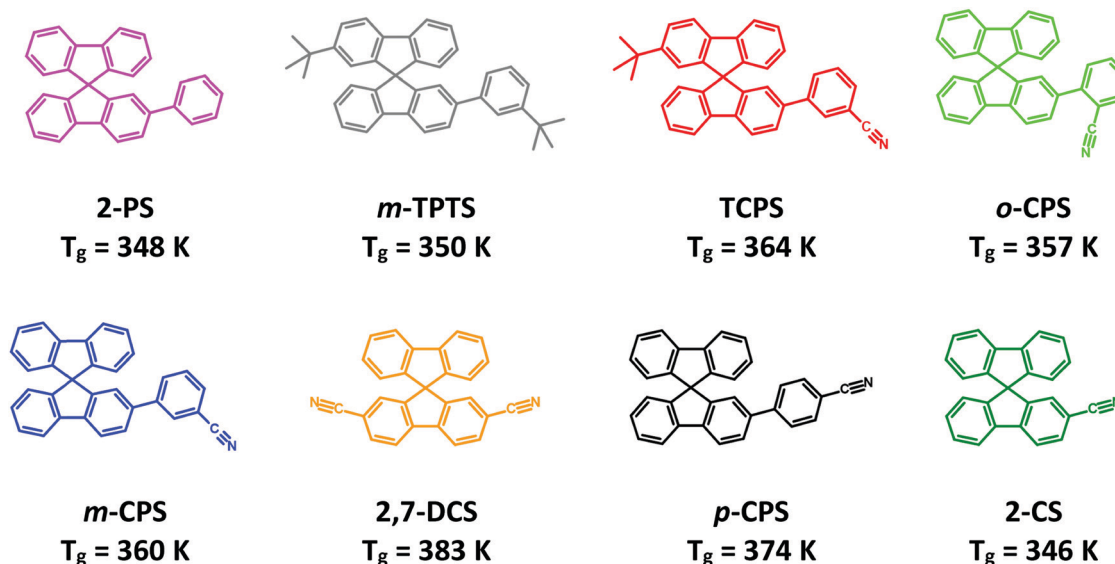


Fig. 1 Structure and glass transition temperature  $T_g$  of the investigated glass formers.

and 2-PS are 2-cyano- and 2-phenylspirobifluorene, respectively. 2,7-DCS stands for the disubstituted 2,7-dicyanospirobifluorene. The compound TCPS corresponds to 2-*tert*-butyl-2'-(3-cyanophenyl)-spirobifluorene, and *m*-TPTS to 2-(*meta-tert*-butylphenyl)-2'-*tert*-butyl-spirobifluorene. The synthesis and DSC characterization of *o*-CPS, *m*-CPS, *p*-CPS, 2-CS, 2,7-DCS, and 2-PS can be found elsewhere.<sup>37</sup> The synthesis route and characterization of the deuterated isomers of *o*-CPS and *m*-CPS as well as of TCPS and *m*-TPTS can be found in the ESI.† The obtained products were purified by sublimation prior to DS measurements. The here considered glass formers can be distinguished by the presence or the absence of strongly dipolar nitrile groups, its position (*o*, *m*, and *p*, appearing before) and as a consequence its dielectric relaxation strength  $\Delta\epsilon_\alpha$ . Table 1 lists molar masses  $M$ , glass transition temperatures  $T_g$ , determined by DSC measurements and by dielectric spectroscopy, and in addition parameters of the spectral analyses presented in the following. Furthermore, we include in Table 1 some properties of two other high  $T_g$  glass formers previously characterized (SBC<sup>39</sup> and DH 379<sup>38</sup>).

In addition, we compare selected systems with mainly low  $T_g$  values as paradigmatic reference systems which well display the characteristic spectral features of molecular glass formers: polybutadiene (PB,  $M = 35.3 \text{ kg mol}^{-1}$ ),<sup>41</sup> toluene (Tol; unpublished work,<sup>42</sup> cf. also ref. 1), tripropyl phosphate (TPP),<sup>43,44</sup> decahydroisoquinoline (DHIQ),<sup>24</sup> 3,3',4,4'-benzophenone tetracarboxylic dianhydride (2-PC, unpublished work<sup>42</sup>) and felodipine (FD, unpublished work<sup>45</sup>).

## 2.2. Differential scanning calorimetry

Differential scanning calorimetry was performed with a Mettler DSC3+ in pierced aluminium pans at  $10 \text{ K min}^{-1}$  under nitrogen flow. The glass transition temperature  $T_g$  was determined as the onset temperature of the step as calculated by Mettler STARe 15.00a software. Results are found in Table 1.

## 2.3. Dielectric spectroscopy

The dielectric permittivity is given by the equation<sup>46,47</sup>

$$\epsilon^*(\omega) = \epsilon'(\omega) - i\epsilon''(\omega) = \epsilon_\infty + \Delta\epsilon \int_0^\infty \frac{d\phi(t)}{dt} e^{-i\omega t} dt \quad (1)$$

where  $\epsilon^*(\omega)$  is the complex dielectric constant,  $\omega = 2\pi\nu$  the angular frequency,  $\epsilon_\infty$  the high frequency permittivity, and  $\phi(t)$  the step-response function. The quantity  $\Delta\epsilon$  is the relaxation strength being linked to the molecular dipole moment.

The main ( $\alpha$ -) dielectric response in glass forming systems is often described either by a Cole–Davidson or Kohlrausch function.<sup>46</sup> In this work, the Kohlrausch function

$$\phi_K(t) = \exp\left[-\left(\frac{t}{\tau_K}\right)^{\beta_K}\right] \quad (2)$$

was applied in terms of its Fourier transform (FT). Here,  $\tau_K$  is the time constant and  $\beta_K$  the stretching parameter. The average relaxation time  $\tau_\alpha$  is then defined by<sup>46</sup>

$$\tau_\alpha = \frac{\tau_K}{\beta_K} \Gamma\left(\frac{1}{\beta_K}\right) \quad (3)$$

while above  $T_g$  the time constants of the  $\alpha$ -relaxation are extracted *via* the FT of eqn (2), below  $T_g$  with the persisting  $\beta$ -process, we extract the time constants  $\tau_\beta$  either *via* peak-picking  $\tau_\beta = (2\pi\nu_{\max})^{-1}$  for clearly recognizable peaks or we apply a distribution of correlation times  $G_\beta(\ln\tau)$  previously introduced for describing the step-response function of a secondary relaxation process. Explicitly, we take<sup>48</sup>

$$G_\beta(\ln\tau) = N_\beta(a,b) \frac{1}{b\left(\frac{\tau}{\tau_m}\right)^a + \left(\frac{\tau}{\tau_m}\right)^{-ab}} \quad (4)$$

**Table 1** Comparison of molar mass  $M$ ,  $T_g$  as determined by dielectric spectroscopy (DS;  $\tau_\alpha(T_g) = 100 \text{ s}$ ) and DSC,<sup>37</sup> dielectric strength  $\Delta\epsilon_\alpha$  at  $1.02T_g$ , Kohlrausch stretching parameter  $\beta_K$ , and time constant  $\tau_0$  as well as activation energy  $E_\beta$  of  $\beta$ -process in units of  $T_g$  for the investigated systems and reference systems (polybutadiene (PB), toluene (Tol), tripropyl phosphate (TPP), decahydro isoquinoline (DHIQ), 3,3',4,4'-benzophenonetetracarboxylic dianhydride (2-PC) and felodipine (FD)); in addition, data for SBC and DH 379

System	$M [\text{g mol}^{-1}]$	$T_g^{\text{DS}} [\text{K}]$	$T_g^{\text{DSC}} [\text{K}]$	$\Delta\epsilon_\alpha$	$\beta_K$	$E_\beta [\text{K}]$	$\tau_0 [\text{s}]$
2-PS	392	348	355	0.034	0.51	—	—
<i>m</i> -TPTS	504	350	357	0.11	0.52	—	—
TCPS	473	364	365	2.21	0.56	19.4	$3.3 \times 10^{-15}$
<i>o</i> -CPS ( $-d_4$ ) <sup>a</sup>	417 (421)	357 (354)	363 (359)	3.24	0.59	26.2	$1.3 \times 10^{-15}$
<i>o</i> -/ <i>m</i> -CPS	417	359	363	1.9	0.62	24.6	$3.4 \times 10^{-15}$
<i>m</i> -CPS ( $-d_4$ )	417 (421)	360 (358)	368 (363)	2.7	0.64	23.1	$8 \times 10^{-16}$
2,7-DCS	366	383	390	0.75	0.65	13.7	$6.5 \times 10^{-15}$
<i>p</i> -CPS	417	374	380	7.65	0.70	14.6	$2.1 \times 10^{-15}$
2-CS	341	346	347	4.8	0.71	16.0	$6.6 \times 10^{-15}$
SBC <sup>39</sup>	809	356	—	0.72	0.50	15.6	$6.3 \times 10^{-16}$
DH 379 <sup>38,55</sup>	1205	374	382	0.66	0.45	14.7	$1.7 \times 10^{-15}$
Toluene <sup>42</sup>	92	117	—	0.25	—	26.1	$4.7 \times 10^{-17}$
TPP <sup>43,44</sup>	224	134	—	24.3	—	23.2	$1.6 \times 10^{-15}$
PB <sup>41</sup>	35.3k	174.5	—	0.082	—	24.1	$5.0 \times 10^{-16}$
DHIQ <sup>24</sup>	139	179.5	—	1.7	—	28.3	$2.1 \times 10^{-16}$
FD <sup>45</sup>	384	313	—	1.12	—	—	—
2-PC <sup>42</sup>	322	330	—	6.93	—	32.3	$2.0 \times 10^{-16}$

<sup>a</sup> ( $-d_4$ ): Compound marked with four deuterium atoms at the spiro core. Details: ESI.

with the normalization factor

$$N_{\beta}(a, b) = \frac{a(1+b)}{\pi} b^{\frac{b}{1+b}} \sin\left(\frac{\pi b}{1+b}\right) \quad (5)$$

and with  $\tau_m$  being the time constant at the maximum of  $G_{\beta}(\ln \tau)$  which is the same as *via* peak-picking. The parameter  $a$  controls the symmetric broadening of the distribution and susceptibility, respectively, while the “asymmetry parameter”  $b$  only affects its high-frequency. Assuming that a distribution of activation energies  $g_{\beta}(E)$  underlies  $G_{\beta}(\ln \tau)$ , and that the time constant at each site in the structurally disordered glass follows an Arrhenius-like temperature dependence,  $\tau_{\beta} = \tau_0 \exp\left(\frac{E}{RT}\right)$ , the temperature dependent distribution  $G_{\beta}(\ln \tau)$  eqn (4) can be mapped to a temperature independent distribution  $g_{\beta}(E)$ :<sup>48</sup>

$$g_{\beta}(E) = N_{\beta}(c, b) \frac{1}{b \exp(c(E - E_m)) + \exp(-cb(E - E_m))} \quad (6)$$

Independent of assuming a particular shape for  $G_{\beta}(\ln \tau)$ , one can directly apply a scaling procedure on the experimental dielectric spectra compiled at different temperatures which compensates for the broadening of  $G_{\beta}(\ln \tau)$  introduced by the underlying distribution  $g_{\beta}(E)$ :<sup>44,49–52</sup>

$$g_{\beta}(E) = g\left(T \ln\left(\frac{\nu_0}{\nu}\right)\right) = \frac{2}{\pi} \frac{\varepsilon''(\nu)}{T \Delta \varepsilon} \quad (7)$$

In words, by plotting the dielectric loss  $\varepsilon''(\nu)$  divided by the temperature  $T$  as a function of the natural logarithm of the inverse frequency multiplied by  $T$ , one gets an estimate of the activation energy distribution of the  $\beta$ -process. In the present analysis, we take the attempt frequency  $\nu_0 = 1/2\pi\tau_0$  from the intercept of plotting the mean time constant *vs.* the reciprocal temperature at infinite temperature (*cf.* Fig. 6A).

For describing the dielectric loss  $\varepsilon''(\nu)$  in the temperature regime, where both,  $\alpha$ - and  $\beta$ -relaxation occur together, we use a Williams–Watts approach.<sup>1,13,53</sup> Thereby, one assumes that the step-response function  $\phi$  is partly decaying by  $\phi_{\beta}$  and then completely decaying *via*  $\phi_{\alpha}$  in the following manner:

$$\phi = [(1 - S)\phi_{\beta} + S]\phi_{\alpha} \quad (8)$$

Hereby,  $(1 - S)$  gives the maximum amount of correlation decaying by  $\phi_{\beta}$  ( $S$  may be taken as order parameter). Here, the function  $\phi_{\alpha}$  is given by a Kohlrausch decay eqn (2), and  $\phi_{\beta}$  is described by the distribution of eqn (4).

The dielectric measurements were carried out with an Alpha-A Analyzer from Novocontrol in the frequency range  $\nu = 10^{-2}$ – $10^6$  Hz. Temperature was kept constant within  $\pm 0.2$  K by using a Quattro-H temperature controller from Novocontrol yielding an absolute accuracy better than  $\pm 0.2$  K. The temperature ranges from 100 up to 400 K. The sample cell was constructed by a design of Wagner and Richert and assures a constant sample volume.<sup>54</sup> The relaxation strength  $\Delta \varepsilon_x$  is determined by a single Kohlrausch fit of the main relaxation close to  $T_g$  without consideration of any further processes and is listed in Table 1.

## 3. Results

### 3.1. Relaxation spectra

Fig. 2A–D show the dielectric loss spectra of *o*-CPS, *m*-CPS, *p*-CPS, and TCPS, all of which possess a nitrile group that is attached *via* a phenyl ring at the spiro core, however, at different positions on the phenyl ring. In the case of TCPS, the core contains in addition a non-polar *tert*-butyl group. The system 2-CS (Fig. 2E) carries one nitrile group directly at the core unit as does 2,7-DCS with two nitrile groups attached (Appendix, Fig. 10A), implying that both molecules are completely rigid. In the case of *p*-CPS, and 2-PS (containing only a phenyl group attached to the core, Fig. 2F), 180 degree jumps of the phenyl ring are expected to occur, yet, this process is dielectrically inactive. Due to the introduced highly polar nitrile group, the dielectric loss of the first five systems (Fig. 2A–E) is rather large. In contrast, the systems 2-PS and *m*-TPTS (see Appendix Fig. 10C) without nitrile groups show a low loss. As 2,7-DCS possesses two nitrile groups symmetrically attached to the core, the partial dipole moments cancel partly, leading to the dielectric loss being somewhat smaller than that of the other nitrile group containing systems. We also measured a mixture of the isomers *o*-CPS and *m*-CPS (*o*/*m*-CPS, Appendix Fig. 10B). No broadening of the main relaxation is observed; thus it appears to behave like a pure glass former. This is of special interest for applications where a crystallization tendency has to be suppressed. In addition, we also measured the systems *o*-CPS-*d*<sub>4</sub> and *m*-CPS-*d*<sub>4</sub>, with one ring of the core deuterated; their spectra (not shown) are equal to those of their protonated counterpart (synthesis route provided in the ESI†).

All liquids exhibit a more or less pronounced DC conductivity which is shown only for one temperature (open squares) in each system and subtracted otherwise for all spectra shown in the Fig. 2A–E, and no more shown for simplicity in Fig. 2F. The systems *o*-CPS, *m*-CPS, and TCPS as well as the mixture *o*/*m*-CPS are type B glass formers with a pronounced and typical  $\beta$ -process.<sup>1</sup> Interestingly, the  $\beta$ -relaxation appears to be absent when the nitrile group is in the *para*-position (*p*-CPS). Instead, one finds a well separated secondary relaxation process at much lower temperatures. A similar behaviour is also found for 2-CS and 2,7-DCS, where the nitrile group is attached directly to the spiro core.

### 3.2. Main relaxation

In order to demonstrate the evolution of the spectra with temperature above  $T_g$  and to compare the different systems, Fig. 3A shows the relaxation spectra scaled by the maximum of the  $\alpha$ -relaxation peak and its frequency, respectively, for selected glass formers, 2-PS, TCPS, *o*-CPS, *m*-CPS, *p*-CPS, and 2-CS in a stacked plot. For comparison, some typical (“reference”) systems like polybutadiene (PB), toluene (Tol), tripropyl phosphate (TPP), decahydroisoquinoline (DHIQ), 3,3',4,4'-benzophenone tetracarboxylic dianhydride (2-PC) and felodipine (FD) are presented in Fig. 3B. The temperature is color-coded, starting in red for the highest temperature and ending in violet for the lowest temperature.

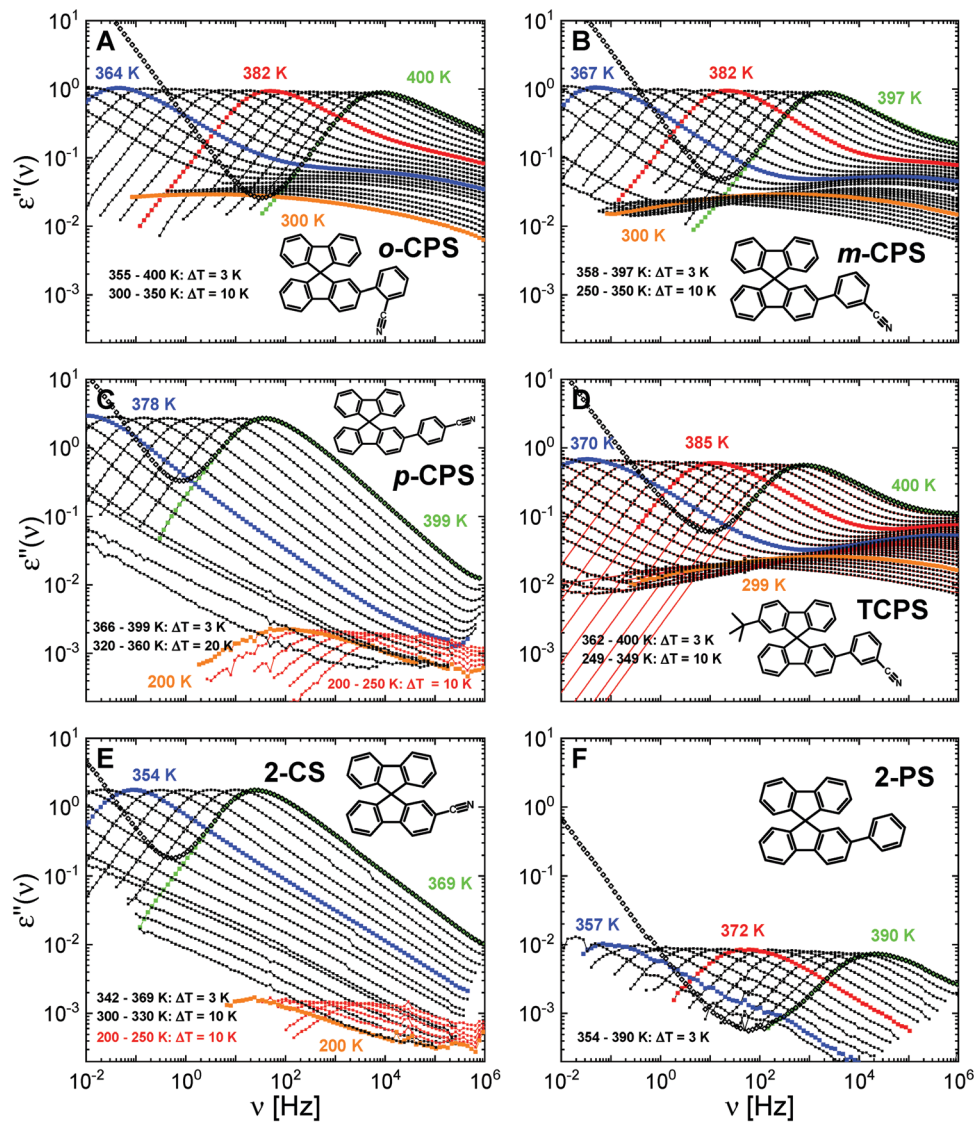


Fig. 2 Dielectric loss spectra of *o*-CPS (A), *m*-CPS (B), *p*-CPS (C), TCPS (D), 2-CS (E), and 2-PS (F). DC conductivity contribution is subtracted; original data is shown in open symbols for the highest temperature. Temperature range and increments are given; coloured curves highlight selected temperatures. Red lines in (D): Interpolations along a Williams–Watts approach with a Kohlrausch function for the  $\alpha$ -relaxation and a symmetric distribution of correlation times for the  $\beta$ -relaxation.

Regarding the  $\alpha$ -relaxation, frequency–temperature superposition (FTS) appears to apply around the peak. Whether it covers also the full high-frequency flank cannot be decided due to the occurrence of a  $\beta$ -relaxation which “spoils” the master curve at these frequencies. The  $\alpha$ -relaxation peaks are describable by a Kohlrausch function (FT of eqn (2)); the stretching parameter  $\beta_K$  values are found in the range 0.51 for 2-PS and 0.71 for 2-CS (*cf.* Table 1 and Fig. 3A). In general, it increases with increasing polarity of the system, a relation which will be discussed below.

Looking in more detail on the spectra exhibiting a  $\beta$ -relaxation in Fig. 3, *i.e.*, the corresponding curves of TCPS, *o*-CPS, and *m*-CPS, and those of the three reference systems PB, Tol, and TPP, a common relaxation pattern is observed: The higher the temperature, the more a broadening of the main relaxation peak is observed due to

the merging of  $\alpha$ - and  $\beta$ -relaxation. *Vice versa*, the lower the temperature the narrower is the  $\alpha$ -peak because the  $\beta$ -relaxation peak separates more and more. This similar spectral evolution is reflected by a colour-coding changing from red at high temperature to violet at low temperature. The systems are distinguished by a different relaxation strength of the  $\beta$ -relaxation with respect to that of the  $\alpha$ -relaxation and by a different spectral separation of the two processes. Whereas in the case of PB or toluene, the  $\beta$ -relaxation displays a rather high relative strength and thus appears to take over the  $\alpha$ -process when merging at high temperatures, for other systems such as TPP or *o*-CPS and *m*-CPS, the  $\beta$ -process exhibits a low strength and thus would rather be “consumed” by the  $\alpha$ -process upon merging. We will come back to this point.

Considering *p*-CPS, 2-CS as well as FD, and 2-PC, no clear evidence of a  $\beta$ -relaxation is found, still, at high frequencies no

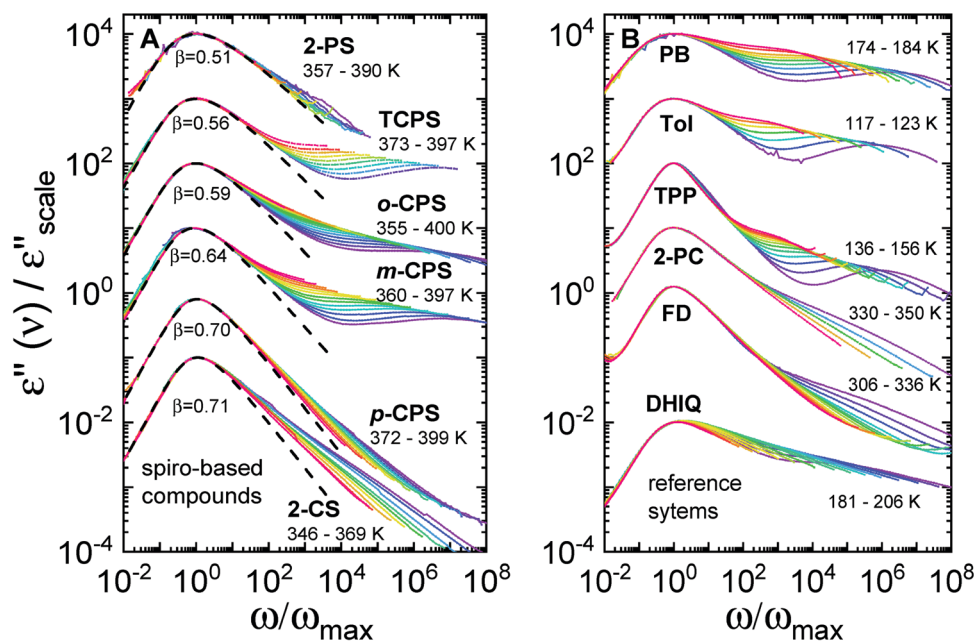


Fig. 3 Master curves (coloured symbols) and respective Kohlrausch fits (dashed black lines, stretching parameter  $\beta_k$  indicated) for (A) 2-PS, TCPS, *o*-CPS, *m*-CPS, *p*-CPS, and 2-CS (top to bottom) and for the reference systems (B) polybutadiene (PB), toluene (Tol), tripropylphosphate (TPP), 3,3',4,4'-benzophenone tetracarboxylic dianhydride (2-PC), felodipine (FD), and decahydroisoquinoline (DHIQ) (top to bottom). Master curves constructed by scaling axes by peak amplitude and frequency, respectively; they are shifted to an arbitrary height. Temperature corresponding to the curves increases from violet to red.

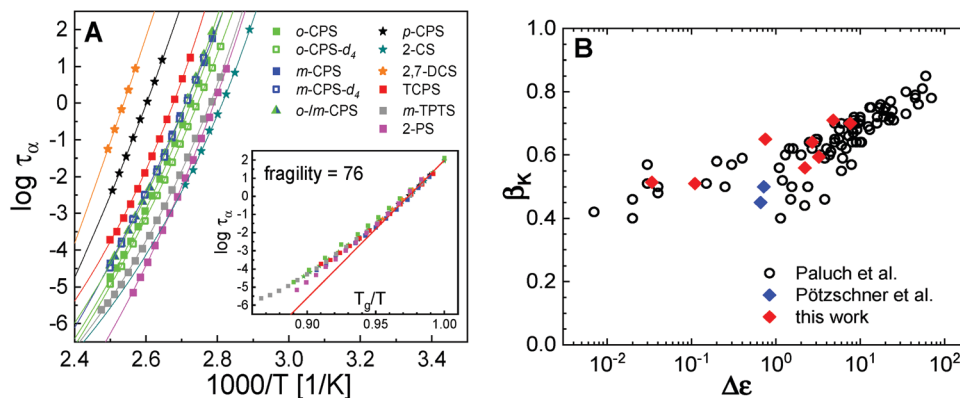


Fig. 4 (A) Time constants  $\tau_\alpha$  as function of inverse temperature for all investigated systems. Lines are VFT extrapolations to determine  $T_g$ . Colour and symbol determine system. Inset: Time constants as function of reduced temperature  $T_g/T$ . (B) Stretching parameter  $\beta_k$  as function of the dielectric relaxation strength  $\Delta\epsilon$  for a large collection of systems from Paluch *et al.*<sup>21</sup> (open black circles), the two high- $T_g$  glass formers SBC and DH 379 from Pötzschner *et al.*<sup>38,39</sup> (blue diamonds), and the herein investigated systems (red diamonds, *cf.* Table 1).

master curve is recognised. In these cases, the curves measured at higher temperatures (marked in red) exhibit a narrower spectrum than those measured at lower temperatures (marked in violet). In other words, an opposite evolution of the color-coding with temperature is found with respect to the spectra discussed before. Assuming FTS still holds for the  $\alpha$ -process, this relaxation pattern can be explained by a broad  $\beta$ -relaxation with a low relaxation strength and a time constant  $\tau_\beta$  being very close to that of the  $\alpha$ -process. This is clearly recognizable for the lowest temperatures in FD and 2-PC, when the ratio  $\tau_\beta/\tau_\alpha$  becomes large leading to the beginning formation a separate peak.

A special relaxation pattern is observed for DHIQ. Here, the peak is the narrowest at the highest temperature, gets broader with decreasing temperatures until a second peak starts to separate out of the main peak and leads for lowest temperatures again to a narrower  $\alpha$ -relaxation peak in combination with a clearly separated  $\beta$ -peak. Therefore, DHIQ is a rare example, where the full merging of the  $\alpha$ - and  $\beta$ -relaxation is observable in the experimental frequency window given by the present spectrometer.

Fig. 4A presents the time constant  $\tau_\alpha(T)$  for all investigated glass formers as a function of the inverse temperature as given by a Kohlrausch fit (*cf.* Fig. 3A). The glass transition temperature

$T_g$  (cf. Table 1) was determined along the definition of  $\tau_\alpha(T_g) = 100$  s, applying a Vogel–Fulcher–Tammann (VFT) fit for extrapolating  $\tau_\alpha(T)$  to low temperatures (lines in Fig. 4A). The so obtained  $T_g$  values agree within few degrees with those determined by DSC (Table 1). There is a slight difference between the deuterated and non-deuterated system of 2–3 K concerning the  $T_g$ . In the inset of Fig. 4A, the time constants are plotted *versus* the reduced reciprocal temperature  $T_g/T$ . Clearly, the fragility of all investigated systems is essentially the same. In the case of 2-PS, the curve is less curved although displaying the same fragility indicating that more than one parameter is needed to characterize  $\tau_\alpha(T_g/T)$ .

As mentioned, the spectra presented in Fig. 3 show the trend that the  $\alpha$ -relaxation is broader, the lower the relaxation strength  $\Delta\epsilon_\alpha$  is, a trend first recognised by Nielsen *et al.*<sup>22</sup> and recently considered by Paluch *et al.*<sup>21</sup> Fig. 4B displays the Kohlrausch stretching parameter  $\beta_K$  as a function of the relaxation strength (cf. Table 1) in a semi-logarithmic plot (instead of a linear plot as done by Paluch *et al.*) as collected in ref. 21. We added the data of the herein investigated glass formers as well as those of ref. 38 and 39. They follow the overall trend.

### 3.3. Secondary relaxation

In order to characterize the merging behaviour of the  $\alpha$ - and  $\beta$ -process, we took the ratio of the amplitude of the  $\beta$ -relaxation peak to that of the  $\alpha$ -peak  $\epsilon''_{\max,\beta}/\epsilon''_{\max,\alpha}$  at a given temperature above  $T_g$  and plotted it against the ratio of the frequency of the  $\beta$ -peak and the  $\alpha$ -peak  $\nu_{\max,\beta}/\nu_{\max,\alpha}$  in a double-logarithmic plot (see Fig. 5A). For all investigated systems, a linear relationship in this representation showing essentially the same slope of  $m = 0.1 \pm 0.01$  can be found, whereas the relative amplitude varies significantly. Quantitatively, this yields a power-law relationship, explicitly:

$$\epsilon''_{\max,\beta}/\epsilon''_{\max,\alpha} \propto \left(\nu_{\max,\beta}/\nu_{\max,\alpha}\right)^{-m} \quad (9)$$

Interestingly, one finds a high relative strength of the  $\beta$ -relaxation for non-polar systems like PB or toluene, whereas the amplitude is small for polar systems like TPP. Moreover, one

gets a rough estimate of the relative strength of the  $\beta$ -process at the merging. As already mentioned, in the case of PB, the  $\beta$ -process appears to take all the relaxation strength of the  $\alpha$ -process, *i.e.*, applying a Williams–Watts approach,<sup>1,13,53</sup> it literally consumes the  $\alpha$ -process. While in the case of TPP, the amplitude of the  $\beta$ -relaxation at the merging becomes only about 10% of that of the  $\alpha$ -process.

We emphasize that eqn (9) is of phenomenological nature, and above we assumed that a linear extrapolation to full merging is permissible. In order to model the merging of both,  $\alpha$ - and  $\beta$ -relaxation in detail, no single model has been generally accepted. Here, we stick to a Williams–Watts approach<sup>1,13,53</sup> which assumes that the full relaxation function is given by a product of the relaxation functions of the two processes (cf. Experimental 2.3, eqn (8)). We applied this model for the case of the spectra of TCPS (cf. Fig. 2D) and 2-PC (Appendix Fig. 10D): The first system displays a rather well resolved  $\beta$ -relaxation, whereas the second is interesting as it shows a comparatively slow  $\beta$ -relaxation strongly submerged under a large  $\alpha$ -relaxation. We assumed for the  $\alpha$ -process a Kohlrausch step-response function and for the  $\beta$ -process a temperature independent symmetric distribution of correlation times (cf. eqn (4) with  $b = 1$ ), which were then combined along eqn (8). As result, we get the relaxation strength of the  $\beta$ -process  $\Delta\epsilon_\beta(T)$  of TCPS (Fig. 5B) as well as the ratio of time constants,  $\tau_\alpha(T)/\tau_\beta(T) = \nu_\beta/\nu_\alpha$  and the relative relaxation strength  $\frac{\Delta\epsilon_\beta}{\Delta\epsilon_\alpha} = \frac{1}{S} - 1$  (cf. eqn (8)) at temperatures above  $T_g$  (Fig. 5B inset). Approximately, again, a power-law is observed but the relative relaxation strength displays higher values compared to the ratio of the amplitudes plotted in Fig. 5A. Regarding the time constants  $\tau_\beta(T)$  of 2-PC and TCPS, both show a stronger temperature dependence above  $T_g$  than below, a phenomenon best recognised when plotted against  $T/T_g$  and well known from literature (Fig. 6B).<sup>4</sup> Such an analysis also yields different stretching parameters of the  $\alpha$ -relaxation compared to that of a simple Kohlrausch fit mainly determined by the relaxation peak. Actually, stretching turns out

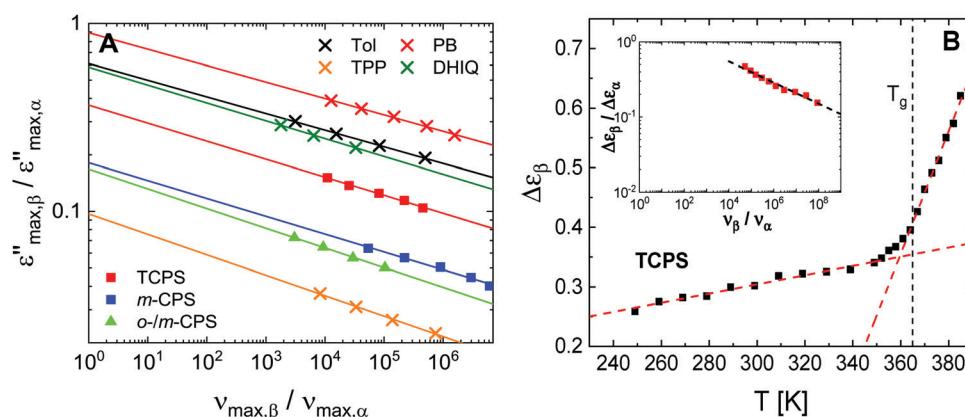
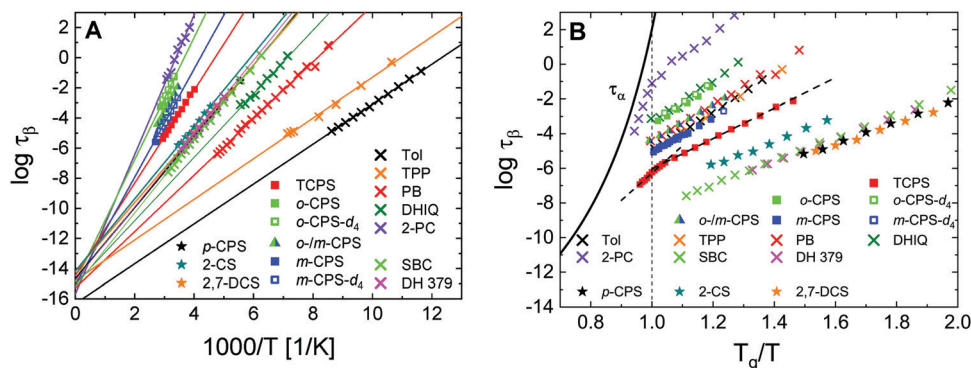


Fig. 5 (A) Relative amplitude of the  $\beta$ -process  $\epsilon''_{\max,\beta}$  with respect to that of the  $\alpha$ -process  $\epsilon''_{\max,\alpha}$  plotted against the relative relaxation frequency  $\nu_{\max,\beta}/\nu_{\max,\alpha}$ . Colour and symbol define system. Lines are linear fits. (B) Relaxation strength  $\Delta\epsilon_\beta(T)$  of TCPS determined from a Williams–Watts approach (cf. Fig. 2D for fits). Dashed red lines indicate the crossover at  $T_g$ . Inset: Relative relaxation strength  $\Delta\epsilon_\beta/\Delta\epsilon_\alpha$  above  $T_g$  as function of  $\nu_\beta/\nu_\alpha$ , which is comparable to (A); a linear but different trend is observed.



**Fig. 6** (A) Time constants  $\tau_\beta$  of the  $\beta$ -process ( $T < T_g$ ) as a function of inverse temperature with linear extrapolation to  $\tau_0$ . Stars:  $p$ -CPS, 2-CS, 2,7-DCS (atypical  $\beta$ -process); squares and triangles:  $o$ -CPS(- $d_4$ ),  $m$ -CPS(- $d_4$ ), mixture  $o$ -/ $m$ -CPS, TCPS; crosses: reference systems (Tol, TPP, PB, DHIQ and 2-PC) as well as SBC<sup>39</sup>, and DH 379.<sup>38</sup> (B) Time constant  $\tau_\beta$  as a function of reduced temperature  $T_g/T$  with "average"  $\alpha$ -process (black line) of herein investigated glass formers. Systems like in (A).  $\tau_\beta$  was determined with a Williams–Watts approach for TCPS (red squares, *cf.* Fig. 2D) and 2-PC (purple crosses, *cf.* Appendix Fig. 10D) also above  $T_g$ .

to be temperature dependent. For example, in the case of TCPS we find  $\beta_K = 0.51$  at  $T_g$  and  $\beta_K = 0.59$  at 400 K under consideration of the  $\beta$ -process. Overall, some care has to be taken when presenting stretching parameters (as in Fig. 4B) just obtained from a single Kohlrausch fit at  $T_g$  without taking the  $\beta$ -relaxation into account. Still, the Williams–Watts approach needs justification within a final theory of the glass transition.

We now focus on temperatures below  $T_g$ . In Fig. 6A, the logarithm of the time constants  $\tau_\beta$  of the investigated (stars, squares, and triangle) and of the reference systems (crosses) are plotted *versus* the inverse temperature. All  $\beta$ -relaxations display an Arrhenius temperature behaviour, with an exponential pre-factor  $\tau_0$  in the range  $10^{-15}$ – $10^{-16}$  s consistent with previous reports,<sup>1,56,57</sup> except for toluene, for which it is about  $10^{-17}$  s and therefore slightly lower. The values of the activation energies (together with those of the attempt time  $\tau_0$ ) are listed in Table 1. Fig. 6B shows the time constants of the  $\beta$ -process as a function of the reduced temperature  $T_g/T$  together with those of the  $\alpha$ -process of the high- $T_g$  systems (the latter as a single line). Whereas the high- $T_g$  systems  $o$ -CPS,  $m$ -CPS, TCPS and the reference systems Tol, PB, DHIQ, and TPP display almost parallel straight lines with a slope close to  $24T_g$  (*cf.* Table 1),

except for 2-PC which shows a somewhat higher slope, the time constants of the systems  $p$ -CPS, 2-CS, 2,7-DCS, DH 379, and SBC are found at higher  $T_g/T$  values and show slopes around  $14T_g$ . However, as we will demonstrate below, the secondary relaxation spectra of  $p$ -CPS, 2-CS, 2,7-DCS (in contrast to DH 379 and SBC) exhibit an atypical evolution with temperature.

As can be noticed from inspecting Fig. 2, below  $T_g$  the spectra of the  $\beta$ -relaxation broaden with lowering temperature, a phenomenon well known.<sup>1,12,14</sup> The spectral broadening can be traced back to an underlying temperature independent distribution of activation energies  $g_\beta(E)$ .<sup>1,14,44,48</sup> Given this and referring to the Experimental section 2.3, the spectra of the  $\beta$ -process measured at the different temperatures can be rescaled along eqn (7) to directly provide the distribution  $g_\beta(E)$ . This was done in Fig. 7A by using the exponential pre-factor provided by the extrapolation in Fig. 6A (*cf.* Table 1). We also included the spectra of 2-PC (see Appendix) which displays a  $\beta$ -relaxation highly submerged with the  $\alpha$ -relaxation, as said. First of all, rather symmetric master curves, *i.e.*, the distributions  $g_\beta(E)$ , are obtained. Second, the distributions shift to higher energies for glass formers with higher  $T_g$ , of course, not surprising due to the trend  $E_\beta \approx 24T_g$  in many cases. The distributions displayed in

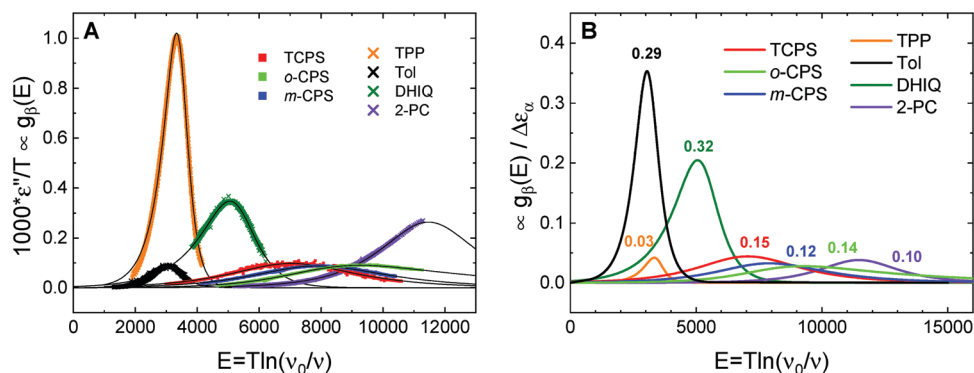


**Fig. 7** (A) Relaxation spectra of  $\beta$ -process ( $T < T_g$ ) scaled along eqn (7) on an absolute scale for TCPS,  $o$ -CPS,  $m$ -CPS as well as TPP, Tol, DHIQ, and 2-PC. Lines are fits along eqn (6) without normalisation. (B) Relative contribution of the  $\beta$ -process at  $0.9T_g$  compared to that of  $\alpha$ -process by plotting fits of (A) divided by  $\Delta \varepsilon_\alpha(T_g)$  (*cf.* Table 1). Numbers indicate integral over the distribution and thus the relative strength  $\Delta \varepsilon_\beta(0.9T_g) / \Delta \varepsilon_\alpha(T_g)$ .

Fig. 7A are not normalized, instead they refer to some reference temperature ( $0.9T_g$  as indicated). Thus, they still reflect the absolute relaxation strength of the  $\beta$ -relaxation, which, like the  $\alpha$ -relaxation, is large in the case of TPP or DHIQ, for example, but rather small for the systems TCPS, *o*-CPS, *m*-CPS, and Tol.

In order to estimate the relative contribution of the  $\beta$ -relaxation with respect to that of the  $\alpha$ -relaxation, we scaled the amplitudes in Fig. 7A by the corresponding values of the relaxation strengths  $\Delta\epsilon_\alpha(T_g)$  – see Fig. 7B, where the  $\Delta\epsilon_\alpha(T_g)$  values were taken from a Kohlrausch fit of the  $\alpha$ -relaxation peak (cf. Table 1). Only the fits of  $g_\beta(E)$  along eqn (6) from Fig. 7A are shown. Now a completely different picture emerges. Whereas due to the large  $\Delta\epsilon_\alpha$  of TPP the  $\beta$ -relaxation shown in Fig. 7A is strong, it shows as a relatively weak contribution in the representation of Fig. 7B. The numbers indicate the integral of the distribution and thus the relative strength of the  $\beta$ -relaxation, i.e.  $\Delta\epsilon_\beta(0.9T_g)/\Delta\epsilon_\alpha(T_g)$ .

The secondary relaxations observed in the systems *p*-CPS, 2-CS, and 2,7-DCS exhibit a different evolution with temperature, as already mentioned. Master curves result just by shifting the spectra at different temperatures along the frequency axis and applying small factors in amplitude to match one at a reference temperature

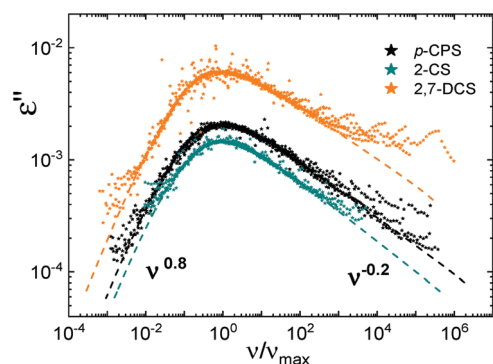


Fig. 8 Master curves of the atypical secondary process in *p*-CPS, 2-CS, and 2,7-DCS, scaled to the maximum of the curve at 220 K solely by shifting along the frequency axis and small adaptations in the amplitude. Dashed lines: interpolation by eqn (4).

(220 K) as shown in Fig. 8. The missing temperature dependence of the width of the spectra prohibits to map these spectra onto a temperature independent distribution of activation energies as done for the typical secondary ( $\beta$ -) relaxations discussed before. Yet, the spectral shape is asymmetric: the low-frequency flank follows a power-law exponent of about 0.8, whereas the high-frequency flank decays with an exponent of about 0.2 by magnitude. The master curves can be interpolated with a distribution of correlation times according to eqn (4). Important to note, the exponential pre-factors of these atypical secondary relaxation processes are quite similar to those regarded as typical (see Fig. 6A).

The distribution of activation energies  $g_\beta(E)$  shown in Fig. 7A, but now normalised, can also be plotted as a function of the reduced energy scale  $T/T_g$  as found in Fig. 9A. As expected, the distributions are centred between 19–35 and of similar width; only in the case of TPP the width is somewhat narrower. In other words, also the width of the  $\beta$ -relaxation increases with  $T_g$ .

Finally, we present in Fig. 9B a collection of activation energy data of the  $\beta$ -process plotted vs.  $T_g$ ,<sup>1,23</sup> extended by the data compiled by the present study (cf. Table 1). Whereas the typical secondary processes observed in this study essentially show an activation energy between 19 and  $35T_g$ , the atypical relaxations are closer to the relationship  $14T_g$ . In the case of SBC, a typical  $\beta$ -relaxation, which shows a broadening of the spectra below  $T_g$ , still a value  $E_\beta = 15.6T_g$  was reported (Table 1), as for several other systems found in Fig. 9B.

## 4. Discussion and conclusion

The dielectric spectra of a collection of specially synthesized high- $T_g$  glass formers with a rather large, non-polar spiro core and more or less polar side groups leading to varying high  $T_g$  values are investigated. All the relaxation features typical of molecular low- $T_g$  systems are rediscovered, that is, relaxation stretching, a more or less pronounced  $\beta$ -process, and a fragility index quite similar to that of other molecular low- $T_g$  glass formers.<sup>19</sup> As in many other

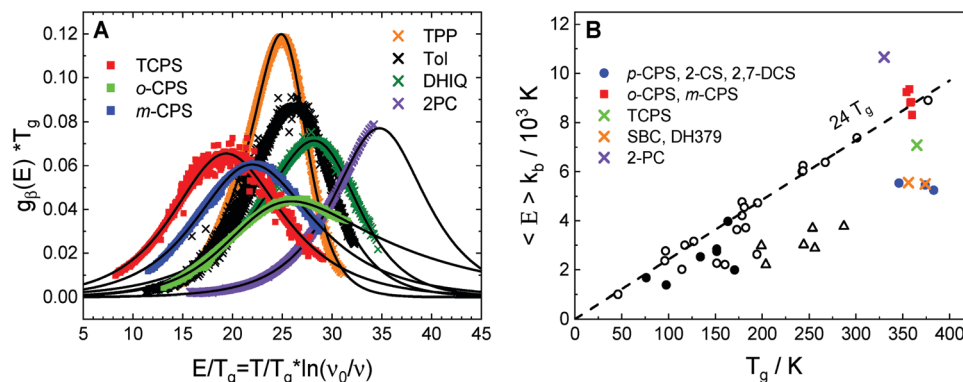


Fig. 9 (A) Normalised distribution  $g_\beta(E)$  scaled by  $T_g$  for TCPS, *o*-CPS, and *m*-CPS (squares) as well as for the reference systems TPP, Tol, DHIQ, and 2-PC (crosses). System is represented by colour and symbol. Black lines are fits along eqn (6). (B) Apparent activation energy of the secondary processes for the herein investigated glass formers (coloured symbols) in comparison to that of other glass formers investigated in ref. 1 and 23 (black symbols). Glass formers showing atypical  $\beta$ -processes are marked in blue. Dashed line gives  $24T_g$ .

glass formers, the appearance of a strong  $\beta$ -process hampers the identification of a possible generic relaxation pattern including  $\alpha$ -peak and excess wing. For example, considering here systems with a rather high (mean) activation of the  $\beta$ -process and thus a low spectral separation of  $\alpha$ - and  $\beta$ -process above  $T_g$ , no traces of an excess wing are found in contrast to systems with a lower activation energy.<sup>17,52</sup> The relaxation stretching in terms of  $\beta_K$  of the  $\alpha$ -relaxation displays the trend to become less with higher relaxation strength  $\Delta\epsilon_\alpha$ , a relationship revealed recently.<sup>21,22</sup> Yet, we do not find any outlier when the direction of the dipole moment introduced by the nitrile group is changed with respect to some molecular axis, a recent finding.<sup>58</sup> Also, the local positioning of the polar nitrile group at the rather large core interacting only *via* van der-Waals forces – potentially having an effect on the stretching<sup>58</sup> – does not change the trend  $\beta_K$  vs.  $\Delta\epsilon_\alpha$  reported by Paluch *et al.*<sup>21</sup>

Well resolved  $\beta$ -relaxations are only found for those glass formers investigated here for which a nitrile group is attached in *o*- or *m*-position of the phenyl ring linked to the rigid spiro core. In the *p*-position, no clearly resolved  $\beta$ -relaxation is observed. Likewise, no discernible  $\beta$ -relaxation peak is observed when one or two nitrile groups are directly attached to the spiro core as in 2-CS and 2,7-DCS. Absence of any nitrile group lowers the relaxation strength  $\Delta\epsilon_\alpha$  significantly, and no typical  $\beta$ -relaxation pattern is recognized, either. Typical for a generic secondary relaxation, *i.e.* a  $\beta$ -process, is the increase of its relaxation amplitude above  $T_g$ , which is found to follow a power-law behaviour with an universal exponent (*cf.* eqn (9)), yet, its relative amplitude, *i.e.* with respect to that of the  $\alpha$ -relaxation, varies strongly. In addition, the separation of  $\alpha$ - and  $\beta$ -process varies significantly because of the fact that  $E_\beta$  varies between 19 and  $35T_g$ , whereas fragility remains essentially the same. However, the power-law behaviour of the amplitudes is a phenomenological finding; a detailed spectral analysis in the frame of the Williams–Watts approach provides quantitative relaxation strengths and time constants. In particular, the temperature dependence of  $\tau_\beta(T)$  shows a crossover to a stronger temperature dependence above  $T_g$ , a phenomenon well known,<sup>1,4,56,59</sup> and the relative strength of the  $\beta$ -process becomes stronger compared to its amplitude (Fig. 5B). The latter can be understood by the fact, that the  $\beta$ -relaxation shows a broader spectrum compared to that of the  $\alpha$ -relaxation.

Generally speaking, on the one hand, there exist systems which clearly show traces of a weak  $\beta$ -process, yet, due to the closeness to the  $\alpha$ -relaxation, no two clearly resolved relaxation peaks are observable above  $T_g$ . On the other hand, there are glass formers which display well resolved secondary relaxation peaks which, given the frequency window of the Alpha-A Analyzer, are only well discernible below  $T_g$ . They belong to the group displaying a mean activation energy close to  $12$ – $15T_g$ , whereas the first group shows values around  $24T_g$ . In the case of DHIQ, the relaxation strength is comparatively strong and the separation of both  $\alpha$ - and  $\beta$ -process is sufficiently large, so that a clear-cut merging from two separate relaxations at low temperature to a single ( $\alpha$ -) peak at high temperatures is observable in the present frequency window. In any case,  $E_\beta$  increases more or less systematically with  $T_g$ , as does the width of the distribution  $g_\beta(E)$ . Plotting  $g_\beta(E)$  as a function of the reduced energy scale  $E/T_g$ , not identical but similar distributions are found with widths changing about a factor 2. As the

actual manifestation of the  $\beta$ -relaxation depends on the temporal separation of  $\alpha$ - and  $\beta$ -process, on amplitude, and width, it is not straight forward to estimate its relative relaxation strength  $\Delta\epsilon_\beta/\Delta\epsilon_\alpha$  from its apparent manifestation in the relaxation spectra. Nevertheless, our results show that  $\Delta\epsilon_\beta/\Delta\epsilon_\alpha$  ranges in the interval 0.03 (TPP)–0.32 (DHIQ).

Applying multi-pulse echo techniques, NMR analyses of neat glasses have identified the  $\beta$ -process as a spatially highly restricted motion of essentially all molecules (a characteristics which might be different in binary glasses<sup>60,61</sup> or polymers<sup>56</sup>).<sup>62,63</sup> Above  $T_g$ , the extent of this spatial restriction becomes less and less which can explain the quick increase of the relaxation strength  $\Delta\epsilon_\beta$  above  $T_g$ .<sup>63–65</sup> Importantly, the NMR relaxation pattern displays rather universal features, which are difficult to reconcile with the quite different relative dielectric relaxation strength  $\Delta\epsilon_\beta/\Delta\epsilon_\alpha$ . These facts appear to challenge a direct mapping of dielectric and NMR results; it is not clear what determines the dielectric relaxation strength of the  $\beta$ -process. Also, on the basis of the NMR results compiled so far, we find it difficult to distinguish between a generic (Johari–Goldstein) and non-generic secondary relaxation except for the three cases reported here, for which the evolution of the dielectric spectra display a completely different pattern.<sup>15</sup> To the best of our knowledge, the latter kind of secondary process was not reported before.

Given the universal relaxation pattern revealed by NMR, we so far interpreted the  $\beta$ -process as a generic cooperative phenomenon.<sup>61–63</sup> Independent of molecular details, the  $\beta$ -process involves an essentially spatially isotropic reorientation of the molecules, though highly hindered. Yet, a possible anisotropic character was discussed by Li-Min Wang & Ngai.<sup>66</sup> In the case of the present glass formers *o*-, *m*-, and *p*-CPS, with a nitrile group in *ortho*-, *meta*-, and *para*-position, respectively, clear-cut differences are observed: With the nitrile group in the *para*-position, only a weak  $\beta$ -process is observed, in contrast to the other two cases with pronounced  $\beta$ -relaxation. Whether this difference of the manifestation of the  $\beta$ -process is an indication of an anisotropic character or a “localized”  $\beta$ -relaxation restricted to the motion of the phenyl ring alone, can be checked by investigating a deuterated core, by <sup>2</sup>H NMR for example – a future task. In the case of toluene, a small, rigid molecule displaying a strong  $\beta$ -process (*cf.* Fig. 3B), labelling the *para*-position by deuterium revealed no difference in the NMR relaxation pattern compared to that given by the fully deuterated phenyl ring.<sup>67</sup> Thus, reorientation around the pseudo  $C_2$  axis alone can be ruled out. Still, there remains the theoretical possibility that the  $\beta$ -process involves an in-plane wobbling of the phenyl ring.

## Conflicts of interest

There are no conflicts to declare.

## Appendix

Fig. 10A–C show the dielectric loss spectra of 2,7-DCS, the 50:50 isomer mixture *o*-/*m*-CPS, and *m*-TPTS. For 3,3',4,4'-benzophenonetetracarboxylic dianhydride (2-PC), the Williams–Watts analysis of the dielectric loss data (*cf.* eqn (8)) with a Kohlrausch

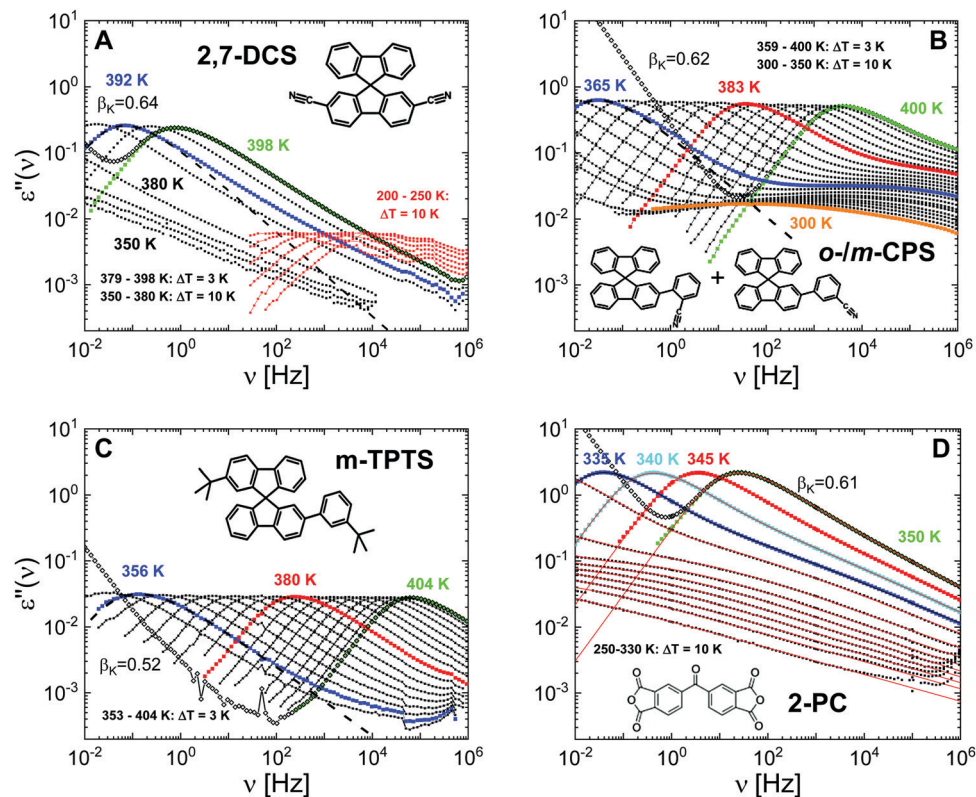


**Fig. 10** Dielectric loss spectra of 2,7-DCS (A), 50:50 isomer mixture *o-/m*-CPS (B), *m*-TPTS (C), and 3,3',4,4'-benzophenonetetracarboxylic dianhydride (2-PC) (D). DC conductivity contribution is subtracted; original data is shown in open symbols for the highest temperature. Coloured curves highlight selected temperatures. In (A)–(C), the dashed black lines show Kohlrausch fits at low temperatures with  $\beta_K$  being indicated. In (D), the red lines show interpolations along a Williams–Watts approach with a Kohlrausch function for the  $\alpha$ -relaxation and a symmetric distribution of correlation times for the  $\beta$ -relaxation (cf. Experimental 2.3).

function (eqn (2)) for the  $\alpha$ -relaxation and a symmetric distribution of correlation times (eqn (4)) for the  $\beta$ -relaxation is demonstrated in Fig. 10D (cf. Experimental 2.3).

## Acknowledgements

This research was funded by the Deutsche Forschungsgemeinschaft (DFG, German Research Foundation), Grant Numbers Schm 703/9-1, RO 907/19, and SFB 840. F. K. acknowledges support from the Elite Network of Bavaria (ENB) within the Elite Study Program Macromolecular Science. TK and ER also acknowledge the support by Jürgen Senker (Department of Inorganic Chemistry III, University Bayreuth) to proceed in the experimental work.

## References

- 1 A. Kudlik, S. Benkhof, T. Blochowicz, C. Tschirwitz and E. A. Rössler, *J. Mol. Struct.*, 1999, **479**, 201–218.
- 2 P. Lunkenheimer, U. Schneider, R. Brand and A. Loidl, *Contemp. Phys.*, 2000, **41**, 15–36.
- 3 T. Blochowicz, A. Brodin and E. A. Rössler in *Advances in Chemical Physics*, ed. S. A. Rice, John Wiley and Sons, Inc., Hoboken, 2006, 127–256.
- 4 G. Floudas, M. Paluch, A. Grzybowski and K. L. Ngai, *Molecular Dynamics of Glass-Forming Systems: Effects of Pressure*, Springer, Berlin, 2011.
- 5 R. Richert in *Advances in chemical physics*, ed. A. R. Dinner and S. A. Rice, Wiley, Hoboken, 2014, pp. 101–195.
- 6 W. Götze, *J. Phys.: Condens. Matter*, 1999, **11**, A1–A45.
- 7 A. Aouadi, C. Dreyfus, M. Massot, R. M. Pick, T. Berger, W. Steffen, A. Patkowski and C. Alba-Simionesco, *J. Chem. Phys.*, 2000, **112**, 9860–9873.
- 8 H. Z. Cummins, *J. Phys.: Condens. Matter*, 2005, **17**, 1457–1470.
- 9 F. Pabst, J. Gabriel, P. Weigl and T. Blochowicz, *Chem. Phys.*, 2017, **494**, 103–110.
- 10 R. Torre, P. Bartolini and R. M. Pick, *Phys. Rev. E: Stat. Phys., Plasmas, Fluids, Relat. Interdiscip. Top.*, 1998, **57**, 1912–1920.
- 11 H. Cang, V. N. Novikov and M. D. Fayer, *Phys. Rev. Lett.*, 2003, **90**, 197401.
- 12 G. P. Johari and M. Goldstein, *J. Chem. Phys.*, 1970, **53**, 2372–2388.
- 13 G. Williams and D. C. Watts, *Trans. Faraday Soc.*, 1971, **67**, 1971–1979.
- 14 L. Wu, *Phys. Rev. B: Condens. Matter Mater. Phys.*, 1991, **43**, 9906–9915.
- 15 K. L. Ngai and M. Paluch, *J. Chem. Phys.*, 2004, **120**, 857–873.
- 16 U. Schneider, R. Brand, P. Lunkenheimer and A. Loidl, *Phys. Rev. Lett.*, 2000, **84**, 5560–5563.

- 17 A. Brodin, C. Gainaru, V. Porokhonsky and E. A. Rössler, *J. Phys.: Condens. Matter*, 2007, **19**, 205104.
- 18 N. Petzold, B. Schmidtke, R. Kahlau, D. Bock, R. Meier, B. Micko, D. Kruk and E. A. Rössler, *J. Chem. Phys.*, 2013, **138**, 12A510.
- 19 R. Böhmer and C. A. Angell, *Phys. Rev. B: Condens. Matter Mater. Phys.*, 1992, **45**, 10091–10094.
- 20 B. Schmidtke, N. Petzold, B. Pötzschner, H. Weingärtner and E. A. Rössler, *J. Phys. Chem. B*, 2014, **118**, 7108–7118.
- 21 M. Paluch, J. Knapik, Z. Wojnarowska, A. Grzybowski and K. L. Ngai, *Phys. Rev. Lett.*, 2016, **116**, 25702.
- 22 A. I. Nielsen, T. Christensen, B. Jakobsen, K. Niss, N. B. Olsen, R. Richert and J. C. Dyre, *J. Chem. Phys.*, 2009, **130**, 154508.
- 23 C. Tschirwitz, S. Benkhof, T. Blochowicz and E. Rössler, *J. Chem. Phys.*, 2002, **117**, 6281–6288.
- 24 C. Gainaru, R. Kahlau, E. A. Rössler and R. Böhmer, *J. Chem. Phys.*, 2009, **131**, 184510.
- 25 Q. Niu, Q. Zhang, W. Xu, Y. Jiang, R. Xia, D. D. C. Bradley, D. Li and X. Wen, *Org. Electron.*, 2015, **18**, 95–100.
- 26 J. Salbeck and F. Weissörtel, *Macromol. Symp.*, 1997, **125**, 121–132.
- 27 J. Pang, Y. Tao, S. Freiberg, X.-P. Yang, M. D'Iorio and S. Wang, *J. Mater. Chem.*, 2002, **12**, 206–212.
- 28 J. Y. Shen, C. Y. Lee, T.-H. Huang, J. T. Lin, Y.-T. Tao, C.-H. Chien and C. Tsai, *J. Mater. Chem.*, 2005, **15**, 2455–2463.
- 29 K. Tsuchiya, S. W. Chang, N. M. Felix, M. Ueda and C. K. Ober, *J. Photopolym. Sci. Technol.*, 2005, **18**, 431–434.
- 30 E. Murotani, J.-K. Lee, M. Chatzichristidi, A. A. Zakhidov, P. G. Taylor, E. L. Schwartz, G. G. Malliaras and C. K. Ober, *ACS Appl. Mater. Interfaces*, 2009, **1**, 2363–2370.
- 31 N. M. Felix, A. de Silva and C. K. Ober, *Adv. Mater.*, 2008, **20**, 1303–1309.
- 32 E. O. Kissi, H. Grohgan, K. Löbmann, M. T. Ruggiero, J. A. Zeitler and T. Rades, *J. Phys. Chem. B*, 2018, **122**, 2803–2808.
- 33 A. Afzal, M. Shahin Thayyil, M. K. Sulaiman and A. R. Kulkarni, *Indian J. Phys.*, 2018, **92**, 565–573.
- 34 F. Pfeiffer, N. M. Felix, C. Neuber, C. K. Ober and H.-W. Schmidt, *Adv. Funct. Mater.*, 2007, **17**, 2336–2342.
- 35 F. Pfeiffer, N. M. Felix, C. Neuber, C. K. Ober and H.-W. Schmidt, *Phys. Chem. Chem. Phys.*, 2008, **10**, 1257–1262.
- 36 M. Hasebe, D. Musumeci and L. Yu, *J. Phys. Chem. B*, 2015, **119**, 3304–3311.
- 37 F. Krohn, C. Neuber, E. A. Rössler and H.-W. Schmidt, *J. Phys. Chem. B*, 2019, **123**, 10286–10293.
- 38 B. Pötzschner, F. Mohamed, A. Lichtinger, D. Bock and E. A. Rössler, *J. Chem. Phys.*, 2015, **143**, 154506.
- 39 B. Pötzschner, F. Mohamed, C. Bächer, E. Wagner, A. Lichtinger, R. Minikejew, K. Kreger, H.-W. Schmidt and E. A. Rössler, *J. Chem. Phys.*, 2017, **146**, 164503.
- 40 V. N. Novikov and E. A. Rössler, *Polymer*, 2013, **54**, 6987–6991.
- 41 J. Hintermeyer, A. Herrmann, R. Kahlau, C. Goiceanu and E. A. Rössler, *Macromolecules*, 2008, **41**, 9335–9344.
- 42 R. Kahlau and E. A. Rössler, unpublished work.
- 43 S. Adishchev, D. Bock, C. Gainaru, R. Kahlau, B. Micko, N. Petzold, B. Pötzschner and E. A. Rössler, *Z. Phys. Chem.*, 2012, **226**, 1149–1168.
- 44 R. Kahlau, T. Dörfler and E. A. Rössler, *J. Chem. Phys.*, 2013, **139**, 134504.
- 45 S. Kachel and E. A. Rössler, unpublished work.
- 46 C. J. F. Böttcher and P. Bordewijk, *Dielectrics in Time-Dependent Fields*, Elsevier, Amsterdam, 1978.
- 47 F. Kremer and A. Schönhals, *Broadband Dielectric Spectroscopy*, Springer, Berlin, 2003.
- 48 T. Blochowicz, C. Tschirwitz, S. Benkhof and E. A. Rössler, *J. Chem. Phys.*, 2003, **118**, 7544–7556.
- 49 K. S. Gilroy and W. A. Phillips, *Philos. Mag. B*, 1981, **43**, 735–746.
- 50 L. Wu and S. R. Nagel, *Phys. Rev. B: Condens. Matter Mater. Phys.*, 1992, **46**, 11198–11200.
- 51 J. Wiedersich, S. V. Adichtchev and E. A. Rössler, *Phys. Rev. Lett.*, 2000, **84**, 2718–2721.
- 52 C. Gainaru, R. Böhmer, R. Kahlau and E. Rössler, *Phys. Rev. B: Condens. Matter Mater. Phys.*, 2010, **82**, 104205.
- 53 A. Arbe, D. Richter, J. Colmenero and B. Farago, *Phys. Rev. E: Stat. Phys., Plasmas, Fluids, Relat. Interdiscip. Top.*, 1996, **54**, 3853–3869.
- 54 H. Wagner and R. Richert, *J. Phys. Chem. B*, 1999, **103**, 4071–4077.
- 55 F. Mohamed, *Dynamics of Advanced Polymer Systems studied by Dielectric Spectroscopy and Rheology: From Binary Glass Formers to Nanocomposites*, Bayreuth, 2018.
- 56 T. Körber, F. Mohamed, M. Hofmann, A. Lichtinger, L. Willner and E. A. Rössler, *Macromolecules*, 2017, **50**, 1554–1568.
- 57 A. Kudlik, C. Tschirwitz, T. Blochowicz, S. Benkhof and E. A. Rössler, *J. Non-Cryst. Solids*, 1998, **235–237**, 406–411.
- 58 A. Jędrzejowska, M. Matussek, K. L. Ngai, K. Grzybowski, K. Jurkiewicz and M. Paluch, *Phys. Rev. E*, 2020, **101**, 10603.
- 59 K. L. Ngai and M. Paluch, *J. Phys. Chem. B*, 2003, **107**, 6865–6872.
- 60 B. Micko, C. Tschirwitz and E. A. Rössler, *J. Chem. Phys.*, 2013, **138**, 154501.
- 61 D. Bock, R. Kahlau, B. Micko, B. Pötzschner, G. J. Schneider and E. A. Rössler, *J. Chem. Phys.*, 2013, **139**, 64508.
- 62 M. Vogel and E. Rössler, *J. Chem. Phys.*, 2001, **114**, 5802–5815.
- 63 M. Vogel, C. Tschirwitz, G. Schneider, C. Koplin, P. Medick and E. Rössler, *J. Non-Cryst. Solids*, 2002, **307–310**, 326–335.
- 64 B. Micko, D. Kruk and E. A. Rössler, *J. Chem. Phys.*, 2013, **138**, 74504.
- 65 M. Vogel, P. Medick and E. A. Rössler, in *Annual Reports on NMR Spectroscopy*, ed. G. A. Webb, Academic Press, Amsterdam, 2005, pp. 231–299.
- 66 L.-M. Wang, Y. Tian, R. Liu and K. L. Ngai, *J. Phys. Chem. B*, 2011, **115**, 719–724.
- 67 D. Bock, T. Körber, F. Mohamed, B. Pötzschner and E. A. Rössler, in *The Scaling of Relaxation Processes*, ed. F. Kremer and A. Loidl, Springer, Cham, 2018.

## Supplementary Information

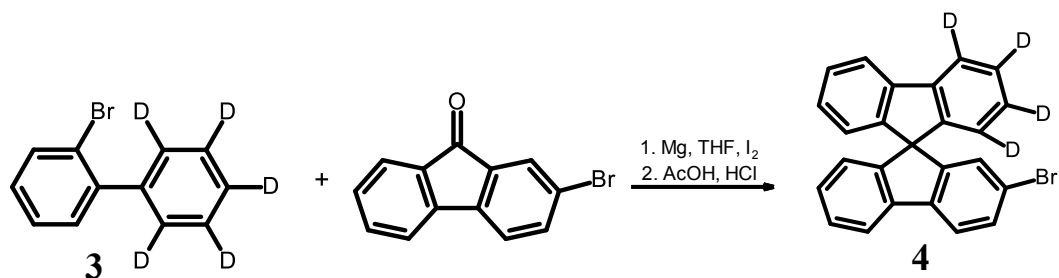
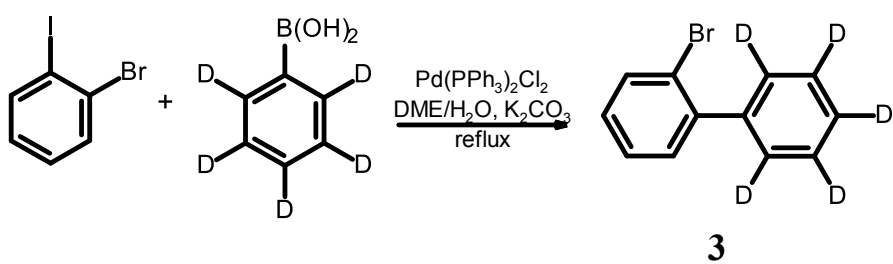
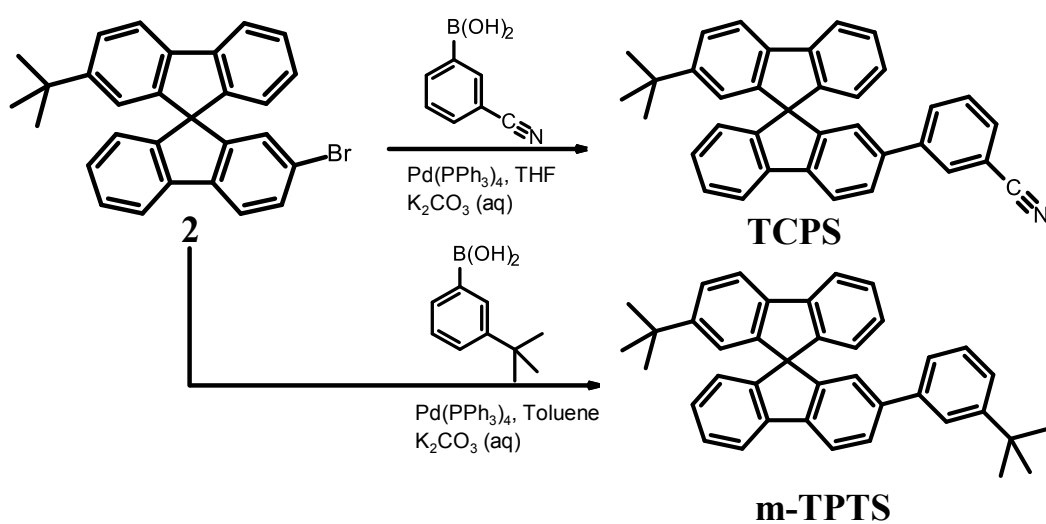
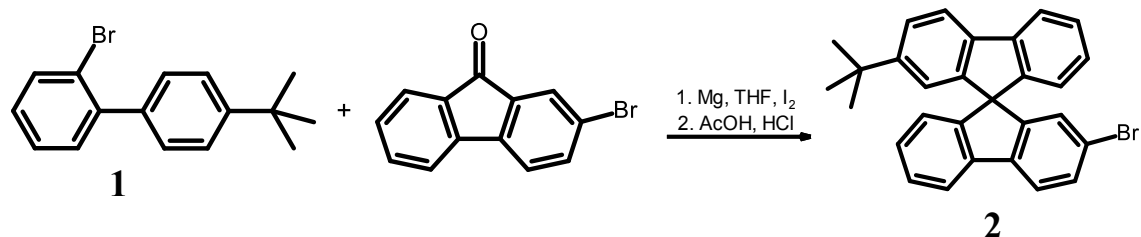
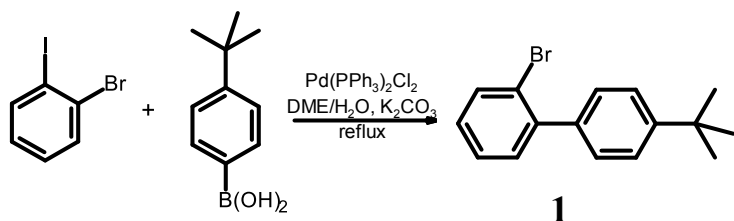
### **Main and secondary relaxations of non-polymeric high- $T_g$ glass formers as revealed by dielectric spectroscopy**

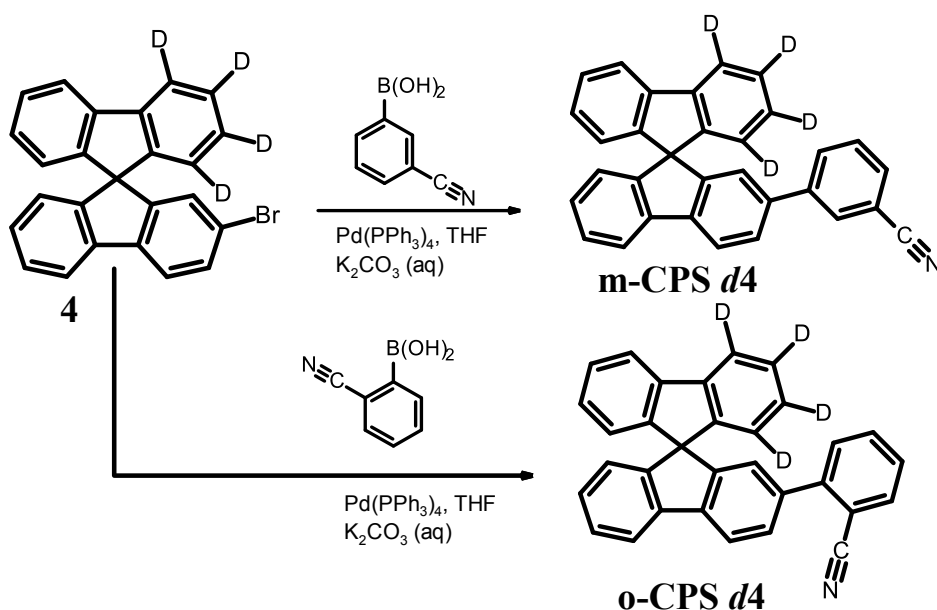
*Thomas Körber,<sup>a</sup> Felix Krohn,<sup>b</sup> Christian Neuber,<sup>b</sup> Hans-Werner Schmidt,<sup>b</sup> and  
Ernst A. Rössler\*<sup>a</sup>*

<sup>a</sup>Department of Inorganic Chemistry III and Northern Bavarian NMR Centre, University of Bayreuth, 95440 Bayreuth, Germany

<sup>b</sup>Department of Macromolecular Chemistry and Bavarian Polymer Institute, University of Bayreuth, 95440 Bayreuth, Germany

## Synthetic route





### Synthetic procedures and $^1\text{H-NMR}$ data

Synthesis of **1**: 7.00 g (24.8 mmol) Iodobromobenzene and 5.291 g (29.7 mmol) of 4-*tert*butylphenylboronic acid are solved in 60 mL of DME and 10 mL of  $\text{H}_2\text{O}$ . 8.55 g of  $\text{K}_2\text{CO}_3$  are added, then the mixture is flushed with Argon under stirring for 30 minutes. 260 mg of  $\text{PdCl}_2(\text{PPh}_3)_2$  are added and Argon is flushed for another 30 minutes. Afterwards the mixture is heated to  $80\text{ }^\circ\text{C}$  for 18 h.

After cooling, DME is removed under reduced pressure, to the residue is given 80 mL of  $\text{H}_2\text{O}$  and 40 mL of Ether. The phases are separated, the aqueous phase is washed with Ether, the combined organic phases are dried over  $\text{MgSO}_4$  and the solvent is removed under reduced pressure. The crude product is further purified by column chromatography with cyclohexane to yield 6.15 g (86 %) of a colourless liquid with a distinct odour.

$^1\text{H NMR}$  (300 MHz,  $\text{CDCl}_3$ ):  $\delta = 1.40$  (s, 9H, *t*-Bu-H), 7.21 (m, 1H, Ar-H), 7.38 (m, 4H, Ar-H), 7.47 (dt, 2H, Ar-H), 7.69 (m, 1H, Ar-H)

Synthesis of **2**: 6.15 g (21.4 mmol) of **1** are mixed with 625 mg of Mg and one spatula tip of  $\text{I}_2$  in 50 mL of dry THF and heated under reflux. 4.66 g (18 mmol) 2-bromo-fluorenone are dissolved in 15 mL of dry THF. After 5 h, the Grignard reagent is transferred to the fluorenone solution with a syringe and stirred under reflux for further 17 h. Then a few drops of HCl are given to the solution upon which it clarifies. THF is removed under reduced pressure, the remaining material is dissolved in 50 mL AcOH and 2 mL of 32 % HCl and heated under reflux

for 4 h. The precipitated product is then filtered, washed with hexane and EtOH, and dried to yield 5.04 g (62 %) of a colourless powder.

<sup>1</sup>H NMR (300 MHz, CDCl<sub>3</sub>): δ = 1.20 (s, 9H, *t*-Bu-H), 6.67 (m, 1H, Ar-H), 6.74 (m, 1H, Ar-H), 6.87 (dd, 1H, Ar-H), 7.12 (m, 2H, Ar-H), 7.37 (qd, 2H, Ar-H), 7.48 (m, 2H, Ar-H), 7.77 (m, 4H, Ar-H)

**Synthesis of TCPS:** 570 mg of **2** (1.3 mmol) are mixed with 240 mg 3-cyanophenylboronic acid (1.62 mmol, 1.25 n) in 100 mL of THF. 60 mL 2 M K<sub>2</sub>CO<sub>3</sub> solution are added and the mixture is stirred under Ar stream for 30 minutes. 120 mg of Pd(PPh<sub>3</sub>)<sub>4</sub> are added and the mixture is stirred under Ar for another 30 minutes and subsequently heated to reflux for 17 h.

After cooling the mixture is filtrated, the phases are separated, the organic phase is washed with brine, dried over MgSO<sub>4</sub> and the solvent is removed under reduced pressure. The crude product is further purified by column chromatography (cyclohexane / ethyl acetate 5:1) to yield 538 mg (85 %) of an off-white powder.

<sup>1</sup>H NMR (300 MHz, CDCl<sub>3</sub>): δ = 1.19 (s, 9H, *t*-Bu-H), 6.71 (m, 1H, Ar-H), 6.77 (m, 2H, Ar-H), 6.92 (dd, 1H, Ar-H), 7.13 (m, 2H, Ar-H), 7.43 (m, 4H, Ar-H), 7.54 (td, 1H, Ar-H), 7.64 (m, 2H, Ar-H), 7.72 (m, 1H, Ar-H), 7.80 – 7.99 (m, 4H, Ar-H)

**Synthesis of *m*-TPTS:** 4.5 g (10 mmol) of **2** are dissolved in 100 mL Toluene with 1.73 g (12.48 mmol) 3-tertbutylphenyl boronic acid. 60 mL 2M K<sub>2</sub>CO<sub>3</sub> solution are added and the mixture is bubbled with Ar for 30 minutes. 336 mg Pd(PPh<sub>3</sub>)<sub>4</sub> are added and Ar is bubbled for another 30 minutes. The mixture is then stirred at 100 °C for 17 h. After the reaction is complete, the phases are separated and the aqueous phase is washed with toluene. The combined organic phases are dried over MgSO<sub>4</sub> and the solvent is evaporated under reduced pressure. The crude product is the purified via column chromatography (cyclohexane / ethyl acetate 5:1 and 100:1) to yield 2.07 g (41 %) of a white powder.

<sup>1</sup>H NMR (300 MHz, CDCl<sub>3</sub>): δ = 1.19 (s, 9H, *t*-Bu-H), 1.32 (s, 9H, *t*-Bu-H), 6.75 (m, 3H, Ar-H), 6.94 (dd, 1H, Ar-H), 7.10 (m, 2H, Ar-H), 7.18 – 7.48 (m, 7H, Ar-H), 7.64 (dd, 1H, Ar-H), 7.77 – 7.95 (m, 4H, Ar-H)

**Synthesis of **3**:** 3.81 g 2-Iodobromobenzene and 2.14 g of phenyl-*d*5-boronic acid are dissolved in 40 mL of DME and 5 mL of H<sub>2</sub>O. 3.64 g of K<sub>2</sub>CO<sub>3</sub> are added, then the mixture is flushed with Argon under stirring for 30 minutes. 118 mg of PdCl<sub>2</sub>(PPh<sub>3</sub>)<sub>4</sub> are added and Argon is flushed for another 30 minutes. Afterwards the mixture is heated to 80 °C for 5 h.

After cooling, DME is removed under reduced pressure, to the residue is given 50 mL of H<sub>2</sub>O and 30 mL of Ether. The phases are separated, the aqueous phase is washed with Ether, the combined organic phases are dried over MgSO<sub>4</sub> and the solvent is removed under reduced pressure. The crude product is further purified by column chromatography with hexane to yield 2.122 g (68 %) of a colourless liquid with a distinct odour.

<sup>1</sup>H NMR (300 MHz, CDCl<sub>3</sub>): δ = 7.23 (m, 1H, Ar-H), 7.33 – 7.42 (m, 2H, Ar-H), 7.70 (m, 1H, Ar-H).

Synthesis of **4**: 2.2 g of **3** are dissolved in 25 mL of dry THF. 0.271 g of Mg and a spatula tip of I<sub>2</sub> are added. The mixture is stirred under reflux for 3 h. 2.41 g of 2-Bromofluorenone are dissolved in 5 mL dry THF. The Grignard reagent is carefully transferred to the fluorenone solution using a syringe. The mixture is stirred for another 18 hours under reflux.

Afterwards, 2 mL of AcOH are added to the mixture, after which the opaque suspension clears. THF is removed under reduced pressure and to the mixture are added 20 mL of AcOH and 1 mL of HCl (32 %). The mixture is stirred under reflux for another 5 h. After cooling, DCM and water are added, the phases are separated and the aqueous phase is washed twice with DCM. The combined organic phase are dried over MgSO<sub>4</sub> and the solvent is removed under reduced pressure to yield 2.505 g (68 %) of a white solid.

<sup>1</sup>H NMR (300 MHz, CDCl<sub>3</sub>): δ = 6.74 (m, 2H, Ar-H), 6.87 (dd, 1H, Ar-H), 7.15 (dt, 2H, Ar-H), 7.40 (m, 2H, Ar-H), 7.50 (dd, 1H, Ar-H), 7.72 (dd, 1H, Ar-H), 7.85 (m, 2H, Ar-H),

Synthesis of **o-CPS d4** and **m-CPS d4**: The synthetic procedure to obtain both compounds from **4** is according to the undeuterated compounds and can be found elsewhere.<sup>1</sup>

**o-CPS d4**: <sup>1</sup>H NMR (300 MHz, CDCl<sub>3</sub>): δ = 6.80 (m, 2H, Ar-H), 6.87 (dd, 1H, Ar-H), 7.16 (qt, 2H, Ar-H), 7.30 – 7.44 (m, 4H, Ar-H), 7.51 (m, 1H, Ar-H), 7.67 (dd, 2H, Ar-H), 7.89 (m, 2H, Ar-H), 7.98 (dd, 1H, Ar-H)

**m-CPS d4**: <sup>1</sup>H NMR (300 MHz, CDCl<sub>3</sub>): δ = 6.78 (m, 2H, Ar-H), 6.92 (dd, 1H, Ar-H), 7.15 (m, 2H, Ar-H), 7.42 (m, 3H, Ar-H), 7.53 (td, 1H, Ar-H), 7.58 – 7.73 (m, 3H, Ar-H), 7.90 (m, 2H, Ar-H), 7.96 (dd, 1H, Ar-H)

#### References:

1. F. Krohn, C. Neuber, E. A. Rössler and H.-W. Schmidt, *J. Phys. Chem. B.*, 2019, **123**, 10286-10293.

---

## Publication 2

**Systematic differences in the relaxation stretching of polar molecular liquids probed by dielectric vs magnetic resonance and photon correlation spectroscopy**

**T. Körber**, R. Stäglich, C. Gainaru,  
R. Böhmer and E. A. Rössler

*The Journal of Chemical Physics*

**153**, 124510 (2020).

DOI: 10.1063/5.0022155

© 2020 AIP Publishing LLC

# Systematic differences in the relaxation stretching of polar molecular liquids probed by dielectric vs magnetic resonance and photon correlation spectroscopy

Cite as: J. Chem. Phys. 153, 124510 (2020); doi: 10.1063/5.0022155

Submitted: 17 July 2020 • Accepted: 30 August 2020 •

Published Online: 29 September 2020



View Online



Export Citation



CrossMark

Thomas Körber,<sup>1</sup>  Robert Stäglich,<sup>1</sup> Catalin Gainaru,<sup>2</sup>  Roland Böhmer,<sup>2</sup>  and Ernst A. Rössler<sup>1,a)</sup> 

## AFFILIATIONS

<sup>1</sup>Anorganische Chemie III and Nordbayerisches NMR Zentrum, Universität Bayreuth, 95440 Bayreuth, Germany

<sup>2</sup>Fakultät Physik, Technische Universität Dortmund, 44221 Dortmund, Germany

<sup>a)</sup> Author to whom correspondence should be addressed: [ernst.roessler@uni-bayreuth.de](mailto:ernst.roessler@uni-bayreuth.de)

## ABSTRACT

Relaxation spectra of molecular glass formers devoid of secondary relaxation maxima, as measured by dielectric spectroscopy (DS), nuclear magnetic resonance (NMR) relaxometry, photon correlation spectroscopy (PCS), and Fabry–Perot interferometry, are quantitatively compared in terms of the Kohlrausch stretching parameter  $\beta_K$ . For a reliable estimate of  $\beta_K$ , the excess wing contribution has to be included in the spectral analysis. The relaxation stretching probed by PCS and NMR varies only weakly among the liquids ( $\beta_K = 0.58 \pm 0.06$ ). It is similar to that found in DS, provided that the liquid is sufficiently nonpolar (relaxation strength  $\Delta\epsilon \lesssim 6$ ). For larger strengths, larger  $\beta_K^{DS}$  (narrowed relaxation spectra) are found when compared to those reported from NMR and PCS. Frequency–temperature superposition (FTS) holds for PCS and NMR. This is demonstrated by data scaling and, for the few glass formers for which results are available, by the equivalence of the susceptibilities  $\chi_{PCS}''(\omega\tau) \propto \chi_{NMR}''(\tau) \propto \chi_{NMR}''(\omega)$ , i.e., measuring at a constant frequency is equivalent to measuring at a constant temperature or constant correlation time. In this context, a plot of the spin–lattice relaxation rate  $R_1(T)$  as a function of the spin–spin relaxation rate  $R_2(T)$  is suggested to reveal the stretching parameter without the need to perform frequency-dependent investigations. Dielectrically, we identify a trend of increasing deviations from FTS with increasing  $\Delta\epsilon$ . Depending on the technique and glass former, the relative relaxation strength of the excess wing varies, whereas its exponent appears to be method independent for a given substance. For polar liquids, we discuss possible reasons for the discrepancy between the results from PCS and NMR as compared to those from DS.

Published under license by AIP Publishing. <https://doi.org/10.1063/5.0022155>

## I. INTRODUCTION

Starting from temperatures well above the melting point down to the glass transition temperature  $T_g$ , the glass transition in supercooled liquids is studied by a wealth of different techniques. They provide a general picture of how the reorientational or density correlation functions evolve in molecular liquids and other glass formers.<sup>1–8</sup> Salient fingerprints of “glassy dynamics” are as follows: (i) The loss of correlation involves two steps—a decay on the picosecond scale and a final slow decay ( $\alpha$ -process). (ii) The latter decay is nonexponential (stretched)

reflecting a non-Lorentzian spectral density/susceptibility. (iii) The characteristic correlation time  $\tau_\alpha$  follows a super-Arrhenius temperature dependence.

Many attempts were undertaken to establish quantitative relationships among the various parameters that describe the “glassy dynamics.” However, few of these remained clear-cut after the database was successively enlarged over the years by adding more (classes of) liquids, more experimental methods, or other temperatures where comparisons are made. When comparing spectral shapes probed with different techniques, more or less pronounced differences may occur when considering susceptibility (or

compliance) vs modulus functions.<sup>9</sup> The present overview will focus only on susceptibility data.

Scrutinizing structural relaxation data of organic as well as inorganic and polymeric glass formers near  $T_g$ , a trend of the stretching exponent to decrease with the extent of fragility was previously found, with fragility describing the steepness of the logarithm of  $\tau_\alpha$  at  $T_g$  when plotted on a reduced scale  $T_g/T$ .<sup>10</sup> A depolarized light scattering study covering the GHz to THz regime for molecular and ionic liquids did not find a correlation with the stretching parameter.<sup>11</sup> Nielsen *et al.* reviewed dielectric relaxation data and reported on the “prevalence of minimum slopes close to  $-1/2$ , corresponding to approximate square root time dependence of the dielectric relaxation function at short times.”<sup>12</sup> Recently, a rheological survey of viscous liquids with different compositions hinted toward a “generic” viscoelastic compliance signature of the  $\alpha$ -relaxation,<sup>13,14</sup> precluding to seek correlations of the rheological relaxation stretching with other quantities. For glycerol, it was shown that the spectral signature of its nuclear magnetic resonance (NMR) and light scattering susceptibilities display the same “generic” shape as obvious from rheology, but different from what is observed in its dielectric response,<sup>13,14</sup> provoking the question how general this finding may be.

Based on “an exhaustive examination of the molecular dynamics in practically all van der Waals molecular glass formers ever probed by dielectric spectroscopy (DS),” Paluch *et al.* recently established a connection between the dielectric relaxation strength  $\Delta\epsilon$  and the stretching parameter  $\beta_K$  (obtained from a Kohlrausch fit) of the  $\alpha$ -process:<sup>15</sup> For larger  $\Delta\epsilon$ , a smaller degree of stretching, i.e., a higher  $\beta_K$ , was found. This correlation was anticipated by Nielsen *et al.* who stated that “There is a clear tendency that large-strength liquids are more Debye-like.”<sup>12</sup> Paluch *et al.* rationalized their findings by assuming that the interaction between the permanent molecular dipoles, due to its contribution to the intermolecular potential, controls the dynamics of the molecular liquid, “making ... the frequency dispersion of the  $\alpha$ -relaxation narrower.”<sup>15</sup> Accepting that the dipolar interaction plays a relevant role for the relaxation stretching, at least when large molecular dipole moments are involved, such a correlation may also be expected to hold for the relaxation stretching probed by non-dielectric experiments, an issue that will be tested in the present contribution.

Many previous surveys focused on the dielectric relaxation, since, here, the database is largest.<sup>10,12,14,16,17</sup> Neglecting cross-correlation effects among the molecular dipole moments, one may consider that dielectric spectroscopy probes first-rank Legendre polynomial reorientational correlation functions.<sup>18</sup> Yet, it is worthwhile to consider also photon correlation spectroscopy (PCS) and nuclear magnetic resonance (NMR) that probe second-rank correlation functions. Using PCS and NMR, an increasing set of data has recently been accumulated. Assuming reorientational diffusion in molecular liquids, one expects that the relaxation times  $\tau_{PCS}$  or  $\tau_{NMR}$  to be three times shorter than  $\tau_{DS}$ ,<sup>18,19</sup> a relationship that was never convincingly documented.<sup>20</sup> According to the results from multidimensional NMR, the limit of rotational diffusion can be excluded for viscous liquids.<sup>19</sup> Instead, a mixture of large- and small-angle jumps is typical, which may explain why the experimentally probed time scales  $\tau_{PCS}$  or  $\tau_{NMR}$  and  $\tau_{DS}$  are often so similar.

Counter to a widespread belief, it is not straightforward to determine the extent of the  $\alpha$ -relaxation stretching unambiguously.

Many studies focus on the stretching at low temperatures, preferably near  $T_g$ . However, the high-frequency flank of the main relaxation peak is not described by a well-defined power law. Instead, secondary features such as an excess wing and/or a  $\beta$ -relaxation show up, and any quantitative analysis of the spectral shape depends on the chosen model and on the considered fitting range.<sup>16,17</sup> The high-frequency flank of the  $\alpha$ -relaxation is additionally superimposed by faster “microscopic” dynamics.<sup>21–23</sup> In other words, a simple comparison of the  $\alpha$ -relaxation shape as measured by different techniques at different temperatures is prone to generate misleading conclusions.

PCS has been used for a long time to explore the long-time behavior of the reorientational correlation function near  $T_g$ .<sup>24–26</sup> Recent efforts extend the time resolution of the PCS technique to cover also secondary relaxations.<sup>8,27,28</sup> Furthermore, studies exploiting the optical Kerr effect (OKE) allow access to the reorientational correlation function in the picosecond to nanosecond regime.<sup>2,29,30</sup> Both the PCS and the OKE techniques probe reorientational dynamics via rank-two correlation functions.<sup>31,32</sup> When comparing the various relaxation stretchings, one has to distinguish not only correlation functions of different rank but also collective vs single particle fluctuations.<sup>33</sup> Whereas  $^2\text{H}$  and  $^{31}\text{P}$  NMR relaxation data usually reflect single-particle fluctuations, this is possibly not the case for PCS<sup>34</sup> and clearly not for DS.<sup>33</sup> Recently, Gabriel *et al.* suggested how to disentangle self-correlation from cross-correlation contributions in the dielectric spectra of glycerol.<sup>35</sup>

All in all, it remains controversial whether the relaxation spectra of supercooled liquids display generic shapes or not and whether the answer to this question depends on the employed experimental technique. Here, we attempt a systematic evaluation of the spectral shape of the main ( $\alpha$ -) relaxation as provided by the three techniques DS, PCS, and NMR that probe reorientational dynamics. From the beginning, we emphasize the preliminary character of the present survey, since the database is still limited. We focus on “type A glass formers,”<sup>36</sup> i.e., on liquids with dielectric spectra that do not display a discernible secondary relaxation peak ( $\beta$ -relaxation) at temperatures above  $T_g$ . In addition to the  $\alpha$ -relaxation peak, their dielectric loss spectra typically exhibit an excess wing,<sup>8,37</sup> a feature that is identified by PCS,<sup>8</sup> OKE,<sup>30</sup> and NMR<sup>38,39</sup> as well. Our survey will indicate that in polar molecular liquids, DS probes a reduced stretching when compared to PCS or NMR relaxometry, both yielding similar  $\beta_K$  values. Whether the degree of stretching is temperature dependent or not has long been discussed under the headings time-temperature superposition or frequency-temperature superposition (FTS).<sup>6,9</sup> In this context, our analysis suggests that FTS applies well for the PCS and NMR susceptibilities, but not generally for DS. Based on NMR spin relaxation data recorded at a *single* frequency, we suggest a simple FTS-based approach that allows one to determine stretching parameters in supercooled liquids.

## II. RELAXATION STRENGTH AND STRETCHING

In Fig. 1, we present dielectric-spectra-based stretching parameters  $\beta_K$  obtained from a single Kohlrausch fit (applied in a frequency range of one decade around the relaxation peak) of various

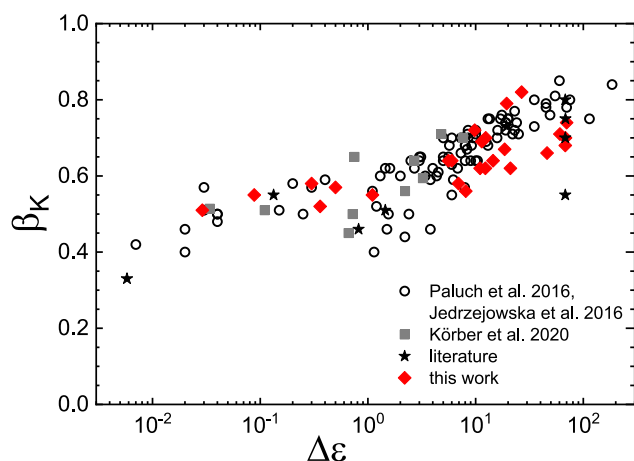


**FIG. 1.** Stretching parameter  $\beta_K$  as obtained from a single Kohlrausch fit of the  $\alpha$ -relaxation peak plotted against the overall dielectric relaxation strength  $\Delta\epsilon$  at  $T_g$ . For propylene glycol and for glycerol, several literature values  $\beta_K$  are shown. Data from the work of Paluch *et al.*,<sup>15</sup> Jedrzejowska *et al.*,<sup>40</sup> and Körber *et al.*<sup>43</sup> are shown. Further literature data are included (stars, cf. Table I).

glass formers measured at  $T_g$  vs the corresponding dielectric relaxation strength  $\Delta\epsilon$ . Figure 1 is similar to a figure previously presented by Paluch *et al.*,<sup>15</sup> but it includes additional data and presents the results on a logarithmic  $\Delta\epsilon$  scale to put emphasis also on the low-polarity regime. In Fig. 1, the data from Paluch *et al.* are shown as open circles,<sup>15,40</sup> further literature data such as for decalin<sup>41</sup> or ibuprofen<sup>42</sup> as stars, our data for *o*-terphenyl, glycerol, and tristyrene, and data for systems shown by Paluch *et al.* but analyzed on the basis of our own measurements as red diamonds (detailed references are included in Table I). Following the work of Paluch *et al.*, in Fig. 1, we also include several type B glass formers. Furthermore, data from a recently presented collection of high- $T_g$  glass formers are added (gray squares).<sup>43</sup> The trend of the previous data by Paluch *et al.*<sup>15</sup> is confirmed: The larger the relaxation strength, the larger is the stretching parameter  $\beta_K$ .

Close to  $T_g$ , the analysis of the dielectric spectra is often affected by the presence of secondary relaxations (like an excess wing and/or a  $\beta$ -relaxation) on the high-frequency flank of the  $\alpha$ -relaxation peak. These features can impede a precise determination of the stretching parameter when applying a single Kohlrausch fit. For example, for some polar liquids for which data are presented in Fig. 1, we find systematically lower  $\beta_K$  values than the work of Paluch *et al.* Actually, in the literature (see Table I) for the stretching parameters of glycerol, one finds values ranging from 0.55 to 0.80 and for propylene glycol from 0.7 to 0.8, although the measured spectra are very similar. The reason for this discrepancy is to be sought in the application of different fit strategies: The more one extends the fitting range toward high frequencies, the lower is the resulting  $\beta_K$ . In any case, in type A liquids, the parameterization of the  $\alpha$ -relaxation, without taking into account the presence of an excess wing, is prone to being unreliable.

### III. PHENOMENOLOGICAL DESCRIPTION OF THE DIELECTRIC SPECTRA

While the nature of the excess wing is still debated,<sup>44–46</sup> the so-called type A glass formers constitute a group of glass formers which exhibit a relatively simple and rather similar dielectric responses near  $T_g$ .<sup>36</sup> Their spectral features were analyzed, e.g., by Nagel and co-workers,<sup>47</sup> who suggested a scaling of the dielectric response that, however, works only approximately in terms of a spectral density representation.<sup>48–50</sup> Later on, the exponent that describes the excess wing using  $\epsilon''(\omega) \propto \omega^{-\gamma}$  was reported to be close to  $\gamma = 0.2$ , while the (apparent) stretching parameter of the  $\alpha$ -process appeared to vary for temperatures close to  $T_g$ .<sup>51</sup> Turning to temperatures well below  $T_g$  for which the  $\alpha$ -relaxation peak has shifted out of the accessible frequency window, the dielectric spectrum in type A glass formers exhibits a power-law behavior  $\epsilon''(\omega) \propto \omega^{-\gamma}$  with a temperature independent exponent  $\gamma$  in the range 0.17–0.23 and an amplitude featuring an exponential temperature dependence.<sup>52</sup>

Figure 2 presents dielectric loss spectra of 15 glass formers investigated close to  $T_g$  by the Bayreuth group, with new *o*-terphenyl data measured using an Andeen-Hagerling 2700A high-precision bridge (HPB). All spectra are scaled in a way to achieve best overlap at frequencies at and below the relaxation maximum. To extend the frequency range, master curves were constructed for a few liquids,<sup>53</sup> including data for temperatures close to  $T_g$ . Clearly, two frequency regions can be distinguished: The region of the  $\alpha$ -relaxation peak and, at high frequencies, that of the excess wing. Even some type B glass formers [e.g., *m*-fluoroaniline (*m*-FAN)]<sup>36</sup> appear to follow a similar relaxation pattern although

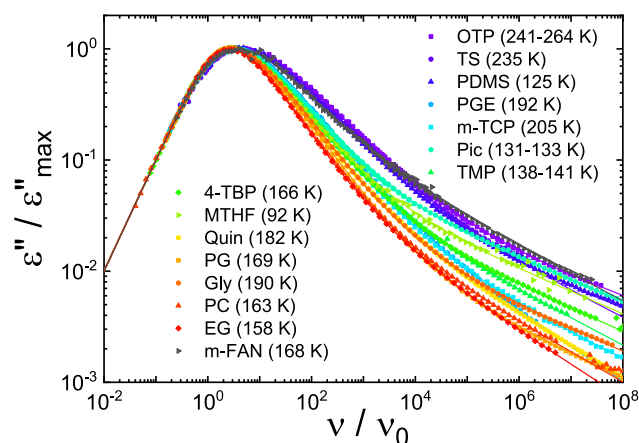


**FIG. 2.** Dielectric spectra of type A glass formers measured close to  $T_g$  that display an excess wing in addition to the main relaxation peak are interpolated by a sum of a Kohlrausch (main relaxation) and a Cole–Davidson (excess wing) susceptibility. Data are represented as symbols and fits as lines. Measurement temperatures are given. If a temperature range is given, the data reflect master curves. One type B system (*m*-FAN, black) is shown as an example for a clearly visible excess wing in addition to a  $\beta$  process (the latter not visible in the presently considered frequency range). See Table I for references and definitions of the acronyms.

**TABLE I.** Glass transition temperature  $T_g$ , dielectric relaxation strength  $\Delta\epsilon$ , stretching parameter  $\beta_K$ , and excess wing exponent  $\gamma$  as obtained using different techniques for various glass formers determined at  $T \approx T_g$ . The table is ordered according to increasing  $\Delta\epsilon$ . Values marked with “(t)” are from analyses in the time domain, while “( $\omega$ )” refers to analyses in the frequency domain. For the liquids analyzed in the present contribution, the reference for the used data is given in the first column if they have been published before. Values from the literature are directly referenced (cf. Figs. 1 and 3). The systems marked with an asterisk (\*) are type B liquids analyzed for Fig. 1.

Glass former	$T_g$ (K)	$\Delta\epsilon$	$\beta_K^{DS}$ single	$\beta_K^{DS}$ composite	$\gamma_{DS}$	$\beta_K^{PCS}$ (t)	$\beta_K^{NMR}$ ( $\omega$ )	$\beta_K^{NMR}$ R <sub>1</sub> (R <sub>2</sub> )
<i>cis</i> -/ <i>trans</i> -decalin (Dec)	135	0.0058 <sup>41</sup>	0.33 <sup>41</sup>					
<i>o</i> -terphenyl (OTP)	246	0.03	0.51	0.55	0.17	0.61 0.59 ( $\omega$ ) 0.57 <sup>54</sup> 0.55 <sup>55</sup> 0.55 <sup>57</sup>	0.62	0.64
Tri-naphthyl benzene (TNB)	345	0.04 <sup>56</sup>	0.50 <sup>56</sup>					
Tristyrene (TS) <sup>58</sup>	233	0.09	0.55	0.57	0.23			
Ibuprofen (Ibu) <sup>42</sup>	225	0.133	0.55 <sup>42</sup>					0.62
Iso-propylene benzene ( <i>i</i> -PB)*	127	0.3	0.58					
Toluene (Tol) <sup>43</sup> *	117	0.36	0.52					0.52
poly(dimethylsiloxane) 311 (PDMS) <sup>58</sup>	125	0.5	0.57	0.57	0.18			
Bis-cresol-C-dimethylether (BKDE)	261	0.82 <sup>59</sup>	0.46 <sup>59</sup>			0.49 <sup>59</sup>		
Triphenyl phosphate (TPhP) <sup>46</sup> *	204	1.1	0.55			0.53 <sup>59</sup> 0.55 <sup>60</sup> 0.54 <sup>61</sup>		
Bis-phenol-C-dimethylether (BMPC)	240	1.45 <sup>59</sup>	0.51 <sup>59</sup>					
$\alpha$ -phenyl <i>o</i> -cresol	219	3.4 <sup>12</sup>	0.6 <sup>12</sup>					
<i>m</i> -tricresyl phosphate ( <i>m</i> -TCP) <sup>8,17</sup>	206	5.6	0.64	0.66	0.23	0.55	0.61 0.56(t)	0.61
Salol (Sal) <sup>62,63</sup>	220	6	0.64			0.64 <sup>64</sup> 0.6 <sup>25</sup> 0.66 <sup>65</sup> 0.68 <sup>65</sup> 0.6		0.62
Dimethyl phthalate (DMP) <sup>66</sup>	193	6.2 <sup>15</sup>	0.59 <sup>15</sup>					
3,3',4,4'-benzophenonetetracarboxylic dianhydride (2-PC) <sup>43</sup> *	330	6.93	0.58					
<i>m</i> -toluidine ( <i>m</i> -Tol)*	187	8.1	0.56					
Quinaldine (Quin) <sup>67</sup>	180	9.8	0.72	0.72	0.28			
Diglycol ether of bisphenol (DGEBA) <sup>46</sup>	253	11	0.62			0.55 <sup>68</sup>		
4-Tert-butyl pyridine (4TBP) <sup>17</sup>	166	11.4	0.69	0.69	0.2			
Phenyl glycidyl ether (PGE)	193	12.3	0.62	0.65	0.29			
Felodipine (Fel) <sup>43</sup> *	313	12.4	0.7					
2-Picoline (Pic) <sup>62</sup>	130	14.5	0.64	0.68	0.19	0.58 <sup>64</sup> 0.55 <sup>26</sup>		
Phenolphthalein dimethylether (PDE)	294	17.5 <sup>15</sup>	0.76 <sup>15</sup>					
Methyl tetrahydrofuran (MTHF) <sup>66,69</sup>	91	18.6	0.67	0.7	0.2	0.6	0.58	0.57
Tributyl phosphate (TBP) <sup>70,71</sup> *	140	19.4	0.79					
<i>m</i> -fluoro aniline ( <i>m</i> -FAN) <sup>16</sup> *	172	21	0.62	0.63	0.24			
Tripropyl phosphate (TPP) <sup>72,73</sup> *	134	26.7	0.82					
Trimethyl phosphate (TMP) <sup>70</sup>	137	46	0.66	0.69	0.24			
Ethylene glycol (EG)	155	60.6	0.71	0.77	0.3			
Glycerol (Gly) <sup>16,35</sup>	186	67.9	0.68 0.55 <sup>74</sup> 0.7 <sup>75</sup> 0.8 <sup>76</sup>	0.69	0.20	0.52 0.58 ( $\omega$ )	0.64	0.64
Propylene glycol (PG) <sup>17</sup>	168	68.2	0.7 0.75 <sup>76</sup> 0.81 <sup>15</sup>	0.71	0.21			
Propylene carbonate (PC) <sup>16</sup>	158	70	0.74	0.75	0.27			

above  $T_g$  they exhibit a  $\beta$ -relaxation peak in addition to an excess wing.

To describe the spectra shown in Fig. 2, which apart from the main relaxation also display an excess wing, we employed an approach inspired by OKE experiments.<sup>30,46</sup> There, two power-law regimes were identified: The one at long times (corresponding to the high-frequency part of the  $\alpha$ -relaxation) refers to the von Schweidler law<sup>23</sup> and the second one (called “intermediate power law”<sup>30</sup>) to the excess wing.<sup>8,37,46</sup> In the susceptibility representation, this leads to a sum of two Cole–Davidson (CD) functions.<sup>18</sup> To analyze the present dielectric spectra, instead of a (low-frequency) CD function, a Kohlrausch function with a stretching parameter  $\beta_K$  is applied. For the dielectric data, it yields better fits. Subsequently, we will call this ansatz “composite fit.” From the lines in Fig. 2, one recognizes that this approach parameterizes the data very satisfactorily. The resulting exponents are listed in Table I. When describing the relaxation peak in terms of a single Kohlrausch function, the stretching parameter depends on the fit interval. In contrast, the present description provides fit-interval-independent  $\alpha$ -stretching parameters. Of course, the validity of the presently chosen phenomenological approach is debatable as long as the nature of the main relaxation probed by dielectric spectroscopy is not fully understood (see Sec. VI, below).

Now, we return to the DS-based observation<sup>12,15</sup> that “large-strength liquids are more Debye-like” and plot the stretching parameters as obtained from the composite fits against the relaxation strength  $\Delta\epsilon$  in Fig. 3. One recognizes that the dielectric stretching parameters from the present analyses (diamonds) are slightly larger than those determined from a single Kohlrausch fit (crosses), as done by Paluch *et al.*<sup>15</sup> More importantly, we find that the trend that  $\beta_K$  increases with increasing  $\Delta\epsilon$  sets in only for relaxation strengths above  $\Delta\epsilon \cong 6$ , a feature already pointed out in Ref. 14.

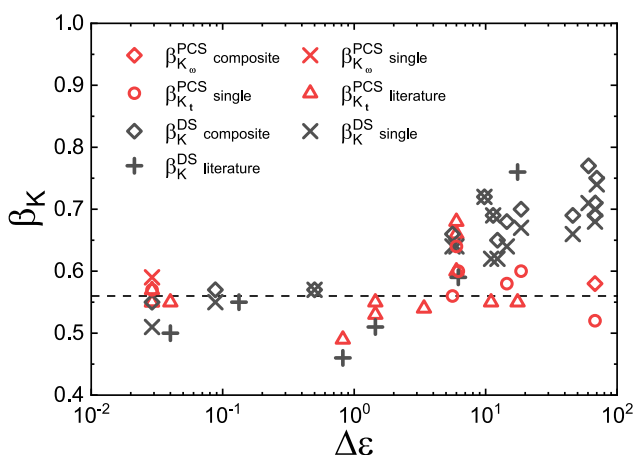


**FIG. 3.** Stretching parameter  $\beta_K^{DS}$  (black) from a single Kohlrausch fit (crosses) as well as from a composite fit (diamonds) of dielectric spectra vs the relaxation strength  $\Delta\epsilon$  for all investigated type A systems. Stretching parameters  $\beta_K^{PCS}$  (red) obtained from PCS are added (subscript t: from time domain data and subscript  $\omega$ : from frequency domain data). Additional PCS literature values (red triangles) and corresponding DS values (plusses) are included (for detailed references, see Table I).

Below  $\Delta\epsilon \cong 6$ , significant scattering is observed for  $\beta_K$ , but no clear-cut trend. To rationalize the low value for decalin,  $\beta_K = 0.33$  (with  $\Delta\epsilon = 0.006$ ), shown in Fig. 1 and not included in Fig. 3, we note that a *cis/trans* mixture was studied, which is possibly more dynamically heterogeneous than neat liquids.<sup>41</sup> As will be discussed next, Fig. 3 also contains  $\beta_K$  data from PCS that are plotted vs the corresponding dielectric relaxation strength taken from the literature (see Table I).

#### IV. COMPARING THE RELAXATION SPECTRA AS OBTAINED BY DIFFERENT TECHNIQUES

It is interesting to compare the dielectric stretching parameters with those provided by PCS because the latter technique allows us to probe the reorientational correlation function close to  $T_g$  directly. Figure 3 includes the PCS results from the literature as well as from our group (see Table I), but the database is still small. Most PCS studies observe and fit only the stretched long-time decay, and thus, one is insensitive to possible excess wing contributions. Corresponding data are marked with “time domain” (open circles and triangles in Fig. 3). Clearly, from Fig. 3, a trend of  $\beta_K^{PCS}$  with the relaxation strength  $\Delta\epsilon$  is not recognizable: The parameter  $\beta_K^{PCS}$  varies within the interval  $0.56 \pm 0.05$  (horizontal line), except for salol and BKDE that lie above and below this interval, respectively. Its mean is close to the dielectric  $\beta_K$  values obtained for liquids with  $\Delta\epsilon \leq 6$ . The polar liquid glycerol is particularly interesting: PCS reports  $\beta_K^{PCS} = 0.52$ – $0.58$ , whereas dielectrically, one finds  $\beta_K^{DS} = 0.69$  (by the composite fit).

In Fig. 4(a), we compare the susceptibility spectra of glycerol as obtained by DS,<sup>16</sup> double-monochromator Fabry–Perot interferometry (FPI),<sup>77</sup> and PCS taken from literature (after Fourier transformation).<sup>35</sup> For  $\omega\tau > 1$ , PCS and FPI reveal similar spectral shapes, but that from DS is narrower. Yet, the exponent describing the excess wings is similar. The FPI data were measured at much higher temperatures than the PCS data. Their good agreement indicates that FTS applies for the light scattering methods, but not for DS. Here, some narrowing is observed at high temperatures (dark blue line at 288 K) even though, due to the limited dynamic range of our dielectric instrument in the MHz-to-GHz range, the high-frequency flank is not fully resolved. Figure 4(a) also includes  $^1\text{H}$ <sup>38</sup> and  $^2\text{H}$  field cycling (FC)<sup>78</sup> as well as  $^2\text{H}$  NMR single-frequency data.<sup>79</sup> Their representation in terms of a master curve assumes FTS to be valid; the origin of the corresponding datasets is explained in detail in Sec. V below. At high frequencies, the NMR data closely traces those from PCS, including the excess wing contribution. The  $^1\text{H}$  FC NMR relaxation spectrum displays a low-frequency shoulder, which is not seen in the other relaxation data ( $\omega\tau < 1$ ). This is a peculiarity of  $^1\text{H}$  NMR relaxation and not found in  $^2\text{H}$  NMR (black squares and magenta stars): Due to an intermolecular contribution to the magnetic dipole–dipole interaction dominating the proton spin–lattice relaxation, in addition to rotational dynamics, it also probes the translational dynamics.<sup>80,81</sup> The agreement of PCS and  $^2\text{H}$  NMR single-frequency data is remarkable, as it suggests that FTS works well for PCS and for NMR. We will come back to this point in Sec. V below.

A similar situation is found for *m*-TCP, for which Fig. 4(b) presents time domain data. The decay curves from  $^{31}\text{P}$  NMR

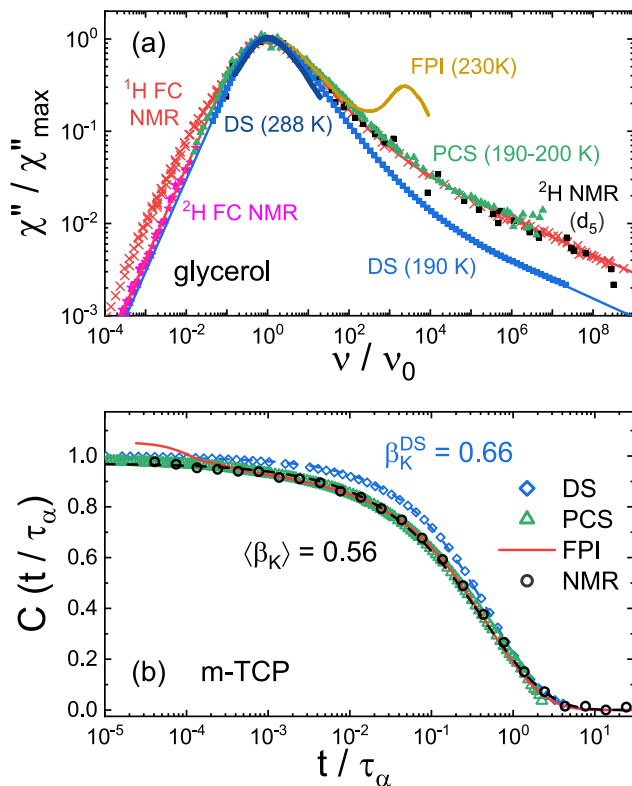


**FIG. 4.** (a) Reorientational susceptibility of glycerol as obtained from DS (blue points and dark blue line),<sup>16</sup> PCS (green triangles: master curve 190 K–200 K),<sup>35</sup> FPI (brown line),<sup>77</sup>  $^1\text{H}$  FC NMR (red crosses: master curve 191 K–360 K),<sup>38</sup>  $^2\text{H}$  FC NMR (magenta stars: master curve 300 K–400 K),<sup>78</sup> and  $^2\text{H}$  single-frequency relaxation (black squares).<sup>79</sup> Composite fits are given for the data from  $^1\text{H}$  FC NMR (red line) and DS (blue line). (b) Reorientational correlation function of *m*-TCP as probed by DS ( $T = 209$  K),<sup>72</sup> PCS ( $T = 210$  K),<sup>8</sup> FPI ( $T = 290$  K),<sup>8</sup> and  $^{31}\text{P}$  NMR stimulated echo ( $T = 209$  K).<sup>82</sup> Except for DS (blue dashed line), the degree of stretching agrees among the various techniques (black dashed line).

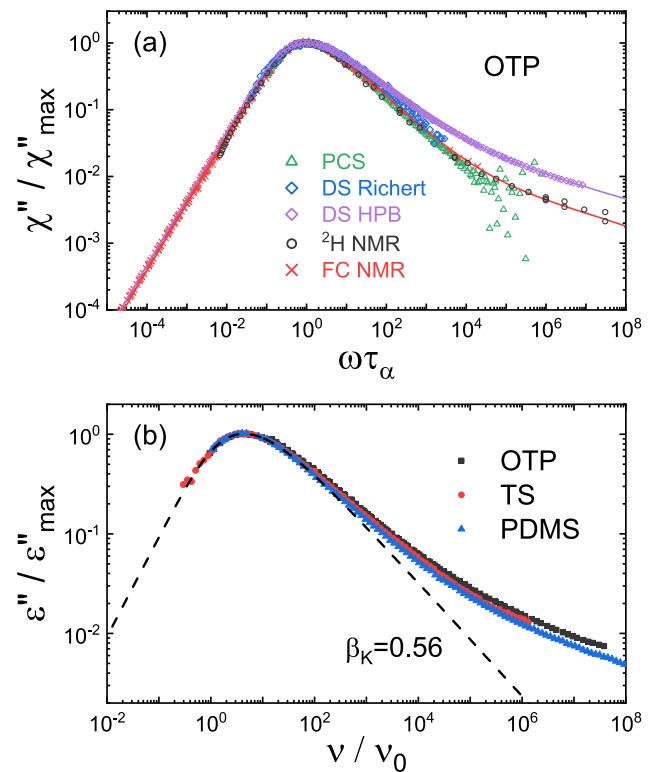


**FIG. 5.** (a) Reorientational susceptibility of *o*-terphenyl as probed by PCS (green triangles),<sup>84</sup> DS [blue diamonds:<sup>83</sup> master curve 248 K–284 K and violet diamonds: high-precision bridge (HPB) master curve 241 K–264 K; present work],  $^1\text{H}$  FC NMR relaxometry (red crosses: master curve 263 K–393 K),<sup>87</sup> and  $^2\text{H}$  NMR single-frequency relaxation (55.2 MHz, black circles).<sup>86</sup> Composite fits are shown for the FC NMR data (red line) and HPB dielectric data (violet line). (b) Scaled dielectric spectra of the three investigated glass formers with the lowest relaxation strengths *o*-terphenyl (OTP), tristyrene (TS),<sup>58</sup> and low-molecular weight PDMS.<sup>58</sup> An average Kohlrausch spectral contribution is shown with an exponent obtained from a composite fit (dashed line).

stimulated-echo experiments<sup>82</sup> (such as PCS providing direct access to the reorientational correlation function) from FPI (after conversion to the time domain) and from PCS measurements<sup>8</sup> are all essentially the same, whereas the DS curve is less stretched.<sup>72</sup> Again, FTS applies for the PCS ( $T = 210$  K) and the FPI ( $T = 290$  K)<sup>8</sup> decays.

As mentioned when discussing Fig. 3, for  $\Delta\epsilon \leq 6$ , the stretching parameters revealed by DS and by PCS resemble each other and are independent of  $\Delta\epsilon$ . This observation suggests that for nonpolar liquids, the relaxation spectra probed using the different techniques essentially agree with each other. This conjecture is directly tested in Fig. 5(a), which displays the susceptibility of *o*-terphenyl, a liquid with a very low molecular dipole moment: We include DS data from the present work and from that from the work of Richert,<sup>83</sup> as well as PCS data from Ref. 84. The DS master curve produced from the data by Richert, not reaching the excess wing

regime, agrees well with our data close to the relaxation peak. Whereas near the peak the DS and PCS spectra are similar, the dielectric spectrum exhibits a relatively strong excess wing. The latter is not discernible in the PCS spectra and is probably below the accessed resolution. Figure 5(a) also contains  $^1\text{H}$  FC NMR<sup>85</sup> and  $^2\text{H}$  NMR single-frequency data.<sup>86</sup> Again, all NMR and PCS results closely follow the same curve. The  $^2\text{H}$  NMR relaxation even displays an excess wing that, compatible with the DS spectrum, is rather low in amplitude. For *o*-terphenyl, a composite fit to the DS and the  $^2\text{H}$  NMR data yields  $\beta_K = 0.55 \pm 0.02$  and  $\beta_K = 0.62 \pm 0.02$ , respectively.

In Fig. 5(b), we present the dielectric spectra of the three investigated liquids with the lowest relaxation strengths for which data from several techniques are available, i.e., *o*-terphenyl ( $\Delta\epsilon = 0.03$ ), tristyrene ( $\Delta\epsilon = 0.09$ ), and PDMS-311 ( $\Delta\epsilon = 0.5$ ). The stretching parameters obtained from a composite fit to the

spectra are all very similar,  $\beta_K = 0.56 \pm 0.02$ . Moreover, the relative relaxation strength of the excess wing is also similar, although obviously not identical. These similarities suggest that for nonpolar liquids, the stretching parameter reaches a certain limit.

Finally, in Fig. 6, we compare the susceptibility spectra of glycerol, *m*-TCP, and *o*-terphenyl collected using PCS and NMR and for *o*-terphenyl also using DS. Following our preceding arguments, all of these spectra are expected to exhibit a similar relaxation peak shape. For *m*-TCP,  $^1\text{H}$  FC relaxometry<sup>88</sup> and  $^{31}\text{P}$  NMR single-frequency relaxation data are included as well.<sup>82</sup> Figure 6 is quite crowded and the PCS spectra (obtained after Fourier transformation) display strong scatter at high frequencies. Nevertheless, one recognizes that among these materials, the width of the  $\alpha$ -relaxation peak that is revealed by the different methods varies much less than the corresponding dielectric spectra. Yet, the relative amplitude of the (weak) excess wing appears to be method and system dependent (for *o*-terphenyl,  $^2\text{H}$  NMR reveals a weaker excess wing than DS), whereas the high-frequency exponent is practically the same and close to 0.2.

Figure 4 suggests that for glycerol (a polar liquid), FTS is applicable for the data from light scattering and from NMR, but not for the dielectric relaxation data. Based on dielectric spectra recorded in a large temperature interval, the validity of FTS is tested in Fig. 7(a) for several glass formers. For all substances, a systematic narrowing is observed as the temperature increases. However, this effect is weakest for the nonpolar liquid tristyrene. In contrast to these dielectric data, the PCS data for OTP, MTHF, and *m*-TCP that are shown in Fig. 7(b) are compatible with the validity of FTS.<sup>8,84,88</sup>

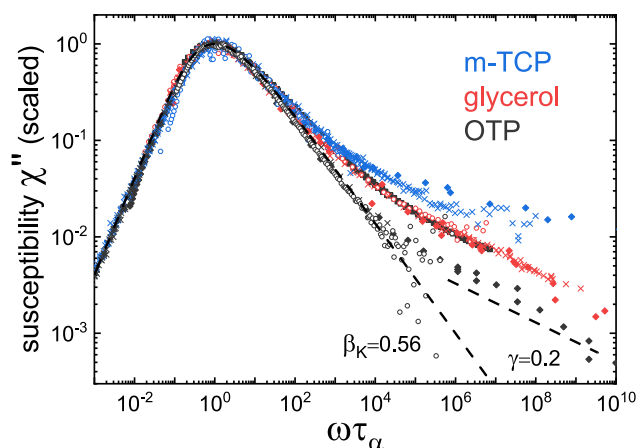


**FIG. 6.** Rotational susceptibility of *m*-TCP (blue) as obtained from PCS (open circles),<sup>8</sup> FC  $^1\text{H}$  NMR relaxometry (plus symbols: master curve 205 K–330 K),<sup>88</sup> and  $^{31}\text{P}$  NMR single-frequency spin relaxation (diamonds: 121.5 MHz).<sup>82</sup> Data for glycerol (red) from PCS (open circles),<sup>35</sup> FC  $^1\text{H}$  relaxometry (crosses),<sup>38</sup> and  $^2\text{H}$  single-frequency spin relaxation (diamonds, 55.2 MHz).<sup>79</sup> Data for *o*-terphenyl (black) from PCS (open circles),<sup>84</sup> FC  $^1\text{H}$  NMR relaxometry (crosses),<sup>87</sup>  $^2\text{H}$  single-frequency spin relaxation (diamonds, 55.2 MHz),<sup>86</sup> and DS (squares). The low-relaxation-strength limit of the  $\alpha$  process from DS is shown as the dashed line ( $\beta_K = 0.56$ ).

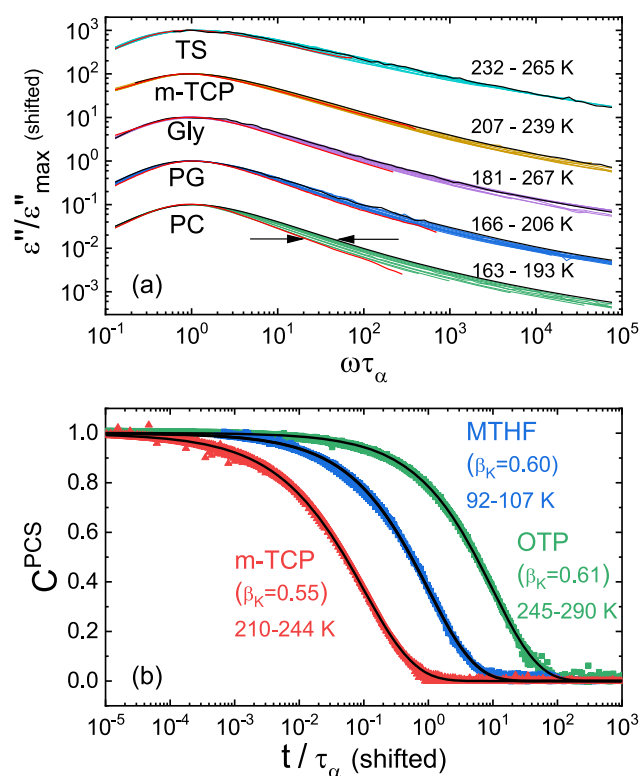


**FIG. 7.** (a) The scaled loss spectra of TS,<sup>58</sup> *m*-TCP,<sup>17</sup> Gly,<sup>16</sup> PG,<sup>17</sup> and PC<sup>16</sup> demonstrate that FTS is not generally applicable for dielectric data. Highest temperatures are marked in red and the lowest temperature in black. For PC, the arrows indicate a  $\omega\tau_\alpha$  variation by a factor of 2. The data are successively shifted after scaling by one decade in amplitude starting with the lowest polarity (TS) and ending with the highest polarity (PC). (b) Master curves of rank-two correlation functions  $C^{\text{PCS}}$  obtained for *m*-TCP,<sup>9</sup> MTHF,<sup>88</sup> and OTP<sup>24</sup> demonstrate the applicability of FTS for these PCS decay curves. For better visualization, the data of *m*-TCP are shifted by one decade to shorter times and the data of OTP by one decade to longer times.

## V. NMR RELAXATION SPECTRA

In Secs. II–IV, we exploited NMR-based susceptibilities and found that they essentially agree with those obtained using PCS. At first glance, this finding is not surprising, as both techniques monitor rank-two reorientational correlation functions—in contrast to DS that probes rank-one correlation functions. Prior to a detailed comparison with the rank-two quantities obtained from FC NMR, it is worthwhile to briefly outline the approach used for arriving at susceptibility master curves on the basis of this technique. The FC method<sup>89–93</sup> measures the frequency dependence of the  $^1\text{H}$  spin-lattice relaxation rate  $R_1(\omega)$  in a frequency range 10 kHz–30 MHz, which reflects the spectral density at the Larmor frequency—see the Bloembergen–Purcell–Pound (BPP)<sup>94</sup> type equations that are presented in Table II (Appendix A). The rate  $R_1(\omega)$  is transformed to the susceptibility representation using  $\chi''_{\text{NMR}}(\omega) \equiv \omega R_1(\omega)$ .<sup>90,93,95,96</sup> To enlarge the effective frequency window, we constructed master curves  $\chi''_{\text{NMR}}(\omega\tau_\alpha)$  by overlapping data recorded in a large temperature interval. The master curve construction was controlled by

comparing the resulting relaxation times with those from other techniques, preferably PCS and FPI. The  $^1\text{H}$  FC NMR (master) spectra were found to agree well with PCS spectra obtained at a single temperature close to  $T_g$  [see Figs. 4(a), 5(a), and 6].

Usually, however,  $R_1$  is measured not as a function of frequency but as a function of temperature for a single or only few frequencies. Still, one can derive the susceptibility function provided that FTS applies. The latter implies that the susceptibility can be expressed in terms of a temperature-independent function  $\chi''$  of a temperature-dependent argument  $\omega\tau_\alpha$ . Thus, it suffices to measure  $R_1(T)$  at a single frequency and, if  $\tau_\alpha(T)$  is known, one still obtains the susceptibility function. This was done for glycerol ( $^2\text{H}$ ),<sup>79</sup>  $m$ -TCP ( $^{31}\text{P}$ ),<sup>82</sup> and OTP ( $^2\text{H}$ ),<sup>86</sup> taking time constant from Refs. 8, 77, and 84, respectively. The resulting relaxation spectra follow the spectra from PCS and  $^1\text{H}$  FC NMR. The identical shapes of the  $\omega R_1(\tau)$  and the  $\omega R_1(\omega)$  spectra clearly confirm that FTS is applicable for the NMR data.

In order to demonstrate directly that FTS applies and that NMR relaxometry and PCS probe the same susceptibility, in Fig. 8, we plot  $R_1/R_1^{\text{max}}$  vs  $\tau_\alpha/\tau_{\text{max}}$  and the corresponding normalized spin-spin relaxation rate  $R_2/R_1^{\text{max}}$  vs  $\tau_\alpha/\tau_{\text{max}}$  for glycerol,  $m$ -TCP, and  $o$ -terphenyl. Here, the variables  $R_1^{\text{max}}$ , denoting the rate maximum, and  $\tau_{\text{max}}$ , the corresponding time constant, are used to “scale out” differences in NMR coupling constants and Larmor frequencies. When introducing the susceptibility derived from the  $^1\text{H}$  FC data into the  $^2\text{H}$  or  $^{31}\text{P}$  NMR relaxation equation connecting the relaxation rates to the spectral density (see Table II, Appendix A) without any fit parameter, the single-frequency data are reproduced perfectly. For  $o$ -terphenyl,  $R_1(\tau_\alpha)$  is reproduced by both the  $^1\text{H}$  susceptibility and the PCS susceptibility derived from Fig. 5(a). For all three glass formers, one notes a high similarity of  $R_1(\tau_\alpha)$  close to the maximum, indicating very similar stretching parameters, yet different excess wing contributions. The difference in  $R_2$  between  $m$ -TCP

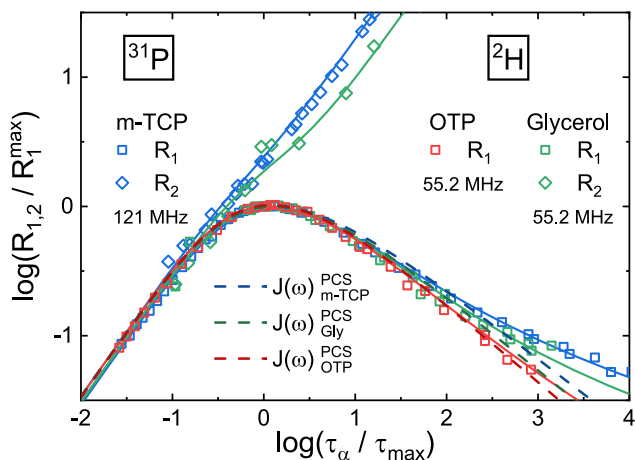


**FIG. 8.** Spin-lattice relaxation rate  $R_1$  and spin-spin relaxation rate  $R_2$  of glycerol<sup>79</sup> and  $m$ -TCP<sup>82</sup> and  $R_1$  of  $o$ -terphenyl<sup>86</sup> as a function of the correlation time  $\tau_\alpha$  as obtained from the literature.<sup>8,77,84</sup> The interpolations using the corresponding spectral density derived from  $^1\text{H}$  FC NMR relaxometry and from PCS are shown as solid and dashed lines, respectively.

and glycerol arises because different interactions dominate in the two substances (cf. Table II, Appendix A).

Given the validity of FTS, NMR offers even another means to determine the susceptibility function:  $R_1(\omega)$  depends on the shape of the spectral density  $J(\omega)$  (or of the susceptibility) and thus is strongly frequency dependent for  $\omega\tau_\alpha \gg 1$ . Conversely,  $R_2(\omega)$  depends essentially only on  $J(0)$ ,<sup>97</sup> i.e., it is independent of the frequency and depends only on the time constant  $\tau_\alpha$ . Hence, a plot of  $R_1$  vs  $R_2$  is expected to provide the essential features of the susceptibility function. To ensure comparability when considering different NMR nuclei and Larmor frequencies, the data are rescaled by the maximum  $R_1^{\text{max}}$  of  $R_1$  or by the rate  $R_2$  at  $R_1^{\text{max}}$ . Technical details regarding this approach can be found in Appendix A.

In Fig. 9(a), we show a collection of  $R_1' = R_1/R_1^{\text{max}}$  vs  $R_2' = R_2/R_2(R_1^{\text{max}})$  based on  $^2\text{H}$  NMR literature data,<sup>69,79,98-100</sup> and Fig. 9(b) features  $^{31}\text{P}$  NMR relaxation data for  $m$ -TCP.<sup>82</sup> The lines in Fig. 9 represent fits using the corresponding BPP type of equations (cf. Table II, Appendix A). Focusing on the  $^2\text{H}$  NMR relaxation data,

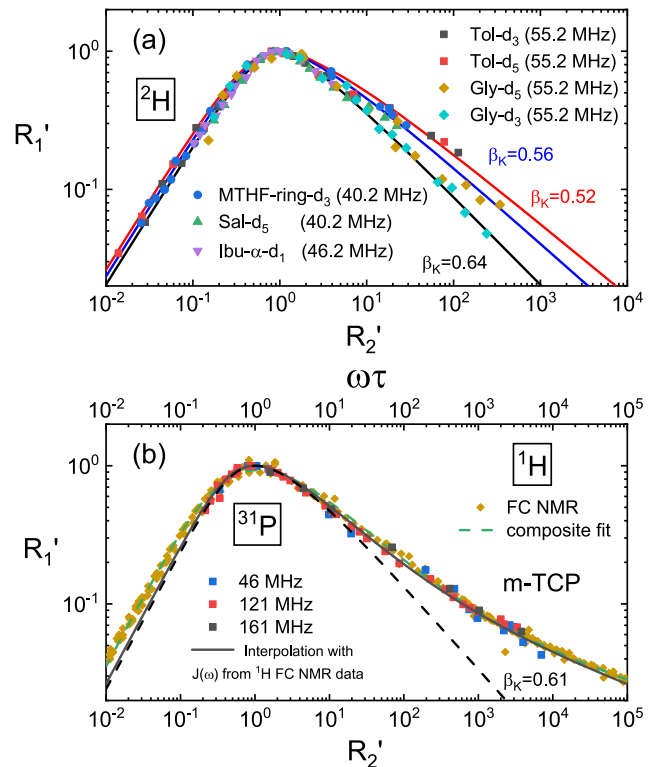


**FIG. 9.** (a) The  $^2\text{H}$  spin-lattice relaxation rate  $R_1' = R_1/R_1^{\text{max}}$  is plotted against the spin-spin relaxation rate  $R_2' = R_2/R_2(R_1^{\text{max}})$  for the supercooled liquids Tol,<sup>98</sup> Gly,<sup>79</sup> MTHF,<sup>69</sup> Sal,<sup>99</sup> and Ibu.<sup>100</sup> The lines are Kohlrausch-like susceptibilities with the indicated exponents. The Larmor frequencies at which the measurements were taken are given. (b)  $^{31}\text{P}$  NMR relaxation rate  $R_1'$  as a function of  $R_2'$  (bottom x-axis)<sup>82</sup> and the FC  $^1\text{H}$  NMR relaxation rate  $R_1'$  as a function of  $\omega\tau$  (top x-axis)<sup>88</sup> of  $m$ -TCP are shown on the same scale. The black solid line ( $^{31}\text{P}$  NMR) is an interpolation according to the spectral density of the  $^1\text{H}$  FC NMR data (green dashed line: composite fit) and the dashed black line corresponds to its Kohlrausch contribution.

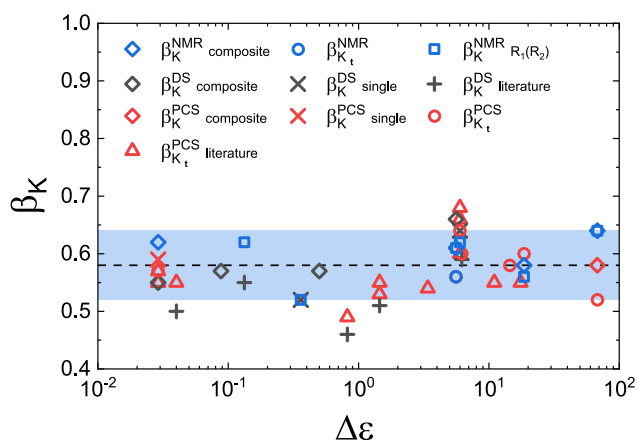


**FIG. 10.** Stretching parameters  $\beta_K^{DS}$  (black),  $\beta_K^{PCS}$  (red), and  $\beta_K^{NMR}$  (blue) as a function of the relaxation strength  $\Delta\epsilon$ . With respect to Fig. 3, the dielectric data correspond to liquids with  $\Delta\epsilon \leq 6$ . Analysis in the  $\omega$  domain: composite fits (diamonds) and single Kohlrausch fits (crosses), analysis in the  $t$  domain: single fits (circles),  $R_1$  vs  $R_2$  analysis (squares). Literature data: triangles (PCS) and plusses (DS).

Fig. 9(a) shows that they all display a similar behavior, with only slight variations in the high-frequency power law. The corresponding stretching parameters agree with those obtained from  $^1\text{H}$  FC NMR spectra and are shown in Fig. 10 together with the stretching parameters from PCS and DS. In Fig. 10, only data for liquids with  $\Delta\epsilon \leq 6$  are included. The Kohlrausch exponents as found using NMR and PCS, as well as using DS for low-polarity liquids, are located in a band defined by  $\beta_K = 0.58 \pm 0.06$ .

Figure 9(b) collects relaxation data of  $m$ -TCP and shows how the different approaches to generate NMR susceptibility spectra nicely agree with each other: The scaled  $^{31}\text{P}$  NMR functions  $R_1(R_2)$  obtained at three Larmor frequencies are seen to form a common master curve. Moreover, taking the  $^1\text{H}$  FC master curve from Fig. 6, a high similarity emerges between  $R_1(\omega\tau)$  and  $R_1(R_2)$ , although different NMR interactions are probed by  $^1\text{H}$  and  $^{31}\text{P}$  NMR. The high-frequency flanks overlap perfectly. On the low-frequency flank, the  $^1\text{H}$  FC curve is somewhat broader because for  $^{31}\text{P}$  ( $I = 1/2$ ) only a single spectral density enters the BPP-type equation, whereas for the  $^1\text{H}$  relaxation, a sum of two spectral densities enters. Taking the spectral density from the composite fit of the  $^1\text{H}$  FC master curve [green dashed line in Fig. 9(b)], the  $^{31}\text{P}$  NMR  $R_1(R_2)$  is perfectly reproduced [black line in Fig. 9(b)]. As already shown in Fig. 6, one recognizes a large excess wing contribution for  $m$ -TCP.

## VI. POSSIBLE REASONS FOR THE OBSERVATION OF NARROW DIELECTRIC RELAXATION SPECTRA IN POLAR LIQUIDS

Previously, we interpreted the difference of the full relaxation spectra (including the excess wing contribution) as reported by DS on the one hand and by PCS and NMR on the other hand by the difference in the rank of the probed reorientational correlation functions.<sup>8,38,88,101</sup> Scaling the two susceptibilities on top of each other in

the region of  $\alpha$ -relaxation peak, one finds that at high frequencies, in the excess wing region, the PCS spectrum of glycerol and  $m$ -TCP exceeds the dielectric spectrum by a factor of 2–3 [see Fig. 4(a) for glycerol]. This factor was rationalized by assuming highly restricted reorientations as the origin of the excess wing—in harmony with  $^2\text{H}$  NMR line shape studies.<sup>45</sup> Consequently, at high frequencies, the susceptibility from PCS is expected to be three times larger than that from DS, here written as  $\chi''_{\lambda=2}(\omega) \approx 3\chi''_{\lambda=1}(\omega)$ .<sup>64,102,103</sup> However, inspecting particularly the  $o$ -terphenyl data shown in Fig. 5(a), one finds that this relation does not generally apply. Gabriel *et al.* also rejected this explanation as it would lead to inconsistencies in the THz regime.<sup>35</sup>

Rather than scaling the susceptibilities in the region of  $\alpha$ -relaxation peak, it is instructive to exploit the recently proposed envelope scaling.<sup>14</sup> Here, the excess wing contributions are collapsed to a high-frequency spectral envelope, which appears to be generic for type A liquids and which describes also the experimental  $\Delta\epsilon(\beta_K)$  data presented by Paluch *et al.*<sup>15</sup> well. As shown in Ref. 14 for glycerol, NMR and LS susceptibilities (which nicely agree in the  $\alpha$ -peak and the excess-wing region) both comply well with this scaling. However, the dielectric spectrum differs: here, the  $\alpha$  response displays a larger relative amplitude, a higher degree of stretching, and a lower characteristic frequency as compared to the other two methods.

Dielectric responses feature self- and cross-correlation terms, which can be associated with single-particle and collective dynamics, respectively.<sup>18</sup> Dielectric spectra are thus expected to feature both contributions which may be disentangled by comparison with single-particle (self-term) probes such as NMR<sup>104,105</sup> or OKE.<sup>106</sup> Explicitly, the collective time constant has been related to the self-correlation time  $\tau_\alpha$  according to  $\tau_{DS} = (fg_K/g')\tau_\alpha$ , where  $f$  represents an internal field correction,  $g_K$  represents the Kirkwood (static) correlation factor, and  $g'$  represents a dynamical correlation factor.<sup>107</sup> Naively, one may even expect that in polar liquids, the dielectric response is bimodal (somehow akin to the situation, e.g., in monohydroxy alcohols<sup>108</sup>), although such a bimodality is easy to overlook and may require dedicated decomposition procedures.<sup>109</sup> Monohydroxy alcohols and related associating liquids<sup>108</sup> are particularly interesting (but possibly special cases) since their separated contributions are assignable to self- and cross-correlations. Recently, a decomposition was proposed<sup>35,71</sup> in which PCS (as another technique potentially sensitive to single-particle dynamics only) is assumed to probe the self-part of the  $\alpha$ -relaxation together with the excess wing contribution.

It seems obvious that the presumed cross-correlation relaxation contribution can be suppressed by diminishing the dipole-dipole interactions via dilution, uncovering a significantly broader self-part of the  $\alpha$ -relaxation. Corresponding studies were presumably first performed by Johari and co-worker<sup>110</sup> and by Williams and co-workers<sup>20</sup> who measured the dielectric loss of polar solutes in a nonpolar solvent such as  $o$ -terphenyl, and  $\beta_K$  was found to be in the range 0.52–0.55, very close to those values reported here from NMR and PCS. Recent work by Pabst *et al.* also exploits the dilution variable.<sup>71</sup>

To assess the cross-correlation relaxation contribution for glycerol, Gabriel *et al.*<sup>35</sup> shifted the dielectric susceptibilities and PCS spectra, both measured at the same temperature, vertically to achieve overlap in the region of the excess wing. In this representation, the

dielectric  $\alpha$ -peak appears larger and shifted to lower frequencies with respect to the PCS  $\alpha$ -peak, thereby experimentally confirming a prediction of the previously introduced envelope scaling.<sup>14</sup> The dielectric spectrum of glycerol was then mimicked by adding a Debye-like low-frequency term to its scaled PCS spectrum. The relative amplitude of the slow dielectric (“collective”) contribution was then assessed in terms of the Kirkwood factor, with the goal to quantify the extent of dielectric cross-correlations for this glass former.<sup>71</sup>

Already Nielsen *et al.*<sup>12</sup> observed that the Kirkwood factor larger than 1 correlates with narrow dielectric spectra. Specifically, they wrote: “Liquids with  $\alpha_{\min} > 0.65$  tend to have Kirkwood correlation factors  $g_K$  significantly larger than unity, reflecting strong correlations between the motions of different dipoles.”<sup>12</sup> Assuming that the spectral shape of the presumed cross-correlation contribution is close to Debye-like,<sup>35</sup> one may argue that the apparent stretching parameter  $\beta_K$  grows with  $g_K$  rather than with  $\Delta\epsilon$ .<sup>15</sup>

Qualitatively, these results fit well to those reported in the present survey. The self-part of the relaxation spectrum may be assumed to be probed by PCS or NMR—and by DS provided that the dielectric relaxation strength is sufficiently small so that cross-correlation effects can be neglected. To further test this idea in Appendix B, we compare the stretching parameters obtained by DS and NMR, spectral enhancements as given by the ratio of the  $\alpha$ -relaxation strengths  $A_{DS}/A_{NMR}$ , dipole moments, and Kirkwood factors  $g_K$ . However, in view of the limited database, no definite answer can be given.

## VII. DISCUSSION AND CONCLUSION

Summarizing and tentatively generalizing our findings for the reorientational dynamics of molecular liquids, a “genuine” stretching parameter  $\beta_K$  of  $0.58 \pm 0.06$  is probed by PCS and NMR and by DS in the limit of low relaxation strengths,  $\Delta\epsilon \leq 6$ . As mentioned, similar values were reported for polar probe molecules in nonpolar solvents.<sup>20</sup> In liquids with higher relaxation strengths, DS reveals larger  $\beta_K$  values. Moreover, for the presently investigated liquids, FTS applies well when probing their relaxation spectra via NMR or PCS. This is obvious from the equivalence of the susceptibilities:  $\chi''_{PCS}(\omega\tau) \propto \chi''_{NMR}(\tau) \propto \chi''_{NMR}(\omega)$ . Various results from neutron scattering,<sup>3,111,112</sup> as well as from molecular simulations,<sup>113,114</sup> hint also at the applicability of FTS. For DS, we identify a trend of increasing FTS violation with increasing relaxation strength. Yet, in nonpolar liquids such as *o*-terphenyl and tristyrene, FTS applies sufficiently well. Given that FTS works for the NMR response, we demonstrated that a simple single-frequency analysis of the spin–lattice relaxation rate  $R_1(T)$  as a function of the spin–spin relaxation rate  $R_2(T)$  is able to yield the stretching parameter. We find satisfying agreement between the  $R_1(R_2)$  results and the relaxation spectrum obtained by FC <sup>1</sup>H NMR relaxometry or PCS. These approaches complement previous determinations of stretching parameters and correlation times  $\tau_\alpha(T)$  that are based on combined measurements of  $R_1$  and  $R_2$ .<sup>79,82,86,98</sup>

It was found that the manifestation of the excess wing depends on the system as well as the technique. Since the relation  $\chi''_{l=2}(\omega) \approx 3\chi''_{l=1}(\omega)$  does not always apply, in contrast to what was previously thought,<sup>8</sup> the relative contribution of the excess wing with respect

to that of the  $\alpha$ -relaxation peak cannot generally be explained by assuming small angular displacements.

High-quality data of more liquids probed by different techniques are obviously needed for a systematic comparison of the relaxation stretching. In particular, the excess wing contribution is not well resolved by many PCS studies. Even from dielectric data covering large dynamic and spectral ranges, it is often difficult to determine the excess wing contribution unambiguously. In any case, the latter has to be accounted for to correctly assess the  $\alpha$ -relaxation stretching. Also, the relation of the relaxation behavior close to  $T_g$ —that is scrutinized in the present publication—to that at high temperature as revealed by FPI needs further attention: Investigating many molecular liquids using this technique, we found<sup>11</sup> a larger variation in the relaxation stretching probed in the low-viscosity regime as compared to that reported in the present article at  $T_g$ .

The present NMR and PCS results suggest that in polar liquids, the dipole–dipole interactions do not *generally* trigger a narrowing of the underlying distribution of molecular reorientation times. One should keep in mind that the correlation of relaxation strength and degree of stretching, demonstrated by Paluch *et al.*,<sup>15</sup> was found by focusing on results from dielectric spectroscopy, a technique for which an extensive database exists. It is suggested that the dipolar associations likely to be present in polar liquids generate the so-called cross terms<sup>115</sup> (a feature fairly unique to dielectric spectroscopy) that are responsible for the joint occurrence of relatively high dielectric strengths and narrow spectral widths observed by Paluch *et al.*<sup>15</sup>

In an attempt to rationalize better why DS reveals a system-specific stretching in polar liquids, we tested (but could not confirm) the notion<sup>35,71</sup> that the spectral enhancement is related to the Kirkwood factor. However, given the relatively small NMR and PCS database, an understanding of narrow dielectric spectra remains a future task in which the clarification of the role played by collective dynamics may become a major issue. For the PCS spectra, at least some impact of collective dynamics on the interaction-induced scattering is present, since it was demonstrated to contribute at high frequencies.<sup>34</sup> Rotational self-correlation functions are probed by <sup>2</sup>H and chemical shift anisotropy (CSA) dominated NMR spin relaxations, yet to a certain extent, these functions will nevertheless reflect the underlying (collective) dynamics.

The main points of our survey regarding the relaxation spectra of a number of (mostly type A) glass formers are that (i) for all viscous liquids studied in the present work, the  $\alpha$ -response as studied using NMR and light scattering shows essentially the same spectral shape and obeys FTS. (ii) This “generic” character of the  $\alpha$  shape is compatible with the previous findings from the analysis of rheological compliance spectra.<sup>13,14</sup> (iii) For liquids with low dipole moment  $\mu$ , items (i) and (ii) also apply for dielectric spectra, while for liquids with high dipole moment, the dielectric spectra gets narrower for increasing  $\mu$  or increasing temperature. (iv) The relative amplitude of the excess wing depends on the substance and technique.

Clearly, more data are needed to further test and refine these findings. When extending the PCS<sup>16</sup> and NMR stretching parameter database, it will be interesting to clarify whether the weak “scatter” observed Fig. 10 is due to experimental uncertainties or whether it reflects peculiarities of the liquids in question. If an extension of the PCS and NMR database confirms the observation of the

presently indicated “genuine” stretching, this raises the question: Should models of the glass transition first aim at understanding this “genuine” behavior or rather focus on the additional information implied by the variation in the degree of dielectrically observed stretching?

## ACKNOWLEDGMENTS

This research was funded by the Deutsche Forschungsgemeinschaft (DFG, German Research Foundation), Grant Nos. RO 907/19, and SFB 840 as well as the EU COST program “European Network on NMR Relaxometry.” T.K., R.S., and E.A.R. gratefully acknowledge the support by Jürgen Senker. We appreciate valuable comments by Kristine Niss.

## APPENDIX A: NMR SUSCEPTIBILITY SPECTRA

Here, we present details that allow one to extract relevant features of spectral densities from NMR measurements, including a novel approach that exploits a parametric plot of  $R_1$  vs  $R_2$  for various nuclei. Explicitly, depending on the relaxation mechanism—quadrupolar (Q) interaction in the case of  $^2\text{H}$  or chemical shift anisotropy (CSA) in the case of  $^{31}\text{P}$ —the expressions for  $R_1$  and  $R_2$  in the extreme narrowing condition ( $\omega\tau_\alpha < 1$ ) and in the slow-motion limit ( $\omega\tau_\alpha > 1$ ) can be derived.<sup>97</sup> Without loss of generality, in the slow-motion limit, we write for a Cole–Davidson or Kohlrausch type spectral density (neglecting for now the excess wing contribution),

$$J(\omega) = \frac{\chi''(\omega\tau)}{\omega} = \frac{(\omega\tau)^{-\beta}}{\omega} \quad \omega\tau \gg 1. \quad (\text{A1})$$

This leads to the expressions for the quadrupolar relaxation ( $I = 1$ ) and for the CSA relaxation ( $I = 1/2$ ) that are summarized in Table II.

For the present purpose, it is not necessary to explicitly specify the coupling constants  $K_Q$  and  $K_{\text{CSA}}$  that are listed in Table II. For both relaxation mechanisms, one finds

$$R_1 \propto R_2 \quad \text{for } \omega\tau < 1 \quad \text{and} \quad R_1 \propto R_2^{-\beta} \quad \text{for } \omega\tau > 1. \quad (\text{A2})$$

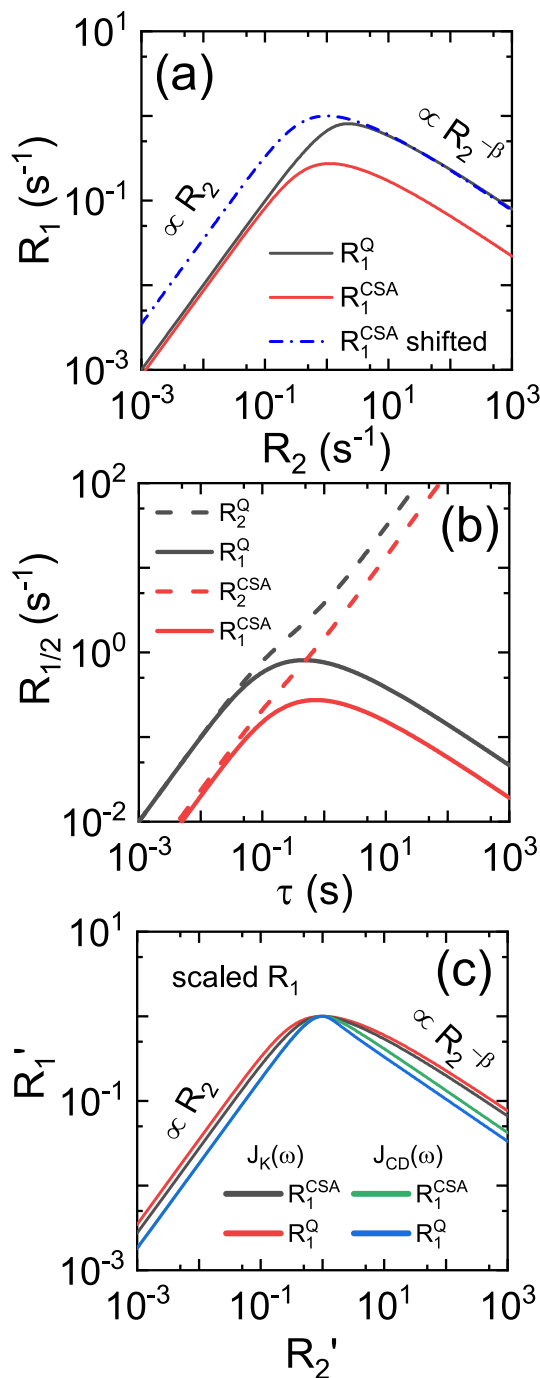
Therefore, assuming a temperature independent exponent  $\beta$  (i.e., FTS), a plot of  $R_1$  vs  $R_2$  yields a curve that resembles a susceptibility function with its high-frequency flank displaying a power law characterized by an exponent  $\beta$ . Near  $\omega\tau \cong 1$ , the details of the  $R_1 = f(R_2)$  curve depend on the relaxation mechanism (see Fig. 11).

Figure 11(a) shows the spin–lattice relaxation rate  $R_1$  vs the spin–spin relaxation rate  $R_2$  based on a Kohlrausch spectral density for quadrupolar and CSA interactions. The corresponding BPP equations are given in Table II. Figure 11(b) shows the corresponding  $R_1$  and  $R_2$  curves as a function of the time constant  $\tau$ . Comparing Kohlrausch with CD spectral densities, in Fig. 11(c), one recognizes that for the same stretching parameter, a Kohlrausch function displays a broader maximum and only at higher frequencies reveals the same power law exponent as the CD function.

A limitation of the  $R_1$  vs  $R_2$  analysis needs to be mentioned: In contrast to the  $R_1$  relaxation, the rate  $R_2$  extracted from the free induction decay (FID) cannot be monitored down to  $T_g$  since entering the highly viscous liquid, the FID and the  $^2\text{H}$  spin–lattice relaxation become nonexponential and a well-defined relaxation rate can no longer be extracted.<sup>19,117</sup> As a consequence,  $R_2$  data are only available for  $\delta_i\tau \ll 1$ , where  $\delta_i$  is roughly given by  $(K_i)^{1/2}$ . For example, in the case of  $^2\text{H}$  NMR, a plot of  $R_1$  vs  $R_2$  covers correlation times shorter than about  $10^{-6}$  s and, in the case of  $^{31}\text{P}$  NMR, shorter than about  $10^{-5}$  s. Thus, the CSA interaction is better suited to map out excess wing contributions. These time scales correspond to rather high temperatures for which  $\beta$ -relaxations should barely interfere. Therefore, also the data of toluene, a typical type B glass former that is well characterized by NMR relaxometry conform to the overall pattern [see Fig. 9(a)].

**TABLE II.** Relation between the NMR relaxation rates  $R_1$  and  $R_2$  and spectral densities  $J$  as mediated by the quadrupolar interaction (Q) or by the chemical shift anisotropy (CSA).  $K_Q$  and  $K_{\text{CSA}}$  denote coupling constants. Due to the presence of two spectral densities for  $^2\text{H}$  spin–lattice relaxation, “true” isothermal spectral densities are not obtained. Yet, the difference to truly isothermal spectral densities is marginal when considering data on logarithmic scales.

Quadrupolar relaxation ( $I = 1$ H, $^2\text{H}$ )		
BPP	$R_1 = K_Q [J(\omega) + 4J(2\omega)]$	$R_2 = \frac{K_Q}{2} [3J(0) + 5J(\omega) + 2J(2\omega)]$
$\omega\tau < 1$	$R_1 = 5K_Q\tau$	$R_2 = 5K_Q\tau$
$\omega\tau > 1$	$R_1 = K_Q \left[ 1 + 2 \cdot 2^{-\beta} \right] \frac{(\omega\tau)^{-\beta}}{\omega}$	$R_2 = \frac{3}{2} K_Q\tau$
CSA relaxation ( $I = 1/2$ , $^{31}\text{P}$ )		
BPP	$R_1 = K_{\text{CSA}} J(\omega)$	$R_2 = \frac{K_{\text{CSA}}}{6} [4J(0) + 3J(\omega)]$
$\omega\tau < 1$	$R_1 = K_{\text{CSA}}\tau$	$R_2 = \frac{7}{6} K_{\text{CSA}}\tau$
$\omega\tau > 1$	$R_1 = K_{\text{CSA}} \frac{(\omega\tau)^{-\beta}}{\omega}$	$R_2 = \frac{4}{6} K_{\text{CSA}}\tau$



**FIG. 11.** (a) Spin-lattice relaxation rate  $R_1$  plotted against the spin-spin relaxation rate  $R_2$ . For the calculations, we assumed a Kohlrausch function and that the  $^2\text{H}$  relaxation is dominated by quadrupolar relaxation and  $^{31}\text{P}$  by CSA relaxation. For better comparability, also, an upward shifted variant of the CSA curve is shown. For this plot, we used the variables  $K_Q = K_{CSA} = 1$ ,  $\omega = 1$ , and  $\beta_K = 0.5$ . (b) The corresponding  $R_1(\tau)$  and  $R_2(\tau)$  functions. (c) Quadrupolar and CSA relaxations assuming a Kohlrausch and a CD spectral density, both with  $\beta = 0.5$ , are compared to each other. The variables  $R_1' = R_1/R_1^{\text{max}}$  and  $R_2' = R_2/R_2(R_1^{\text{max}})$  are used to be insensitive to variations in coupling constants and Larmor frequencies.

**TABLE III.** Comparison of susceptibility stretching parameters  $\beta_K$  from DS and NMR, as well as the calculated  $\alpha$ -process amplitude ratio  $A_{DS}/A_{NMR}$  (assuming same CD excess wing contribution), the dielectric relaxation strength  $\Delta\epsilon$ , the dipole moment  $\mu$ , and the density  $\rho$  at room temperature as well as the refractive index  $n$  used to calculate the Kirkwood factor  $g_K$  for OTP, MTHF, *m*-TCP, and glycerol.<sup>118</sup> The molecular dipole moment of OTP was calculated via density functional theory (DFT) in analogy to the method explained in the supplementary material of Ref. 119.

	$\beta_K^{DS}$	$\beta_K^{NMR}$	$A_{DS}/A_{NMR}$	$\Delta\epsilon$	$\mu$ (D)	$\rho$ (kg m <sup>-3</sup> )	$n$	$g_K$
OTP	0.55	0.62	0.43	0.016	0.16	1046 <sup>120</sup>	1.6 <sup>120</sup>	0.8
MTHF	0.70	0.58	1.9	18.6	1.58 <sup>121</sup>	863 <sup>122</sup>	1.41 <sup>122</sup>	1.87
Gly	0.69	0.64	3	74	2.67 <sup>123</sup>	1303 <sup>124</sup>	1.49 <sup>124</sup>	2.54
<i>m</i> -TCP	0.66	0.61	5.2	5.6	3.05 <sup>125</sup>	1150 <sup>126</sup>	1.55 <sup>126</sup>	0.77

## APPENDIX B: AMPLITUDE RATIO COMPARED TO OTHER QUANTITIES

When seeking correlations of the amplitude ratio  $A_{DS}/A_{NMR}$  with other quantities, we focus on the NMR susceptibility as reference since here (as compared to PCS), more data are available for comparison with dielectric spectra including the excess wing contribution. Table III shows that the exponent  $\beta_K$  increases from 0.57 to 0.70 as the ratio of the relaxation strengths increases from 0.43 to 5.2. However, a trend of the  $\alpha$ -process amplitude ratio with  $g_K$  is not observed, different from an anticipation implied by the findings of Ref. 35 for glycerol. Instead, the spectral enhancement ratio  $A_{DS}/A_{NMR}$  appears to grow with the dipole moment.

## DATA AVAILABILITY

The data that support the findings of this study are available from the corresponding author upon reasonable request.

## REFERENCES

- P. Lunkenheimer, U. Schneider, R. Brand, and A. Loid, "Glassy dynamics," *Contemp. Phys.* **41**, 15 (2000).
- G. Hinze, D. D. Brace, S. D. Gottke, and M. D. Fayer, "A detailed test of mode-coupling theory on all time scales: Time domain studies of structural relaxation in a supercooled liquid," *J. Chem. Phys.* **113**, 3723 (2000).
- A. Tölle, "Neutron scattering studies of the model glass former *ortho*-terphenyl," *Rep. Prog. Phys.* **64**, 1473 (2001).
- K. Binder and W. Kob, *Glassy Materials and Disordered Solids: An Introduction to Their Statistical Mechanics* (World Scientific, New Jersey, 2005).
- T. Blochowicz, A. Brodin, and E. A. Rössler, "Evolution of the dynamic susceptibility in supercooled liquids and glasses," in *Advances in Chemical Physics: Fractals, Diffusion, and Relaxation in Disordered Complex Systems*, edited by W. T. Coffey and Y. P. Kalmykov (John Wiley & Sons, Inc., Hoboken, NJ, 2006), Vol. 133, p. 127.
- G. Floudas, M. Paluch, A. Grzybowski, and K. Ngai, *Molecular Dynamics of Glass-Forming Systems: Effects of Pressure* (Springer, Berlin, Heidelberg, 2011).
- P. G. Wolynes and V. Lubchenko, *Structural Glasses and Supercooled Liquids: Theory, Experiment, and Applications* (Wiley, Hoboken, NJ, 2012).
- N. Petzold, B. Schmidtke, R. Kahlau, D. Bock, R. Meier, B. Micko, D. Kruk, and E. A. Rössler, "Evolution of the dynamic susceptibility in molecular glass formers:

- Results from light scattering, dielectric spectroscopy, and NMR," *J. Chem. Phys.* **138**, 12A510 (2013).
- <sup>9</sup>K. Niss and T. Hecksher, "Perspective: Searching for simplicity rather than universality in glass-forming liquids," *J. Chem. Phys.* **149**, 230901 (2018).
- <sup>10</sup>R. Böhmer, K. L. Ngai, C. A. Angell, and D. J. Plazek, "Nonexponential relaxations in strong and fragile glass formers," *J. Chem. Phys.* **99**, 4201 (1993).
- <sup>11</sup>B. Schmidtke, N. Petzold, B. Pötzschner, H. Weingärtner, and E. A. Rössler, "Relaxation stretching, fast dynamics, and activation energy: A comparison of molecular and ionic liquids as revealed by depolarized light scattering," *J. Phys. Chem. B* **118**, 7108 (2014).
- <sup>12</sup>A. I. Nielsen, T. Christensen, B. Jakobsen, K. Niss, N. B. Olsen, R. Richert, and J. C. Dyre, "Prevalence of approximate square root(t) relaxation for the dielectric alpha process in viscous organic liquids," *J. Chem. Phys.* **130**, 154508 (2009).
- <sup>13</sup>S. P. Bierwirth, R. Böhmer, and C. Gainaru, "Generic primary mechanical response of viscous liquids," *Phys. Rev. Lett.* **119**, 248001 (2017).
- <sup>14</sup>C. Gainaru, "Spectral shape simplicity of viscous materials," *Phys. Rev. E* **100**, 020601 (2019).
- <sup>15</sup>M. Paluch, J. Knapik, Z. Wojnarowska, A. Grzybowski, and K. L. Ngai, "Universal behavior of dielectric responses of glass formers: Role of dipole-dipole interactions," *Phys. Rev. Lett.* **116**, 025702 (2016).
- <sup>16</sup>T. Blochowicz, C. Tschirwitz, S. Benkhof, and E. A. Rössler, "Susceptibility functions for slow relaxation processes in supercooled liquids and the search for universal relaxation patterns," *J. Chem. Phys.* **118**, 7544 (2003).
- <sup>17</sup>T. Blochowicz, C. Gainaru, P. Medick, C. Tschirwitz, and E. A. Rössler, "The dynamic susceptibility in glass forming molecular liquids: The search for universal relaxation patterns II," *J. Chem. Phys.* **124**, 134503 (2006).
- <sup>18</sup>C. J. F. Böttcher and P. Bordewijk, *Dielectrics in Time-Dependent Fields*, 2nd completely revised edition (Elsevier, Amsterdam, 1978).
- <sup>19</sup>R. Böhmer, G. Diezemann, G. Hinze, and E. Rössler, "Dynamics of supercooled liquids and glassy solids," *Prog. Nucl. Magn. Reson. Spectrosc.* **39**, 191 (2001).
- <sup>20</sup>G. Williams, "Molecular motion in glass-forming systems," *J. Non-Cryst. Solids* **131-133**, 1 (1991).
- <sup>21</sup>H. Z. Cummins, G. Li, Y. H. Hwang, G. Q. Shen, W. M. Du, J. Hernandez, and N. J. Tao, "Dynamics of supercooled liquids and glasses: Comparison of experiments with theoretical predictions," *Z. Phys. B* **103**, 501 (1997).
- <sup>22</sup>W. Götzke, "Recent tests of the mode-coupling theory for glassy dynamics," *J. Phys.: Condens. Matter* **11**, A1-A45 (1999).
- <sup>23</sup>A. Aouadi, C. Dreyfus, M. Massot, R. M. Pick, T. Berger, W. Steffen, A. Patkowski, and C. Alba-Simionesco, "Light scattering study of the liquid-glass transition of meta-toluidine," *J. Chem. Phys.* **112**, 9860 (2000).
- <sup>24</sup>G. Fytas and T. Dorfmueller, "Photon correlation spectroscopy of liquid 2,4-pentanediol near the glass point," *Mol. Phys.* **47**, 741 (1982).
- <sup>25</sup>D. L. Sidebottom and C. M. Sorensen, "Light scattering study of the glass transition in salol," *Phys. Rev. B* **40**, 461 (1989).
- <sup>26</sup>A. Patkowski, M. Paluch, and H. Kriegs, "Dynamic light scattering studies of supercooled phenylphthalene-dimethylether dynamics under high pressure," *J. Chem. Phys.* **117**, 2192 (2002).
- <sup>27</sup>J. Gabriel, F. Pabst, and T. Blochowicz, "Debye process and  $\beta$ -relaxation in 1-propanol probed by dielectric spectroscopy and depolarized dynamic light scattering," *J. Phys. Chem. B* **121**, 8847 (2017).
- <sup>28</sup>J. Gabriel, F. Pabst, A. Helbling, T. Böhmer, and T. Blochowicz, "Nature of the Debye-process in monohydroxy alcohols: 5-methyl-2-hexanol investigated by depolarized light scattering and dielectric spectroscopy," *Phys. Rev. Lett.* **121**, 035501 (2018).
- <sup>29</sup>R. Torre, P. Bartolini, and R. Pick, "Time-resolved optical Kerr effect in a fragile glass-forming liquid, salol," *Phys. Rev. E* **57**, 1912 (1998).
- <sup>30</sup>H. Cang, V. N. Novikov, and M. D. Fayer, "Logarithmic decay of the orientational correlation function in supercooled liquids on the ps to ns time scale," *J. Chem. Phys.* **118**, 2800 (2003).
- <sup>31</sup>S. Kinoshita, Y. Kai, M. Yamaguchi, and T. Yagi, "Direct comparison between ultrafast optical Kerr effect and high-resolution light scattering spectroscopy," *Phys. Rev. Lett.* **75**, 148 (1995).
- <sup>32</sup>A. Brodin and E. A. Rössler, "Depolarized light scattering versus optical Kerr effect. II. Insight into the dynamic susceptibility of molecular liquids," *J. Chem. Phys.* **126**, 244508 (2007).
- <sup>33</sup>D. Kivelson and P. Madden, "Theory of dielectric relaxation," *Mol. Phys.* **30**, 1749 (1975).
- <sup>34</sup>A. Patkowski, W. Steffen, H. Nilgens, E. W. Fischer, and R. Pecora, "Depolarized dynamic light scattering from three low molecular weight glass forming liquids: A test of the scattering mechanism," *J. Chem. Phys.* **106**, 8401 (1997).
- <sup>35</sup>J. P. Gabriel, P. Zourchang, F. Pabst, A. Helbling, P. Weigl, T. Böhmer, and T. Blochowicz, "Intermolecular cross-correlations in the dielectric response of glycerol," *Phys. Chem. Chem. Phys.* **22**, 11644 (2020).
- <sup>36</sup>A. Kudlik, S. Benkhof, T. Blochowicz, C. Tschirwitz, and E. Rössler, "The dielectric response of simple organic glass formers," *J. Mol. Struct.* **479**, 201 (1999).
- <sup>37</sup>U. Schneider, R. Brand, P. Lunkenheimer, and A. Loidl, "Excess wing in the dielectric loss of glass formers: A Johari-Goldstein  $\beta$  relaxation?," *Phys. Rev. Lett.* **84**, 5560 (2000).
- <sup>38</sup>C. Gainaru, O. Lips, A. Troshagina, R. Kahlau, A. Brodin, F. Fujara, and E. A. Rössler, "On the nature of the high-frequency relaxation in a molecular glass former: A joint study of glycerol by field cycling NMR, dielectric spectroscopy, and light scattering," *J. Chem. Phys.* **128**, 174505 (2008).
- <sup>39</sup>M. Flämig, M. Hofmann, N. Fatkullin, and E. A. Rössler, "NMR relaxometry: The canonical case glycerol," *J. Phys. Chem. B* **124**, 1557 (2020).
- <sup>40</sup>A. Jedrzejowska, K. L. Ngai, and M. Paluch, "Modifications of structure and intermolecular potential of a canonical glassformer: Dynamics changing with dipole-dipole interaction," *J. Phys. Chem. A* **120**, 8781 (2016).
- <sup>41</sup>K. Duvvuri and R. Richert, "Dynamics of glass-forming liquids. VI. Dielectric relaxation study of neat decahydro-naphthalene," *J. Chem. Phys.* **117**, 4414 (2002).
- <sup>42</sup>A. Minecka, E. Kaminska, D. Heczko, M. Tarnacka, I. Grudka-Flak, M. Bartoszek, A. Zięba, R. Wrzaliak, W. E. Śmiszek-Lindert, M. Dulski, K. Kaminski, and M. Paluch, "Studying molecular dynamics of the slow, structural, and secondary relaxation processes in series of substituted ibuprofens," *J. Chem. Phys.* **148**, 224505 (2018).
- <sup>43</sup>T. Körber, F. Krohn, C. Neuber, H.-W. Schmidt, and E. A. Rössler, "Main and secondary relaxations of non-polymeric high-Tg glass formers as revealed by dielectric spectroscopy," *Phys. Chem. Chem. Phys.* **22**, 9086 (2020).
- <sup>44</sup>K. L. Ngai and M. Paluch, "Classification of secondary relaxation in glass-formers based on dynamic properties," *J. Chem. Phys.* **120**, 857 (2004).
- <sup>45</sup>M. Vogel, P. Medick, and E. A. Rössler, "Secondary relaxation processes in molecular glasses studied by nuclear magnetic resonance spectroscopy," in *Annual Reports on NMR Spectroscopy*, edited by G. A. Webb (Academic Press, 2005), Vol. 56, p. 231.
- <sup>46</sup>A. Brodin, C. Gainaru, V. Porokhonskyy, and E. A. Rössler, "Evolution of dynamic susceptibility in molecular glass formers—A critical assessment," *J. Phys.: Condens. Matter* **19**, 205104 (2007).
- <sup>47</sup>P. K. Dixon, L. Wu, S. R. Nagel, B. D. Williams, and J. P. Carini, "Scaling in the relaxation of supercooled liquids," *Phys. Rev. Lett.* **65**, 1108 (1990).
- <sup>48</sup>A. Kudlik, S. Benkhof, R. Lenk, and E. Rössler, "Spectral shape of the  $\alpha$ -process in supercooled liquids revisited," *Europhys. Lett.* **32**, 511 (1995).
- <sup>49</sup>R. L. Leheny, N. Menon, and S. R. Nagel, "Comment on 'Spectral shape of the  $\alpha$ -process in supercooled liquids revisited,'" *Europhys. Lett.* **36**, 473 (1996).
- <sup>50</sup>A. Kudlik, T. Blochowicz, S. Benkhof, and E. Rössler, "Reply to Comment on 'Spectral shape of the  $\alpha$ -process in supercooled liquids revisited,'" *Europhys. Lett.* **36**, 475 (1996).
- <sup>51</sup>C. Gainaru, R. Kahlau, E. A. Rössler, and R. Böhmer, "Evolution of excess wing and  $\beta$ -process in simple glass formers," *J. Chem. Phys.* **131**, 184510 (2009).
- <sup>52</sup>C. Gainaru, R. Böhmer, R. Kahlau, and E. Rössler, "Energy landscape in molecular glasses probed by high-resolution dielectric experiments," *Phys. Rev. B* **82**, 104205 (2010).
- <sup>53</sup>The use of a mastercurve is particularly important for *o*-terphenyl because the high-precision bridge covers only three decades in frequency.
- <sup>54</sup>D. L. Sidebottom, B. V. Rodenburg, and J. R. Changstrom, "Connecting structure and dynamics in glass forming materials by photon correlation spectroscopy," *Phys. Rev. B* **75**, 132201 (2007).
- <sup>55</sup>G. Fytas, T. Dorfmueller, and C. H. Wang, "Pressure- and temperature-dependent homodyne photon correlation studies of liquid *o*-terphenyl in the supercooled state," *J. Phys. Chem.* **87**, 5041 (1983).

- <sup>56</sup>R. Richert, K. Duvvuri, and L.-T. Duong, "Dynamics of glass-forming liquids. VII. Dielectric relaxation of supercooled *tris*-naphthylbenzene, squalane, and decahydroisoquinoline," *J. Chem. Phys.* **118**, 1828 (2003).
- <sup>57</sup>X. R. Zhu and C. H. Wang, "Homodyne photon-correlation spectroscopy of a supercooled liquid: 1,3,5-*tri*- $\alpha$ -naphthyl benzene," *J. Chem. Phys.* **84**, 6086 (1986).
- <sup>58</sup>J. Hintermeyer, A. Herrmann, R. Kahlau, C. Goiceanu, and E. A. Rössler, "Molecular weight dependence of glassy dynamics in linear polymers revisited," *Macromolecules* **41**, 9335 (2008).
- <sup>59</sup>G. Meier, B. Gerharz, D. Boese, and E. W. Fischer, "Dynamical processes in organic glassforming van der Waals liquids," *J. Chem. Phys.* **94**, 3050 (1991).
- <sup>60</sup>A. Patkowski, J. Gapinski, and G. Meier, "Dynamics of supercooled van der Waals liquid under pressure. A dynamic light scattering study," *Colloid Polym. Sci.* **282**, 874 (2004).
- <sup>61</sup>C. H. Wang, R. J. Ma, G. Fytas, and T. Dorfmueller, "Laser light scattering studies of the dynamics of molecular reorientation of a viscoelastic liquid:  $\alpha$ -Phenyl *o*-cresol," *J. Chem. Phys.* **78**, 5863 (1983).
- <sup>62</sup>C. Gainaru, A. Rivera, S. Putselyk, G. Eska, and E. A. Rössler, "Low-temperature dielectric relaxation of molecular glasses: Crossover from the nearly constant loss to the tunneling regime," *Phys. Rev. B* **72**, 174203 (2005).
- <sup>63</sup>S. Benkhof and E. A. Rössler, "Relaxation data of Salol" (unpublished).
- <sup>64</sup>A. Brodin, R. Bergman, J. Mattsson, and E. A. Rössler, "Light scattering and dielectric manifestations of secondary relaxations in molecular glassformers," *Eur. Phys. J. B* **36**, 349 (2003).
- <sup>65</sup>L. Comez, S. Corezzi, D. Fioretto, H. Kriegs, A. Best, and W. Steffen, "Slow dynamics of salol: A pressure- and temperature-dependent light scattering study," *Phys. Rev. E* **70**, 011504 (2004).
- <sup>66</sup>B. Schmidtke, N. Petzold, R. Kahlau, and E. A. Rössler, "Reorientational dynamics in molecular liquids as revealed by dynamic light scattering: From boiling point to glass transition temperature," *J. Chem. Phys.* **139**, 084504 (2013).
- <sup>67</sup>T. Körber, R. Minikejew, B. Pötzschner, D. Bock, and E. A. Rössler, "Dynamically asymmetric binary glass formers studied by dielectric and NMR spectroscopy," *Eur. Phys. J. E* **42**, 143 (2019).
- <sup>68</sup>L. Comez, D. Fioretto, L. Palmieri, L. Verdini, P. A. Rolla, J. Gapinski, T. Pakula, A. Patkowski, W. Steffen, and E. W. Fischer, "Light-scattering study of a supercooled epoxy resin," *Phys. Rev. E* **60**, 3086 (1999).
- <sup>69</sup>F. Qi, T. El Goresy, R. Böhmer, A. Döb, G. Diezemann, G. Hinze, H. Sillescu, T. Blochowicz, C. Gainaru, E. Rössler, and H. Zimmermann, "Nuclear magnetic resonance and dielectric spectroscopy of a simple supercooled liquid: 2-methyl tetrahydrofuran," *J. Chem. Phys.* **118**, 7431 (2003).
- <sup>70</sup>R. Kahlau, T. Dörfler, and E. A. Rössler, "Secondary relaxations in a series of organic phosphate glasses revealed by dielectric spectroscopy," *J. Chem. Phys.* **139**, 134504 (2013).
- <sup>71</sup>F. Pabst, A. Helbling, J. Gabriel, P. Weigl, and T. Blochowicz, "Dipole-dipole correlations and the Debye-process in the dielectric response of non-associating glass forming liquids," *Phys. Rev. E* **102**, 010606 (2020).
- <sup>72</sup>S. Adishchev, D. Bock, C. Gainaru, R. Kahlau, B. Micko, N. Petzold, B. Pötzschner, and E. A. Rössler, "Reorientational dynamics of organophosphate glass formers—A joint study by <sup>31</sup>P NMR, dielectric spectroscopy and light scattering," *Z. Phys. Chem.* **226**, 1149 (2012).
- <sup>73</sup>D. Bock, R. Kahlau, B. Micko, B. Pötzschner, G. J. Schneider, and E. A. Rössler, "On the cooperative nature of the  $\beta$ -process in neat and binary glasses: A dielectric and nuclear magnetic resonance spectroscopy study," *J. Chem. Phys.* **139**, 064508 (2013).
- <sup>74</sup>P. Lunkenheimer, A. Pimenov, B. Schiener, R. Böhmer, and A. Loidl, "High-frequency dielectric spectroscopy on glycerol," *Europhys. Lett.* **33**, 611 (1996).
- <sup>75</sup>K. L. Ngai and R. W. Rendell, "Comparison between frequency-dependent specific heat and dielectric relaxation of glycerol and propylene glycol," *Phys. Rev. B* **41**, 754 (1990).
- <sup>76</sup>C. A. Angell and D. L. Smith, "Test of the entropy basis of the Vogel–Tammann–Fulcher equation: Dielectric relaxation of polyalcohols near  $T_g$ ," *J. Phys. Chem.* **86**, 3845 (1982).
- <sup>77</sup>A. Brodin and E. A. Rössler, "Depolarized light scattering study of glycerol," *Eur. Phys. J. B* **44**, 3 (2005).
- <sup>78</sup>M. Flämig, M. Becher, M. Hofmann, T. Körber, B. Kresse, A. F. Privalov, L. Willner, D. Kruk, F. Fujara, and E. A. Rössler, "Perspectives of deuteron field-cycling NMR relaxometry for probing molecular dynamics in soft matter," *J. Phys. Chem. B* **120**, 7754 (2016).
- <sup>79</sup>W. Schnauss, F. Fujara, and H. Sillescu, "The molecular dynamics around the glass transition and in the glassy state of molecular organic systems: A <sup>2</sup>H-nuclear magnetic resonance (NMR) study," *J. Chem. Phys.* **97**, 1378 (1992).
- <sup>80</sup>D. Kruk, R. Meier, and E. A. Rössler, "Nuclear magnetic resonance relaxometry as a method of measuring translational diffusion coefficients in liquids," *Phys. Rev. E* **85**, 020201 (2012).
- <sup>81</sup>R. Meier, D. Kruk, J. Gmeiner, and E. A. Rössler, "Intermolecular relaxation in glycerol as revealed by field cycling <sup>1</sup>H NMR relaxometry dilution experiments," *J. Chem. Phys.* **136**, 034508 (2012).
- <sup>82</sup>E. Rössler and P. Eiermann, "Reorientational dynamics in supercooled *m*-tricyresyl phosphate: Its relation to main and secondary relaxation—<sup>31</sup>P nuclear magnetic resonance study of relaxation, line shape, and stimulated echo," *J. Chem. Phys.* **100**, 5237 (1994).
- <sup>83</sup>R. Richert, "On the dielectric susceptibility spectra of supercooled *o*-terphenyl," *J. Chem. Phys.* **123**, 154502 (2005).
- <sup>84</sup>N. Petzold and E. A. Rössler, "Light scattering study on the glass former *o*-terphenyl," *J. Chem. Phys.* **133**, 124512 (2010).
- <sup>85</sup>R. Meier, D. Kruk, A. Bourdick, E. Schneider, and E. A. Rössler, "Inter- and intramolecular relaxation in molecular liquids by field cycling <sup>1</sup>H NMR relaxometry," *Appl. Magn. Reson.* **44**, 153 (2013).
- <sup>86</sup>T. Dries, F. Fujara, M. Kiebel, E. Rössler, and H. Sillescu, "<sup>2</sup>H-NMR study of the glass transition in supercooled *ortho*-terphenyl," *J. Chem. Phys.* **88**, 2139 (1988).
- <sup>87</sup>R. Meier, R. Kahlau, D. Kruk, and E. A. Rössler, "Comparative studies of the dynamics in viscous liquids by means of dielectric spectroscopy and field cycling NMR," *J. Phys. Chem. A* **114**, 7847 (2010).
- <sup>88</sup>B. Schmidtke, N. Petzold, M. Flämig, and E. A. Rössler, "From boiling point down to the glass transition - dynamics of molecular liquids described by a generalized Angell plot," in *Fragility of Glass-Forming Liquids*, edited by A. L. Greer (Hindustan Book Agency, New Delhi, 2014), p. 129.
- <sup>89</sup>R. Kimmich and E. Anordo, "Field-cycling NMR relaxometry," *Prog. Nucl. Magn. Reson. Spectrosc.* **44**, 257 (2004).
- <sup>90</sup>R. Meier, D. Kruk, and E. A. Rössler, "Intermolecular spin relaxation and translation diffusion in liquids and polymer melts: Insight from field-cycling <sup>1</sup>H NMR relaxometry," *ChemPhysChem* **14**, 3071 (2013).
- <sup>91</sup>F. Fujara, D. Kruk, and A. F. Privalov, "Solid state field-cycling NMR relaxometry: Instrumental improvements and new applications," *Prog. Nucl. Magn. Reson. Spectrosc.* **82**, 39 (2014).
- <sup>92</sup>R. Kimmich and N. Fatkullin, "Self-diffusion studies by intra- and intermolecular spin-lattice relaxometry using field-cycling: Liquids, plastic crystals, porous media, and polymer segments," *Prog. Nucl. Magn. Reson. Spectrosc.* **101**, 18 (2017).
- <sup>93</sup>M. Flämig, M. Hofmann, A. Lichtinger, and E. A. Rössler, "Application of proton field-cycling NMR relaxometry for studying translational diffusion in simple liquids and polymer melts," *Magn. Reson. Chem.* **57**, 805 (2019).
- <sup>94</sup>N. Bloembergen, E. M. Purcell, and R. V. Pound, "Relaxation effects in nuclear magnetic resonance absorption," *Phys. Rev.* **73**, 679 (1948).
- <sup>95</sup>S. Kariyo, C. Gainaru, H. Schick, A. Brodin, V. N. Novikov, and E. A. Rössler, "From a simple liquid to a polymer melt: NMR relaxometry study of polybutadiene," *Phys. Rev. Lett.* **97**, 207803 (2006).
- <sup>96</sup>S. Kariyo, A. Herrmann, C. Gainaru, H. Schick, A. Brodin, V. N. Novikov, and E. A. Rössler, "Erratum. From a simple liquid to a polymer melt: NMR relaxometry study of polybutadiene [Phys. Rev. Lett. 97, 207803 (2006)]," *Phys. Rev. Lett.* **100**, 109901 (2008).
- <sup>97</sup>A. Abragam, *The Principles of Nuclear Magnetism* (Clarendon Press, Oxford, 1961).
- <sup>98</sup>E. Rössler and H. Sillescu, "<sup>2</sup>H NMR Study of supercooled toluene," *Chem. Phys. Lett.* **112**, 94 (1984).
- <sup>99</sup>R. Böhmer, A. Döb, G. Hinze, H. Sillescu, H. Kolshorn, M. Vogel, and H. Zimmermann, "Deuteron and carbon magnetic resonance studies of supercooled liquid and glassy salol," *J. Chem. Phys.* **112**, 5884 (2000).
- <sup>100</sup>S. Bauer, M. Storek, C. Gainaru, H. Zimmermann, and R. Böhmer, "Molecular motions in supercooled and glassy ibuprofen: Deuteron magnetic resonance and high-resolution rheology study," *J. Phys. Chem. B* **119**, 5087 (2015).

- <sup>101</sup>G. Diezemann, R. Böhmer, G. Hinze, and H. Sillescu, "Reorientational dynamics in simple supercooled liquids," *J. Non-Cryst. Solids* **235-237**, 121 (1998).
- <sup>102</sup>M. J. Lebon, C. Dreyfus, Y. Guissani, R. M. Pick, and H. Z. Cummins, "Light scattering and dielectric susceptibility spectra of glassforming liquids," *Z. Phys. B* **103**, 433 (1997).
- <sup>103</sup>T. Blochowicz, A. Kudlik, S. Benkhof, J. Senker, E. Rössler, and G. Hinze, "The spectral density in simple organic glass formers: Comparison of dielectric and spin-lattice relaxation," *J. Chem. Phys.* **110**, 12011 (1999).
- <sup>104</sup>A. Volmari and H. Weingärtner, "Cross terms and Kirkwood factors in dielectric relaxation of pure liquids," *J. Mol. Liq.* **98-99**, 295 (2002).
- <sup>105</sup>T. Yamaguchi, H. Furuhashi, T. Matsuoka, and S. Koda, "Dynamic solvophobic effect and its cooperativity in the hydrogen-bonding liquids studied by dielectric and nuclear magnetic resonance relaxation," *J. Phys. Chem. B* **112**, 16633 (2008).
- <sup>106</sup>R. Buchner and G. Heftner, "Interactions and dynamics in electrolyte solutions by dielectric spectroscopy," *Phys. Chem. Chem. Phys.* **11**, 8984 (2009).
- <sup>107</sup>P. Madden and D. Kivelson, "A consistent molecular treatment of dielectric phenomena," in *Advances in Chemical Physics*, edited by I. Prigogine and S. A. Rice (John Wiley & Sons, Inc., Hoboken, NJ, USA, 1984), p. 467.
- <sup>108</sup>R. Böhmer, C. Gainaru, and R. Richert, "Structure and dynamics of monohydroxy alcohols - milestones towards their microscopic understanding, 100 years after Debye," *Phys. Rep.* **545**, 125 (2014).
- <sup>109</sup>Y. Z. Chua, A. R. Young-Gonzales, R. Richert, M. D. Ediger, and C. Schick, "Dynamics of supercooled liquid and plastic crystalline ethanol: Dielectric relaxation and AC nanocalorimetry distinguish structural  $\alpha$ - and debye relaxation processes," *J. Chem. Phys.* **147**, 014502 (2017).
- <sup>110</sup>G. P. Johari and M. Goldstein, "Viscous liquids and the glass transition. II. Secondary relaxations in glasses of rigid molecules," *J. Chem. Phys.* **53**, 2372 (1970).
- <sup>111</sup>E. Bartsch, F. Fujara, B. Geil, M. Kiebel, W. Petry, W. Schnauss, H. Sillescu, and J. Wuttke, "Signatures of the glass transition in a van der Waals liquid seen by neutrons and NMR," *Physica A* **201**, 223 (1993).
- <sup>112</sup>J. Wuttke, W. Petry, and S. Pouget, "Structural relaxation in viscous glycerol: Coherent neutron scattering," *J. Chem. Phys.* **105**, 5177 (1996).
- <sup>113</sup>W. Kob and H. C. Andersen, "Kinetic lattice-gas model of cage effects in high-density liquids and a test of mode-coupling theory of the ideal-glass transition," *Phys. Rev. E* **48**, 4364 (1993).
- <sup>114</sup>L. J. Lewis and G. Wahnström, "Molecular-dynamics study of supercooled *ortho*-terphenyl," *Phys. Rev. E* **50**, 3865 (1994).
- <sup>115</sup>M. Cook, D. C. Watts, and G. Williams, "Correlation function approach to the dielectric behaviour of amorphous polymers," *Trans. Faraday Soc.* **66**, 2503 (1970).
- <sup>116</sup>After this paper was submitted PCS data of more supercooled liquids have become available, see F. Pabst, J. Gabriel, T. Böhmer, P. Weigl, A. Helbling, T. Richter, P. Zourchang, T. Walther, and T. Blochowicz, "Universal structural relaxation in supercooled liquids," [arXiv:2008.01021](https://arxiv.org/abs/2008.01021).
- <sup>117</sup>B. Geil and G. Hinze, "Influence of data treatment on the shape of  $^2\text{H}$  NMR  $T_1$  curves," *Chem. Phys. Lett.* **216**, 51 (1993).
- <sup>118</sup>L.-M. Wang and R. Richert, "Identification of dielectric and structural relaxations in glass-forming secondary amides," *J. Chem. Phys.* **123**, 054516 (2005).
- <sup>119</sup>C. S. Zehe, J. A. Hill, N. P. Funnell, K. Kreger, K. P. van der Zwan, A. L. Goodwin, H.-W. Schmidt, and J. Senker, "Polarisation auf der Mesoskala durch geometrische Frustration in kolumnaren supramolekularen Kristallen," *Angew. Chem.* **129**, 4502 (2017).
- <sup>120</sup>See <https://www.chembk.com/en/chem/o-terphenyl> for *o*-Terphenyl, 18 June 2020.
- <sup>121</sup>M. G. Faizullin, R. V. Galeev, and A. K. Mamleev, "Microwave spectrum of 2-methyltetrahydrofuran," *Russ. J. Phys. Chem.* **91**, 2275 (2017).
- <sup>122</sup>See <https://www.chembk.com/en/chem/2-Methyltetrahydrofuran> for 2-Methyltetrahydrofuran, 18 June 2020.
- <sup>123</sup>Y. E. Ryabov, Y. Hayashi, A. Gutina, and Y. Feldman, "Features of supercooled glycerol dynamics," *Phys. Rev. B* **67**, 132202 (2003).
- <sup>124</sup>See <https://www.chembk.com/en/chem/56-81-5> for Glycerol, 18 June 2020.
- <sup>125</sup>C. W. N. Cumper and A. P. Thurston, "Electric dipole moments and molecular conformations of aromatic amines, phosphites, and phosphates," *J. Chem. Soc., B* **1971**, 422.
- <sup>126</sup>See <https://pubchem.ncbi.nlm.nih.gov/compound/Tri-M-cresyl-phosphate> for National Center for Biotechnology Information, PubChem Compound Summary for CID 11232, Tri-M-cresyl phosphate, 18 June 2020.

---

## Publication 3

### **Dynamically asymmetric binary glass formers studied by dielectric and NMR spectroscopy**

**T. Körber**, R. Minikejew, B. Pötzschner,  
D. Bock and E. A. Rössler

*The European Physical Journal E*

**42**, 143 (2019)

DOI: 10.1140/epje/i2019-11909-5

© EDP Sciences / Società Italiana di Fisica /  
Springer-Verlag GmbH Germany,  
part of Springer Nature, 2019

# Dynamically asymmetric binary glass formers studied by dielectric and NMR spectroscopy\*

Th. Körber, R. Minikejew, B. Pötzschner, D. Bock, and E.A. Rössler<sup>a</sup>

Universität Bayreuth, Anorganische Chemie III and Nordbayerisches NMR-Zentrum, D-95440 Bayreuth, Germany

Received 30 May 2019 and Received in final form 18 September 2019

Published online: 20 November 2019

© EDP Sciences / Società Italiana di Fisica / Springer-Verlag GmbH Germany, part of Springer Nature, 2019

**Abstract.** We investigate the component dynamics in asymmetric binary glass formers. Focusing on the dielectric spectra of the high- $T_g$  components m-tricresyl phosphate and quinaldine mixed with toluene as low- $T_g$  component, the broadend spectra cannot be described by Kohlrausch or Cole-Davidson (CD) functions. Instead, we apply a generalized CD function which allows to control the width of the susceptibility independently of its high-frequency flank. The spectra show a common broadening and failure of the frequency-temperature superposition with increasing toluene concentration. This is confirmed by stimulated echo experiments showing an increased stretching of the probed orientational correlation function. In analogy to the definition of  $T_g$ , we consider “isodynamic points”. For each component, a different but linear concentration dependence of  $1/T_{iso}$  is revealed, indicating different time scales. Qualitatively, we do not find significant differences for the present mixtures with  $T_g$ -contrasts of 63–89 K compared to those with larger  $T_g$ -contrast ( $\Delta T_g > 170$  K): Whereas the high- $T_g$  component shows relaxation features similar to those of neat glass formers, yet, with “atypical” weak relaxation broadening, the faster low- $T_g$  component displays pronounced dynamic heterogeneities. This is supported by scrutinizing NMR relaxation data of several mixtures investigated previously as a function of concentration. A universal evolution of the dynamics of the high- $T_g$  as well as the low- $T_g$  component is suggested for mixtures with high  $\Delta T_g$ .

## 1 Introduction

Pure glass formers were extensively investigated in the past [1–10]. The next experimental challenge is to characterize the dynamics of binary glass formers. Whereas technologically relevant polymer-additive (or polymer-plasticizer) systems were the subject of intensive research [11–22] less is known about non-polymeric mixed glasses [8, 21–28], in particular, about such systems with a high  $T_g$ -contrast of their components as it is usually the case in polymer-plasticizer systems. These “dynamically asymmetric” mixtures may be taken as model systems for binary glass formers with significant size disparity of their components. Here, one may ask to what extent the dynamics of the small molecules in a more or less rigid matrix of large molecules still resembles that of neat glass formers, and whether the small molecules undergo a new kind of glass transition [22], for example. In a series of papers, we investigated the component dynamics in such binary glass formers by dielectric as well as by NMR spectroscopy [29–

35]. Mixtures with a  $T_g$ -contrast of their components up to  $\Delta T_g \cong 250$  K were studied. In addition to polymers, specially synthesized non-polymeric glass formers were considered as high- $T_g$  component and mixed with a low- $T_g$  liquid [33, 34]. It turned out that the compiled dynamic scenario does not differ significantly when taking a polymeric or non-polymeric high- $T_g$  component.

At all concentrations, two separated main relaxation processes –  $\alpha_1$  (referring to the dynamics invoked by the slow high- $T_g$  component) and  $\alpha_2$  (referring to the faster dynamics of the low- $T_g$  or additive component) – are identified in addition to some  $\beta$ -process (cf. fig. 1). Dielectric studies revealed that the two relaxation processes are not completely decoupled: A temperature-dependent fraction of the low- $T_g$  molecules participates in the dynamics of the high- $T_g$  component [22, 28, 34]. Each process involves liquid-like, isotropic reorientations as confirmed by  $^2\text{H}$  and  $^{31}\text{P}$  NMR experiments. The high- $T_g$  component shows relaxation features similar to that of a neat glass former, *i.e.*, a Kohlrausch-like reorientational correlation loss is observed, though some broadening of the relaxation is found. The low- $T_g$  component displays significantly faster dynamics and pronounced dynamic heterogeneities. This may lead to, depending on the concentration, quasi-logarithmic correlation functions. In

\* Contribution to the Topical Issue “Dielectric Spectroscopy Applied to Soft Matter” edited by Simone Napolitano.

<sup>a</sup> e-mail: [ernst.roessler@uni-bayreuth.de](mailto:ernst.roessler@uni-bayreuth.de)  
(corresponding author)

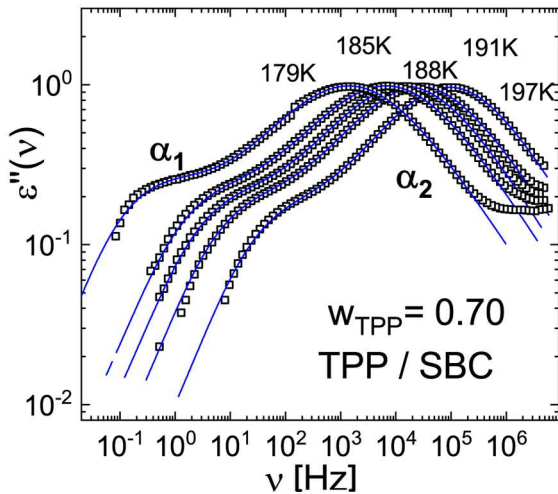


**Fig. 1.** Dielectric spectra of the mixture tripropyl phosphate (TPP)/SBC with a mass fraction of  $w_{\text{TPP}} = 0.70$ . SBC is a spirobichroman derivate with  $T_g = 356$  K [34]. Lines: interpolations by a superposition of a Kohlrausch ( $\alpha_1$ ) and a Havriliak-Negami susceptibility ( $\alpha_2$ ).

other words, an extremely broad distribution of correlation times  $G(\ln \tau_{\alpha_2})$  in comparison to a moderately wide distribution  $G(\ln \tau_{\alpha_1})$  is found when the  $T_g$ -contrast is sufficiently large. Importantly, the spectra of the  $\alpha_2$ -process are strongly broadened on the low-frequency flank (see fig. 1), in contrast to what is observed in neat glass formers. The dynamic heterogeneities are transient in nature as proven by 2D exchange NMR [18,33,36]. Thus, liquid-like (isotropic) reorientation of the low- $T_g$  additive as well as exchange within its distribution  $G(\ln \tau_{\alpha_2})$  is observed in an essentially rigid matrix of the high- $T_g$  component.

In a joint analysis of dielectric and NMR spectroscopy the time constants of each component were derived (cf. fig. 2(a)), clearly demonstrating the strong separation of the dynamics. Accordingly, two glass transition temperatures  $T_{g1}(w_2)$  and  $T_{g2}(w_2)$  with non-trivial concentration dependences can be identified; an example is given in fig. 2(b) for m-tricresyl phosphate (m-TCP) mixed with another spirobichroman derivate “DH” as the high- $T_g$  glass former [33]. Concentrations are always given in terms of mass fraction of the low- $T_g$  component  $w_2$ . It is well established that such systems (including polymer-plasticizer systems) exhibit two glass transition temperatures albeit they are fully miscible [13,15,28,37–40]. Even polymer blends show this phenomenon [41,42]. The peculiar trace of  $T_{g2}(w_2)$  showing a maximum at intermediate concentration  $w_{\text{m-TCP}}$  (fig. 2(b)), however, was not reported before. Yet, many studies on polymer-plasticizer systems did not investigate the full concentration range. The phenomenon is a direct consequence of the fragile-to-strong transition observed for the time constant  $\tau_{\alpha_2}$  at low additive concentrations (cf. fig. 2(a),  $w_2 = 0.34$ ), a feature also reported by other studies on binary glass formers [22,30], for example. The crossover is found close to  $T_{g1}$ .

As the distribution  $G(\ln \tau_{\alpha_2})$  is asymmetrically broadened, in particular, on the long-time flank and overall

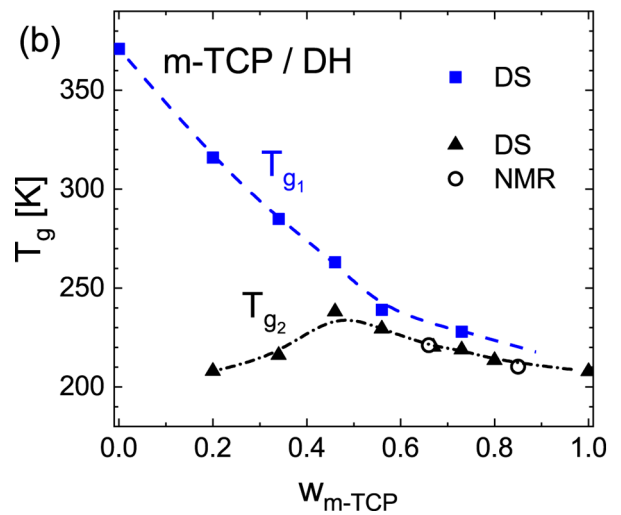
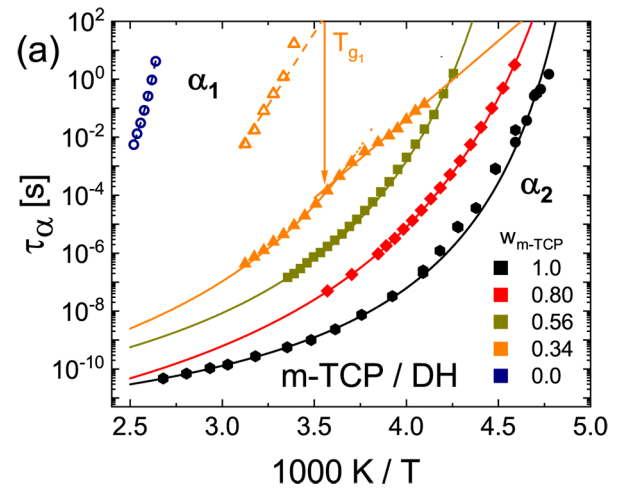


**Fig. 2.** (a) Relaxation times of the low- $T_g$  component m-tricresyl phosphate (m-TCP,  $T_g = 206$  K) and of the high- $T_g$  component (“DH”, a spirobichroman derivate with  $T_g = 382$  K) as well as in the mixtures [33]. Mass fraction is defined by color; open symbols represent  $\alpha_1$ - and filled symbols  $\alpha_2$ -process. (b) Glass transition temperatures,  $T_{g1}$  and  $T_{g2}$ , as revealed by DS and NMR for the mixture m-TCP/DH [33]; lines serve as guides for the eye.

broadens with decreasing temperature, the problem of defining an appropriate correlation time allowing to compare different experiments becomes an issue, especially for lower concentrations of the low- $T_g$  component  $w_2$ . In this case, the time constants extracted from the dielectric relaxation maximum (the most probable time constant) are not mean correlation times in the strict sense reflecting the correlation time  $\tau_{\alpha_2}$  as defined by the integral over the distribution function  $G(\ln \tau_{\alpha_2})$ . In the time domain,  $\tau$  is given by the integral over the correlation function which is determined by its long-time decay, which, as said, is highly stretched in the case of the additive relaxation. The maximum in  $T_{g2}(w_{\text{add}})$  may even disappear if one can access  $\tau_{\alpha_2}$  in a proper way which is obviously difficult in binary systems facing an extremely broadened dielectric spectrum and an overlap with the contribution

of the high- $T_g$  component. Of course, the actual fragile-to-strong transition cannot be explained in such a way; this phenomenon always leads to a lowering of  $T_{g2}$  at low additive concentrations. As we deal in the present study with the spectral evolution of the high- $T_g$  component with only subtle changes with respect to the spectra of the pure component, the problem is less severe.

For completeness, we mention that recently a somewhat different interpretation of the dynamics in binary glass formers was derived from essentially the same experimental basis [43,44]. The authors argue that the here discussed  $\alpha_2$ -relaxation is actually a mixture of a  $\beta$ -relaxation and the “true”  $\alpha_2$ -relaxation. By this interpretation, again no maximum in  $T_{g2}(w_2)$  appears. As sketched above we do favor a different interpretation due to the conclusive NMR results.

The design of the above discussed experiments was such that the low- $T_g$  component, for example, TPP, dominated the dielectric response, *i.e.*, TPP displays a dipole moment which is much larger than that of the high- $T_g$  components. Thus, the dielectric spectra directly reflected the dynamics of TPP embedded in the high- $T_g$  matrix. Surprisingly, however, two main relaxation peaks were observed (cf. fig. 1). As said, this suggests that there exists a second sub-ensemble of TPP molecules which shares the dynamics of the high- $T_g$  molecules. Similar conclusions were drawn by Blochowicz and coworkers [22,28]. For the present study two decisive things were changed. First, systems were chosen with a smaller  $T_g$ -contrast, specifically toluene/quinaldine (quin) ( $\Delta T_g = 63$  K) and toluene/m-TCP ( $\Delta T_g = 89$  K). Second, the high- $T_g$  component carries a significantly higher dipole moment compared to that of the additive and thus dominates the dielectric spectrum. This allows us to analyze the change of  $G(\ln \tau_{\alpha_1})$  in more detail compared to our previous experiments. Again, employing the  $^2\text{H}$  and  $^{31}\text{P}$  nucleus as additional NMR probes, we assume that both techniques, NMR and dielectric spectroscopy, have to be interpreted along the same lines, as both probe solely reorientational dynamics, yet in terms of the second and first Legendre polynomial correlation function, respectively. The results, particularly obtained from measuring the spin-lattice relaxation, are compared to a plethora of data we compiled in previous studies. As will be demonstrated, we find strong indications for a relaxation pattern in binary glass formers controlled essentially by the  $T_g$ -contrast.

## 2 Experimental and spectra analysis

### 2.1 Dielectric spectra

The dielectric permittivity is given by the equation [45,46]

$$\varepsilon^*(\omega) = \varepsilon'(\omega) - i\varepsilon''(\omega) = \varepsilon_\infty + \Delta\varepsilon \int_0^\infty -\frac{d\phi(t)}{dt} e^{-i\omega t} dt, \quad (1)$$

where  $\varepsilon^*(\omega)$  is the complex dielectric constant,  $\omega$  the angular frequency,  $\varepsilon_\infty$  the high-frequency permittivity, and  $\phi(t)$  the step-response function.

The dielectric response in binary glass formers cannot be described by a Cole-Davidson or Kohlrausch function. In the case of the high- $T_g$  component, we applied a generalization of the pulse-response function of the CD function introduced by Kahlau *et al.* [47] which allows controlling its high-frequency flank independently of its overall width. The latter is given by [45]

$$\varphi_{CD}(t) = -\dot{\phi}_{CD}(t) = \frac{1}{\tau_{CD}\Gamma(\beta)} \left(\frac{t}{\tau_{CD}}\right)^{\beta-1} e^{-\frac{t}{\tau_{CD}}} \quad (2)$$

and the step-response function by

$$\phi_{CD}(t) = \frac{1}{\Gamma(\beta)} \int_{\frac{t}{\tau_{CD}}}^\infty x^{\beta-1} e^{-x} dx = \frac{\Gamma(\beta, \frac{t}{\tau_{CD}})}{\Gamma(\beta)} \quad (3)$$

with

$$\Gamma(\beta) = \int_0^\infty x^{\beta-1} e^{-x} dx \quad (4)$$

denoting the Gamma function and

$$\Gamma(\beta, y) = \int_y^\infty x^{\beta-1} e^{-x} dx \quad (5)$$

being the upper incomplete Gamma function. The generalized pulse-response function  $\phi_g(t)$  can be introduced modifying  $\phi_{CD}(t)$  by adding a stretching parameter  $\alpha$  to the exponential expression, *i.e.*, changing the exponential term in eq. (3) to a Kohlrausch expression.

$$\phi_g(t) = \frac{\int_{\frac{t}{\tau_g}}^\infty x^{\beta-1} e^{-x^\alpha} dx}{\int_0^\infty x^{\beta-1} e^{-x^\alpha} dx}. \quad (6)$$

An alternative definition of  $\phi_g(t)$  which is more suitable for a numerical implementation of the model function is given by

$$\phi_g(t) = \frac{1}{\Gamma(\frac{\beta}{\alpha})} \int_{(\frac{t}{\tau_g})^\alpha}^\infty y^{\frac{\beta}{\alpha}-1} e^{-y} dy = \frac{\Gamma(\frac{\beta}{\alpha}, (\frac{t}{\tau_g})^\alpha)}{\Gamma(\frac{\beta}{\alpha})} \quad (7)$$

with the (mean) correlation time  $\tau$  defined by the integral over the step correlation function or equivalently by the spectral density at zero frequency (see below)

$$\tau = \tau_g \frac{\Gamma(\frac{1+\beta}{\alpha})}{\Gamma(\frac{\beta}{\alpha})}. \quad (8)$$

It is obvious that  $\phi_g(t) = \phi_{CD}(t)$  for  $\alpha = 1$  and  $\beta = \beta_{CD}$  (cf. eq. (3)). For  $\alpha = \beta_K$ ,  $\phi_g(t)$  gives the Kohlrausch step response function  $\phi_K(t)$ . In other words, the generalized function includes the case of a CD and a Kohlrausch response. In the case that the parameters are not very small the ratio  $\tau/\tau_g$  is not far from unity.

In addition to the main relaxation peak described by the Fourier transform of eq. (7), some of the spectra show an excess wing which is described by an additional CD spectrum with the condition  $\tau_g = \tau_{CD}$  as done before in the case of neat glass formers [48].

The imaginary part of eq. (1) can be expressed by

$$\varepsilon''(\omega) = \Delta\varepsilon\omega\phi''(\omega) = \Delta\varepsilon\chi''(\omega), \quad (9)$$

where the normalized spectral density  $\phi''(\omega)$  is given by the Fourier transform of the step-response function  $\phi(t)$  and  $\chi''(\omega)$  denotes the normalized dynamic susceptibility. In the limit of low frequencies one can write

$$\varepsilon''(\omega)/\Delta\varepsilon = \omega\tau. \quad (10)$$

Here,  $\tau$  is the mean correlation time as given by eq. (8) or equivalently by  $\phi''(\omega = 0)$ . Equation (10) allows to construct master curves by shifting the normalized dielectric spectra  $\varepsilon''(\omega)/\Delta\varepsilon$  solely along the  $\omega$  axis until agreement is found at low frequencies with the straight line given by  $\omega^1$ . The resulting shift factors are identical with the mean correlation time  $\tau$ , in the present case with  $\tau_\alpha$ . This procedure is applied to analyze the atypically broadened spectra in the binary glass formers.

The dielectric measurements were carried out with an Alpha-A Analyzer from Novocontrol in the frequency range  $\nu = 10^{-2}$ – $10^6$  Hz. Temperature was kept constant within  $\pm 0.2$  K by using a Quatro-H temperature controller from Novocontrol yielding an absolute accuracy better than  $\pm 0.2$  K. For the mixture toluene/m-TCP, we measured the mass fractions  $w_{tol} = 0.21, 0.45, 0.70$  and  $0.88$ . In the case of the mixture toluene/quinaldine, we measured  $w_{tol} = 0.25, 0.50, 0.70$  and  $0.90$ . The error of these concentrations was estimated to  $\pm 0.02$ .

## 2.2 NMR Relaxation

The  $^{31}\text{P}$  NMR relaxation is determined by the fluctuations of the chemical shift anisotropy (CSA) [49,50]. The relative contribution to the relaxation from heteronuclear dipolar coupling is weak at the applied high magnetic field, and in the case of homonuclear coupling it is negligible due to the large distance between the phosphorus nuclei in the investigated mixtures [51]. The  $^2\text{H}$  relaxation is caused by the fluctuations of the quadrupolar interaction [49,50]. The relaxation rates  $1/T_1$  and  $1/T_2$  are linked to the spectral density  $\phi''(\omega)$  at multiples of the Larmor frequency  $\omega_L$ . In the case of the CSA interaction one gets

$$\frac{1}{T_1} = K^{CSA}\phi''(\omega_L), \quad (11)$$

$$\frac{1}{T_2} = \frac{1}{6}K^{CSA}[4\phi''(0) + 3\phi''(\omega_L)], \quad (12)$$

$$\text{with } K^{CSA} = \frac{2}{15}(\Delta\sigma_{CSA}\omega_L)^2 = \frac{2}{15}\left(\frac{3}{2}\delta_{CSA}\right)^2. \quad (13)$$

$\Delta\sigma$  gives the frequency-independent shielding parameter, while the anisotropy parameter  $\delta_{CSA}$  can be directly determined from the width of  $^{31}\text{P}$  powder spectrum.

In the case of the quadrupolar interaction the relaxation rates are given by

$$\frac{1}{T_1} = \frac{2}{15}\delta_Q^2[\phi''(\omega_L) + 4\phi''(2\omega_L)], \quad (14)$$

$$\frac{1}{T_2} = \frac{1}{15}\delta_Q^2[3\phi''(0) + 5\phi''(\omega_L) + 2\phi''(2\omega_L)], \quad (15)$$

$$\text{with } \delta_Q = \frac{3eQeq}{4\hbar}. \quad (16)$$

$\delta_Q$  is the anisotropy parameter given by the interaction of the quadrupolar moment ( $eQ$ ) with the electric field gradient ( $eq$ ), which can be determined directly from the splitting of the satellites of the  $^2\text{H}$  solid state (Pake) spectrum at low temperatures. In both cases,  $^2\text{H}$  and  $^{31}\text{P}$  NMR, the spectral density  $\phi''(\omega)$  is given by the Fourier transform of the second Legendre polynomial reorientational correlation function.

Reorientational time constants can then be estimated at the  $T_1$ -minimum via the condition  $\omega_L\tau \cong 1$  for  $^{31}\text{P}$  NMR and  $\omega_L\tau \cong 0.62$  for  $^2\text{H}$  NMR. Here, the most probable time constant is estimated which is not identical with that of eq. (8). However, for the present case of rather narrow relaxation spectra, the difference can be safely ignored. Under extreme narrowing condition ( $\omega_L\tau \ll 1$ ), *i.e.*,  $\phi''(\omega) \cong \phi''(0)$  in eqs. (11), (12) and (14), (15) respectively,  $\frac{1}{T_1} = \frac{1}{T_2} = \frac{2}{3}\delta_Q^2\tau$  holds in the case of  $^2\text{H}$  NMR and  $\frac{1}{T_1} = K^{CSA}\tau$  in the case of  $^{31}\text{P}$  NMR independent of a specific model for  $\phi''(\omega)$ . In this case, the time constant  $\tau$  is identical to that of eq. (8). In the slow motion limit ( $\omega_L\tau \gg 1$ ), only  $1/T_2$  is directly linked to the time constant  $\tau = \phi''(0)$ , which leads to  $\frac{1}{T_2} = \frac{2}{3}K^{CSA}\tau$  for  $^{31}\text{P}$  NMR and  $\frac{1}{T_2} = \frac{1}{5}\delta_Q^2\tau$  for  $^2\text{H}$  NMR, whereas the relationship for  $1/T_1$  depends on details of the spectral density.

The spin-lattice relaxation measurements were performed with an inversion recovery pulse sequence at higher and with a saturation recovery pulse sequence at lower temperatures. The spin-spin relaxation time  $T_2$  was obtained from the spectral width of the Lorentzian line ( $T_2 = 1/(\pi\Delta\nu_{FWHM})$ ) in the liquid when inhomogeneous broadening can be neglected.

In this study, we investigated the mixture toluene/m-TCP with NMR. Therefore, we used deuterated toluene to apply  $^2\text{H}$  NMR at the Larmor frequency  $\omega_L = 2\pi \cdot 46.05$  MHz. We measured  $w_{tol} = 0.21, 0.51$  with toluene- $d_5$  and  $w_{tol} = 0.84$  with toluene- $d_8$ , where we then extracted the corresponding  $T_1$ -relaxation times for toluene- $d_5$ . To investigate the m-TCP dynamics, which is direct accessible via  $^{31}\text{P}$  NMR, the following mass fractions  $w_{tol}$  were measured:  $w_{tol} = 0.0, 0.21, 0.51$  and  $0.84$  at the Larmor frequency  $\omega_L = 2\pi \cdot 162$  MHz.

## 2.3 Stimulated echo experiment

From the decay of the stimulated echo, the full reorientational correlation function of the second Legendre polynomial is accessible, *i.e.*, the rank-two reorientational correlation function is probed [52–54]. In the present case

of  $I = 1/2$  nuclei, the three-pulse echo sequence ( $90^\circ$ - $t_p$ - $90^\circ$ - $t_m$ - $90^\circ$ ) with appropriate pulse phases is applied and the echo amplitude is measured for different mixing times  $t_m$ , for a constant short evolution time  $t_p$ . If the second and third pulse is shifted by  $90^\circ$  compared to the first pulse, then the sine-sine reorientational correlation function  $F_{t_p}^{\text{sin}}(t_m)$  is probed. For the decay of the stimulated echo  $I(t_m, t_p)$ , one finds

$$I(t_m, t_p) \propto \langle \sin(\omega(0)t_p) \sin(\omega(t_m)t_p) \rangle \exp\left(-\left(\frac{t_m}{T_1}\right)\right) = F_{t_p}^{\text{sin}}(t_m) \exp\left(-\left(\frac{t_m}{T_1}\right)\right), \quad (17)$$

where  $F_{t_p}^{\text{sin}}(t_m)$  is damped by the spin-lattice relaxation.  $\omega$  refers to the frequency in the rotating frame. For a short evolution time  $t_p$ , the correlation function  $F_{t_p}^{\text{sin}}(t_m)$  approximates the rank-two reorientational correlation function  $C_2(t)$

$$\lim_{t_p \rightarrow 0} F_{t_p}^{\text{sin}}(t_m) \propto \langle \omega(0)\omega(t_m) \rangle \propto C_2(t), \quad (18)$$

which is interpolated by the generalized CD function introduced above (cf. eq. (7)).

### 3 Results

#### 3.1 NMR spin-lattice relaxation – a common scenario

A first qualitative picture is provided by measuring the  $^2\text{H}$  and  $^{31}\text{P}$  spin-lattice relaxation rate  $R_1 = 1/T_1$  as a function of temperature. In fig. 3 we consider the rate  $R_1$  vs. the temperature of the mixture toluene- $d_5$  ( $T_g = 117\text{K}$ ) with m-TCP ( $T_g = 206\text{K}$ ). The experiment is analogous to plotting the dielectric loss  $\varepsilon''$  measured at a given frequency as function of  $T$ . In fig. 3(a) the results obtained by  $^2\text{H}$  NMR are shown, *i.e.*, the dynamics of the low- $T_g$  component toluene is reflected. Whereas for neat toluene a narrow and high relaxation peak is observed, it successively broadens and lowers its amplitude upon adding m-TCP. In addition, the maximum shifts to higher temperatures indicating a slowing-down of the dynamics due to the anti-plasticizer effect of m-TCP. The strong broadening of the relaxation peak and the decreasing of its amplitude is a direct consequence of the emergence of pronounced dynamic heterogeneities induced by concentration fluctuations in binary glass formers. They are described by a distribution  $G(\ln \tau_{\alpha_2})$  becoming broader and broader at lower toluene concentrations. Even indications of a bimodal distribution are found.

In fig. 3(b) the results from the  $^{31}\text{P}$  NMR spin-lattice relaxation rate are displayed originating from the dynamics of the high- $T_g$  component m-TCP. Now, a slight opposite effect is recognized: The relaxation maximum weakly increases with adding toluene to m-TCP, and it shifts to lower temperatures due to the plasticizer effect of toluene. These findings clearly demonstrate that, depending on

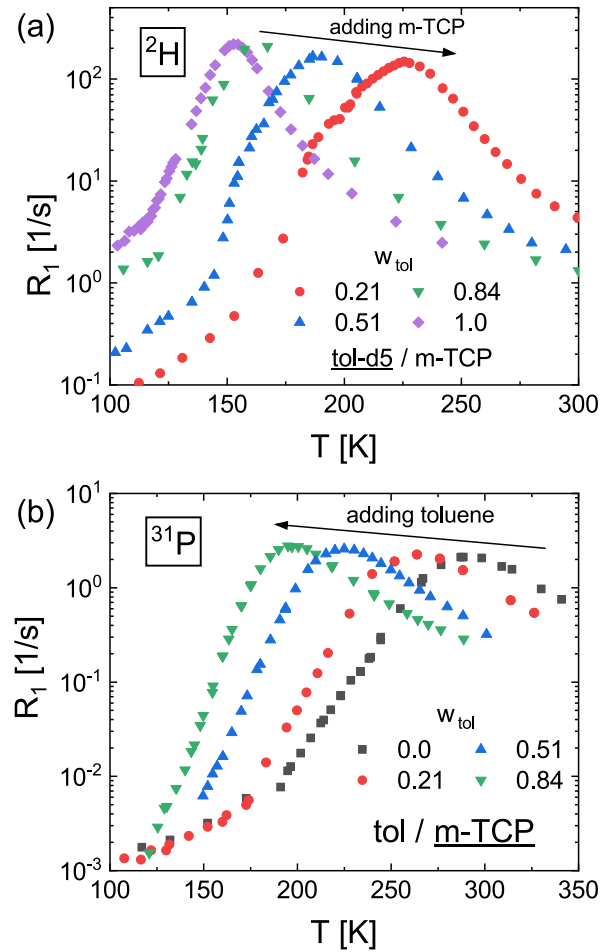


**Fig. 3.** Spin-lattice relaxation rate  $R_1 = 1/T_1$  as a function of temperature for different concentrations  $w_{\text{tol}}$ : (a) toluene in the mixture toluene/m-TCP probed by  $^2\text{H}$  NMR. Pure toluene data adapted from [55,56]. (b) m-TCP in the same mixture with toluene probed by  $^{31}\text{P}$  NMR.

whether being the high- or the low- $T_g$  component, the dynamics of the component is quite different: The high- $T_g$  component displays dynamics close to that of neat glass formers, while the low- $T_g$  component exhibits strong dynamic heterogeneities which may even involve a bimodal  $G(\ln \tau_{\alpha_2})$ , as said.

A first estimate of the respective time constants can be drawn from the condition  $\omega_L \tau_{\alpha_2} \cong 0.62$  ( $^2\text{H}$  NMR) and  $\omega_L \tau_{\alpha_1} \cong 1$  ( $^{31}\text{P}$  NMR). As mentioned, an estimate of the most probable time constant is given (cf. sect. 2.2). The results are included in fig. 10 (stars). Clearly, similar time constants are found at quite different temperatures. The  $\tau_{\alpha_2}$  of toluene is found at lower temperature. In other words, toluene reorients faster than m-TCP, as expected. The differences in the dynamics can be directly identified when comparing the NMR spectra – see fig. 4. In contrast to systems with larger  $T_g$ -contrast [31,33], the dynamic decoupling is not that strong and therefore the lineshape changes of each component take place at comparable temperatures. Still, the changes set in at slightly

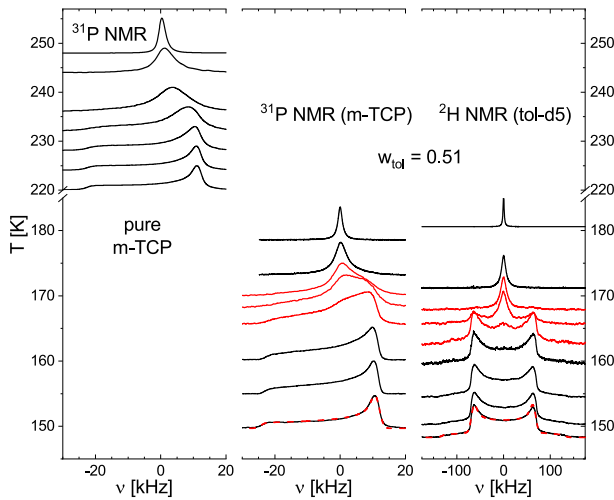


**Fig. 4.**  $^2\text{H}$  and  $^{31}\text{P}$  NMR spectra of the mixture toluene/m-TCP with  $w_{\text{tol}} = 0.51$ . Their baseline defines the temperature. The temperature range with two-phase spectra is marked. At lowest temperatures, the dashed lines show the fits of the solid state spectra to determine the corresponding coupling constant  $\delta_{Q/CSA}$ . On the left side, the  $^{31}\text{P}$  NMR spectra of pure m-TCP are shown for comparison.

higher temperatures for m-TCP. One finds “two-phase” spectra (indicating dynamic heterogeneities) for toluene, yet, in a rather small temperature interval. Furthermore, two-phase spectra are recognized for m-TCP as well. This means, that not only  $G(\ln \tau_{\alpha_2})$  is broadened in the mixture but also  $G(\ln \tau_{\alpha_1})$ , which was not always observable in our previous investigations. Such two-phase spectra are characterized by a superposition of a liquid (Lorentzian) line and a solid-state spectrum with different weighting factors changing with temperature [57, 52]. The strong plasticizer effect of toluene is seen comparing the NMR spectra for pure m-TCP with those in the mixture (cf. fig. 4).

The results of the spin-lattice relaxation rates presented in fig. 3 are very similar to those reported for other previously investigated binary glass formers with a much higher  $T_g$ -contrast [29, 32, 33, 58] and also for the toluene/polystyrene system investigated long time ago [59, 60]. This is demonstrated in fig. 5, where the relaxation rate at the relaxation maximum (an isodynamical point when measured at the same Larmor frequency) normalized to its value of the neat component is plotted against the mass fraction  $w_2$  of the low- $T_g$  component. This is shown for the case of  $^2\text{H}$  NMR relaxation in fig. 5(a) and for  $^{31}\text{P}$  NMR in fig. 5(b). Semi-quantitatively this normalized rate  $R_1^{\text{max}}(w_2)/R_1^{\text{max}}(w_2 = 1)$  is a measure of the width of the underlying susceptibility or distribution  $G(\ln \tau)$ , with respect to that of the neat component (like a dielectric width parameter).

In the case of toluene (probed by  $^2\text{H}$  NMR) mixed with polystyrene (PS,  $T_g = 373$  K) [59, 60],  $R_1^{\text{max}}(w_2)/R_1^{\text{max}}(w_2 = 1)$  (right scale) decreases with decreasing  $w_2$  and reaches very small values at lowest  $w_2$  in fig. 5(a). In other words, the distribution  $G(\ln \tau_{\alpha_2})$  of the low- $T_g$  component becomes extremely broad in the case of a large

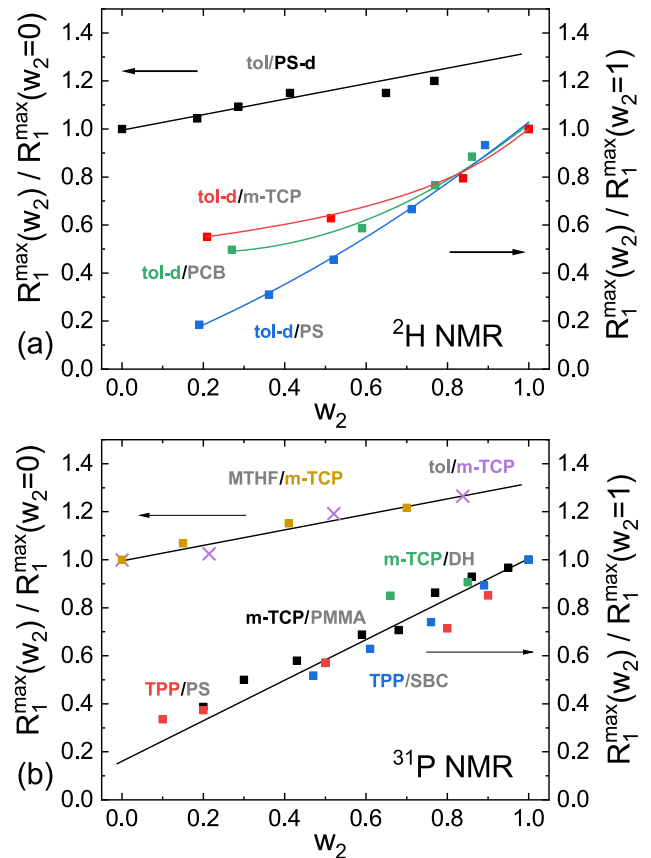


**Fig. 5.** (a) Normalized relaxation rate maxima  $R_1^{\text{max}}(w_2)/R_1^{\text{max}}(w_2 = 1)$  (right scale) in the case of the low- $T_g$  component toluene and  $R_1^{\text{max}}(w_2)/R_1^{\text{max}}(w_2 = 0)$  (left scale) in the case of various high- $T_g$  components, as revealed by  $^2\text{H}$  NMR on the deuterated components [29, 60]. (b) Corresponding normalized relaxation rate maxima as obtained by  $^{31}\text{P}$  NMR of the phosphorus containing components [32–34]. Color gives the measured component of the mixtures. The  $T_g$ -contrast is 89 K for the system toluene (tol)/m-TCP, 110 K for MTHF/m-TCP, 129 K for tol/PCB and at least 170 K up to 250 K for all other systems analyzed (cf. text).

$T_g$ -contrast and low concentration  $w_2$ . Similar trends were found for toluene mixed with PCB54 (a polychlorinated biphenyl;  $T_g = 246$  K) [29], and for the present systems toluene/m-TCP, respectively, yet the broadening is less pronounced as in the case of toluene/PS; the width of  $G(\ln \tau_{\alpha_2})$  appears to saturate at some finite value at lowest values  $w_2$ . Comparing the three systems, the final broadening at lowest  $w_2$  (i.e., at highest concentration of the high- $T_g$  component) is the higher the smaller the  $T_g$ -contrast is. Regarding the  $^2\text{H}$  results for the deuterated high- $T_g$  component PS, a weak opposite effect is observed: Adding toluene to PS, its relaxation spectrum appears to become somewhat narrower, i.e.,  $R_1^{\text{max}}(w_2)/R_1^{\text{max}}(w_2 = 0)$  (left scale) increases by dilution.

Completely analogous results are obtained from  $^{31}\text{P}$  NMR. Here, we compare the mixtures TPP/PS [32], TPP/SBC [34], m-TCP/PMMA [32], and m-TCP/DH [33]. Due to the  $T_g$ -contrast being rather high in all

these cases (about 170 K and higher), a common behavior is observed for  $R_1^{\max}(w_2)/R_1^{\max}(w_2 = 1)$  (right scale) *vs.*  $w_2$ , *i.e.*, in all cases, the low- $T_g$  component displays an extremely broad  $G(\ln \tau_{\alpha_2})$  at low  $w_2$  values. In contrast, m-TCP playing the role of the high- $T_g$  component in the systems toluene/m-TCP (present work) and methyl tetrahydrofuran (MTHF;  $T_g = 96$  K)/m-TCP [32],  $R_1^{\max}(w_2)/R_1^{\max}(w_2 = 0)$  (left scale) displays a weak opposite effect. Dilution of m-TCP with a low- $T_g$  component appears to somewhat narrow the distribution  $G(\ln \tau_{\alpha_1})$ .

The indication that  $G(\ln \tau_{\alpha_2})$  broadens upon mixing with a high- $T_g$  component is also well documented by DS, for example as seen in fig. 1, where a strong broadening on the low-frequency flank is recognized for the major peak reflecting the dynamics of the low- $T_g$  component. In contrast, the case of the high- $T_g$  component is less obvious as all previously compiled dielectric spectra were dominated by the signal of a highly polar low- $T_g$  component leading to a purely resolved  $\alpha_2$ -peak. The spectral analyses were carried out by assuming a Kohlrausch function for describing  $G(\ln \tau_{\alpha_1})$  as in the case of neat glass formers [30]. However, its width also increased, yet, weakly with adding the low- $T_g$  component which is at variance with the trend observed by the NMR relaxation data in fig. 5. We will come back to this point later.

## 3.2 Evolution of the dielectric spectra

### 3.2.1 Toluene/m-tricresyl phosphate

In the present paper, we discuss in detail the spectral evolution of the high- $T_g$  component. This became possible via DS choosing high- $T_g$  components with a much higher dipole moment compared to that of the low- $T_g$  component. In fig. 6(a), we show the dielectric spectra of neat toluene and m-TCP. The amplitudes of the corresponding relaxation peaks differ by about one and a half decades. We thus assume that except for highest toluene concentrations the DS spectra are dominated by the m-TCP signal. The spectra of the mixture  $w_2 = 0.45$  toluene/m-TCP, as measured, are included in fig. 6(a). Clearly, the spectra are broadened in comparison with those of neat m-TCP. In addition, a weak  $\beta$ -relaxation is observed in pure toluene as well as in the mixture.

In order to allow for a quantitative comparison of the dielectric spectra at the different concentrations and to determine the mean time constant (cf. eq. (8)) in a model independent way as a function of temperature, we apply the procedure explained above providing master curves (cf. sect. 2.1), *i.e.*, we plot  $\varepsilon''(\omega)/\Delta\varepsilon$  *vs.*  $\omega\tau^{-1}$  in fig. 7 after the DC contribution is subtracted. In the case of pure m-TCP, this low frequency limit is not fully recovered. The relaxation strength  $\Delta\varepsilon$  is determined from the real part  $\varepsilon'(\omega)$ , and the master curves are obtained by shifting  $\varepsilon''(\omega)/\Delta\varepsilon$  solely along the  $\omega$  axis until agreement with the straight line  $\varepsilon''(\omega)/\Delta\varepsilon = \omega$  is achieved on the low-frequency flank. For control, we show in fig. 6(b) the (averaged) relaxation strength  $\Delta\varepsilon$  as a function of  $w_2$  after Curie correction and averaging over the weak temperature dependence of  $\Delta\varepsilon$ . A

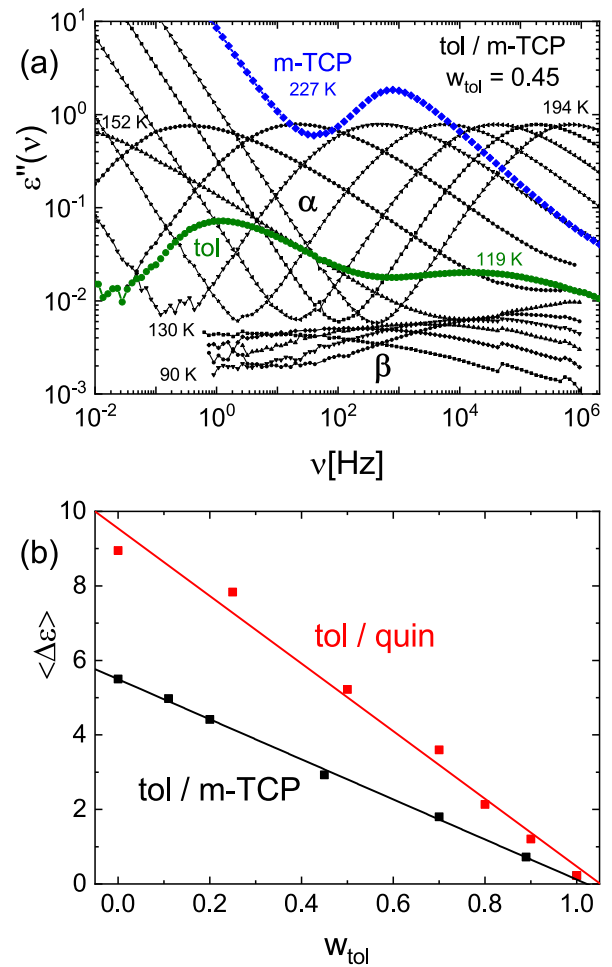


**Fig. 6.** (a) Dielectric spectra of neat toluene (green circles) and of neat m-TCP (blue diamonds) as measured. In addition, the spectra of the mixture  $w_{tol} = 0.45$  toluene/m-TCP are displayed for the  $\alpha$ -process ( $T = 152$  K– $194$  K,  $\Delta T = 6$  K, black points) and the  $\beta$ -process ( $T = 90$  K– $130$  K,  $\Delta T = 10$  K, black points). (b) Averaged relaxation strength defined as  $\langle \Delta\varepsilon \rangle = \langle \Delta\varepsilon \cdot T \rangle / \langle T \rangle$  of the (polar) high- $T_g$  component m-TCP and quinaldine (quin), respectively, mixed with toluene as a function of mass fraction  $w_{tol}$ .

linear dependence is revealed confirming the assumption that the response reflects the signal from m-TCP even at highest toluene concentrations. The data of the system toluene/quinaldine are included (see below); here, possibly a weak non-linear concentration dependence shows up.

The following features are observed in fig. 7. i) Starting with pure m-TCP up to the  $w_2 = 0.21$  mixture, FTS applies, yet, the overall peak becomes somewhat broader with respect to that of neat m-TCP (dashed line). ii) The excess wing, well recognized in the pure m-TCP, becomes more and more difficult to be identified due to a broader relaxation peak. iii) For concentration  $w_2 = 0.45$  and higher, FTS fails and the relaxation broadens further. iv) It appears that the high-frequency flank remains essentially the same although the overall width of the spectra becomes broader. v) At the highest toluene concentrations ( $w_2 = 0.70$  and  $w_2 = 0.88$ ), spectral contributions from

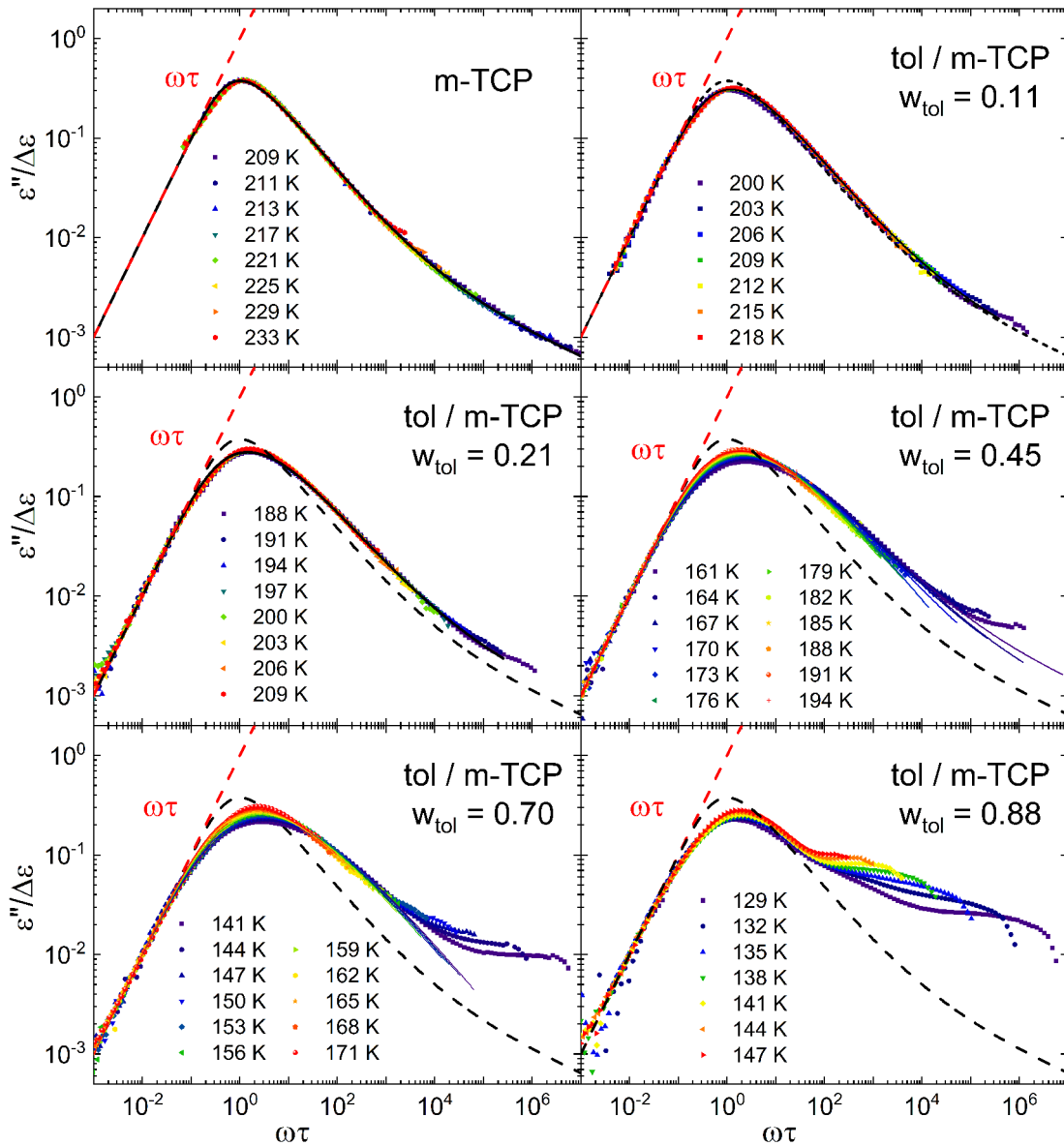


**Fig. 7.** Master curves of the dielectric spectra of the mixture toluene/m-TCP at different temperatures and different mass fractions of toluene. Straight dashed line represents low-frequency limit  $\omega\tau$ . For comparison, the fit of the master curve of neat m-TCP is added in each case (black dashed line). The fits, a superposition of the GCD (main peak) and CD function (excess wing), are shown as solid lines. The corresponding parameters are given in fig. 8.

toluene are observed at high frequencies, in particular, a  $\beta$ -relaxation typical of toluene is recognized. The spectra cannot be described by a Kohlrausch or Cole-Davidson function as it is well established when concentration fluctuations come into play [61]. Applying the latter functions, for example, it is not possible to keep the high-frequency exponent fixed and vary the overall width. Hence, we take recourse to the generalization of the Cole-Davidson and Kohlrausch functions introduced by Kahlau *et al.* (subsequently abbreviated GCD function; cf. sect. 2.1) [47]. The susceptibility function allows to describe an overall broadened relaxation peak (set by the parameter  $\alpha$ ) independently of its high-frequency flank (set by the parameter  $\beta$ ). For low values  $w_2$ , an additional CD function was used

to interpolate the excess wing at highest frequencies. At higher concentrations, as said, it cannot be clearly identified any longer. The corresponding fits are included in fig. 7 and well reproduce the experimental spectra. Yet, the quality of the fits with a constant parameter  $\beta$  appears to become worse at highest  $w_2$ .

Figure 8 summarizes the fit results regarding the parameter  $\alpha = \alpha(T)$ . The high-frequency parameter  $\beta$  can be kept constant, *i.e.*,  $\beta = 0.62$  as for neat m-TCP for which a temperature independent parameter  $\alpha = 0.80$  is found. Here, we give the average values  $\langle\alpha\rangle$  as no systematic trends are found. As the value of the parameter  $\alpha$  is rather high, the spectral shape of neat m-TCP is close to that of a CD function ( $\alpha = 1$ ) as found before [51].

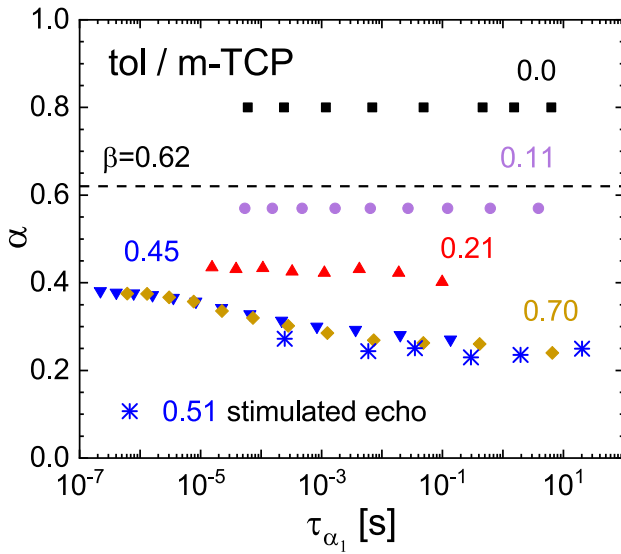


**Fig. 8.** Width parameter  $\alpha$  of the GCD function as a function of the time constants  $\tau_{\alpha_1}$  as given for different toluene mass fractions (colour coded) of the system toluene/m-TCP. The horizontal line represents the value of the parameter  $\beta$  assumed the same for all concentrations and temperatures. For comparison we added the results of the NMR stimulated echo experiment in the case of the  $w_2 = 0.51$  mixture.

Adding toluene brings the parameter down to  $\alpha \cong 0.58$  at  $w_2 = 0.11$ , *i.e.*, the spectral shape is close to a Kohlrausch function. At  $w_2 = 0.21$  the parameter becomes  $\alpha \cong 0.40$ . At higher concentrations ( $w_2 = 0.45$  and  $w_2 = 0.70$ ) a temperature dependence is revealed with values  $\alpha \cong 0.25$  at lowest temperatures and  $\alpha \cong 0.40$  at highest temperatures, indicating the failure of FTS. Yet, the quality of the fits becomes worse. It appears, that the high-frequency flank is not constant any longer. For the highest concentration ( $w_2 = 0.88$ ), we refrain therefore to perform fits. In this case, spectral contributions from toluene are well recognized.

Summarizing these results, we see a clear broadening of the dielectric spectra of the high- $T_g$  component m-TCP upon adding toluene and a failure of FTS at high  $w_2$ . The described trend of the spectral evolution can also be monitored by  $^{31}\text{P}$  NMR applying the stimulated echo method [52,53]. It reveals the second Legendre polynomial reorientational correlation function  $C_2(t)$  directly in the time domain instead of the spectrum of  $C_1(t)$  as measured by DS, actually, in essentially the same time/frequency window. Figure 9 gives some examples for toluene/m-TCP and for MTHF/m-TCP (previously investigated [32]). In fig. 9(a) we consider the changes with respect to the concentration. In both systems the correlation decay becomes more stretched compared to that of neat m-TCP when adding MTHF or toluene, respectively. In fig. 9(b) the temperature dependence of the decays of the mixture  $w_2 = 0.51$  toluene/m-TCP is shown. Fitting a GCD function again with  $\beta = 0.62$  to the decay for these data, essentially the same results for  $\alpha(T)$  are obtained as in the case of the dielectric data – see fig. 8. We conclude

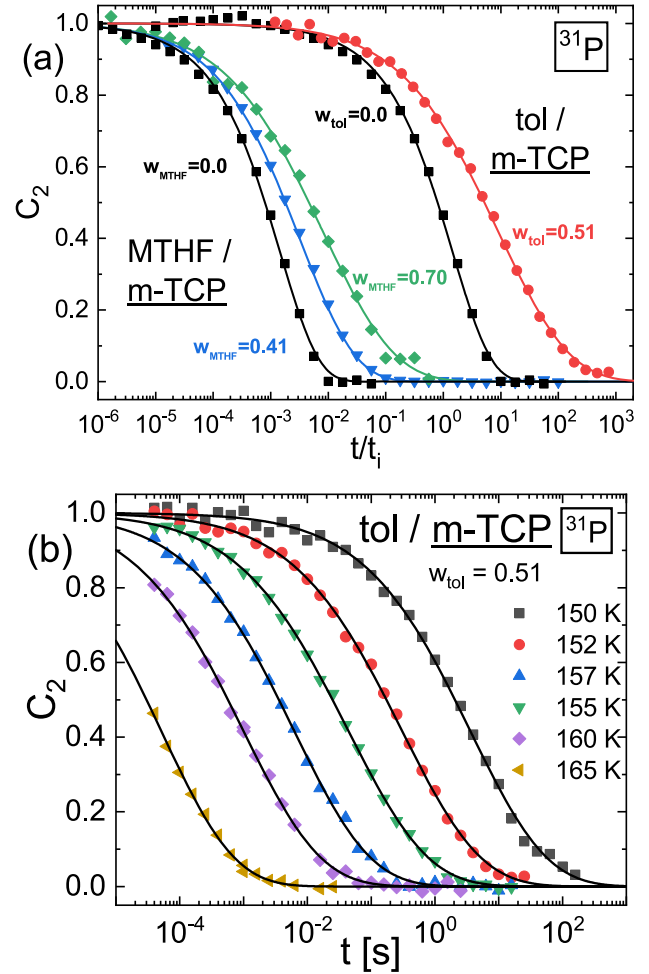


**Fig. 9.** (a)  $^{31}\text{P}$  NMR stimulated echo decays of the mixtures MTHF/m-TCP (left) and toluene/m-TCP (right), respectively. For better visualization, the decay curves for a given system are normalized to the initial decays and a further arbitrary shift was taken to discriminate the decays of the two systems. The corresponding mass fractions  $w_2$  are given. The decays are interpolated by the GCD function keeping the parameter  $\beta = 0.62$  constant. (b) Temperature-dependent  $^{31}\text{P}$  NMR stimulated echo decays of the mixture toluene/m-TCP with  $w_2 = 0.51$ , which are interpolated the same way as in (a).

that NMR stimulated echo and DS monitor consistently the “unconventional” spectral evolution – in the sense that CD or Kohlrausch functions do not apply – of the main relaxation of the high- $T_g$  component.

The trend of the spin-lattice relaxation rate  $R_1$  at the maximum (cf. fig. 5), which indicates a slight narrowing of the m-TCP susceptibility upon dilution with toluene, however, cannot be explained by the evolution of the dielectric spectra and stimulated echo decays. Here, one has to keep in mind that the NMR relaxation maximum occurs in the ns correlation time regime, *i.e.*, at significantly higher temperatures compared to the DS spectra, and from fig. 8, it is impossible to decide what values are reached at high temperatures. As an opposite effect is observed, *i.e.*, the relaxation rate  $R_1(T)$  of m-TCP becomes

sharper and higher (by about 20%) upon adding toluene, some relative enhancement in the spectral density with respect to that of neat m-TCP has to occur. One candidate is the excess wing. Possibly it disappears more and more in the mixture. Indeed, the excess wing is not any longer observed for  $w_2 \geq 0.70$  in the DS spectra. We emphasize that the apparent narrowing of the  $R_1(T)$  is also observed by  $^2\text{H}$  NMR in the case of the (deuterated) high- $T_g$  matrix PS, thus a generic explanation is needed (cf. fig. 5(a)). Presently, yet, we cannot find a final solution for this finding.

Figure 10(a) presents the time constants of the neat systems toluene [62] and m-TCP [51] as reported previously. Additionally, the time constants of the  $\beta$ -process, another relaxation feature well recognized in neat toluene and also observed in the mixtures, are added. As in many binary glass formers, the time constant  $\tau_\beta$  depends only weakly or even not at all on the concentration [26, 63, 64]. An average activation energy of  $\Delta E_\beta = 23.3 \frac{\text{kJ}}{\text{mol}} = 24.0 \cdot RT_g^{\text{tol}}$  is observed for all studied concentrations. We note, however, as  $T_g$  changes with concentration the relationship  $E_\beta \cong 24 RT_g$  observed for many neat glass formers does not hold any longer in the mixtures [65].

In fig. 10(b) all the time constants from DS and NMR in the mixture toluene/m-TCP are displayed. Regarding the NMR analysis, as already discussed, one gets a first estimate for the time constant from the maximum condition of  $R_1(T)$ , and the stimulated echo decays yield further data at low temperatures. The full spectral density determining the spin-lattice relaxation is unknown so far. Therefore, we further analyzed the data only in the extreme narrowing limit, for which the extracted time constants are independent of the particular spectral density. For this purpose, the NMR coupling constants are needed which are accessible from the solid-state spectrum observed at low temperature, *i.e.*, in the limit of rigid molecules (cf. fig. 4 and sect. 2.2). Taking  $\delta_Q/2\pi \cong 132 \text{ kHz}$  for  $^2\text{H}$  NMR and  $\delta_{CSA}/2\pi \cong 26 \text{ kHz}$  for  $^{31}\text{P}$  NMR obtained from fits, the resulting time constants are added in fig. 10(b). Clearly, the dynamics of the components is decoupled; about 1.5 decades difference is revealed at high temperatures.

The conventionally defined glass transition temperature  $T_g$  is an isodynamic point, *i.e.*, it reflects the temperature at which the main relaxation time is  $\tau_\alpha = 100 \text{ s}$ . However, if such long time constants are experimentally not reached, one can choose other definitions. Here we stick to the condition  $\tau_\alpha(T_g^{1s}) = 1 \text{ s}$  for the time constant of the high- $T_g$  component m-TCP measured by DS. A continuous slightly non-linear decrease of  $T_g^{1s}$  is observed in fig. 11(a) with increasing  $w_2$ . Other isodynamic points are given by the temperature yielding a maximum in the spin-lattice relaxation rate  $R_1(T)$ . It refers to the relaxation time  $\tau = \frac{0.62}{2\pi \cdot 46 \cdot 10^6} \text{ s} \approx 2.1 \text{ ns}$  in the case of  $^2\text{H}$  NMR (toluene) and  $\tau = \frac{1}{2\pi \cdot 162 \cdot 10^6} \text{ s} \approx 0.98 \text{ ns}$  for  $^{31}\text{P}$  NMR (m-TCP). Actually, both time constants are quite close, and therefore define  $T_g^{\text{NMR}}$ , which when plotted *versus*  $w_2$  directly reflects the decoupling of the component dynamics in the ns regime. Indeed, this is observed in fig. 11(a):

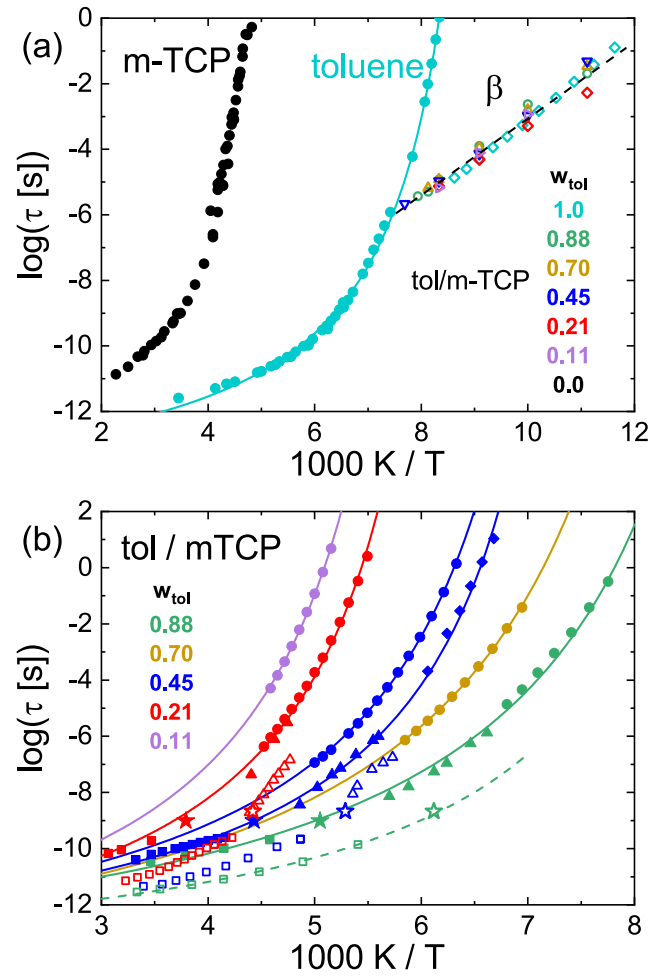


**Fig. 10.** (a) Time constants of neat m-TCP and neat toluene, respectively, as obtained by NMR, DS and other methods from literature [51,62]. In addition, the relaxation times of the  $\beta$ -process of the mixture toluene/m-TCP as determined by DS (open symbols). (b) Time constants of m-TCP and toluene in their mixture by DS (circles), respectively, as revealed by  $^{31}\text{P}$  NMR ( $\alpha_1$ : filled symbols) and by  $^2\text{H}$  NMR ( $\alpha_2$ : open symbols).  $\tau$  determined from  $T_1$ -minima (stars), from high-temperature  $T_1$  relaxation data (squares), from  $T_2$  relaxation times (triangles) and from  $^{31}\text{P}$  stimulated echo data (diamonds). NMR concentrations differ slightly from those shown for DS ( $w_{\text{tol}}^{\text{NMR}} = 0.51, 0.84$ ).

$T_g^{\text{NMR}}$  for toluene and m-TCP are significantly different; that of toluene is lower than that of m-TCP. Inspecting the corresponding NMR data of toluene/PS (included in fig. 11(a)) a similar behavior is observed, yet the  $T_g^{\text{NMR}}$ -difference of the two components is much larger. We also added the result  $T_g^{1s}(w_2)$  of the high- $T_g$  component quinaldine in the mixture toluene/quinaldine (blue line). As will be discussed below, the  $T_g$ -contrast is somewhat smaller than in the case of toluene/m-TCP. In any case, the present NMR relaxation data do not cover slow dynamics, and thus cannot detect a possible fragile-to-strong transition, possibly observed in  $\tau_{\alpha_2}(T)$ .

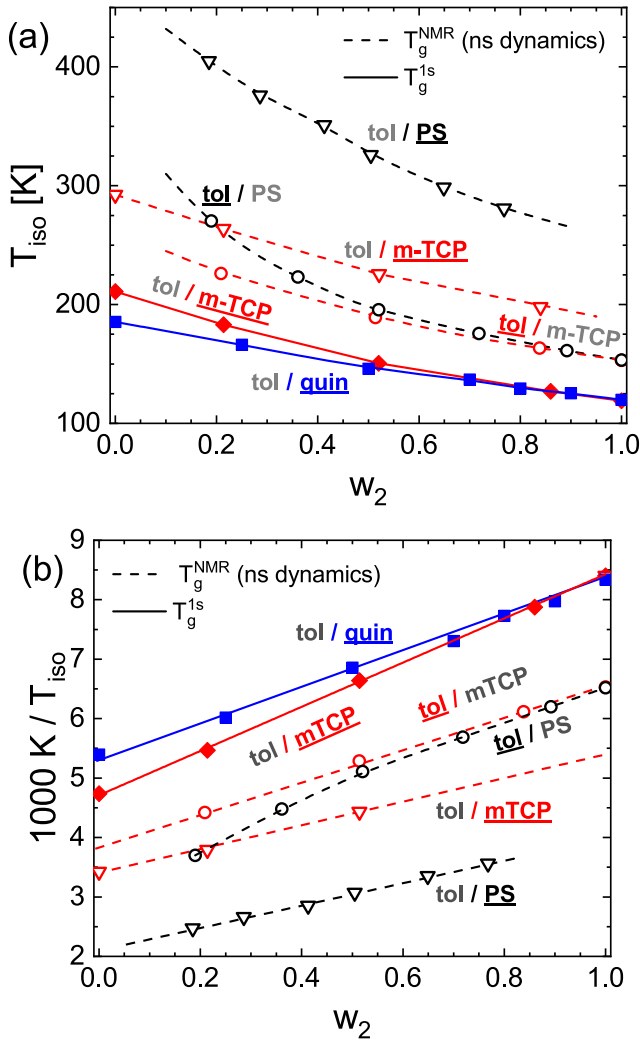


**Fig. 11.** (a) Isodynamic points  $T_g^{1s}$  (solid lines) and  $T_g^{NMR}$  (dashed lines, from  $^2\text{H}$  and  $^{31}\text{P}$  NMR) plotted *versus* mass fraction  $w_2$  of the systems toluene (tol)/m-TCP, toluene/quinaldine (quin), and toluene/polystyrene (PS), respectively. System is given by color and component by symbol. Lines are guides for the eye. (b) Data as in (a) plotted in terms of reciprocal temperatures  $1000/T_g^{1s}$  and  $1000/T_g^{NMR}$ , respectively, *vs.* concentration. Lines are linear interpolations with exception of toluene/PS (open black circles).

One can also plot the reciprocal  $1/T_g^i$  values as a function of  $w_2$  as done in fig. 11(b) where we also plotted the data for toluene/PS [60] and for toluene/quinaldine (see below). In this representation a linear behavior is observed for low- $T_g$ -contrast systems. In the case of toluene/PS, the linear behavior is observed for PS, whereas a weak deviation is found in the case of toluene. Thus, in some approximation the reciprocal glass temperature follows a kind of Gordon-Taylor (or Fox) formula [66] for both components  $i = 1, 2$  separately:

$$\frac{1}{T_{g_i}}(w_i) = \frac{1 - w_i}{T_{g_i}^\infty} + \frac{w_i}{T_{g_i}^{pure}}. \quad (19)$$

The value  $T_{g_i}^{pure}$  is the  $T_g$  of the pure component while  $T_{g_i}^\infty$  is the extrapolated value of  $T_g$  for infinite dilution. Importantly, the values  $T_{g_{1/2}}^\infty$  are not the same as  $T_{g_{2/1}}^{pure}$  of the second pure component. Such a relationship is well established for polymer blends [61,67], where the concept of self-concentration comes into play, but also applicable for polymer plasticizer systems [60].

### 3.2.2 Toluene/quinaldine

The binary glass former toluene/quinaldine was solely studied by DS. Again, the relaxations strength of quinaldine (quin) is much larger than that of toluene (tol) and even larger than that of m-TCP (cf. fig. 6(b)). Hence, the DS spectra reflect essentially the dynamics of quinaldine as affected by toluene in the mixture. In fig. 12 the corresponding master curves (after DC contribution is subtracted) are shown for six concentrations. As in the case of toluene/m-TCP, at low concentrations ( $w_2 = 0.0$  and 0.25) FTS essential works and a weak overall broadening is observed with the high-frequency flank not significantly changing its exponent. At higher concentrations broadening continues, yet, FTS fails more and more. Again, the spectra can be described by a GCD function ( $\beta = 0.65$ ) with an additional CD function to describe the excess wing at low  $w_2$  values. But this fit fails more and more at high  $w_2$ . In particular, it appears that the assumption of a  $w_2$ -independent parameter  $\beta$  does not hold at high  $w_2$  any longer. At  $w_2 = 0.90$  contributions from the toluene relaxation are clearly recognized at the high-frequency flank.

The corresponding parameters  $\alpha$  and  $\beta$  as a function of  $\tau_{\alpha_1}$  are found in fig. 13, for the cases interpolating the spectra appears to work. Quite similar parameters are found as in the case of toluene/m-TCP (cf. fig. 8). As the quality of the spectra at high values of  $w_2$  does not allow a reasonable fit at all temperatures and thus does not allow a full comparison among the two mixtures, we further apply a phenomenological analysis. Plotting the full width at half maximum ( $F$ ) of the dielectric spectra normalized by the value  $F_0$  of a Debye function, for both m-TCP and quinaldine mixed with toluene, respectively, as a function of  $w_2$  – see fig. 15 in appendix A – allows this comparison. In this model-independent representation of the spectral evolution, essentially the same behavior is observed.

As the master curve construction (fig. 12) allows to determine the time constants of the high- $T_g$  component in a model-independent manner, we get time constants  $\tau_{\alpha_1}(T)$  of quinaldine with toluene even in the cases no appropriate fits with the GCD function are possible (see fig. 14(a)). In the case when reliable fits are possible, the same results are reported for the mean relaxation time given by eq. (8) (open *vs.* filled symbols). The corresponding  $T_g^{1s}$  and  $1/T_g^{1s}$ , respectively, are included in fig. 11 and show an analogue linear behavior as in the case of toluene/m-TCP. The smaller  $T_g$ -contrast of toluene/quinaldine is clearly recognized.

Figure 14(b) displays the time constants of the neat systems toluene and the time constants of the well

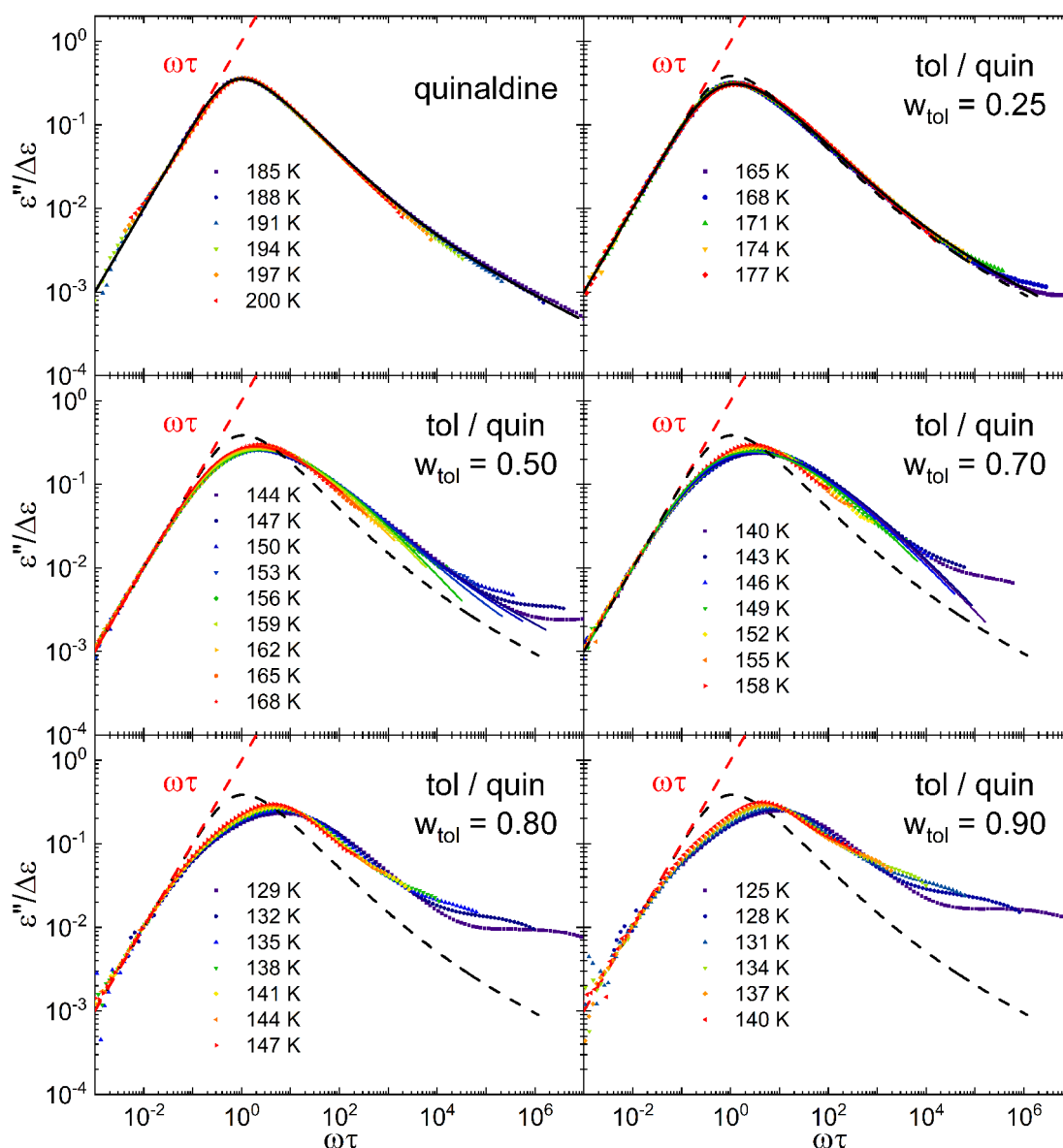


**Fig. 12.** Master curves of the dielectric spectra of the mixture toluene (tol)/quinaldine (quin) at different temperatures and different mass fractions of toluene  $w_{tol}$ . Straight dashed line represents low-frequency limit  $\omega\tau$ . Fits are included as far as possible as solid lines. For comparison, the fit of the master curve of neat quinaldine is added in each case (black dashed line).

recognizable  $\beta$ -process in this mixture.  $\tau_\beta(w)$  depends only weakly on the concentration like in the mixture toluene/m-TCP. An average activation energy over all concentrations of  $\Delta E_\beta = 25.6 \frac{\text{kJ}}{\text{mol}} = 26.4 \cdot RT_g^{tol}$  is observed for an assumed Arrhenius temperature dependence, which is only slightly higher compared to that of neat toluene and in the mixture with m-TCP (cf. fig. 10(a)).

#### 4 Discussion and conclusions

Compiling the component selective NMR relaxation rate maxima of various mixtures investigated before as well as in the present study as a function of concentration, a common scenario is revealed. It appears that only the  $T_g$ -

contrast controls the evolution of the relaxation spectrum with concentration. In the case of a large contrast, larger than, say, 150 K, a universal pattern is observed independent of what component is considered and what NMR probe is employed ( $^2\text{H}$  or  $^{31}\text{P}$  NMR) (cf. fig. 5). As the relaxation rates probe the component dynamics in the ns range, indications of the behavior leading to a maximum in  $T_{g2}(w_2)$  cannot be discovered in these data sets. The latter phenomenon being a direct consequence of the fragile-to-strong transition appearing only close to  $T_{g1}$  (cf. fig. 2) still deserves further studies. Comparing qualitatively the results of the present mixtures with  $T_g$ -contrasts of 63–89 K to those with larger  $T_g$ -contrast, we do not find significant differences: Whereas the high- $T_g$  component shows relaxation features similar to those of neat glass formers,

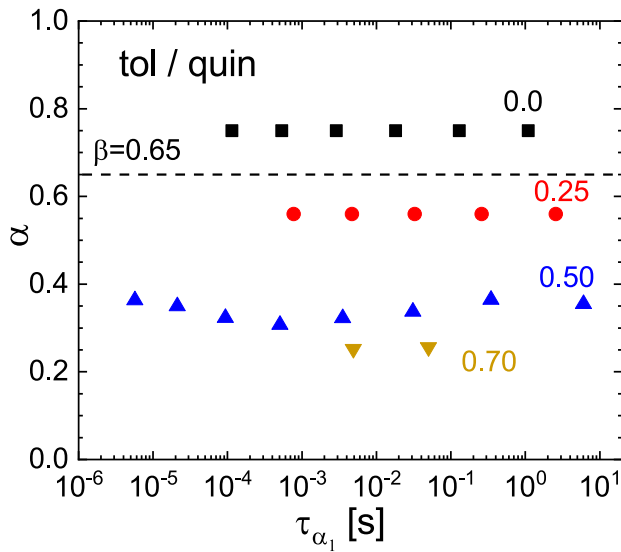


**Fig. 13.** Width parameter  $\alpha$  of the GCD function as a function of the time constants  $\tau_{\alpha_1}$  as given for different toluene mass fractions  $w_2$  (color coded) of the system toluene/quinaldine. The horizontal line represents the value of the parameter  $\beta$  assumed the same for all shown concentrations and temperatures.

yet, with a weak relaxation broadening, the faster low- $T_g$  component displays pronounced dynamic heterogeneities.

Specifically, we investigated the spectral evolution in two binary mixtures with a moderate  $T_g$ -contrast, namely quinaldine and m-TCP mixed with toluene ( $\Delta T_g = 63\text{ K} - 89\text{ K}$ ). Due to the large dipole moment of the high- $T_g$  component, the dielectric response is dominated by the high- $T_g$  constituent. Therefore we were able to consider details of the evolution of  $G(\ln \tau_{\alpha_1})$  which was not done before. It turns out, that the spectral evolution upon adding toluene shows a low-frequency broadening which cannot be described by a Kohlrausch or CD function at low  $w_2$  values. We applied a recently introduced GCD function which allows to control the width of the susceptibility peak independent of that of the high-frequency flank. Furthermore, by constructing susceptibility master curves on an absolute scale, a model independent way to determine the average correlation times for complex susceptibilities was demonstrated. Quinaldine and m-TCP as high- $T_g$  components essentially display the same spectral changes with  $w_2$ , thus suggesting a universal spectral evolution of the high- $T_g$  component in binary molecular glass formers. This does not hold in the case of mixtures of associated liquids for which quite different spectral evolutions are observed [68]. Still, we cannot provide a final explanation for the opposite effect observed for the spin-lattice relaxation rate  $R_1(T)$  of the high- $T_g$  component. The relaxation maximum of  $R_1(T)$  probing dynamics at high temperatures appears to indicate a narrowing of  $G(\ln \tau_{\alpha_1})$ , in contrast to what is reported by the DS and NMR stimulated echo experiments for lower temperatures.

The dynamics of binary mixtures consisting of particles (lacking orientational degrees of freedom) with different size was also investigated by MD simulations [69–

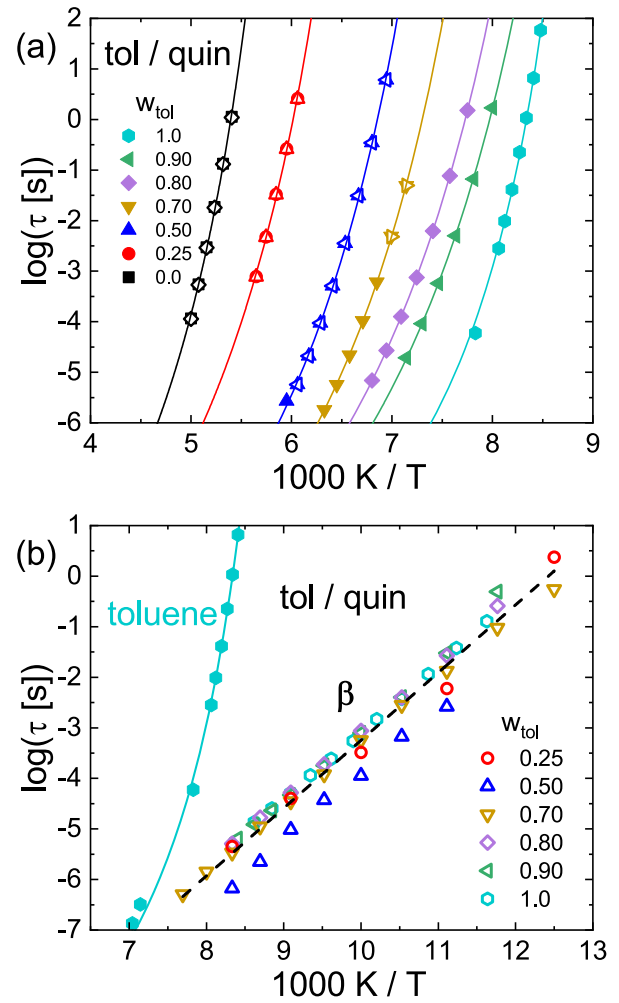


**Fig. 14.** (a) Time constants of quinaldine in the mixture with toluene obtained by the master curve construction (filled symbols) and by the GCD fit (open symbols) of the dielectric spectra. In addition, time constants of pure toluene are included. (b) The relaxation times of the  $\beta$ -process in the mixture. For comparison, the relaxation times of the  $\alpha$ - and  $\beta$ -process of pure toluene are included. The dashed line gives an Arrhenius interpolation.

73]. Here, a dynamical decoupling of both particle species was reported. The large particles exhibit a standard glass transition controlled by the cage effect, while the small particles still remain mobile within the arrested matrix of the large particles. In particular, when the size disparity is larger than 2.5 (by diameter ratio) quasi-logarithmic decays are visible in the density-density correlator, but less pronounced in the self-correlation function [71–73]. In this limit, one may speak about confinement effects revealed by the additive dynamics. As in our experiments, the dynamics of the small (fast) particles is qualitatively different compared to that of the large (slow) particles.

Previously, the dynamical heterogeneities typical of binary glass formers were explained in terms of thermally driven concentration fluctuations [74, 75] or so-called self-concentration effects [67], *i.e.*, the presence of local compo-

sition heterogeneity. In this context, a very recent MD simulation is of interest, which investigated a mixture of two water-like model molecules with different polarities such that the dynamical contrast is large whereas the mixture remains miscible in a sufficiently large temperature interval [76]. Again, dynamical decoupling was observed and the fast component displays quasi-logarithmic correlation decays together with a sub-diffusive regime in the mean square displacement. In contrast, the dynamics of the slow component resembles essentially that of neat glass formers. The growing concentration fluctuations upon cooling, characteristic of approaching spinodal decomposition, control the spatially heterogeneous dynamics. Specifically, in contrast to the behavior of ensemble-averaged data, the dynamics of the components does not strongly differ when studied as a function of the *local* concentration. However, the probability of finding a certain concentration fluctuation is narrow in the case of the slow component whereas it is broadly distributed for the fast component. Thereby, the authors are able to understand the qualitatively different dynamics of the slow and the fast component, respectively. Of course, the MD model was constructed to mimic water-specific interactions, and so far one can only diagnose the high similarities of the phenomena reported by our experiments.

Clearly, concentration fluctuations are of relevance, however, in the case of dynamically very asymmetric mixtures, additional confinement effects may come into play as emphasized by theoretical studies. For example, the phenomenon was investigated by the mode coupling theory (MCT) where a dynamic decoupling of large and small particles is anticipated, if the components differ sufficiently in size [77–79]. In that case, the smaller particles retain mobility below  $T_g$  of the larger ones and undergo a localization transition in the confinement of a frozen matrix. In this respect, work on MCT in so-called quenched-annealed systems [80,81] and simulations for a Lorentz-gas model [82] may be relevant. In such systems, MCT predicts higher-order singularities [69,83,84] in the vicinity of which the correlation functions of the smaller molecules become extremely broad and quasi-logarithmic decay curves are expected as observed in simulations and experiments.

Financial support by the Deutsche Forschungsgemeinschaft (DFG) through the projects RO 907/19 is acknowledged. We especially appreciate the hospitality of Prof. Dr. Jürgen Senker and his whole group, giving us the possibility to proceed in our work.

**Publisher's Note** The EPJ Publishers remain neutral with regard to jurisdictional claims in published maps and institutional affiliations.

## Appendix A.

Figure 15 shows the full width at half maximum  $F_0$  of a Debye function over the value of the investigated dielectric spectra  $F$ , for both m-TCP and quinaldine mixed

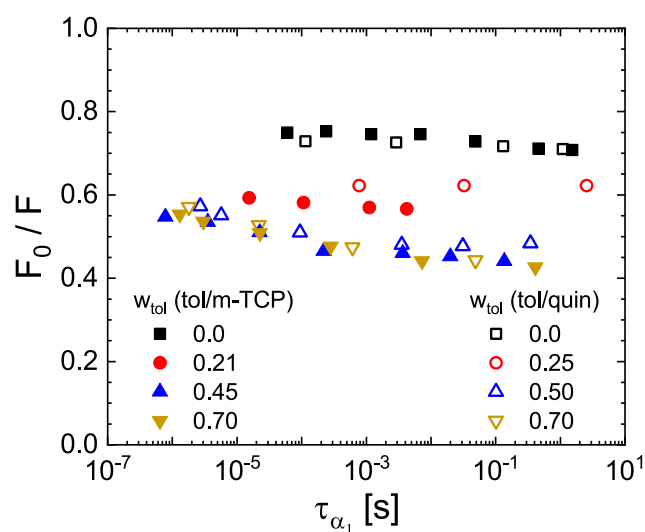


**Fig. 15.** Full width at half maximum  $F_0$  of a Debye function over the value of the investigated dielectric spectra  $F$  as a function of the time constants  $\tau_{\alpha_1}$ , for both m-TCP (filled symbols) and quinaldine (open symbols), respectively, in their mixtures with toluene.

with toluene, respectively, as a function of  $\tau_{\alpha_1}$  and concentration. Similar changes are observed for both mixtures.

## Author contribution statement

TK performed the NMR experiments on the mixture, supplemented by some experiments of DB. RM carried out the DS measurements. The analysis was done by TK supported by BP and RM. All of this was done in discussion with EAR as the group leader. The manuscript was prepared by TK and EAR.

## References

1. M.D. Ediger, *Annu. Rev. Phys. Chem.* **51**, 99 (2000).
2. P. Lunkenheimer, U. Schneider, R. Brand, A. Loidl, *Contemp. Phys.* **41**, 15 (2000).
3. J.C. Dyre, *Rev. Mod. Phys.* **78**, 953 (2006).
4. T. Blochowicz, A. Brodin, E.A. Rössler, in *Advances in Chemical Physics*, edited by W.T. Coffey, Y.P. Kalmykov (John Wiley & Sons, Inc., Hoboken, NJ, 2006) p. 127.
5. A. Cavagna, *Phys. Rep.* **476**, 51 (2009).
6. L. Berthier, G. Biroli, *Rev. Mod. Phys.* **83**, 587 (2011).
7. R. Richert, *Annu. Rev. Phys. Chem.* **62**, 65 (2011).
8. G. Floudas, M. Paluch, A. Grzybowski, K. Ngai, *Molecular Dynamics of Glass-Forming Systems: Effects of Pressure* (Springer, Berlin, Heidelberg, 2011).
9. P.G. Wolynes, V. Lubchenko, *Structural Glasses and Supercooled Liquids: Theory, Experiment, and Applications* (Wiley, Hoboken, NJ, 2012).
10. N. Petzold, B. Schmidtke, R. Kahlau, D. Bock, R. Meier, B. Micko, D. Kruk, E.A. Rössler, *J. Chem. Phys.* **138**, 12A510 (2013).
11. L.A. Utracki, *Polymer Alloys and Blends: Thermodynamics and Rheology* (Hanser, Munich, 1989).

12. P.J. Hains, G. Williams, *Polymer* **16**, 725 (1975).
13. D.J. Plazek, E. Riande, H. Markovitz, N. Raghupathi, *J. Polym. Sci. Polymer Phys. Ed.* **17**, 2189 (1979).
14. M.A. Desando, S. Walker, W.H. Baarschers, *J. Chem. Phys.* **73**, 3460 (1980).
15. M. Scandola, G. Ceccorulli, M. Pizzoli, *Polymer* **28**, 2081 (1987).
16. M. Nakazawa, O. Urakawa, K. Adachi, *Macromolecules* **33**, 7898 (2000).
17. T.R. Lutz, Y. He, M.D. Ediger, *Macromolecules* **38**, 9826 (2005).
18. D. Bingemann, N. Wirth, J. Gmeiner, E.A. Rössler, *Macromolecules* **40**, 5379 (2007).
19. S. Cervený, Á. Alegría, J. Colmenero, *Phys. Rev. E* **77**, 31803 (2008).
20. G. Goracci, A. Arbe, A. Alegría, Y. Su, U. Gasser, J. Colmenero, *J. Chem. Phys.* **144**, 154903 (2016).
21. T. Blochowicz, C. Karle, A. Kudlik, P. Medick, I. Roggatz, M. Vogel, C. Tschirwitz, J. Wolber, J. Senker, E. Rössler, *J. Phys. Chem. B* **103**, 4032 (1999).
22. T. Blochowicz, S. Schramm, S. Lusceac, M. Vogel, B. Stühn, P. Gutfreund, B. Frick, *Phys. Rev. Lett.* **109**, 35702 (2012).
23. T. Blochowicz, E.A. Rössler, *J. Chem. Phys.* **122**, 224511 (2005).
24. M.D. Ediger, T.R. Lutz, Y. He, *J. Non-Cryst. Solids* **352**, 4718 (2006).
25. K. Kessairi, S. Capaccioli, D. Prevosto, M. Lucchesi, P. Rolla, *J. Chem. Phys.* **127**, 174502 (2007).
26. D. Cangialosi, A. Alegría, J. Colmenero, *J. Chem. Phys.* **128**, 224508 (2008).
27. S. Capaccioli, K. Kessairi, M.S. Thayyil, D. Prevosto, M. Lucchesi, *J. Non-Cryst. Solids* **357**, 251 (2011).
28. T. Blochowicz, S.A. Lusceac, P. Gutfreund, S. Schramm, B. Stühn, *J. Phys. Chem. B* **115**, 1623 (2011).
29. B. Micko, C. Tschirwitz, E.A. Rössler, *J. Chem. Phys.* **138**, 154501 (2013).
30. R. Kahlau, D. Bock, B. Schmidtke, E.A. Rössler, *J. Chem. Phys.* **140**, 44509 (2014).
31. D. Bock, R. Kahlau, B. Pötzschner, T. Körber, E. Wagner, E.A. Rössler, *J. Chem. Phys.* **140**, 94505 (2014).
32. D. Bock, N. Petzold, R. Kahlau, S. Gradmann, B. Schmidtke, N. Benoit, E.A. Rössler, *J. Non-Cryst. Solids* **407**, 88 (2015).
33. B. Pötzschner, F. Mohamed, A. Lichtinger, D. Bock, E.A. Rössler, *J. Chem. Phys.* **143**, 154506 (2015).
34. B. Pötzschner, F. Mohamed, C. Bächer, E. Wagner, A. Lichtinger, R. Minikejew, K. Kreger, H.-W. Schmidt, E.A. Rössler, *J. Chem. Phys.* **146**, 164503 (2017).
35. D. Bock, T. Körber, F. Mohamed, B. Pötzschner, E.A. Rössler, in *The Scaling of Relaxation Processes*, edited by F. Kremer, A. Loidl (Springer, Cham, 2018) p. 173.
36. P. Medick, M. Vogel, E. Rössler, *J. Magn. Reson.* **159**, 126 (2002).
37. M. Pizzoli, M. Scandola, G. Ceccorulli, *Eur. Polym. J.* **23**, 843 (1987).
38. D.A. Savin, A.M. Larson, T.P. Lodge, *J. Polym. Sci. B: Polym. Phys.* **42**, 1155 (2004).
39. Y. Miwa, K. Usami, K. Yamamoto, M. Sakaguchi, M. Sakai, S. Shimada, *Macromolecules* **38**, 2355 (2005).
40. J.E.G. Lipson, S.T. Milner, *J. Polym. Sci. B: Polym. Phys.* **44**, 3528 (2006).
41. A.N. Gaikwad, E.R. Wood, T. Ngai, T.P. Lodge, *Macromolecules* **41**, 2502 (2008).
42. K. Mpoukouvalas, G. Floudas, *Macromolecules* **41**, 1552 (2008).
43. S. Valenti, S. Capaccioli, K.L. Ngai, *J. Chem. Phys.* **148**, 54504 (2018).
44. K.L. Ngai, S. Valenti, S. Capaccioli, to be published in *J. Non-Cryst. Solids* (2019) <https://doi.org/10.1016/j.jnoncrysol.2019.119573>.
45. C.J.F. Böttcher, P. Bordewijk, *Dielectrics in Time-Dependent Fields* (Elsevier, Amsterdam, 1978).
46. F. Kremer, A. Schönhals, *Broadband Dielectric Spectroscopy* (Springer, Berlin, Heidelberg, 2003).
47. R. Kahlau, D. Kruk, T. Blochowicz, V.N. Novikov, E.A. Rössler, *J. Phys.: Condens. Matter* **22**, 365101 (2010).
48. C. Gainaru, O. Lips, A. Troshagina, R. Kahlau, A. Brodin, F. Fujara, E.A. Rössler, *J. Chem. Phys.* **128**, 174505 (2008).
49. A. Abragam, *The Principles of Nuclear Magnetism* (Clarendon Press, Oxford, 1961).
50. H.W. Spiess, in *Dynamic NMR Spectroscopy*, edited by P. Diehl, E. Fluck, R. Kosfeld (Springer, Berlin, Heidelberg, 1978) p. 55.
51. S. Adishchev, D. Bock, C. Gainaru, R. Kahlau, B. Micko, N. Petzold, B. Pötzschner, E.A. Rössler, *Z. Phys. Chem.* **226**, 1149 (2012).
52. R. Böhmer, G. Diezemann, G. Hinze, E. Rössler, *Prog. Nucl. Magn. Reson. Spectrosc.* **39**, 191 (2001).
53. F. Fujara, S. Wefing, H.W. Spiess, *J. Chem. Phys.* **84**, 4579 (1986).
54. K. Schmidt-Rohr, H.W. Spiess, *Multidimensional Solid-State NMR and Polymers* (Academic Press, London, 1994).
55. G. Hinze, H. Sillescu, *J. Chem. Phys.* **104**, 314 (1996).
56. M. Vogel, P. Medick, E.A. Rössler, in *Annual Reports on NMR Spectroscopy*, edited by G.A. Webb (Academic Press, 2005) p. 231.
57. E. Rössler, M. Taupitz, K. Börner, M. Schulz, H.-M. Vieth, *J. Chem. Phys.* **92**, 5847 (1990).
58. D. Bock, PhD Thesis, University Bayreuth, 2015.
59. E. Rössler, in *Lecture Notes in Physics*, edited by Th. Dorfmüller, G. Williams, Vol. **277** (Springer, Berlin, Heidelberg, 1987) p. 144.
60. E. Rössler, PhD Thesis, University Mainz, 1984.
61. G. Katana, E.W. Fischer, T. Hack, V. Abetz, F. Kremer, *Macromolecules* **28**, 2714 (1995).
62. B. Schmidtke, N. Petzold, R. Kahlau, E.A. Rössler, *J. Chem. Phys.* **139**, 84504 (2013).
63. B. Pötzschner, F. Mohamed, C. Bächer, E. Wagner, A. Lichtinger, D. Bock, K. Kreger, H.-W. Schmidt, E.A. Rössler, *J. Chem. Phys.* **146**, 164504 (2017).
64. D. Bock, R. Kahlau, B. Micko, B. Pötzschner, G.J. Schneider, E.A. Rössler, *J. Chem. Phys.* **139**, 64508 (2013).
65. A. Kudlik, S. Benkhof, T. Blochowicz, C. Tschirwitz, E. Rössler, *J. Mol. Struct.* **479**, 201 (1999).
66. M. Gordon, J.S. Taylor, *J. Appl. Chem.* **2**, 493 (1952).
67. T.P. Lodge, T.C.B. McLeish, *Macromolecules* **33**, 5278 (2000).
68. M.H. Jensen, C. Gainaru, C. Alba-Simionesco, T. Hecksher, K. Niss, *Phys. Chem. Chem. Phys.* **20**, 1716 (2018).
69. F. Sciortino, P. Tartaglia, E. Zaccarelli, *Phys. Rev. Lett.* **91**, 268301 (2003).

70. T. Voigtmann, J. Horbach, Phys. Rev. Lett. **103**, 205901 (2009).
71. A.J. Moreno, J. Colmenero, Phys. Rev. E **74**, 21409 (2006).
72. A.J. Moreno, J. Colmenero, J. Chem. Phys. **125**, 164507 (2006).
73. T. Sentjabrskaja, E. Zaccarelli, C.D. Michele, F. Sciortino, P. Tartaglia, T. Voigtmann, S.U. Egelhaaf, M. Laurati, Nat. Commun. **7**, 11133 (2016).
74. G. Floudas, W. Steffen, E.W. Fischer, W. Brown, J. Chem. Phys. **99**, 695 (1993).
75. A. Zetsche, E.W. Fischer, Acta Polym. **45**, 168 (1994).
76. N. Müller, M. Vogel, J. Chem. Phys. **150**, 64502 (2019).
77. J. Bosse, Y. Kaneko, Phys. Rev. Lett. **74**, 4023 (1995).
78. S.-H. Chong, W. Götze, A.P. Singh, Phys. Rev. E **63**, 11206 (2000).
79. T. Voigtmann, EPL **96**, 36006 (2011).
80. V. Krakoviack, Phys. Rev. Lett. **94**, 65703 (2005).
81. J. Kurzidim, D. Coslovich, G. Kahl, J. Phys.: Condens. Matter **23**, 234122 (2011).
82. F. Höfling, T. Franosch, E. Frey, Phys. Rev. Lett. **96**, 165901 (2006).
83. K. Dawson, G. Foffi, M. Fuchs, W. Götze, F. Sciortino, M. Sperl, P. Tartaglia, T. Voigtmann, E. Zaccarelli, Phys. Rev. E **63**, 11401 (2000).
84. M. Sperl, Phys. Rev. E **68**, 31405 (2003).



---

## Publication 4

### Reorientational dynamics of highly asymmetric binary non-polymeric mixtures – a dielectric spectroscopy study

T. Körber, F. Krohn, C. Neuber,  
H.-W. Schmidt and E. A. Rössler

*Physical Chemistry Chemical Physics*

**23**, 7200-7212 (2021).

DOI: 10.1039/d0cp06652d

© Royal Society of Chemistry 2021



Cite this: *Phys. Chem. Chem. Phys.*, 2021, **23**, 7200

# Reorientational dynamics of highly asymmetric binary non-polymeric mixtures – a dielectric spectroscopy study

Thomas Körber,<sup>a</sup> Felix Krohn,<sup>b</sup> Christian Neuber,<sup>b</sup> Hans-Werner Schmidt<sup>b</sup> and Ernst A. Rössler<sup>\*a</sup>

We present an analysis of dielectric spectra measured for a specially designed non-polymeric asymmetric binary glass former characterized by a large difference of the component's  $T_g$  ( $\Delta T_g = 216$  K). We cover the whole additive concentration range from 4% up to 90% (by mass). Two main relaxations  $\alpha_1$  and  $\alpha_2$  are identified, which are characterized by well separated time scales and are attributed to the dynamics associated with the high- $T_g$  component ( $\alpha_1$ ) and the low- $T_g$  component ( $\alpha_2$ ). Frequency-temperature superposition does not apply. To cope with the extraordinary spectral broadening, we introduce a model consisting of a generalized Cole–Davidson ( $\alpha_1$ ) and a Havriliak–Negami function with a low frequency truncation ( $\alpha_2$ ). Whereas the  $\alpha_1$ -relaxation reflects essentially homogeneous dynamics and its spectra mainly broaden on the high-frequency flank of the relaxation peak, the  $\alpha_2$ -relaxation becomes broader on the low-frequency side reflecting pronounced dynamic heterogeneity in a more or less arrested matrix of high- $T_g$  molecules. From the extracted time constants, two glass transition temperatures  $T_{g1}$  and  $T_{g2}$  can be derived, showing a non-trivial concentration dependence for  $T_{g2}$ . Supplementary, we find a  $\beta$ -relaxation. The total relaxation strength  $\Delta\epsilon$  strongly deviates from ideal mixing, and therefore care has to be taken interpreting the corresponding  $\Delta\epsilon_{\alpha_i}$  as representation of molecular populations.

Received 25th December 2020,  
 Accepted 3rd March 2021

DOI: 10.1039/d0cp06652d

[rsc.li/pccp](http://rsc.li/pccp)

## Introduction

The dynamics of neat glass-formers was extensively investigated in the last decades, and a clear picture of the evolution of the dynamics has emerged.<sup>1–5</sup> Yet, a full understanding of the glass transition phenomenon has still to be accomplished. In recent years, interest has been drawn to the understanding of binary glass forming mixtures. A relevant technological field is a typical polymer–plasticizer system or a polymer blend, both of which were intensively reviewed.<sup>6–10</sup> Significantly less is known about mixtures of non-polymeric compounds, especially dynamically asymmetric systems, that are systems having a high  $T_g$ -contrast. These mixtures may be taken as model systems for binary glass formers with significant molecular size disparity of their components and have also sparked the interest of molecular dynamics simulations and theoretical studies.<sup>11–17</sup>

While early experimental studies suggested a single  $T_g$  to be a necessity in fully miscible systems,<sup>18</sup> the existence of two  $T_g$  in

dynamically asymmetric systems is now widely accepted which reflects a decoupling of the component dynamics.<sup>19–21</sup> For example, two glass transitions are observed in miscible polymer blends,<sup>21</sup> polymer–plasticizer systems,<sup>19,22</sup> and mixtures of non-polymeric organic glasses<sup>23–25</sup> by means of dielectric spectroscopy (DS),<sup>22,26,27</sup> nuclear magnetic resonance spectroscopy (NMR),<sup>28–30</sup> differential scanning calorimetry (DSC),<sup>7,31</sup> and neutron scattering.<sup>32</sup> In such mixtures, a broadening of the underlying relaxation time distributions as compared to the neat materials is usually observed, and frequency-temperature superposition (FTS) fails pronouncedly.<sup>22,33,34</sup>

In a series of papers, we investigated component-selectively the dynamics in dynamically highly asymmetric binary glass formers, polymeric and non-polymeric, by dielectric as well as by <sup>2</sup>H and <sup>31</sup>P NMR spectroscopy.<sup>22,24,35</sup> In particular, we started a program synthesizing stable non-polymeric high- $T_g$  glass formers based on a spirobifluorene central unit.<sup>36,37</sup> Mixtures with a  $T_g$ -contrast of their components up to  $\Delta T_g \cong 250$  K were studied. Two more or less separated main relaxations,  $\alpha_1$  associated with the slow dynamics of the high- $T_g$  component and  $\alpha_2$  the faster one of the low- $T_g$  component (additive) were observed. For the  $\alpha_1$ -process, the well-known plasticizer effect is observed, *i.e.* an acceleration of the dynamics upon mixing.

<sup>a</sup> Department of Inorganic Chemistry III and Northern Bavarian NMR Centre, University of Bayreuth, 95440 Bayreuth, Germany.  
 E-mail: [ernst.roessler@uni-bayreuth.de](mailto:ernst.roessler@uni-bayreuth.de)

<sup>b</sup> Department of Macromolecular Chemistry and Bavarian Polymer Institute, University of Bayreuth, 95440 Bayreuth, Germany

The corresponding relaxation spectra appeared to broaden only weakly and FTS still applies approximately. Usually, they can be fitted with a Kohlrausch function. For the  $\alpha_2$ -process, an anti-plasticizer effect is observed. At low additive concentrations a crossover of the time constants  $\tau_{\alpha_2}$  to an Arrhenius-like temperature dependence is observed for  $T \leq T_{g1}$ . This “fragile-to-strong” transition was found in several other systems.<sup>22,31,38</sup>

As confirmed by NMR, strong dynamic heterogeneities appear for the low- $T_g$  component showing a quasi-logarithmic correlation loss and involving isotropic reorientation in a more or less arrested matrix of the high- $T_g$  component.<sup>28,35</sup> Thus, the  $\alpha_2$ -process was regarded as a second main ( $\alpha$ )-relaxation. In DSC experiments, a second yet broadened glass step was found, allowing  $T_{g1}$  and  $T_{g2}$  to be determined in addition to DS. It turned out that the dynamic scenario does not differ significantly when taking a polymeric or non-polymeric high- $T_g$  component. Recently, investigating systems with smaller  $T_g$  contrast ( $\Delta T_g = 63$ – $89$  K), we found indications that also the dynamics of the high- $T_g$  component displays some extent of dynamic heterogeneity.<sup>34</sup> In any case, given the broad and overlapping relaxation spectra, their analysis becomes a challenge and their interpretation is still controversially debated.<sup>39,40</sup>

Two features deserve to be particularly mentioned. First, interpreting the  $\alpha_1$ - and  $\alpha_2$ -process, respectively, as a separate glass transition, the mass concentration dependence  $T_{g1}(w_{\text{additive}})$  displays the well-established monotonously decrease starting with  $T_g$  of the high- $T_g$  component. The peculiar trace of  $T_{g2}(w_{\text{additive}})$ , however, showing a maximum at intermediate additive concentration was not reported before but found in all investigated systems with a high  $T_g$ -contrast.<sup>22,24,35</sup> Yet, many studies on polymer–plasticizer systems did not investigate the full concentration range. Moreover, in the limit of low additive concentrations the second DSC step becomes highly broadened which may prevent a clear-cut determination of  $T_{g2}$ . Second, the design of our experiments was such that the low- $T_g$  component dominated the dielectric response. Thus, the dielectric spectra directly reflect its dynamics. Surprisingly, however, two dielectric relaxation peaks were observed, and comparing the respective relaxation strengths, we suggested that there exists a second sub-ensemble of additive molecules which follows the dynamics of the high- $T_g$  molecules. Similar conclusions were drawn by Blochowicz and co-workers.<sup>23,31</sup> Analysing the relaxation strength, it appeared that the fraction of additive molecules being linked to the  $\alpha_1$ -process continuously decreased upon increasing temperature until it finally disappears.

Our previous studies on non-polymeric asymmetric mixtures were hampered by the fact that the samples tend to de-mix and partly crystallize around room-temperature.<sup>24</sup> Furthermore, in order to probe the dynamics of the high- $T_g$  component by  $^2\text{H}$  NMR a deuterated phenyl group was attached to the spirobifluorene unit. However, the occurring phenyl-flip hampered a detailed analysis of the  $\alpha_1$ -process by NMR.<sup>35</sup> In the present contribution, we introduce a new non-polymeric asymmetric binary system not prone to de-mixing and crystallization. It is composed of the high- $T_g$  component *m*-TPTS

( $T_g = 350$  K) and the additive tripropyl phosphate (TPP;  $T_g = 134$  K), thus featuring a  $T_g$ -contrast of 216 K (see Fig. 1 for chemical structure). One of the four phenyl rings constituting the spirobifluorene unit can be deuterated and thus,  $^2\text{H}$  NMR can probe the dynamics of the rigid core of the glass former as will be demonstrated in a follow-up study. The additive TPP is already well-investigated as a neat glass-former<sup>41,42</sup> and as the low- $T_g$  component in our previous binary systems; its dynamics will be probed by  $^{31}\text{P}$  NMR.<sup>22,35</sup> The dielectric behaviour of neat *m*-TPTS was reported recently.<sup>37</sup> In the present publication we report on the DSC and DS experiments. In a forthcoming paper, we will complement our investigations by presenting the results from the NMR investigations.<sup>43</sup>

## Experimental

### Materials

Fig. 1 shows the chemical structures of the two used components in the present study. The high- $T_g$  glass former 2-(*m*-*tert*-butylphenyl)-2'-*tert*-butyl-9,9'-spirobi[9*H*]fluorene (*m*-TPTS) was synthesized along the lines described in ref. 37. The compound was purified by sublimation. The low- $T_g$  additive tripropyl phosphate (TPP; Sigma Aldrich) was rectified by the distillation over a vigreux column under reduced pressure before use. For the dielectric measurements with 50% or higher TPP content (by weight percentage), a solution was prepared in a vial and transferred into the sample-cell *via* a pipette. At 50% and lower TPP content, a certain amount of *m*-TPTS amorphous powder was filled into the sample cell and re-vitrified. The amount of *m*-TPTS was chosen to yield 50–60 mg of the mixture in order to ensure a completely filled sample volume in the DS cell. Then, an appropriate amount of liquid TPP was added to the *m*-TPTS, the DS cell was tightly sealed, and treated at elevated temperature (80–130 °C) for a prolonged time (1–3 days) to ensure complete mixing of both compounds in the cell. To prove the tightness of the cell, mass was controlled before and after tempering. DS measurements were conducted from highest to lowest temperature. Equilibrium of the mixture was ensured by a following measurement of selected temperatures from the lowest to the highest temperature, whereby the obtained spectra were identical in all cases. After the DS or DSC measurement was completed, the finally measured concentration of both compounds was determined by high-resolution NMR with an error of 1%. Mixtures with mass percentage  $w_{\text{TPP}} = 4\%$ , 10%, 20%, 30%, 40%, 50%, 70% and 90% of TPP were measured.

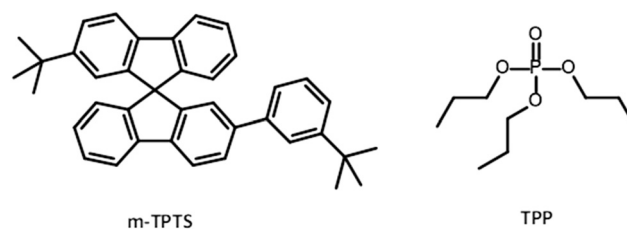


Fig. 1 Chemical structures of the high- $T_g$  component *m*-TPTS and the low- $T_g$  component tripropyl phosphate (TPP) used for the binary mixtures.

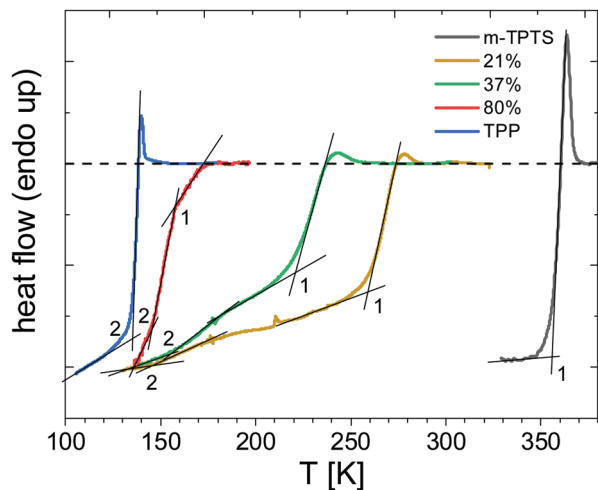


Fig. 2 DSC measurements (coloured lines) for the neat compounds *m*-TPTS (grey) and TPP (blue), as well as in the mixture with  $w_{\text{TPP}} = 0.21$  (yellow), 0.37 (green) and 0.80 (red). All DSC measurements are scaled to a common baseline (dashed line) and comparable total heights. Lines indicate the crossing points determining the  $T_g$ 's and the numbers denote the corresponding relaxation process (cf. Fig. 13).

Like in polymer plasticizer systems, we call TPP throughout this work the plasticizer or additive.

### Differential scanning calorimetry

Differential scanning calorimetry (DSC) was performed at Mettler Laboratories in sealed Al-pans at a heating rate of  $10 \text{ K min}^{-1}$ . Sample preparation was according to the procedure established for DS measurements. In Fig. 2 DSC curves of the neat compounds and the mixtures  $w_{\text{TPP}} = 0.21$ , 0.37 and 0.80, scaled to a common baseline and comparable heights, are shown. In the mixtures, two steps are found. Corresponding  $T_g$  values are determined as onset of the observed step. The first step (1), coming from high temperatures, gets smaller and broader with increasing  $w_{\text{TPP}}$ , whereas the second one (2) decreases and broadens strongly with decreasing  $w_{\text{TPP}}$ . Therefore, the steps at low temperatures are attributed to the glass transition temperature of the  $\alpha_2$ -process ( $T_{g_2}$ ), whereas the high temperature steps correspond to  $T_{g_1}$ . The concentration dependence of both  $T_g$ 's is shown in Fig. 13 together with the DS results and will be discussed below. Such kind of DSC curves were already observed in previous investigations of binary glasses.<sup>22,23</sup>

### Dielectric spectroscopy

The dielectric permittivity is described by the equation<sup>44,45</sup>

$$\varepsilon^*(\omega) = \varepsilon'(\omega) - i\varepsilon''(\omega) = \varepsilon_\infty + \Delta\varepsilon \int_0^\infty \frac{d\phi(t)}{dt} e^{-i\omega t} dt \quad (1)$$

where  $\varepsilon^*(\omega)$  is the complex dielectric constant,  $\omega = 2\pi\nu$  the angular frequency with  $\nu$  being the frequency,  $\varepsilon_\infty$  the high frequency permittivity, and  $\phi(t)$  the step-response function. The quantity  $\Delta\varepsilon$  denotes the relaxation strength which is linked to the molecular dipole moment.

The dielectric response of neat glass formers is often described either by a Cole–Davidson (CD) or Kohlrausch function.<sup>44</sup> In binary systems, however, these functions are no more applicable due to strongly varying peak shapes depending on concentration and temperature. Furthermore, at least in a certain concentration range, two relaxations  $\alpha_1$  (slow main relaxation) and  $\alpha_2$  (fast main relaxation) with different characteristic evolutions are found.<sup>22,24,35</sup>

Therefore, we use the generalized Cole–Davidson relaxation function (GCD) introduced by Kahlau *et al.*,<sup>46</sup> to describe the  $\alpha_1$ -relaxation<sup>34</sup> and the widely used Havriliak–Negami relaxation function (HN) to describe the  $\alpha_2$ -relaxation.<sup>44,47</sup> The step-response of the GCD can be numerically calculated along:

$$\phi_{\text{GCD}}(t) = \frac{\Gamma\left(\frac{b_{\text{GCD}}}{a_{\text{GCD}}}, \left(\frac{t}{\tau_{\text{GCD}}}\right)^a\right)}{\Gamma\left(\frac{b_{\text{GCD}}}{a_{\text{GCD}}}\right)} \quad (2)$$

This model function, which is used in terms of its Fourier Transform (cf. eqn (1)), consists of three parameters  $\tau_{\text{GCD}}$ , defining the peak position,  $a_{\text{GCD}}$  giving a measure of the overall width of the peak and the high-frequency power law exponent  $b_{\text{GCD}}$ . The mean correlation time  $\langle\tau_{\text{GCD}}\rangle$  of the GCD is well defined and a Debye-like low-frequency behaviour ( $\varepsilon'' \propto \omega^{-1}$ ) is granted.<sup>46</sup> The GCD includes also the cases of a Kohlrausch ( $a = b$ ) and a CD relaxation function ( $a = 1$ ). The HN distribution, applied to describe the spectra associated with the low- $T_g$  component, can be directly expressed as permittivity function:<sup>44</sup>

$$\varepsilon^*(\omega) = \varepsilon_\infty + \frac{\Delta\varepsilon_{\text{HN}}}{(1 + (i\omega\tau_{\text{HN}})^{a_{\text{HN}}})^{b_{\text{HN}}}} \quad (3)$$

with the dielectric loss  $\varepsilon''_{\text{HN}} = \Delta\varepsilon_{\text{HN}} \cdot \chi''_{\text{HN}}$ :

$$\chi''_{\text{HN}}(\omega) = \frac{\sin(b_{\text{HN}}\phi)}{\left(1 + 2(\omega\tau_{\text{HN}})^{a_{\text{HN}}}\cos\left(\frac{\pi a_{\text{HN}}}{2}\right) + (\omega\tau_{\text{HN}})^{2(a_{\text{HN}})}\right)^{\frac{b_{\text{HN}}}{2}}}$$

$$\phi = \arctan\left(\frac{(\omega\tau_{\text{HN}})^{a_{\text{HN}}}\sin\left(\frac{\pi a_{\text{HN}}}{2}\right)}{1 + (\omega\tau_{\text{HN}})^{a_{\text{HN}}}\cos\left(\frac{\pi a_{\text{HN}}}{2}\right)}\right) \quad (4)$$

$\tau_{\text{HN}}$  is the characteristic relaxation time,  $a_{\text{HN}}$  the low-frequency limit power law exponent and  $c_{\text{HN}} = a_{\text{HN}}b_{\text{HN}}$  the high-frequency power law exponent. No mean time constant can be defined because the integral over the corresponding relaxation function  $\phi_{\text{HN}}(t)$  is not finite. The most probable time constant, which reflects the relaxation peak can be determined by peak-picking or from the fit parameters.<sup>44,47</sup>

From a purely phenomenological point, one can safely state that the liquid-like dynamics of the low- $T_g$  component is governed by a broad distribution of correlation times with essentially two cut-offs  $\tau_{\alpha_2}$  and  $\tau_{\alpha_1}$ , which allow to define two  $T_g$  values,  $T_{g_1}$  and  $T_{g_2}$ . In between these limits the dynamics spans over a large time window, in particular at low additive concentrations. Due to this fact and the problem, that the HN function does not display the correct low-frequency behaviour

$\varepsilon'' \propto \omega^1$ , we introduced a cut-off function. We calculated the pulse response function  $\varphi_{\text{HN}} = -d\phi_{\text{HN}}(t)/dt$  of a HN relaxation function *via* numerical FT (applying a kind of Filon algorithm)<sup>48</sup> of  $\chi''_{\text{HN}}$  and derivation. Then, we multiplied  $\varphi_{\text{HN}}$  with an exponential cut-off ( $\tau_{\text{C}}$ ), which is defined by the longest time constant in our system, the average time constant of the  $\alpha_1$ -relaxation ( $\tau_{\text{C}} = \langle \tau_{\alpha_1} \rangle$ ).

$$\varphi_{\text{HNC}}(t) = \varphi_{\text{HN}}(t) \cdot \exp\left(-\frac{t}{\tau_{\text{C}}}\right) \quad (5)$$

The corresponding step-response function  $\phi_{\text{HNC}}(t)$  is derived *via* numerical integration and normalization ( $\phi_{\text{HNC}}(t=0) = 1$ ). *Via* FT we finally received our HN relaxation function with cut-off (HNC). This leads to a low-frequency power law with exponent  $a_{\text{HNC}}$  and a  $\omega^1$  behaviour at lowest frequencies. Whenever both relaxations  $\alpha_1$  and  $\alpha_2$  are observed in the dielectric spectra, we use an additive ansatz to describe the dielectric loss as combination of the GDC and HNC relaxation function:

$$\varepsilon''(\omega) = \Delta\varepsilon_{\text{GCD}} \cdot \chi''_{\text{GCD}}(\omega) + \Delta\varepsilon_{\text{HNC}} \cdot \chi''_{\text{HNC}}(\omega) \quad (6)$$

which we subsequently call “composite fit”. If only one process is in the measurement window, we use either GCD or HN. In Fig. 3, we give some examples of the GCD (blue dashed lines) and the HNC function (red dashed lines,  $\tau_{\text{C}} = \langle \tau_{\text{GCD}} \rangle$ ) and its superposition (composite fit, black lines) as it will be applied to interpolate the measured dielectric spectra of the mixtures.

To get comparable time constants  $\tau$  for both relaxations, we can only use the most probable time constant defined by the peak position *via* “peak-picking” ( $\omega_{\text{P}} = 2\pi\nu_{\text{P}} = 1/\tau$ ).

Especially in systems with a high DC conductivity, relevant spectral contributions are often hidden under and sometimes even not visible after subtracting the DC conductivity contribution ( $\text{DC} \propto \omega^{-1}$ ). Therefore, Wübbenhorst *et al.*<sup>49</sup> introduced an

ohmic-conduction-free dielectric loss representation ( $\partial\varepsilon'$ ) from the real part of the dielectric susceptibility  $\varepsilon'$ :

$$\partial\varepsilon' \equiv -\frac{\pi}{2} \frac{\partial\varepsilon'(\omega)}{\partial \ln \omega} \quad (7)$$

This representation results in peaks at the same peak position but somewhat different spectral shape. The exact used procedure and further details are described elsewhere.<sup>49–51</sup> Hence more subtle features can be resolved in  $\partial\varepsilon'$  compared to  $\varepsilon''$ . One has to mention, that for a complete description of  $\partial\varepsilon'$ , the corresponding interpolations must be calculated the same way (eqn (7)).

Dielectric measurements were carried out with an Alpha-A Analyzer from Novocontrol in the frequency range  $\nu = 10^{-2}$ – $10^6$  Hz. Temperature was kept constant within  $\pm 0.2$  K by using a Quattro-H temperature controller from Novocontrol yielding an absolute accuracy better than  $\pm 0.2$  K. Applied temperatures ranged from 100 up to 400 K. The completely sealed sample cell was adapted to a design assuring a constant sample volume.<sup>52</sup>

## Results

### Pure components

Fig. 4 shows the dielectric spectra of the neat components TPP (black squares) and *m*-TPTS (black triangles) at selected temperatures. For both compounds the  $\alpha$ -relaxation is observed which shifts to higher frequencies with increasing temperature. For TPP, a pronounced  $\beta$ -relaxation persisting below  $T_{\text{g}}$  is observed at high frequencies which was analysed earlier.<sup>37,53</sup> For *m*-TPTS, no  $\beta$ -relaxation is observed, however, the high-frequency flank is made up of a crossover from one power-law behaviour to a second with a lower exponent, reflecting the so-called excess wing.<sup>2,5,54</sup> The relaxation strength at  $T \approx 1.02T_{\text{g}}$  of *m*-TPTS ( $\Delta\varepsilon_{m\text{-TPTS}} \approx 0.1$ ) is about a factor of 240 smaller than that of TPP ( $\Delta\varepsilon_{\text{TPP}} \approx 24$ ), reflecting the non-polar nature of the

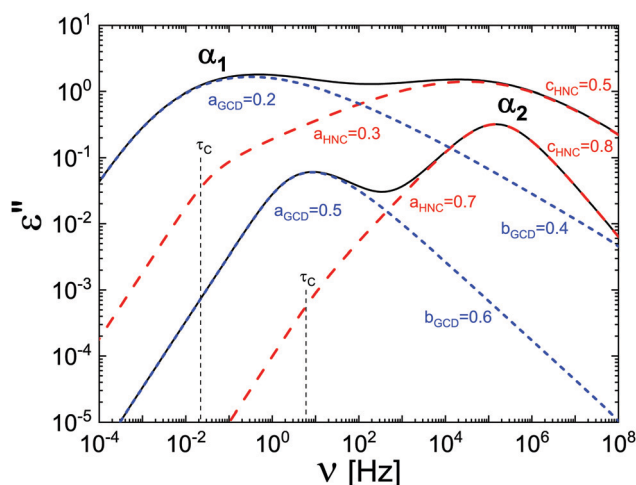


Fig. 3 Calculated dielectric loss spectra for two sets of parameters ( $\Delta\varepsilon_{\text{GCD}} = \Delta\varepsilon_{\text{HNC}}$  and  $\Delta\varepsilon_{\text{GCD}} = 0.5 \cdot \Delta\varepsilon_{\text{HNC}}$ ,  $\tau_{\text{GCD}} = 0.01$  s,  $\tau_{\text{HNC}} = 1 \times 10^{-6}$  s). Blue dashed lines are GCD functions, red dashed lines are HNC functions with cut-off  $\tau_{\text{C}} = \langle \tau_{\text{GCD}} \rangle$ , and the black lines are the corresponding composite functions.

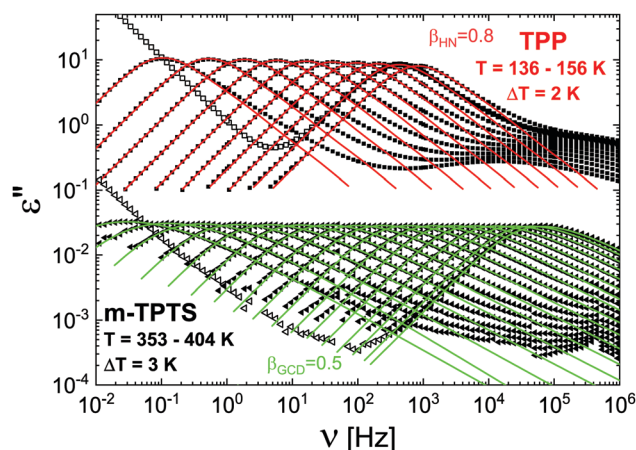


Fig. 4 Selected dielectric spectra  $\varepsilon''$  of neat TPP (squares) and neat *m*-TPTS (triangles). DC conductivity is shown only for one temperature for each system (open symbols) and subtracted for TPP. Fits by a HN function  $\beta_{\text{HN}} = \beta_{\text{CD}} = 0.80$  are shown as red lines (parameters *cf.* Fig. 6), GCD fits as green lines (parameters *cf.* Fig. 9).

hydrocarbon *m*-TPTS. Thus, DS predominately probes TPP in the present mixtures except for lowest TPP concentrations. For *m*-TPTS, no crystallization behaviour is observed, whereas crystallization may occur above 156 K for TPP.

The TPP relaxation spectra are interpolated by a HN function (cf. eqn (5)) yielding  $a_{\text{HN}} = 1$  and  $b_{\text{HN}} = 0.80$  (red lines), which corresponds to a simple CD function. We disregard the contribution of the  $\beta$ -relaxation in the present context focusing on the two main relaxations. In the case of *m*-TPTS we apply a GCD function (green lines) with  $b_{\text{GCD}} = 0.5$  and  $a_{\text{GCD}}(T)$ , changing slightly with temperature (cf. Fig. 8), showing a spectral shape close to a Kohlrausch function. The resulting  $T_g$  value defined by  $\tau(T_g) = 100$  s for *m*-TPTS is 350 K, that of TPP is  $T_g = 134$  K, as reported prior.<sup>37,41</sup>

### High additive (TPP) concentrations ( $w_{\text{TPP}} = 0.90$ and $0.70$ )

Mixtures with a strongly varying concentration of TPP in *m*-TPTS were measured. Starting with high TPP concentrations, Fig. 5(a) shows the dielectric spectra of  $w_{\text{TPP}} = 0.90$  (black squares) and for comparison that of neat TPP at single temperature (green diamonds). The DC conductivity was subtracted; for  $T = 162$  K, the original spectrum is shown (open squares). The HN fits of the relaxation spectra are shown as red lines.

As expected, the signal amplitude of the mixture is lower than that of neat TPP. Due to the anti-plasticizer effect, the spectra are shifted to lower frequencies. Furthermore, a strongly temperature dependant broadening on the low-frequency flank is observed, while the high-frequency is just slightly broader. Thus, FTS does not apply any longer in the mixture. Clearly, the spectra in Fig. 5(a) reflect the relaxation of the polar additive TPP and we denote it the  $\alpha_2$ -relaxation. The appearance of the  $\beta$ -process remains essentially the same but will be addressed later on separately (cf. section  $\beta$ -Process).

As discussed in the Experimental section, our phenomenological approach assumes that the spectral contribution of the low- $T_g$  additive stretches between the two cut-offs  $\tau_{\alpha_2}$  and  $\tau_{\alpha_1}$ , yet, the latter limit does not show up at high additive concentrations. Thus, we are left with an interpolation by a simple HN distribution which considers the additional broadening of the spectra at low frequencies. The corresponding parameters  $a_{\text{HN}}(T)$  and  $c_{\text{HN}}$  are shown in Fig. 6. Whereas the high-frequency parameter  $c_{\text{HN}} = 0.74$  is virtually temperature-independent and only slightly smaller compared to pure TPP ( $c_{\text{HN}} = 0.8$ ), the low-frequency exponent  $a_{\text{HN}}(T)$  decreases strongly from 0.81 to 0.52 with lowering temperature. Given the strong temperature dependence of  $a_{\text{HN}}(T)$ , one may speculate that at highest temperatures the CD limit  $a_{\text{HN}} = 1$  is reached and the spectral form approaches that of neat TPP. Similar features are observed for  $w_{\text{TPP}} = 0.70$  (cf. Appendix Fig. 17). The FTS violation is even stronger with  $a_{\text{HN}}$  decreasing from 0.55 to 0.25 with decreasing temperature and a high frequency exponent of  $c_{\text{HN}} = 0.65$ .

This is further demonstrated in Fig. 5(b) where selected spectra measured at different temperatures are scaled to the peak position and amplitude for the two mixtures  $w_{\text{TPP}} = 0.90$

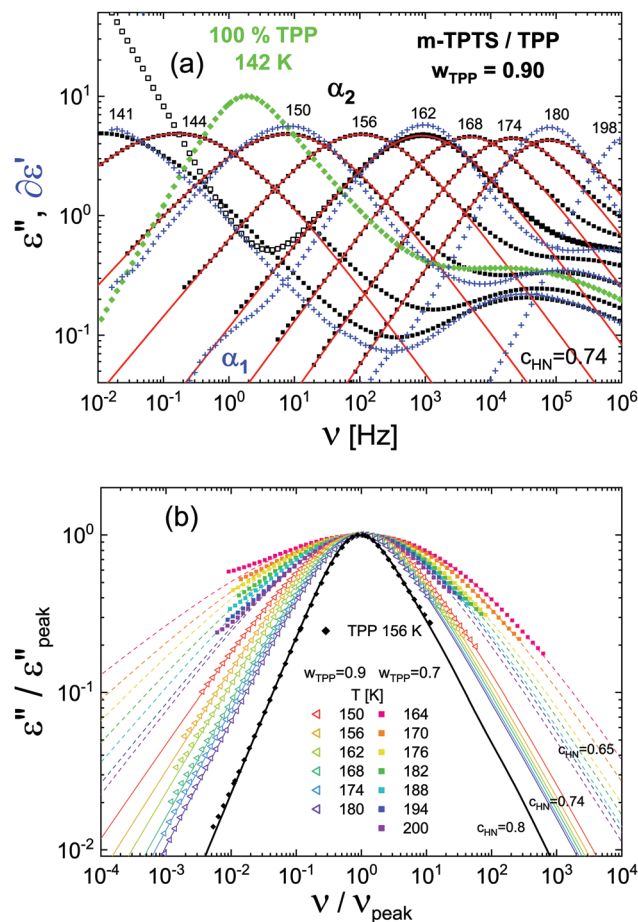


Fig. 5 (a) Dielectric spectra  $\epsilon''$  of the mixture  $w_{\text{TPP}} = 0.90$  (black squares, HN fits as red lines) and for comparison a spectrum of neat TPP (green diamonds). DC conductivity contribution is subtracted. For selected temperatures, derivative data  $\partial\epsilon''$  (blue crosses) are shown. An additional relaxation contribution is recognized at lowest intensities ( $\alpha_1$ ), which cannot be resolved in  $\epsilon''$ . (b) Rescaled curves of  $w_{\text{TPP}} = 0.90$  (open triangles) and  $0.70$  (squares) scaled on the peak position and amplitude for selected temperatures in comparison to neat TPP.  $\beta$ -Relaxation and DC contributions are suppressed.

(open triangles, lines),  $0.70$  (squares, dashed lines) and compared to that of neat TPP (black diamonds). For both concentrations, the spectra clearly broaden with decreasing temperature mainly on the low-frequency flank but even the spectrum at highest temperature is significantly broader than that of neat TPP. The actual small changes in the high-frequency exponent  $c_{\text{HN}}$  are indicated. Evidently, the overall width drastically increases with decreasing TPP content.

One of the challenges during the data analysis of  $w_{\text{TPP}} = 0.70$  was the strong not addressable DC conductivity contribution. In order overcome this problem and to get a better resolution at low frequencies, where even subtracting the DC conductivity may still obscure some relaxation features, we took recourse to the derivative method  $\partial\epsilon''$  outlined in the Experimental section (eqn (7)). Indeed, one recognizes already for  $w_{\text{TPP}} = 0.90$  a very weak shoulder at  $T \leq 180$  K (blue crosses, Fig. 5(a)) which probably originates from a relaxation associated with the high- $T_g$

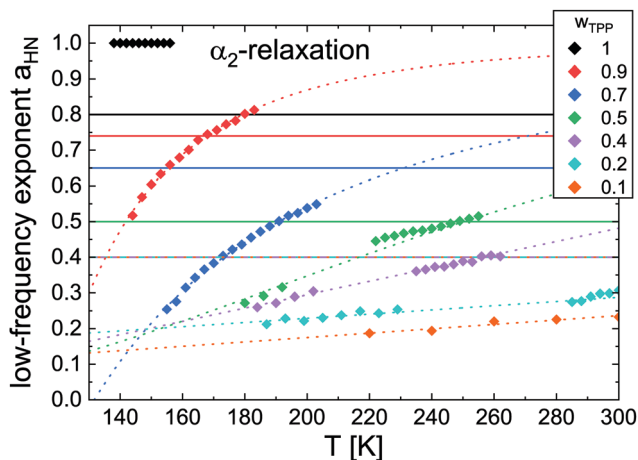


Fig. 6 HN(C) fit parameters of the spectral analysis regarding the  $\alpha_2$ -relaxation. Low-frequency exponent  $a_{\text{HN(C)}}$  as diamonds and constant high-frequency exponent  $c_{\text{HN(C)}}$ , determined at lowest temperatures, as solid lines. For  $w_{\text{TPP}} \leq 0.4$ ,  $c_{\text{HN(C)}}$  was kept constant at 0.4. Colour specifies the concentration and dotted lines are guides for the eye.

component ( $\alpha_1$ ). However, a full quantitative analysis is not possible. Therefore, we estimate only the time constants  $\tau_{\alpha_1}$  via peak picking after subtracting the low-frequency power law behaviour of the  $\alpha_2$ -relaxation, as given by  $\partial\epsilon'$ . In the case of  $w_{\text{TPP}} = 0.70$  (blue crosses, Appendix Fig. 17), the low-frequency contribution is much larger, but still we refrain from quantitatively singling out this relaxation feature and determine only the time constants again via peak picking. All time constants determined for  $w_{\text{TPP}} = 0.90$  and  $0.70$  are shown in Fig. 12 and will be discussed in the context of the results of all mixtures.

#### Low additive (TPP) concentrations – ( $w_{\text{TPP}} = 0.04$ and $0.10$ )

Turning to the other end of the concentration range, in Fig. 7 the dielectric spectra of  $w_{\text{TPP}} = 0.10$  are shown. The DC conductivity was subtracted, but original data is shown for  $T = 390$  K (open diamonds). Clearly, now two separate relaxations can be identified, which we attribute to the  $\alpha_1$ -process (black squares, high temperatures) and the  $\alpha_2$ -process (open triangles, low temperatures). Additionally, at even lower temperatures, a  $\beta$ -relaxation is observed, but omitted for clarity and will be discussed separately. For selected temperatures, the derivative relaxation data  $\partial\epsilon'$  is added (blue crosses), which is only slightly sharper as expected for broad peaks.<sup>49</sup>

In contrast to the high-TPP concentration mixtures, the dominating  $\alpha_1$ -relaxation is associated with the high- $T_g$  component whereas the  $\alpha_2$ -relaxation again with the additive component. We note that although the polarity of neat TPP is by a factor of about 240 larger than that of *m*-TPTS, the amplitude of the corresponding  $\alpha_2$ -relaxation is remarkably small; yet, it is extremely broad. Below we will consider the relaxation strength in detail (cf. Fig. 11). The  $\alpha_1$ -relaxation exhibits significant overall broadening, especially on the high-frequency flank, which increases with decreasing temperature. Thus, also for the high- $T_g$  component FTS is violated. At low-frequencies, the expected  $\omega^1$  behaviour can be identified as expected for the slowest process of

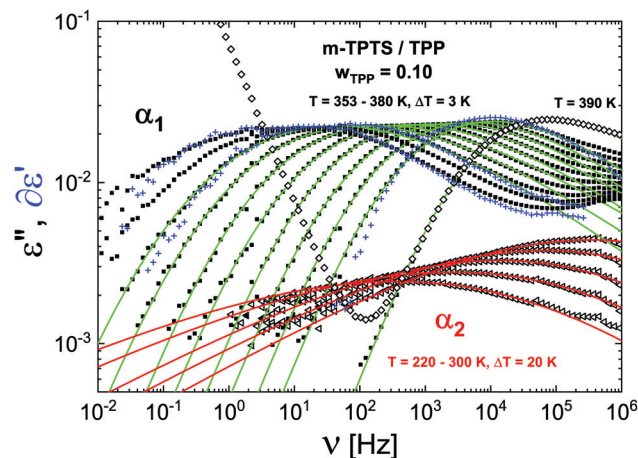


Fig. 7 Dielectric spectra  $\epsilon''$  of the mixture  $w_{\text{TPP}} = 0.10$  displaying two relaxations  $\alpha_1$  (squares) and  $\alpha_2$  (open triangles). DC conductivity contribution is subtracted; original data is shown for  $T = 390$  K (open diamonds). Temperatures are indicated. Green lines are GCD fits, red lines are HN fits. Fit parameters are included in Fig. 6, 8 and 11. For selected temperatures, the derivative data  $\partial\epsilon'$  is shown (blue crosses).

a liquid. Similar results are found for  $w_{\text{TPP}} = 0.04$ , which is shown in the Appendix (Fig. 18). Therefore, the spectral analysis will be discussed in the following for both concentrations.

To quantify the described relaxation features, the  $\alpha_1$ -relaxation is interpolated by a GCD function (green lines in Fig. 7 and 18), and the corresponding parameter  $a_{\text{GCD}}(T)$  and  $b_{\text{GCD}}(T)$  are included in Fig. 8(a). We remind, that the GCD function always displays a Debye-behaviour ( $\propto \omega^1$ ) at low frequencies, the high-frequency exponent is given by  $b_{\text{GCD}}$  and  $a_{\text{GCD}}$  specifies the overall width. In the mixtures, in addition to  $a_{\text{GCD}}$ , also  $b_{\text{GCD}}$  shows a significant temperature dependence and gets overall smaller with increasing  $w_{\text{TPP}}$ . In the case of  $w_{\text{TPP}} = 0.10$  even a broad GCD function is unable to interpolate the broadest spectra at the two lowest temperatures ( $T = 353$  K,  $356$  K), possibly indicating even a bimodal structure.

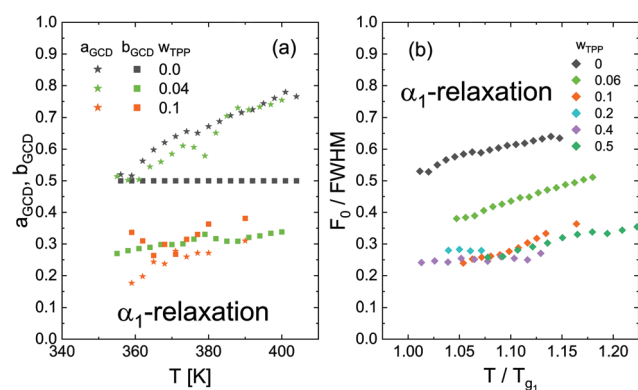


Fig. 8 (a) Parameter of the GCD function interpolating  $\alpha_1$ -relaxation for the lowest concentrations as function of temperature. Peak width parameter  $a_{\text{GCD}}$  (stars) and  $b_{\text{GCD}}$  (diamonds). The concentration is colour coded. (b) Inverse logarithmic FWHM of the  $\alpha_1$ -process as function of the reduced temperature ( $T/T_{g1}$ ), normalized by the FWHM of a Debye function ( $F_0$ ). The used DS glass transition temperatures are shown in Fig. 13.

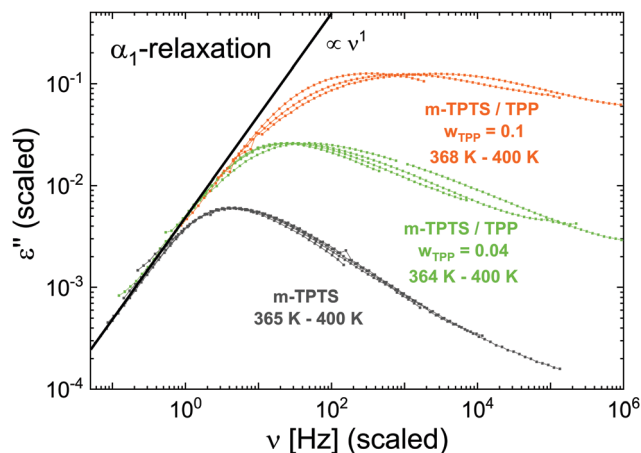


Fig. 9 Master curves of the  $\alpha_1$ -relaxation, scaled to the low-frequency flank ( $\propto \nu^1$ ), of neat *m*-TPTS (black) and mixtures with  $w_{\text{TPP}} = 0.04$  (green) and 0.10 (orange), respectively. The mixture data is shifted in height for better visualization.

As the parameters in Fig. 8(a) exhibit some scatter and it is difficult to fully grab the temperature evolution of the spectra, for convenience, we plot in Fig. 8(b) their inverse logarithmic half width (1/FWHM) in relation to that of a Debye function ( $F_0 = 1.14$ ). Clearly, the spectra associated with the high- $T_g$  component become broader with increasing  $w_{\text{TPP}}$  and exhibit a strong temperature dependence which is very similar when plotted on the reduced temperature scale  $T/T_{g1}$ . We added only up to 10% of TPP and already get  $\alpha_1$ -relaxation spectra by almost a factor of 3 broader compared to those of neat *m*-TPTS. Additionally, one has to discern, that the relaxation strength  $\Delta\epsilon_{\alpha_1}$  grows for increasing additive content  $w_{\text{TPP}}$  (cf. Fig. 11(b)) in contrast to a simple ideal mixing prospect.

The described results can directly be observed, recasting the low  $w_{\text{TPP}}$  data in Fig. 9, scaled to provide the common low-frequency behaviour  $\epsilon''(\omega) \propto \omega^1$ . The temperature dependent spectral broadening in particular on the high-frequency flank compared to neat *m*-TPTS is obvious – a different behaviour compared to that of the spectra of TPP in the mixture ( $\alpha_2$ -relaxation) – and hence FTS fails, as said.

The  $\alpha_2$ -relaxation in Fig. 7 (open triangles) appears as a very broad relaxation with a very low amplitude, well separated from the  $\alpha_1$ -relaxation. In other words, an extremely broad distribution of relaxation times  $G(\ln \tau_{\alpha_2})$  in the limit of low additive concentrations is found. The spectra of  $w_{\text{TPP}} = 0.10$  are fitted by simple HN functions (red lines), the corresponding parameters are included in Fig. 6. Extremely low values of the low-frequency exponent  $a_{\text{HN}}(T)$  are found and FTS fails again. In the case of  $w_{\text{TPP}} = 0.04$ , the signal almost disappears in the background noise (cf. Appendix Fig. 18) and therefore we refrained from fitting the spectra and determined only the time constants *via* peak-picking (cf. Fig. 12).

#### Intermediate additive (TPP) concentrations ( $w_{\text{TPP}} = 0.20$ , 0.04 and 0.50)

We now focus on intermediate concentrations including the samples with  $w_{\text{TPP}} = 0.20$ , 0.40 and 0.50. Fig. 10(a)–(c) show the

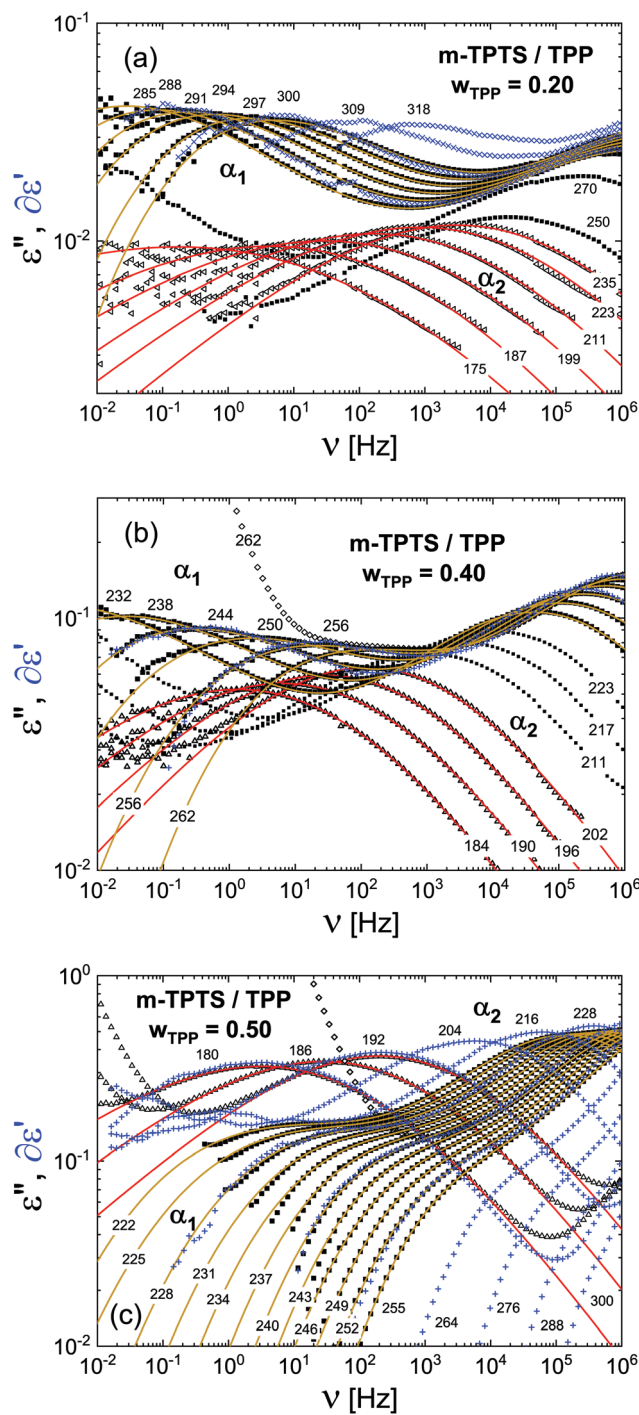


Fig. 10 Dielectric spectra  $\epsilon''$  of (a)  $w_{\text{TPP}} = 0.20$ , (b) 0.40 and (c) 0.50 (squares). DC conductivity contribution is subtracted (if possible). Original data is shown for one temperature (open diamonds). Temperatures in K are given. Yellow lines denote composite fits, red lines are HN fits to  $\alpha_2$  (open triangles). Fit parameters are included in Fig. 6, 8 and 11. For selected temperatures, the derivative data  $d\epsilon''/d\nu$  is shown (blue crosses).

corresponding dielectric spectra after subtraction of the DC conductivity. In all cases, two main relaxations can clearly be observed in a single spectrum, *i.e.*, at high frequencies the  $\alpha_2$ -relaxation is recognized whereas at low frequencies the

$\alpha_1$ -relaxation is found. The relative intensity of the  $\alpha_1$ -relaxation to that of the  $\alpha_2$ -relaxation decreases from almost similar to much smaller with increasing  $w_{\text{TPP}}$ . Thereby, also the time constants of both processes come closer with increasing TPP concentration. Furthermore, the ratio of the amplitudes  $\alpha_1/\alpha_2$  is strongly temperature dependent, decreasing with increasing temperature for all concentrations. As in the limiting cases discussed above, the  $\alpha_2$ -relaxation broadens on the low-frequency flank, whereas  $\alpha_1$ -relaxation mainly on the high-frequency flank. Again, as expected for the slowest relaxation of a liquid, its low-frequency flank still follows the relation  $\varepsilon''(\omega) \propto \omega^{-1}$ .

As in all cases both  $\alpha$ -relaxations overlap more or less strongly, we apply a composite fit (yellow lines) composed by a sum of a HN function ( $\alpha_2$ -relaxation) with a cut-off (HNC) at  $\langle\tau_{\alpha_1}\rangle$  and a GCD function ( $\alpha_1$ -relaxation) – see eqn (6). Starting with  $w_{\text{TPP}} = 0.20$  (Fig. 10(a)), the high-temperature data (black squares) are well described. The low-temperature spectra (open triangles) displaying solely the  $\alpha_2$ -relaxation are interpolated by a simple HN function (red lines). Here again, the low-frequency temperature dependent broadening is recognized. Analogous fits have been carried out for the other two concentrations (Fig. 10(b) and (c)). All shape parameters of the  $\alpha_2$ -relaxation are included in Fig. 6, showing that the overall stretching increases with decreasing  $w_{\text{TPP}}$  while the almost linear temperature dependence gets weaker. The FWHM of the  $\alpha_1$ -relaxation is added in Fig. 8(b), indicating some kind of saturation in the overall width for  $w_{\text{TPP}} \geq 0.10$  and similar temperature dependence for all concentrations on the reduced scale  $T/T_{g_1}$ .

Additionally, derivative data  $\partial\varepsilon'$  (blue crosses) are included in Fig. 10, showing perfect agreement with  $\varepsilon''$  and providing further insight for higher temperatures, once a composite fit is no more possible due to the  $\alpha_2$ -relaxation leaving the measurement window. In particular, the  $w_{\text{TPP}} = 0.50$  sample provides the best glimpse into the temperature dependence of the two sub-spectra in the mixture. The relatively weak  $\alpha_1$ -relaxation decreases in amplitude up to the highest temperature measured and becomes less and less separated from the  $\alpha_2$ -relaxation, which itself increases in amplitude with temperature. One could speculate that the  $\alpha_1$ -relaxation could even disappear at highest temperatures.<sup>31</sup> But still, the  $\omega^{-1}$  behaviour respectively the introduced cut off at the low frequencies of the slowest process ( $\alpha_1$ ) can prominently be observed in the derivative data  $\partial\varepsilon'$ . Another feature is important to be mentioned: although the sample contains only 50–80% of the weakly polar high- $T_g$  component, the  $\alpha_1$ -relaxation strength is much higher than that of the neat  $m$ -TPTS.

Next, we consider quantitatively the relaxation strength  $\Delta\varepsilon$  of the two main relaxations as revealed by our analysis for all investigated concentrations, corrected for the Curie law ( $\Delta\varepsilon(w_{\text{TPP}}, T) \cdot T$ ), in Fig. 11(a). As the relaxation strengths become much smaller than expected from a linear concentration dependence, we plotted the data on a semi-log scale. Starting at high  $w_{\text{TPP}} \geq 0.70$ , the total relaxation strength  $\Delta\varepsilon$  is determined purely by the relaxation strength  $\Delta\varepsilon_{\alpha_2}$  (open circles) of TPP (*cf.* Fig. 5 and 17), showing only a slight deviation from a

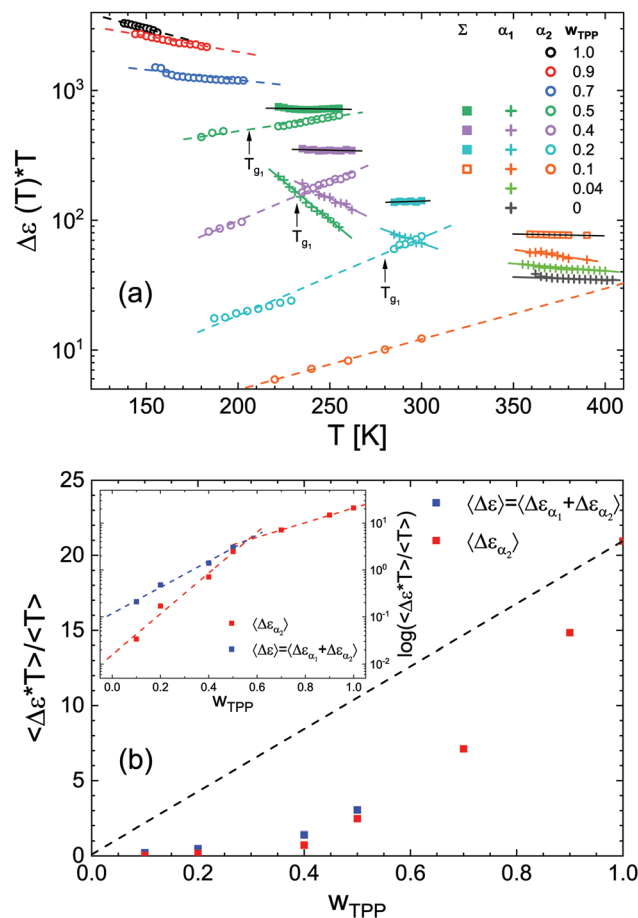


Fig. 11 (a) Curie corrected relaxation strength  $\Delta\varepsilon(w_{\text{TPP}}) \cdot T$  for  $\alpha_1$  (pluses),  $\alpha_2$  (circles) and the sum of both (squares) on a logarithmic scale. The gap in between  $\alpha_2$  data of one concentration is due to the used composite fit at high  $T$  and HN fit at low  $T$ . In between, no appropriate fit was possible. Lines are guides for the eye. For  $w_{\text{TPP}} = 0.10$ ,  $\Delta\varepsilon_{\alpha_2}$  was linearly approximated (dashed orange line) and used to calculate the total  $\Delta\varepsilon$  (orange open squares). (b) Temperature averaged relaxation strength  $\langle\Delta\varepsilon(w_{\text{TPP}}) \cdot T\rangle / \langle T\rangle$  for the  $\alpha_2$ -relaxation (red squares) and the overall relaxation  $\Delta\varepsilon$  (blue squares). Dashed line shows the expected behavior for ideal mixing. Inset: Logarithmic y-axis with lines as guide for the eye.

Curie temperature behaviour with a tendency to become stronger towards pure TPP. For  $w_{\text{TPP}} < 0.70$ , essentially a Curie law applies for  $\Delta\varepsilon$  (squares). For intermediate concentrations  $w_{\text{TPP}} = 0.20$  up to 0.50,  $\Delta\varepsilon$  is composed of strongly temperature dependent relaxation strengths  $\Delta\varepsilon_{\alpha_1}$  and  $\Delta\varepsilon_{\alpha_2}$ . Thereby  $\Delta\varepsilon_{\alpha_1}(T)$  (crosses) decreases with increasing temperature. On the other hand,  $\Delta\varepsilon_{\alpha_2}(T)$  (open circles) shows an opposite effect. In the case of  $w_{\text{TPP}} = 0.20$  and 0.40, the two relaxations exhibit similar strengths ( $\Delta\varepsilon_{\alpha_1}(T)$  crosses  $\Delta\varepsilon_{\alpha_2}(T)$ ) although the relaxation strength of the neat components differ by a factor of 240.

Correspondingly, at lowest  $w_{\text{TPP}} \leq 0.10$ , the relaxation strength  $\Delta\varepsilon_{\alpha_1}$ , which is associated with the high- $T_g$  component, shows an enhanced relaxation strength, with a slight negative temperature dependence, compared to neat  $m$ -TPTS. In contrast,  $\Delta\varepsilon_{\alpha_2}(T)$  shows a very small absolute value for  $w_{\text{TPP}} = 0.10$  (orange circles), but is growing with temperature. Assuming this temperature dependence to hold up to highest temperatures

(dashed orange line), one receives for the total relaxation strength  $\Delta\epsilon$  again a constant value (orange open squares) at temperatures, where  $\Delta\epsilon_{\alpha_1}$  was analyzed.

To get an overview of the concentration dependence of  $\Delta\epsilon(w_{\text{TPP}})$ , the mean relaxation strength after Curie correction ( $(\Delta\epsilon(w_{\text{TPP}}, T) \cdot T) / \langle T \rangle$ ) is displayed in Fig. 11(b). As the contribution of the  $\alpha_1$ -relaxation can be ignored at  $w_{\text{TPP}} \geq 0.70$ , the relaxation strength  $\Delta\epsilon_{\alpha_2}$  (red squares) represents essentially the total  $\Delta\epsilon$ , as said. Only at  $w_{\text{TPP}} \leq 0.50$  the total strength  $\Delta\epsilon$  (blue squares) is larger than that of  $\Delta\epsilon_{\alpha_2}$ . Importantly, the concentration dependence strongly deviates from a linear dependence expected for ideal mixing (dashed line). For example, adding only 30% of the high- $T_g$  component reduces  $\Delta\epsilon_{\alpha_2}$  by a factor of about 4. A linear concentration dependence is actually observed for the  $\beta$ -relaxation (see Fig. 15). Once again, we emphasize that this strongly anomalous behaviour is not caused by filling factors lower than one as special care has been taken to assure complete filling. A similar finding was reported for a polymeric mixture before.<sup>28</sup> The inset of Fig. 11(b) shows the dependence on logarithmic scales, revealing two “branches” of exponential concentration dependence above and below  $w_{\text{TPP}} = 0.50$ . From the strongly non-ideal concentration dependence of  $\Delta\epsilon_{\alpha_1}(T)$  and  $\Delta\epsilon_{\alpha_2}(T)$ , severe doubts appear interpreting such behaviour as changes in molecular populations – as done before (*cf.* also Discussion).<sup>22,23,31</sup>

## Time constants and $T_g$

Fig. 12 shows the most probable time constants as determined by “peak-picking” for the main relaxations showing a distinguishable peak from dielectric loss data  $\epsilon''(\omega)$  ( $\tau_{\alpha_1}$ : filled circles,  $\tau_{\alpha_2}$ : open diamonds) and derivative data  $\partial\epsilon'$  ( $\tau_{\alpha_1}$ : pluses,  $\tau_{\alpha_2}$ : crosses). Additionally, to settle the high temperature behaviour, NMR time constants from  $T_1$  relaxation data are added ( $\tau_{\alpha_1}$ : stars,  $\tau_{\alpha_2}$ : open stars).<sup>43</sup>

The trend as observed in the spectra is confirmed in the time constants: with low TPP concentrations, both processes are far apart and cannot be seen in a single spectrum due to the frequency window of the DS analyser. Upon mixing, both processes approach each other until they can be both detected in a single spectrum for concentrations  $w_{\text{TPP}} \geq 0.20$ . Specifically, at  $w_{\text{TPP}} \geq 0.50$ , the  $\alpha_1$ -relaxation times  $\tau_{\alpha_1}$  (pluses) are all determined from the derivative relaxation data  $\partial\epsilon'$ , due to its enhanced sensitivity – for the first time up to highest concentrations (compared to previous work<sup>22,24</sup>). The corresponding time constants  $\tau_{\alpha_2}$  from this method (crosses) perfectly match them from  $\epsilon''$  (open diamonds). A non-Arrhenius temperature behaviour is generally observed for the  $\alpha_1$ -process. The corresponding  $T(\tau_{\alpha_1} = 100 \text{ s}) = T_{g_1}$  values are displayed in Fig. 13. A continuous decrease with increasing TPP content is observed, a behaviour well documented for many mixed systems (plasticizer effect).

For the  $\alpha_2$ -process, a non-Arrhenius behaviour is observed for neat TPP and binary mixtures down to  $w_{\text{TPP}} = 0.50$  (Fig. 12(a)). For lower concentrations  $w_{\text{TPP}} \leq 0.40$  an Arrhenius temperature dependence is observed (Fig. 12(b)). For decreasing TPP concentrations the apparent activation energy of this process

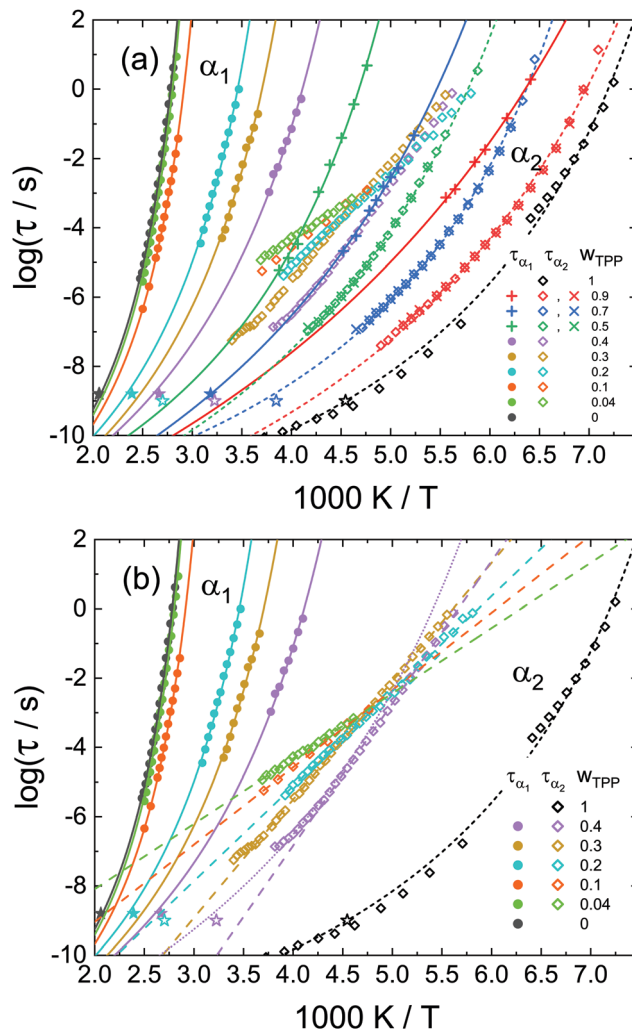


Fig. 12 Time constants  $\tau$  from peak picking for the  $\alpha_1$ - (filled circles, pluses, stars) and the  $\alpha_2$ -process (open diamonds, crosses, open stars). Concentration is colour coded. For  $c_{\text{TPP}} = 0.9, 0.7$  and  $0.5$ , the time constants (pluses and crosses) are determined from  $\partial\epsilon'$ . Stars are from NMR relaxation.<sup>43</sup> (a) Non-Arrhenius temperature dependence is shown as lines ( $\alpha_1$ ) and dashed lines ( $\alpha_2$ ). (b) Selected time constants from (a) in the concentration range with Arrhenius temperature dependence of  $\tau_{\alpha_2}$ . Neat components for comparison.

decreases. As confirmed by NMR,<sup>43</sup> the  $\alpha_2$ -process reflects an isotropic reorientation of the TPP molecules and thus one can define a second glass transition temperature,  $T_{g_2}$  by extrapolating to  $\tau(T_g) = 100 \text{ s}$ . The curve  $T_{g_2}(w_{\text{TPP}})$  passes through a maximum with decreasing  $w_{\text{TPP}}$  (*cf.* Fig. 13), a behaviour reported in other dynamically asymmetric binary glasses.<sup>22,24</sup> We note that even at high TPP concentrations we are able to identify two distinct  $T_g$  values from DS. The such obtained  $T_g$  values are confirmed by our DSC experiments.

A subtle feature may be recognized when inspecting  $\tau_{\alpha_2}(T)$  in detail for concentrations for which an Arrhenius temperature dependence is observed (*cf.* Fig. 12(b)). At high temperatures,  $\tau_{\alpha_2}(T)$  deviates from the extrapolation of the Arrhenius behaviour and the data display a weak non-Arrhenius trace. This feature may be a reminiscence of a fragile-to strong transition occurring close to  $T_{g_1}$ , a phenomenon observed before.<sup>22,31</sup>

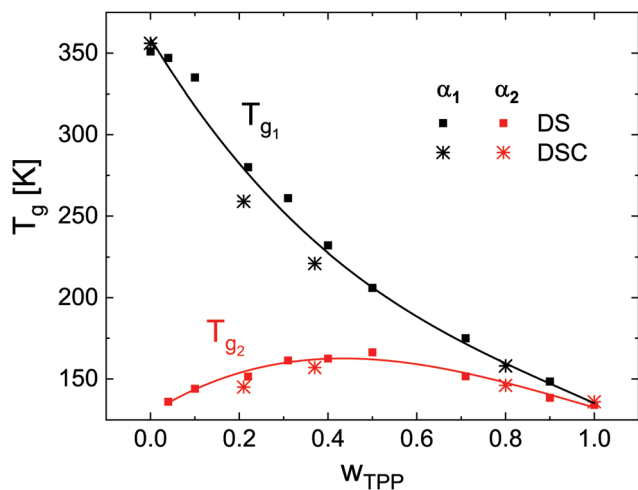


Fig. 13 Glass transition temperature  $T_g(w_{\text{TPP}})$  from DS (squares) and DSC (stars).  $T_{g_1}$  ( $\alpha_1$ -process,  $m$ -TPTS dynamics) is shown in black and  $T_{g_2}$  ( $\alpha_2$ -process, TPP dynamics) in red.

## $\beta$ -Process

In contrast to neat  $m$ -TPTS, neat TPP displays a  $\beta$ -relaxation, which is observed in all mixtures, too. Fig. 14(a) shows exemplarily the dielectric susceptibility spectra of neat TPP and of the binary mixtures  $w_{\text{TPP}} = 0.04, 0.30$  and  $0.70$  at temperatures between 100 K and 140 K, displaying solely the  $\beta$ -relaxation.

As expected from a relaxation process determined by a distribution of activation energies,<sup>54</sup> the amplitude decreases with decreasing temperature while the spectra broaden. Furthermore, the intensity of the  $\beta$ -relaxation decreases with decreasing TPP concentration. More precisely, the corresponding relaxation strength  $\Delta\epsilon_{\beta}(T = 100 \text{ K})$  increases linearly with  $w_{\text{TPP}}$  (see Fig. 15). The relaxation strength  $\Delta\epsilon_{\beta}$  was determined with an appropriate fitting function.<sup>55</sup> In addition, a weak but continuous shift of the relaxation maxima to higher frequencies is observed for decreasing  $w_{\text{TPP}}$ . This can directly be seen in Fig. 14(b), where the time constants  $\tau_{\beta}$  extracted from the

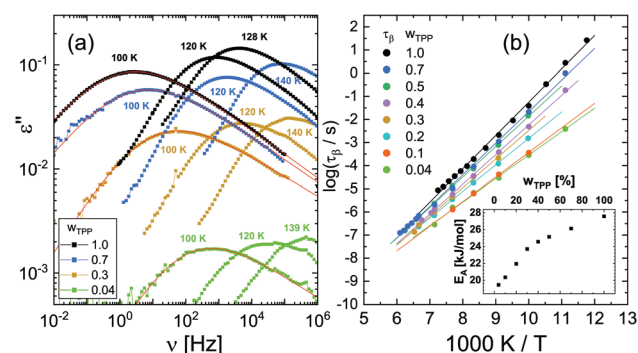


Fig. 14 (a) Dielectric spectra  $\epsilon''$  of neat TPP and the binary mixtures  $w_{\text{TPP}} = 0.04, 0.30$  and  $0.70$  at temperatures between 100 K and 140 K. Red lines are interpolations to determine the relaxation strength  $\Delta\epsilon_{\beta}$  with an appropriate fitting function.<sup>55</sup> Concentration is colour coded. (b) Time constants of the  $\beta$ -process  $\tau_{\beta}(T)$  at different concentrations. Inset displays the concentration dependence of the activation energy.

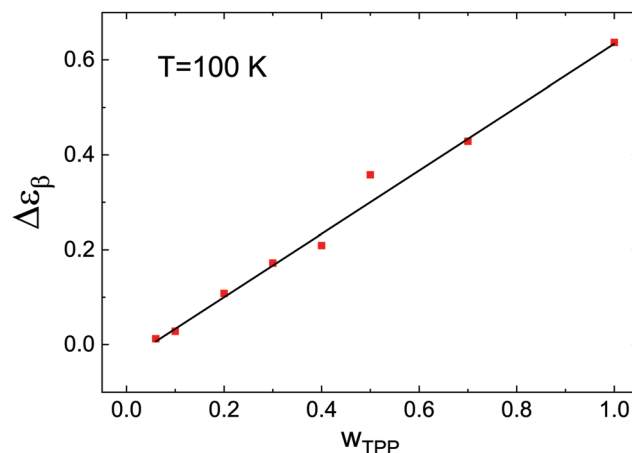


Fig. 15  $\beta$ -Relaxation strength  $\Delta\epsilon_{\beta}(w_{\text{TPP}})$  determined at  $T = 100 \text{ K}$  with an appropriate fitting function.<sup>55</sup>

relaxation peaks ( $\tau_{\beta} = 1/(2\pi\nu_p)$ ) are shown. An Arrhenius like temperature dependence is found for all concentrations. The corresponding activation energy  $E_{\text{A}\beta}$  changes with concentration, which is shown as inset in Fig. 14(b). Whereas the  $\beta$ -relaxation of neat TPP shows an activation energy of  $E_{\text{A}\beta} = 27.4 \text{ kJ mol}^{-1}$ , the value steadily decreases to  $E_{\text{A}\beta} = 19.5 \text{ kJ mol}^{-1}$  at a concentration  $w_{\text{TPP}} = 0.04$ . It has to be mentioned, that such a large concentration dependence was not found in our previous investigated binary mixtures, although, TPP was used as additive.<sup>22,29</sup> But only for completeness, the  $\beta$ -relaxation is shown here. Therefore, we will not further discuss this process.

## Discussion and conclusion

With the present non-polymeric asymmetric binary glass former, we are able to cover the full concentration range ( $0.04 \leq w_{\text{TPP}} \leq 0.90$ ) by dielectric spectroscopy. As said, our previous studies were hampered by the fact that the samples tend to de-mix/crystallize. In addition to a secondary  $\beta$ -process, two main relaxation processes,  $\alpha_1$  and  $\alpha_2$ , are identified at all concentrations. They are characterized by well separated time scales. We attribute  $\alpha_1$  to the dynamics associated with the high- $T_g$  component and  $\alpha_2$  with that of the additive (low- $T_g$  component).

Compared to the relaxation spectra of neat glass formers, the evolution of the relaxation spectra shows unusual features which are again summarized in Fig. 16. Just for didactic purpose, we re-scaled the spectra in a way to document best the evolution of the component spectra with concentration. Whereas the  $\alpha_1$ -relaxation broadens on the high-frequency flank of the relaxation peak, the  $\alpha_2$ -relaxation becomes broader on the low-frequency side progressively with adding additive or high- $T_g$  component, respectively. Basically, the broadening of the component's spectra is only confined by the time constant of the other component. As expected for the slowest relaxation in a liquid, the low-frequency flank of the  $\alpha_1$ -relaxation displays a  $\epsilon'' \propto \omega^1$  behaviour (see Fig. 16). In both cases FTS does not apply any longer and the spectra cannot be reproduced by

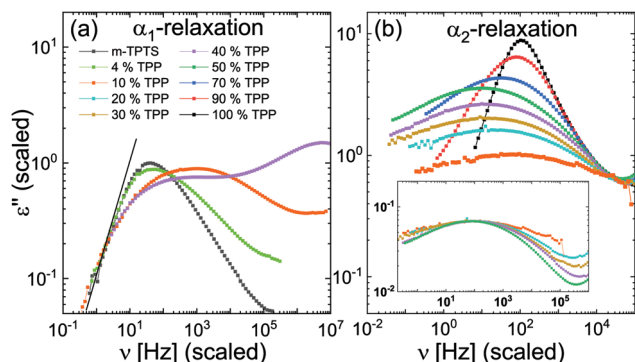


Fig. 16 Overview of the dielectric spectra evolution with concentration for (a) the  $\alpha_1$ -relaxation and (b) the  $\alpha_2$ -relaxation. Comparable time constants/temperatures were used. The concentration is colour coded. The  $\alpha_1$ -relaxation spectra were scaled on the low frequency side and the  $\alpha_2$ -relaxation spectra on the high frequency side. Inset of (b):  $\alpha_2$ -relaxation spectra scaled onto peak position and height.

functions of Kohlrausch- or CD-type, for example. At lowest additive concentration, the  $\alpha_2$  spectra become such broad that they tend to disappear in the noise of the instrument; no saturation of the broadening is observed at lowest TPP concentration (see inset of Fig. 16(b)) in contrast to the behaviour of the  $\alpha_1$ -relaxation (cf. Fig. 8(b)). For example, it is a remarkable fact that at  $w_{\text{TPP}} = 0.04$  (cf. Fig. 18) still highly decoupled dynamics of TPP is observed in an essentially arrested high- $T_g$  matrix. Thus, it is difficult to foresee the transition to the infinite-dilution limit, expecting that a single added molecule probes the dynamics of the high- $T_g$  component. All in all, the described spectral features closely resemble those in polymer-additive systems.<sup>22,28</sup>

Regarding the time constants of the additive ( $\alpha_2$ -relaxation), one observes a crossover from a non-Arrhenius temperature dependence at high concentration to an Arrhenius at low concentration. There is some indication that a “fragile-to strong” transition is also observed for a given concentration, *i.e.*, around  $T_{g_1}$ ,  $\tau_{\alpha_2}(T)$  crosses over to Arrhenius behaviour upon cooling. Anticipating our results from a follow-up NMR study which are supported by our previous investigations,<sup>28,30</sup> the dynamics of the TPP molecules is dynamically strongly heterogeneous: molecules undergo isotropic liquid-like reorientation on very different time scales. This allows us to define a second isodynamic point  $T_{g_2} = T_{g_2}(w_{\text{TPP}})$ , which passes through a maximum indicating extreme separation of the component dynamics at low additive concentration. Of course, this temperature characterizes the slow-down of the additive dynamics in an essentially arrested high- $T_g$  matrix, thus may involve a different type of glass transition as suggested by MD simulations as well as analyses by mode coupling theory.<sup>13,14,16,56</sup> Specifically, a dynamical decoupling of large and small particle species was reported. The large particles exhibit a standard glass transition controlled by the cage effect, while the small particles still remain mobile within the arrested matrix of the large particles and undergo finally at lowest temperatures a localization transition. In contrast, and in accordance with our results, the dynamics of the high- $T_g$  component *m*-TPTS is essentially homogeneous.<sup>43</sup> In this context, another MD

simulation is of interest, which investigated a mixture of two water-like model molecules with different polarities such that the dynamical contrast is large whereas the mixture remains miscible.<sup>17</sup> Again, dynamical decoupling was observed and the fast component displays quasi-logarithmic correlation decays together with a sub-diffusive regime in the mean square displacement. In contrast, the dynamics of the slow component resembles essentially that of neat glass formers. The growing concentration fluctuations upon cooling, characteristic of approaching spinodal decomposition, control the spatially heterogeneous dynamics.

This difference of the dynamics leads us to a different interpretation of the observed broadening of the spectra of the high- $T_g$  and the low- $T_g$  component, respectively. On the one hand, the low-frequency broadening of the additive spectra, indeed, reflects heterogeneous dynamics. The corresponding “true” time constant as given by the spectral density at zero frequency (or as integral over the correlation function) is determined by the longest time, which is actually difficult to access because the low-frequency flank is partly obscured by the spectral contribution associated with the high- $T_g$  component. Consequently, the TPP time constants  $\tau_{\alpha_2}(T)$  given in Fig. 12 represent the most probable time constant reflecting the major part of the spectrum of the TPP sub-ensemble. The difference between  $T_{g_1}$  and  $T_{g_2}$  specifies the extent of time scale separation in the mixture. We emphasize that around  $T_{g_2}$  a broad glass step is also monitored in the DSC signal (cf. Fig. 2). On the other hand, the spectra of the high- $T_g$  component become overall broader and, importantly, display a stronger relaxation strength compared to that of the neat component. For example, adding only 4% TPP, the spectra significantly broaden (see Fig. 16). However, the corresponding high-frequency broadening of the spectra does not originate from molecules that reorient isotropically at those frequencies. These spectral features are probably of similar quality as that of the excess wing documented in the spectra of neat glass formers. It is a kind of precursor relaxation of the main relaxation.

The most unusual result reported by our study and not covered by our previous investigations concerns the concentration dependence of the total dielectric relaxation strength  $\Delta\epsilon$ . Due to the low polarity of the high- $T_g$  component, it basically reflects the relaxation strength of the additive. While  $\Delta\epsilon(T)$  essentially follows a Curie law, its concentration dependence strongly deviates from that expected by ideal mixing. Actually, this is not observed for the case when a high- $T_g$  component carries the high dipole moment.<sup>34</sup> Thus, care has to be taken to interpret the fraction  $\Delta\epsilon_{\alpha_2}/\Delta\epsilon$  as reflecting the corresponding population of the respective sub-ensemble of the component.

Here, recent simulation work of the dielectric spectra of molecular binary systems may be of relevance.<sup>57</sup> It indicates significant difference between the collective (coherent) and the self (incoherent) reorientational dynamics. In particular, the coherent additive correlation function shows in addition to a short time decay a plateau essentially persisting up to a time scale on the order of that of the matrix – a feature not observed in the incoherent correlation function. In other words, the

collective dynamics of the additive only fully decays to zero when the matrix relaxes, whereas the incoherent dynamics lead to a low-frequency broadening with a cut-off at the time scale of the high- $T_g$  dynamics as modelled by our approach. For example, a single additive molecule could leave the matrix sites on the time scale  $\tau_{\alpha_2}$  but other molecules visit an identical site, thus keeping some correlations up to the time scale  $\tau_{\alpha_1}$ , at which the matrix relaxes. Similar effects were reported when simulating mixtures of particles (lacking orientational degrees of freedom) of disparate sizes.<sup>13</sup>

Like Blochowicz and co-workers,<sup>22,23,31</sup> we previously interpreted the higher relaxation strength of the  $\alpha_1$ -relaxation with respect to the that of the neat system as an indication that part of the additive molecules take part in the  $\alpha_1$ -relaxation of the high- $T_g$  component and finally are released at a certain high temperature.<sup>24,28</sup> Possibly, as the simulations suggest, the enhanced relaxation strength of the  $\alpha_1$ -relaxation may also result from a persistent correlation induced by the high- $T_g$  matrix on the TPP molecules: in any case, the strongly enhanced relaxation strength  $\Delta\epsilon_{\alpha_1}$  must not be interpreted as reflecting an underlying distribution of the liquid-like high- $T_g$  component dynamics. Given that <sup>31</sup>P NMR probes single-particle (incoherent) dynamics, our follow-up NMR study will address the question up to what extent the enhanced relaxation strength  $\Delta\epsilon_{\alpha_1}$  can be attributed to a slow TPP sub-ensemble. Thus, in applying different NMR techniques, we will re-iterate the sketched issues.

## Conflicts of interest

There are no conflicts to declare.

## Appendix

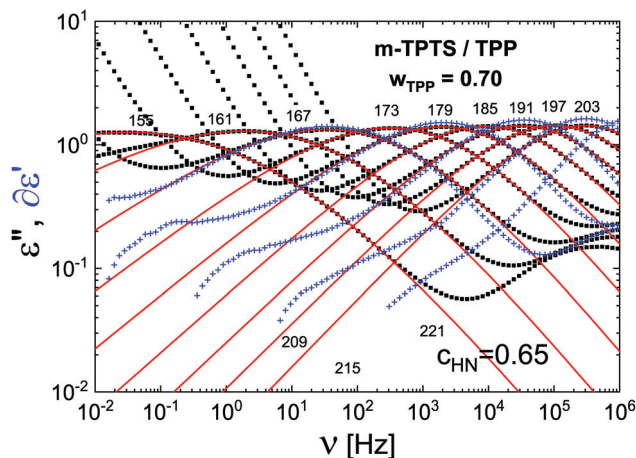


Fig. 17 Dielectric spectra  $\epsilon''$  of the binary mixture  $w_{\text{TPP}} = 0.90$  (black squares, HN fits as red lines). For selected temperatures, the derivative relaxation data  $\partial\epsilon'/\partial\nu$  (blue crosses) are shown. An additional low intensity relaxation contribution is recognized at lowest frequencies ( $\alpha_1$ ), which cannot be resolved in  $\epsilon''$ . Fit parameters are included in Fig. 6 and 11.

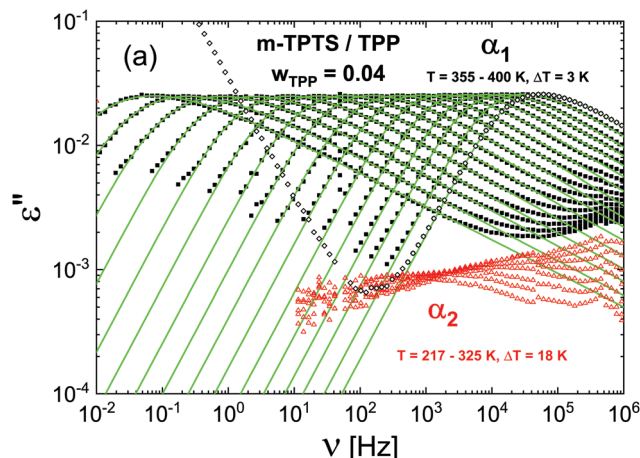


Fig. 18 Dielectric spectra  $\epsilon''$  of  $w_{\text{TPP}} = 0.04$  (squares,  $\alpha_2$ -spectra as open red triangles). Original data is shown for  $T = 400$  K (open diamonds). Green lines are GCD-fits. Fit parameters are included in Fig. 8 and 11.

## Acknowledgements

This research was funded by the Deutsche Forschungsgemeinschaft (DFG, German Research Foundation), Grant Numbers Schm 703/9-1, RO 907/19, and SFB 840. F. K. acknowledges support from the Elite Network of Bavaria (ENB) within the Elite Study Program Macromolecular Science. T. K. and E. R. also acknowledge the support by Simon Winterstein and Jürgen Senker.

## References

- M. D. Ediger, *Annu. Rev. Phys. Chem.*, 2000, **51**, 99–128.
- P. Lunkenheimer, U. Schneider, R. Brand and A. Loidl, *Contemp. Phys.*, 2000, **41**, 15–36.
- G. Floudas, M. Paluch, A. Grzybowski and K. Ngai, *Molecular dynamics of glass-forming systems. Effects of pressure*, Springer, Berlin, Heidelberg, 2011.
- P. G. Wolynes and V. Lubchenko, *Structural glasses and supercooled liquids. Theory, experiment, and applications*, Wiley, Hoboken, New Jersey, 2012.
- N. Petzold, B. Schmidtke, R. Kahlau, D. Bock, R. Meier, B. Micko, D. Kruk and E. A. Rössler, *J. Chem. Phys.*, 2013, **138**, 12A510.
- P. J. Hains and G. Williams, *Polymer*, 1975, **16**, 725–729.
- M. Scandola, G. Ceccorulli and M. Pizzoli, *Polymer*, 1987, **28**, 2081–2084.
- Y. He, T. R. Lutz, M. D. Ediger, M. Pitsikalis, N. Hadjichristidis and E. D. von Meerwall, *Macromolecules*, 2005, **38**, 6216–6226.
- T. R. Lutz, Y. He and M. D. Ediger, *Macromolecules*, 2005, **38**, 9826–9835.
- G. Goracci, A. Arbe, A. Alegría, Y. Su, U. Gasser and J. Colmenero, *J. Chem. Phys.*, 2016, **144**, 154903.
- Y. Kaneko and J. Bosse, *J. Non-Cryst. Solids*, 1996, **205–207**, 472–475.

- 12 S.-H. Chong, W. Götze and A. P. Singh, *Phys. Rev. E: Stat., Nonlinear, Soft Matter Phys.*, 2000, **63**, 11206.
- 13 A. J. Moreno and J. Colmenero, *J. Chem. Phys.*, 2006, **125**, 164507.
- 14 T. Voigtmann and J. Horbach, *Phys. Rev. Lett.*, 2009, **103**, 205901.
- 15 T. Voigtmann, *EPL*, 2011, **96**, 36006.
- 16 T. Sentjabrskaja, E. Zaccarelli, C. D. Michele, F. Sciortino, P. Tartaglia, T. Voigtmann, S. U. Egelhaaf and M. Laurati, *Nat. Commun.*, 2016, **7**, 11133.
- 17 N. Müller and M. Vogel, *J. Chem. Phys.*, 2019, **150**, 64502.
- 18 L. A. Utracki and B. D. Favis, in *Handbook of Polymer Science and Technology*, ed. N. P. Cheremisinoff, Marcel Dekker, Inc., New York, 1989.
- 19 M. Pizzoli, M. Scandola and G. Ceccorulli, *Eur. Polym. J.*, 1987, **23**, 843–846.
- 20 T. Sakaguchi, N. Taniguchi, O. Urakawa and K. Adachi, *Macromolecules*, 2005, **38**, 422–428.
- 21 T. P. Lodge, E. R. Wood and J. C. Haley, *J. Polym. Sci., Part B: Polym. Phys.*, 2006, **44**, 756–763.
- 22 R. Kahlau, D. Bock, B. Schmidtke and E. A. Rössler, *J. Chem. Phys.*, 2014, **140**, 44509.
- 23 T. Blochowicz, S. A. Lusceac, P. Gutfreund, S. Schramm and B. Stühn, *J. Phys. Chem. B*, 2011, **115**, 1623–1637.
- 24 B. Pötzschner, F. Mohamed, A. Lichtinger, D. Bock and E. A. Rössler, *J. Chem. Phys.*, 2015, **143**, 154506.
- 25 S. P. Bierwirth, C. Gainaru and R. Böhmer, *J. Chem. Phys.*, 2018, **149**, 44509.
- 26 J. Colmenero and A. Arbe, *Soft Matter*, 2007, **3**, 1474–1485.
- 27 D. Cangialosi, A. Alegria and J. Colmenero, *J. Chem. Phys.*, 2007, **126**, 204904.
- 28 D. Bock, R. Kahlau, B. Pötzschner, T. Körber, E. Wagner and E. A. Rössler, *J. Chem. Phys.*, 2014, **140**, 94505.
- 29 B. Pötzschner, F. Mohamed, C. Bächer, E. Wagner, A. Lichtinger, D. Bock, K. Kreger, H.-W. Schmidt and E. A. Rössler, *J. Chem. Phys.*, 2017, **146**, 164504.
- 30 D. Bock, T. Körber, F. Mohamed, B. Pötzschner and E. A. Rössler, in *The Scaling of Relaxation Processes*, ed. F. Kremer and A. Loidl, Springer, Cham, Switzerland, 2018, pp. 173–201.
- 31 T. Blochowicz, S. Schramm, S. Lusceac, M. Vogel, B. Stühn, P. Gutfreund and B. Frick, *Phys. Rev. Lett.*, 2012, **109**, 35702.
- 32 B. Frick, C. Alba-Simionesco, G. Dosseh, C. Le Quellec, A. J. Moreno, J. Colmenero, A. Schönhals, R. Zorn, K. Chrissopoulou, S. H. Anastasiadis and K. Dalnoki-Veress, *J. Non-Cryst. Solids*, 2005, **351**, 2657–2667.
- 33 D. Bock, N. Petzold, R. Kahlau, S. Gradmann, B. Schmidtke, N. Benoit and E. A. Rössler, *J. Non-Cryst. Solids*, 2015, **407**, 88–97.
- 34 T. Körber, R. Minikejew, B. Pötzschner, D. Bock and E. A. Rössler, *Eur. Phys. J. E: Soft Matter Biol. Phys.*, 2019, **42**, 143.
- 35 B. Pötzschner, F. Mohamed, C. Bächer, E. Wagner, A. Lichtinger, R. Minikejew, K. Kreger, H.-W. Schmidt and E. A. Rössler, *J. Chem. Phys.*, 2017, **146**, 164503.
- 36 F. Krohn, C. Neuber, E. A. Rössler and H.-W. Schmidt, *J. Phys. Chem. B*, 2019, **123**, 10286–10293.
- 37 T. Körber, F. Krohn, C. Neuber, H.-W. Schmidt and E. A. Rössler, *Phys. Chem. Chem. Phys.*, 2020, **22**, 9086–9097.
- 38 C. Lorthioir, A. Alegria and J. Colmenero, *Phys. Rev. E: Stat., Nonlinear, Soft Matter Phys.*, 2003, **68**, 31805.
- 39 S. Valenti, S. Capaccioli and K. L. Ngai, *J. Chem. Phys.*, 2018, **148**, 54504.
- 40 K. L. Ngai, S. Valenti and S. Capaccioli, *J. Non-Cryst. Solids*, 2019, 119573.
- 41 S. Adishchev, D. Bock, C. Gainaru, R. Kahlau, B. Micko, N. Petzold, B. Pötzschner and E. A. Rössler, *Z. Phys. Chem.*, 2012, **226**, 1149–1168.
- 42 R. Kahlau, T. Dörfler and E. A. Rössler, *J. Chem. Phys.*, 2013, **139**, 134504.
- 43 T. Körber and E. A. Rössler, 2021, to be published.
- 44 C. J. F. Böttcher and P. Bordewijk, *Dielectrics in time-dependent fields*, Elsevier, Amsterdam, 2nd edn, 1978.
- 45 F. Kremer and A. Schönhals, *Broadband Dielectric Spectroscopy*, Springer, Berlin, Heidelberg, 2003.
- 46 R. Kahlau, D. Kruk, T. Blochowicz, V. N. Novikov and E. A. Rössler, *J. Phys.: Condens. Matter*, 2010, **22**, 365101.
- 47 S. Havriliak and S. Negami, *Polymer*, 1967, **8**, 161–210.
- 48 T. Blochowicz, PhD thesis, Universität Bayreuth, 2003.
- 49 M. Wübbenhorst and J. van Turnhout, *J. Non-Cryst. Solids*, 2002, **305**, 40–49.
- 50 A. Savitzky and M. J. E. Golay, *Anal. Chem.*, 1964, **36**, 1627–1639.
- 51 P. A. Gorry, *Anal. Chem.*, 1990, **62**, 570–573.
- 52 H. Wagner and R. Richert, *J. Phys. Chem. B*, 1999, **103**, 4071–4077.
- 53 D. Bock, R. Kahlau, B. Micko, B. Pötzschner, G. J. Schneider and E. A. Rössler, *J. Chem. Phys.*, 2013, **139**, 64508.
- 54 A. Kudlik, S. Benkhof, T. Blochowicz, C. Tschirwitz and E. Rössler, *J. Mol. Struct.*, 1999, **479**, 201–218.
- 55 T. Blochowicz, C. Tschirwitz, S. Benkhof and E. A. Rössler, *J. Chem. Phys.*, 2003, **118**, 7544–7555.
- 56 A. J. Moreno and J. Colmenero, *Phys. Rev. E: Stat., Nonlinear, Soft Matter Phys.*, 2006, **74**, 21409.
- 57 T. Böhmer, R. Horstmann, J. Gabriel, F. Pabst, M. Vogel and T. Blochowicz, 2021, to be published.

---

## Publication 5

**Reorientational dynamics in highly  
asymmetric binary low-molecular mixtures  
– a quantitative comparison of dielectric  
and NMR spectroscopy results**

**T. Körber, B. Pötzschner, F. Krohn and E. A. Rössler**

*The Journal of Chemical Physics*

**155**, 024504 (2021)

DOI: 10.1063/5.0056838

© 2021 AIP Publishing LLC

# Reorientational dynamics in highly asymmetric binary low-molecular mixtures—A quantitative comparison of dielectric and NMR spectroscopy results

Cite as: J. Chem. Phys. 155, 024504 (2021); doi: 10.1063/5.0056838

Submitted: 14 May 2021 • Accepted: 14 June 2021 •

Published Online: 9 July 2021



View Online



Export Citation



CrossMark

Thomas Körber,<sup>1</sup> Björn Pötzschner,<sup>1</sup> Felix Krohn,<sup>2</sup> and Ernst A. Rössler<sup>1,a)</sup>

## AFFILIATIONS

<sup>1</sup>Department of Inorganic Chemistry III and Northern Bavarian NMR Centre, University of Bayreuth, 95440 Bayreuth, Germany

<sup>2</sup>Department of Macromolecular Chemistry and Bavarian Polymer Institute, University of Bayreuth, 95440 Bayreuth, Germany

<sup>a)</sup>Author to whom correspondence should be addressed: [ernst.roessler@uni-bayreuth.de](mailto:ernst.roessler@uni-bayreuth.de)

## ABSTRACT

Previously, we scrutinized the dielectric spectra of a binary glass former made by a low-molecular high- $T_g$  component 2-(*m*-*tert*butylphenyl)-2'-*tert*butyl-9,9'-spirobi[9H]fluorene (*m*-TPTS;  $T_g = 350$  K) and low- $T_g$  tripropyl phosphate (TPP;  $T_g = 134$  K) [Körber *et al.*, Phys. Chem. Chem. Phys. **23**, 7200 (2021)]. Here, we analyze nuclear magnetic resonance (NMR) spectra and stimulated echo decays of deuterated *m*-TPTS- $d_4$  ( $^2\text{H}$ ) and TPP ( $^{31}\text{P}$ ) and attempt to understand the dielectric spectra in terms of component specific dynamics. The high- $T_g$  component ( $\alpha_1$ ) shows relaxation similar to that of neat systems, yet with some broadening upon mixing. This correlates with high-frequency broadening of the dielectric spectra. The low- $T_g$  component ( $\alpha_2$ ) exhibits highly stretched relaxations and strong dynamic heterogeneities indicated by “two-phase” spectra, reflecting varying fractions of fast and slow liquid-like reorienting molecules. Missing for the high- $T_g$  component, such two-phase spectra are identified down to  $w_{\text{TPP}} = 0.04$ , indicating that isotropic reorientation prevails in the rigid high- $T_g$  matrix stretching from close to  $T_g^{\text{TPP}}$  to  $T_{g_1}(w_{\text{TPP}})$ . This correlates with low-frequency broadening of the dielectric spectra. Two  $T_g$  values are defined:  $T_{g_1}(w_{\text{TPP}})$  displays a plasticizer effect, whereas  $T_{g_2}(w_{\text{TPP}})$  passes through a maximum, signaling extreme separation of the component dynamics at low  $w_{\text{TPP}}$ . We suggest understanding the latter counter-intuitive feature by referring to a crossover from “single glass” to “double glass” scenario revealed by recent MD simulations. Analyses reveal that a second population of TPP molecules exists, which is associated with the dynamics of the high- $T_g$  component. However, the fractions are lower than suggested by the dielectric spectra. We discuss this discrepancy considering the role of collective dynamics probed by dielectric but not by NMR spectroscopy.

Published under an exclusive license by AIP Publishing. <https://doi.org/10.1063/5.0056838>

## I. INTRODUCTION

The dynamics of neat glass-formers was studied extensively in the last few decades.<sup>1–6</sup> The next challenge is understanding binary systems. Here, dynamically asymmetric systems, which are systems displaying a high  $T_g$ -contrast of their components, are of particular interest. As an example, polymer–plasticizer systems have been investigated since long.<sup>7–13</sup> Moreover, mixtures of non-polymeric low-molecular components may be taken as model systems for binary glass formers with significant molecular size disparity of their components.<sup>14–19</sup> Such systems have therefore

created the interest of molecular dynamics simulations and theoretical studies.<sup>20–28</sup>

Continuing our previous work on investigating component-selectively the dynamics in highly asymmetric binary glass formers, polymeric<sup>12,29</sup> as well as non-polymeric,<sup>18,30</sup> by dielectric (DS) as well as by nuclear magnetic resonance (NMR) spectroscopy, we recently introduced a new non-polymeric asymmetric binary system not prone to de-mixing and crystallization.<sup>31</sup> It is composed of a high- $T_g$  component *m*-TPTS ( $T_g = 350$  K) and an additive tripropyl phosphate (TPP;  $T_g = 134$  K), thus displaying a  $T_g$ -contrast of 216 K (see Fig. 1 for chemical structures). In a preceding

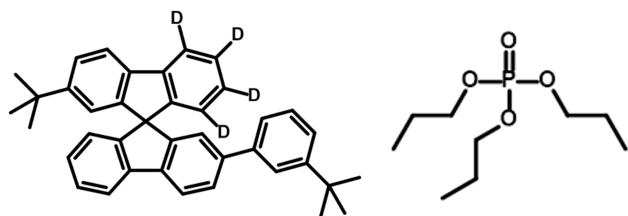


**FIG. 1.** Chemical structures of the high- $T_g$  component  $m$ -TPTS- $d_4$  (left) and the low- $T_g$  component TPP (right) used for the binary mixtures.

publication (denoted subsequently “Part I”), we analyzed its DS and differential scanning calorimetry (DSC) response.<sup>31</sup> Here, we will focus on component-selective NMR investigations.

Compared to the relaxation spectra of neat glass formers,<sup>1,32</sup> the dielectric spectra show unusual features in this system.<sup>31</sup> Two more or less separated and broadened main relaxations,  $\alpha_1$  associated with the slow dynamics of the high- $T_g$  component and  $\alpha_2$ , the faster one, associated with the low- $T_g$  component (additive) dynamics, are observed. Whereas the  $\alpha_1$ -relaxation broadens on the high-frequency flank of its relaxation peak upon adding the additive, the  $\alpha_2$ -relaxation broadens on the low-frequency side [cf. Fig. 2(a)]. In both cases, frequency-temperature superposition (FTS) does not apply and the spectra cannot be reproduced by functions such as of Kohlrausch- or Cole-Davidson (CD)-type. The broad  $\alpha_2$  spectra clearly indicate pronounced dynamic heterogeneities. While the time constants  $\tau_{\alpha_1}(T)$  display a typical non-Arrhenius behavior and a plasticizer effect in  $T_{g_1}(w_{TPP})$ , those of the additive  $\tau_{\alpha_2}(T)$  show a crossover from a non-Arrhenius temperature dependence at high additive concentrations to Arrhenius at low concentrations. Determined by DS and DSC,  $T_{g_2}(w_{TPP})$  passes through a maximum, indicating extreme separation of the component dynamics at

low  $w_{TPP}$  [see Fig. 2(b)], a phenomenon observed in several asymmetric mixtures investigated by our group but still controversially discussed.<sup>12,18,33,34</sup>

The puzzling result emerging from our dielectric study concerns the concentration dependence of the dielectric relaxation strengths [see Fig. 11(b) and the inset of Fig. 2(a)], where we plotted the relative dielectric relaxation strength  $\Delta\epsilon_1/\Delta\epsilon$  as a function of temperature and the total  $\Delta\epsilon$  as a function of concentration  $w_{TPP}$  (by mass percentage).<sup>31</sup> Due to the very low polarity of the high- $T_g$  component in contrast to that of the additive ( $\Delta\epsilon$  is by a factor of about 260 smaller at their respective  $T_g$ ), it is expected that the dielectric spectra essentially reflect the signal of the additive. However, the individual  $\Delta\epsilon_i$  exhibit atypical changes with temperature,  $\Delta\epsilon_1$  growing and  $\Delta\epsilon_2$  decreasing with lowering temperature and, importantly,  $\Delta\epsilon_1$  becomes higher than the relaxation strength of the pure (non-polar) high- $T_g$  component already at lowest additive concentrations. Moreover, whereas the total strength  $\Delta\epsilon(T)$  essentially follows a Curie law, its concentration dependence strongly deviates from that expected by ideal mixing. We previously interpreted the enhanced (relative)  $\alpha_1$ -relaxation strength as an indication that part of the additive molecules take part in the  $\alpha_1$ -relaxation of the high- $T_g$  component and finally are released at high temperature.<sup>11,18,29</sup> However, given the unusual behavior of the relaxation strength, care has to be taken to interpret the fraction  $\Delta\epsilon_i/\Delta\epsilon$  as reflecting the corresponding population of the respective sub-ensemble of the component. Possibly, as the simulations suggest, the enhanced relaxation strength of the  $\alpha_1$ -relaxation may also result from a persistent correlation induced by the high- $T_g$  matrix on the TPP molecules.<sup>35</sup>

In Sec. III, we present results from  $^2\text{H}$  NMR (probing the high- $T_g$  component) and from  $^{31}\text{P}$  NMR (probing the additive dynamics). One of the four phenyl rings constituting the spirobifluorene unit is deuterated, and thus,  $^2\text{H}$  NMR probes the dynamics of

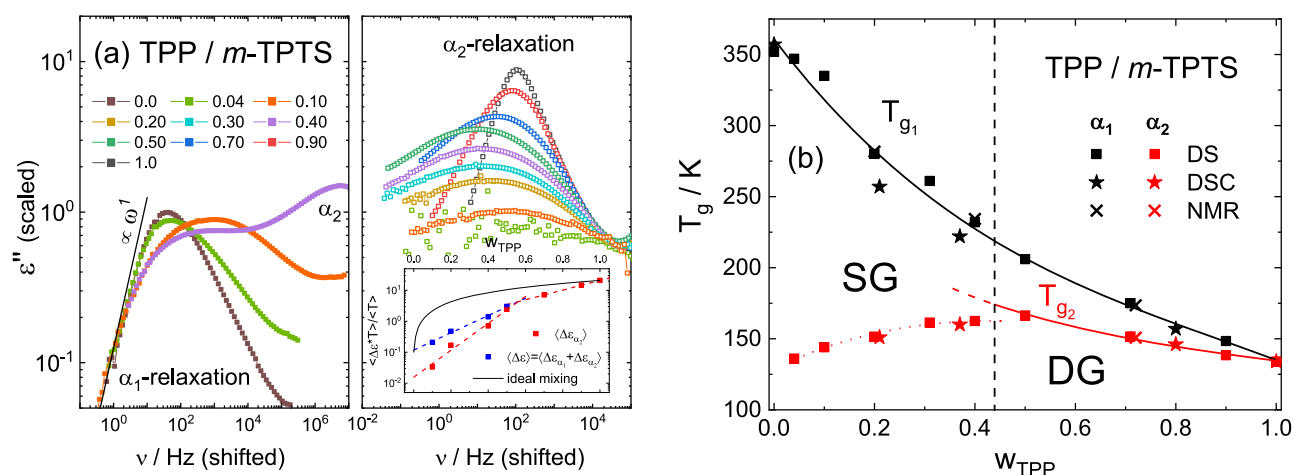


**FIG. 2.** (a) Evolution of the dielectric spectra of the  $\alpha_1$ -relaxation (high- $T_g$  component dynamics, squares) and  $\alpha_2$ -relaxation (additive dynamics, open squares) of the mixture TPP/ $m$ -TPTS with concentration  $w_{TPP}$  (color coded).<sup>31</sup> The spectra are scaled on the common low-frequency side ( $\alpha_1$ ), respectively, on the high-frequency side ( $\alpha_2$ ). Inset: temperature averaged relaxation strength  $\langle \Delta\epsilon(w_{TPP}) \cdot T \rangle / \langle T \rangle$  of the  $\alpha_2$ -relaxation (red squares) and the overall relaxation  $\Delta\epsilon$  (blue squares).<sup>31</sup> Black line: expected behavior for ideal mixing. (b) Glass transition temperatures  $T_{g,1,2}(w_{TPP})$  from DS (squares), DSC (stars),<sup>31</sup> and NMR measurements (crosses). Transition from fluid to single glass (SG), respectively, double glass (DG), scenario suggested by recent MD simulations (cf. Sec. IV).<sup>28</sup>

its rigid core. Given that  $^2\text{H}$  and  $^{31}\text{P}$  NMR probe single-particle (incoherent) dynamics, our present study will address the question that up to what extent the enhanced dielectric relaxation strength of the  $\alpha_1$ -relaxation, for example, can indeed be attributed to a slow TPP sub-ensemble attached more or less to the high- $T_g$  component. We will focus on analyzing NMR line shapes, stimulated echo decays, and spin relaxation times with the final goal to provide a consistent interpretation of the results of both, dielectric and NMR spectroscopy. Anticipating our results, although the dielectric relaxation strengths cannot be quantitatively mapped to those from NMR, there exists a second population of additive molecules associated with the dynamics of the high- $T_g$  component, yet its fraction is smaller than suggested by DS. Furthermore, we propose to understand the counter-intuitive behavior of  $T_{g_2}(w_{\text{TPP}})$  in terms of a crossover from a “double glass” to a “single glass” transition as found in recent MD simulations of mixtures of hard spheres with a highly disparate size,<sup>28</sup> which is already sketched in Fig. 2(b) and will be discussed later (cf. Sec. IV).

## II. EXPERIMENTAL AND METHODOLOGICAL SECTION

### A. Systems

Figure 1 shows the chemical structures of the two used components. The high- $T_g$  glass former 2-(*m*-*tert*butylphenyl)-2'-*tert*butyl-9,9'-spirobi[9H]fluorene (*m*-TPTS) was synthesized along the lines described in Ref. 32 and purified by sublimation. Its phenyl ring deuterated counterpart (*m*-TPTS- $\text{d}_4$ , cf. Fig. 1) is synthesized analogously and described in detail in the [supplementary material](#). Its dielectric characterization is shown in the [Appendix](#) (Fig. 13). The low- $T_g$  component tripropyl phosphate (TPP; Sigma-Aldrich) was rectified by distillation and will be called “additive” in the following. Its characterization was done previously.<sup>36,37</sup> The *m*-TPTS- $\text{d}_4$  powder was inserted into a standard 5 mm NMR glass tube and flame sealed for the neat sample. For the mixtures, the corresponding amount of TPP was added in the NMR tube and the total mass was controlled before and after flame sealing. Then, all samples were annealed for several days at 120 °C to ensure complete mixing and weighed before inserting them into the NMR probe. Thereby, NMR samples of TPP in *m*-TPTS- $\text{d}_4$  with mass concentrations of  $w_{\text{TPP}} = 0.2, 0.4,$  and  $0.72 \pm 0.01$  were prepared. Additionally, one sample with  $w_{\text{TPP}} = 0.04$  was made with non-deuterated *m*-TPTS.

### B. Dielectric spectroscopy

The dielectric measurements were performed on an Alpha-A Analyzer (Novocontrol) in the frequency range  $\nu = 10^{-2}$ – $10^6$  Hz. Temperature was regulated within  $\pm 0.1$  K by using a Quatro-H temperature controller from Novocontrol with an absolute accuracy better than  $\pm 0.2$  K. The dielectric spectra of pure *m*-TPTS- $\text{d}_4$  were interpolated by a Generalized Cole–Davidson (GCD)<sup>38</sup> function as done in Part I for the  $\alpha_1$ -process. The GCD correlation function is analytically defined via

$$\phi_{\text{GCD}}(t) = \frac{\Gamma\left(\frac{b_{\text{GCD}}}{a_{\text{GCD}}}, \left(\frac{t}{\tau_{\text{GCD}}}\right)^a\right)}{\Gamma\left(\frac{b_{\text{GCD}}}{a_{\text{GCD}}}\right)} \quad (1)$$

and can be used in terms of its Fourier transform to describe the dielectric spectra. Here, “ $\Gamma$ ” denotes the gamma function. The parameter  $\tau_{\text{GCD}}$  describes the peak position,  $a_{\text{GCD}}$  gives a measure of the overall width of the relaxation peak, and  $b_{\text{GCD}}$  describes the high-frequency power law exponent (for details, cf. Ref. 38). The average time constant is given by

$$\langle \tau_{\alpha_1} \rangle = \langle \tau_{\text{GCD}} \rangle = \tau_{\text{GCD}} \cdot \Gamma\left(\frac{1 + b_{\text{GCD}}}{a_{\text{GCD}}}\right) / \Gamma\left(\frac{b_{\text{GCD}}}{a_{\text{GCD}}}\right). \quad (2)$$

The GCD includes the cases of a Kohlrausch ( $a_{\text{GCD}} = b_{\text{GCD}}$ ) and CD function ( $a_{\text{GCD}} = 1$ ).

### C. Nuclear magnetic resonance (NMR) spectroscopy

All NMR experiments were performed on a Bruker Avance III spectrometer with a 9.4 T Spectrospin cryomagnet. This results in a  $^{31}\text{P}$  Larmor frequency of  $\omega_L/2\pi = 161.98$  MHz and a  $^2\text{H}$  frequency of  $\omega_L/2\pi = 61.48$  MHz. The low temperature measurements (100–330 K) were performed with a home-built double resonance probe for the  $^{31}\text{P}$  and a home-built single resonance probe for the  $^2\text{H}$  NMR experiments in an Oxford CF1200 cryostat, which was cooled by liquid nitrogen and operated via an Oxford temperature controller (ITC-503/Mercury ITC). The temperature was measured via an additional Cernox temperature sensor. For higher temperatures up to 500 K, a standard Bruker high-temperature probe was used for both nuclei, which was controlled via an internal VTC unit and pressurized heated air. A temperature calibration was performed with  $\text{PbNO}_2$  according to Ref. 39. A temperature stability of at least  $\pm 0.5$  K was reached, with a maximal deviation from the true temperature of 2 K at high temperatures and 1 K at low temperatures.

### D. NMR spectra and relaxation

Solid-state spectra were recorded with a Hahn-echo pulse sequence ( $^{31}\text{P}$ ,  $90^\circ - t_p - 180^\circ$ ) or a solid-echo pulse sequence ( $^2\text{H}$ ,  $90^\circ - t_p - 90^\circ$ ), with an inter-pulse delay of  $t_p = 20 \mu\text{s}$ .  $^1\text{H}$ - $^{31}\text{P}$  dipolar decoupling was applied for all  $^{31}\text{P}$  NMR spectra during the acquisition of the FID. The  $90^\circ$  pulse length was about  $2.1 \mu\text{s}$  for  $^2\text{H}$  and  $2.7 \mu\text{s}$  for  $^{31}\text{P}$  experiments.

The interaction of the nuclear quadrupolar moment (Q) with the electric field gradient (EFG) governs the  $^2\text{H}$  NMR spectra. The shift of the NMR frequency  $\omega(\theta)$  with respect to the Larmor frequency  $\omega_L$  is given by<sup>40,41</sup>

$$\omega(\theta) = \pm \delta_Q/2 (3 \cos^2(\theta) - 1 - \eta \sin^2(\theta) \cos(2\varphi)) \quad (3)$$

and depends on the spherical angles ( $\theta, \varphi$ ) between the direction of the magnetic field  $B_0$  and the principal EFG tensor axis. The anisotropy of the quadrupolar tensor is specified by the parameter  $\delta_Q$ , the asymmetry by the parameter  $\eta$ . In the case of  $^{31}\text{P}$  NMR of TPP, the dominant interaction is the chemical shift anisotropy (CSA).<sup>40,41</sup> The dependence of the NMR frequency on the orientation is similar to that of  $^2\text{H}$  NMR [cf. Eq. (3)];  $\delta_Q$  has to be replaced by the chemical shift anisotropy (CSA) coupling  $\delta_{\text{CSA}}$  and only the positive sign is valid. For TPP, a symmetric CSA tensor  $\eta = 0$  is found. The CSA interaction leads to a characteristic asymmetric powder spectrum, and the quadrupolar interaction leads to a symmetric Pake spectrum if the molecular reorientation is slower than the NMR time scale ( $\tau_\alpha \gg \frac{1}{\delta}$ ) and isotropically distributed as it is the

case in glasses. For high temperatures well above  $T_g$ , fast isotropic reorientation characterized by the time constant  $\tau_{\alpha_i}$  leads to a collapse of the solid-state spectrum to a central Lorentzian line. In the limit of magnetic field inhomogeneities not spoiling the free induction decay (FID), the width  $\Delta\nu_{FWHM}$  (in Hz) of the Lorentzian line is linked to the spin–spin relaxation time  $T_2$ , which controls the FID via  $T_2 = \frac{1}{\pi\Delta\nu_{FWHM}}$ . In the case of  $^2\text{H}$  NMR, the rate  $R_2 = 1/T_2$  is calculated by<sup>40</sup>

$$\begin{aligned} \frac{1}{T_2} &= \frac{1}{15} \delta_Q^2 [3J(0) + 5J(\omega_L) + 2J(2\omega_L)] \\ &\cong \frac{1}{5} \delta_Q^2 J(0) \text{ (for } \omega_L \tau_{\alpha_1} \gg 1) \end{aligned} \quad (4)$$

and in the case of  $^{31}\text{P}$  NMR by<sup>40</sup>

$$\frac{1}{T_2} = \frac{1}{6} K^{CSA} [4J(0) + 3J(\omega_L)] \cong \frac{2}{3} K^{CSA} J(0) \text{ (for } \omega_L \tau_{\alpha_2} \gg 1), \quad (5)$$

with  $K^{CSA} = \frac{2}{15} \left(\frac{3}{2} \delta_{CSA}\right)^2$ , and the mean correlation time  $J(0) = \langle \tau_{\alpha_i} \rangle$ . A further estimate of time constants  $\tau_{\alpha_i}$  can be obtained from the spin–lattice relaxation rate  $R_1(T) = 1/T_1(T)$ . For  $^2\text{H}$  NMR, the condition  $\omega_L \langle \tau_{\alpha_1} \rangle \approx 0.616$  is valid at the temperature of the maximum rate  $R_1^{\max}$ , and at even higher temperatures,  $(\omega_L \tau_{\alpha_1} \ll 1)$ ,  $R_1$  is directly associated with  $\tau_{\alpha_1}$  according to  $R_1 = \frac{2}{3} \delta_Q^2 \langle \tau_{\alpha_1} \rangle$ . For  $^{31}\text{P}$  NMR, the maximum condition reads  $\omega_L \langle \tau_{\alpha_2} \rangle \approx 1$ , and the high temperature limit is given by  $R_1 = K^{CSA} \langle \tau_{\alpha_2} \rangle$ .

In the mixtures, the low- $T_g$  component TPP ( $\alpha_2$ ) undergoes isotropic reorientation, which is subject to a broad distribution of correlation times  $G(\ln \tau_{\alpha_2})$  yielding so-called “two-phase spectra.”<sup>42–44</sup> They can be described by a superposition of a Lorentzian line  $L(\omega)$  and a solid-state  $^{31}\text{P}$  powder spectrum  $P_{CSA}(\omega)$ ,

$$S(\omega, T) = W(T)L(\omega) + (1 - W(T))P_{CSA}(\omega), \quad (6)$$

with a weighting factor  $W = \int_0^{\tau_{cut}} G(\ln \tau) d \ln \tau$ , where  $\tau_{cut}$  is defined by the typical time scale of the experiment:  $\tau_{cut} \approx 1/\delta$ .<sup>44,45</sup> In the case of a broad distribution  $G(\ln \tau)$ , spectral contributions from sub-ensembles with correlation times on the order of the NMR time scale ( $\tau \approx 1/\delta$ ) can be neglected due to the small fraction of molecules in the intermediate exchange limit and due to the reduction in their signal intensity in the Hahn/solid echo applied for monitoring the spectra. In Part I, the  $\alpha_2$ -relaxation spectra were described by a Havriliak–Negami (HN)<sup>46,47</sup> function with a cutoff at the time constant of the  $\alpha_1$ -process. Explicitly, the corresponding pulse response function was multiplied by an exponential cut-off. This approach was applied to parameterize the HN distribution  $G(\ln \tau_{\alpha_2})$  such as to describe the particular behavior of  $W(T)$  and to analyze the  $^{31}\text{P}$  stimulated echo decays (see below). The parameters  $\tau_0$ ,  $a_{HN}$ , and  $c_{HN} = a_{HN} \cdot b_{HN}$  define the peak position and low- and high-frequency slopes, respectively, of the corresponding HN susceptibility  $\chi''_{HN}(\omega)$ .

### E. Reorientational correlation function probed by stimulated echo decay

The decay of the stimulated echo provides direct access to the reorientational correlation function  $C_2(t)$  of the second

Legendre polynomial  $P_2(\theta)$ . In the case of  $^{31}\text{P}$  NMR, a three-pulse echo sequence ( $90^\circ - t_{ev} - 90^\circ - t_m - 90^\circ$ ) with appropriate pulse phases is employed, and the echo amplitude is measured for different mixing times  $t_m$  for a constant evolution time  $t_{ev}$  to yield the sine–sine reorientational correlation function.<sup>44,48</sup> Regarding  $^2\text{H}$  NMR, a four-pulse sequence ( $90^\circ - t_{ev} - 45^\circ - t_m - 45^\circ - t_p - 90^\circ$ ) is applied.<sup>49</sup> The decay is described by

$$\begin{aligned} I(t_m, t_{ev}) &\propto \langle \sin(\omega(0)t_{ev}) \sin(\omega(t_m)t_{ev}) \rangle \cdot F_{\text{damp}}(t_m) \\ &\propto F_{t_{ev}}^{\text{sin}}(t_m) \cdot F_{\text{damp}}(t_m). \end{aligned} \quad (7)$$

The sin–sin correlation function  $F_{t_{ev}}^{\text{sin}}(t_m)$  can be rewritten as<sup>44,49</sup>

$$F_{t_{ev}}^{\text{sin}}(t_m) = (1 - F_\infty) \cdot F_{2,t_{ev}}(t_m) + F_\infty. \quad (8)$$

The value  $F_\infty$  depends on the motional mechanism and the evolution time  $t_{ev}$ . In the case of isotropic motion, short  $t_{ev}$  and  $^2\text{H}$  NMR,  $F_\infty$  is typically on the order of a few percent and  $F_{2,t_{ev}}$  becomes close to  $C_2(t_m)$ . For  $^{31}\text{P}$  NMR,  $F_\infty$  is under these conditions even smaller and neglectable. An evolution time  $t_{ev} = 10 \mu\text{s}$  was applied for both  $^{31}\text{P}$  and  $^2\text{H}$  NMR, whereby the short-time limit is fulfilled.<sup>48,50</sup> The damping function  $F_{\text{damp}}(t_m)$  differs for the two nuclei. In the case of  $^2\text{H}$  NMR, it is given by the quadrupolar relaxation time  $T_{1Q}$ , which can be determined at highest temperatures as decay of  $F_\infty$ . The temperature dependence of  $T_{1Q}(T)$  roughly matches that of the spin–lattice relaxation time  $T_1$ , and a constant proportionality was assumed:  $T_{1Q}(T) \propto T_1(T)$ . For the  $^{31}\text{P}$  NMR experiments, the damping is directly given by the spin–lattice relaxation time  $T_1(T)$ . However, additionally, for longest times, spin diffusion effects come into play, which are exemplarily shown in the Appendix for one sample (Fig. 14). As introduced before, in the case of  $^2\text{H}$  NMR probing the high- $T_g$  component, the stimulated echo decay is interpolated by  $\phi_{GCD}(t)$  [cf. Eq. (1)], whereas that of the additive dynamics is interpolated by the FT of a HN function. For low additive concentrations, we have to introduce an additional temperature dependent residual plateau value  $f_{\alpha_1}(T)$  ( $C_2 = \phi_{HN} + f_{\alpha_1}$ ) to quantify the fraction of additive molecules not relaxing on the observable time scale, presumably the  $\alpha_1$ -relaxation.

## III. RESULTS OF THE TPP/ $m$ -TPTS MIXTURES

### A. $^2\text{H}$ NMR spectra of the high- $T_g$ component

We start with presenting the  $^2\text{H}$  NMR spectra of  $m$ -TPTS- $d_4$  in the three mixtures together with those of the pure compound in Fig. 3. All spectra show basically the same kind of transition as observed for pure  $m$ -TPTS- $d_4$ : Within a small temperature range above  $T_g$ , the solid-state powder (Pake) spectrum collapses to give way to a Lorentzian with a width quickly decreasing upon further heating, features well known from investigations of pure glass formers.<sup>44</sup> In between, there is some gap where spectra cannot be recorded since  $T_2$  is too short. The only difference in the mixtures is the temperature at which this transition sets in. The more TPP is added, the more the transition shifts to lower temperatures. This is nothing else than the well-known plasticizer effect.<sup>51</sup> Qualitatively, the nature of the dynamics remains essentially unchanged in the

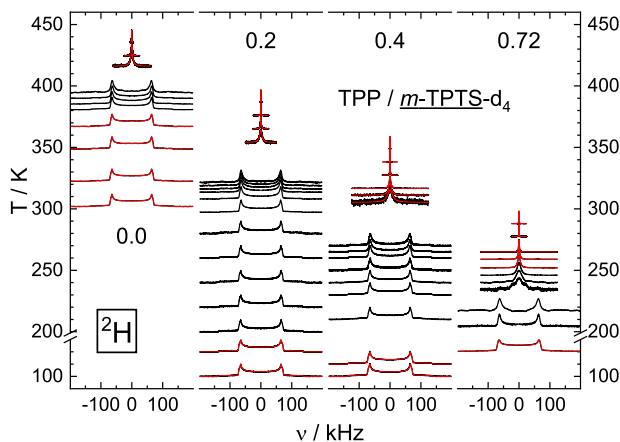


**FIG. 3.**  $^2\text{H}$  NMR spectra (black lines) of neat  $m\text{-TPTS-d}_4$  ( $w_{\text{TPP}} = 0.0$ ) and of the mixture TPP/ $m\text{-TPTS-d}_4$  for the concentrations  $w_{\text{TPP}}$  (mass percentage) as indicated. Baseline of the spectrum gives the measurement temperature. Red lines: fits by a Lorentzian line at high temperatures and a Pake spectrum at low temperatures.

mixtures. The quadrupolar interaction parameters  $\delta_Q/2\pi = (137 \pm 2)$  kHz and  $\eta = 0.04 \pm 0.01$  are determined for lowest temperatures for each sample and shown together with  $\delta_{\text{CSA}}$  of the  $^{31}\text{P}$  spectra in Fig. 5(b). Only a slight temperature dependent reduction of one percent of  $\delta_Q$  per 100 K is found. From the width of the Lorentzian line, correlation times  $\langle \tau_{\alpha_1}(T) \rangle$  are extracted along Eq. (4) and included in Fig. 8(b). These data complement the time constants obtained by the stimulated echo decays (see below) to higher temperatures.

### B. $^{31}\text{P}$ NMR spectra of the low- $T_g$ component

The corresponding spectra of the additive are given in Fig. 4. The spectra of pure TPP exhibit a smooth transition from an asymmetric powder spectrum at low temperatures ( $T \leq 150$  K), now determined by the CSA interaction, to a Lorentzian at high temperature ( $T \geq 165$  K). Here, no gap as in the case of  $^2\text{H}$  NMR (cf. Fig. 3) is observed due to the much smaller  $\delta_{\text{CSA}}$  compared to  $\delta_Q$ . However, the transition in the mixtures is qualitatively different. At lowest temperatures, powder spectra are found again, and at highest temperatures, Lorentzian lines are observed. At intermediate temperatures, however, the so-called “two-phase” spectra are observed over a wide temperature range. They comprise a superposition of a solid-state spectrum and a central Lorentzian line with its weight increasing continuously with temperature. Such spectra are indicative of a broad distribution of correlation times  $G(\ln \tau_{\alpha_2})$ .<sup>45</sup> The simultaneous presence of fast (on the NMR time scale) isotropic dynamics (Lorentzian line) and slow dynamics (powder spectrum) clearly demonstrates this. Thus, in contrast to the dynamics of the high- $T_g$  component, pronounced motional heterogeneities govern the dynamics of the additive. Regarding the three mixtures ( $w_{\text{TPP}} = 0.2, 0.4,$  and  $0.72$ ), the temperature interval for which such two-phase spectra are recorded broadens with the decreasing additive concentration (blue dashed lines in Fig. 4) and shifts to higher temperatures reflecting the “anti-plasticizer” effect. In order to test the situation in the limit of very low additive concentrations, we included in Fig. 4 a

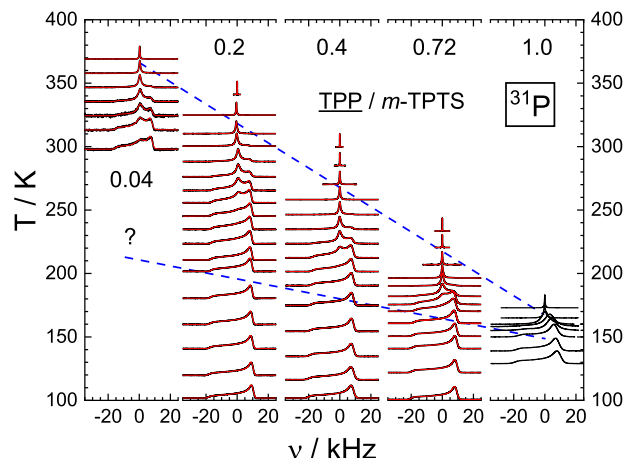


**FIG. 4.**  $^{31}\text{P}$  NMR spectra (black lines) of neat TPP ( $w_{\text{TPP}} = 1.0$ ) and of the mixture TPP/ $m\text{-TPTS-d}_4$  for additive concentrations  $w_{\text{TPP}}$  as indicated. The baseline of the spectra gives the measurement temperature. Red lines: fits by a Lorentzian line at high temperatures and a solid-state powder spectrum at low temperatures. Weighted superposition (two-phase spectra) at intermediate temperatures; temperature range marked by the blue dashed lines. Spectra of neat TPP from Ref. 36.

few spectra measured for a mixture with  $w_{\text{TPP}} = 0.04$ . Clearly, strong dynamic heterogeneities are even observed in this limit.

We note that although the additive molecules show a clear-cut CSA powder spectrum, the molecules are actually not rigid at least at not too low temperature. They perform slow isotropic reorientation as was proven several times by measuring 2D exchange spectra of similar mixtures.<sup>29,52,53</sup> Moreover, 2D NMR demonstrates that the motional heterogeneities are actually dynamic in the sense that slow and fast molecules mutually exchange their time constants basically on the same time scale as the slow reorientation proceeds.<sup>29,52,53</sup>

As said, the spectra in the mixture can be interpolated by a superposition of both a CSA powder spectrum and a Lorentzian line [cf. Eq. (6)]. For the mixture  $w_{\text{TPP}} = 0.4$ , the two-phase spectra and the corresponding fits are shown in Fig. 5(a). The fits yield the corresponding weighting factors  $W(T)$  reflecting the fraction of liquid-like molecules (cf. Fig. 6, red symbols/lines). We note a subtle observation when analyzing the  $^{31}\text{P}$  NMR solid state spectra over a wide temperature range. In contrast to the quadrupolar anisotropy parameter  $\delta_Q$ , that of the CSA interaction ( $\delta_{\text{CSA}}$ ) displays a considerable temperature dependence [see Fig. 5(b)]. Starting at low temperatures with a common linear temperature dependence of 2 kHz per 100 K for all concentrations, the decrease accelerates when the two-phase spectra show up.

The strongly decoupled dynamics of the low- and high- $T_g$  component is directly seen in Fig. 5(c) for  $w_{\text{TPP}} = 0.4$ . At about 250 K, almost all TPP molecules perform a liquid-like motion (Lorentzian line), whereas the  $m\text{-TPTS-d}_4$  molecules display a powder spectrum indicating slow or even arrested dynamics. This is also evidenced in Fig. 6: Regarding the  $w_{\text{TPP}} = 0.20$  sample, the weighting factor of TPP reaches 0.8 at about 300 K, i.e., 80% of the molecules reorient fast, whereas the  $m\text{-TPTS-d}_4$  spectrum is still a solid-state spectrum. Clearly, two isotropic processes  $\alpha_1$  and  $\alpha_2$  are involved, and their dynamics is expected to differ more and more with decreasing  $w_{\text{TPP}}$ . Yet, while the distribution  $G(\ln \tau_{\alpha_1})$  is rather narrow and

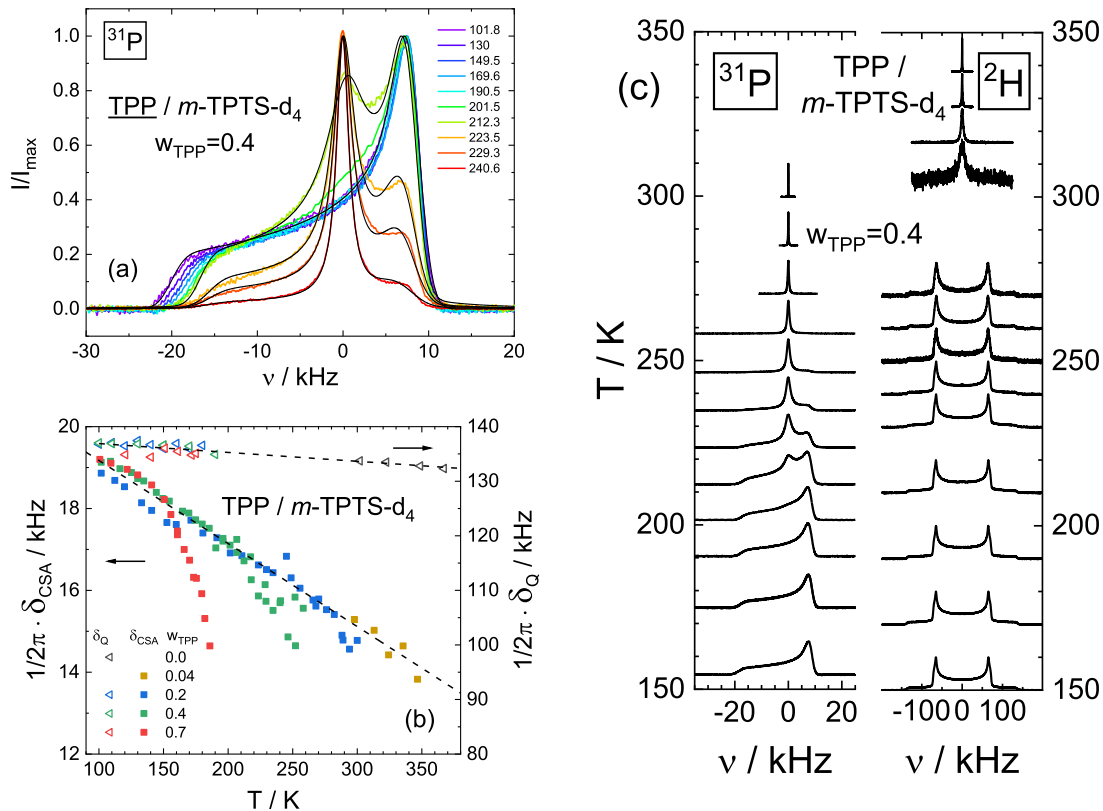


**FIG. 5.** (a)  $^{31}\text{P}$  NMR spectra of the mixture  $w_{\text{TPP}} = 0.4$  with fits (black lines) for temperatures with two-phase spectra and the lowest temperatures. Temperature is color-coded. (b)  $^{31}\text{P}$  NMR coupling constant  $\frac{\delta_{\text{CSA}}}{2\pi}(w_{\text{TPP}}, T)$  and  $\frac{\delta_Q}{2\pi}(w_{\text{TPP}}, T)$  from  $^2\text{H}$  spectra as a function of temperature. (c) Spectra of the  $w_{\text{TPP}} = 0.4$  sample for TPP (left side) and  $m$ -TPTS- $d_4$  (right side).

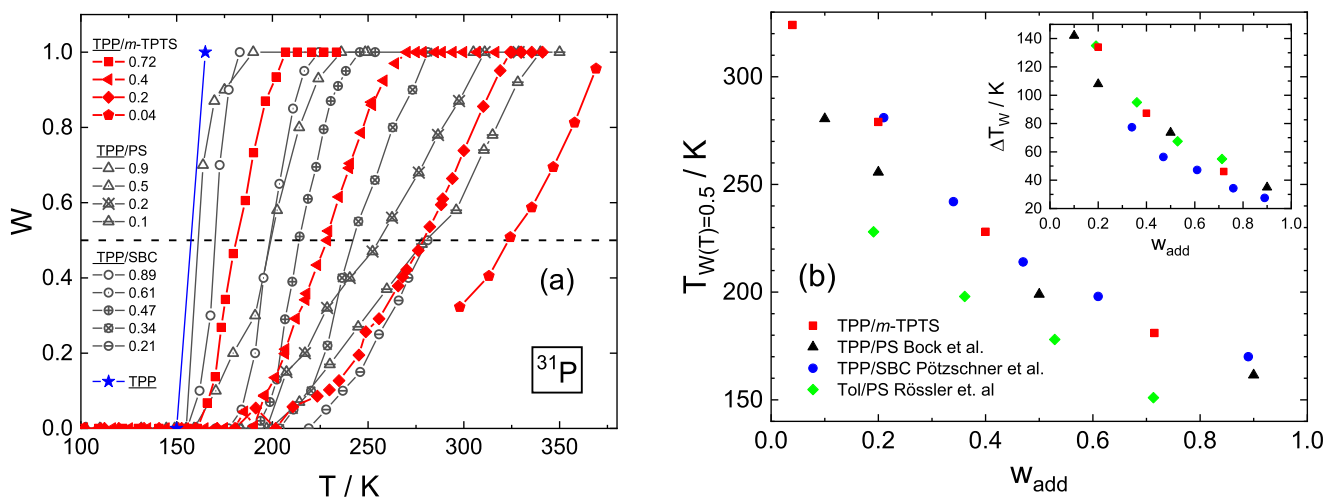


**FIG. 6.** (a) Weighting factor  $W(T)$  for the mixtures TPP/ $m$ -TPTS- $d_4$  (red symbols,  $\Delta T_g = 222$  K), TPP/polystyrene (gray triangles,  $\Delta T_g = 200$  K),<sup>29</sup> and TPP/SBC (gray circles,  $\Delta T_g = 222$  K).<sup>30</sup> The additive concentration  $w_{\text{TPP}}$  is given by the filling of the corresponding symbol. Pure TPP (blue stars) is given as reference for a transition without two-phase spectra. (b) Temperature of  $W(T) = 0.5$  as a function of the additive concentration  $w_{\text{add}}$  for the three systems and for toluene/polystyrene ( $\Delta T_g = 256$  K).<sup>45</sup> Note that components have slightly different  $T_g$ 's. Inset: width of the two-phase temperature region  $\Delta T_W$  for the different systems and concentrations.

still qualitatively similar to that in neat glass formers,<sup>44</sup> the distribution  $G(\ln \tau_{\alpha_2})$  is becoming very broad at low TPP concentrations, indicative of pronounced dynamic heterogeneities.

Here, a note is worthwhile. It is well established that applying solid-echo techniques, a significant loss of signal may occur for the intermediate spectra:  $\tau \sim 1/\delta$ .<sup>54–57</sup> In the present context analyzing <sup>31</sup>P spectra, this could lead to a partial loss of contributions from the distribution  $G(\ln \tau_{\alpha_2})$ . Already the mere fact of observing clear-cut two-phase spectra, however, demonstrates the presence of a very broad distribution that reduces these signal losses.<sup>55</sup> The effect is further reduced by choosing a rather short pulse delay  $t_p$  as was done here. More precisely,  $\delta^* t_p$  as a measure of potential losses has to be made as small as possible. Due to  $\delta_{CSA}$  being by a factor of six smaller compared to  $\delta_Q$ , signal reduction is no issue in the present <sup>31</sup>P NMR spectra. The situation is quite different for the <sup>2</sup>H spectra of the high- $T_g$  component (see Fig. 3). Here, the motional process relevant of collapsing the solid-state spectrum is narrowly distributed such that the NMR signal is completely lost for a certain temperature range. We were not able to find indications of a two-phase character in the <sup>2</sup>H spectra of the high- $T_g$  component *m*-TPTS-d<sub>4</sub>.

Several dynamically asymmetric glass formers were studied so far by our group, polymeric as well as non-polymeric with similar high  $T_g$ -contrast, and the results for  $W(T)$  are included in Fig. 6(a).<sup>29,30,45</sup> Very similar traces are recognized. In order to compare the different systems, we plot in Fig. 6(b) the temperature at which  $W(T) = 0.50$ . A quite similar behavior is revealed: The temperature  $T_{W=0.5}$  decreases more or less linearly with the increasing additive concentration (plasticizer effect), whereas the interval for which two-phase spectra are observed [ $\Delta T_W$ , inset of Fig. 6(b)] grows almost linearly with the decreasing additive concentration. This trend holds even down to a concentration of  $w_{TPP} = 0.1$ .

Regarding Fig. 6(b), one has to keep in mind that the absolute  $T_g$  values of the components are somewhat different.

Given the quite universal manifestation of two-phase spectra as characteristics of additive dynamics, we undertake a first attempt to understand the dielectric  $\alpha_2$ -relaxation of the present mixture TPP/*m*-TPTS in terms of the NMR spectra. As discussed, it is not clear whether  $\Delta\epsilon_i/\Delta\epsilon$  from DS indeed reflects the fraction of two populations of molecules associated with the dynamics of the high- $T_g$  and the low- $T_g$  component, respectively. Explicitly, we ask whether one can interpolate  $W(T)$  by integrating  $G(\ln \tau_{\alpha_2})$ , determining the dielectric susceptibility of  $\alpha_2$ -relaxation as it evolves with temperature. Therefore, we use the temperature dependent parameters of our DS analysis (Part I: Figs. 6, 8, and 12) and calculate the distribution corresponding to the truncated HN function. Explicitly, to account for the introduced cutoff at the time constant of the dielectric  $\alpha_1$ -process ( $\tau_c = \langle \tau_{\alpha_1}^{DS} \rangle$ ),  $G(\ln \tau_{\alpha_2})$  is cut-off at this time constant, too [cf. Fig. 7(b)]. One recognizes directly the strong broadening of  $G(\ln \tau_{\alpha_2})$  with decreasing temperature (solid lines). The weighting factor  $W(T)$  of the <sup>31</sup>P spectra is then calculated along Eq. (6). The resulting curve  $W(T)$  is shown in Fig. 7(a) for the different concentrations  $w_{TPP}$  as dotted lines in the corresponding color and compared to the experimental result (symbols).

Satisfactory agreement is found for the high concentrations  $w_{TPP} = 0.72$  and 0.4; for  $w_{TPP} = 0.72$ , a slight temperature shift is recognizable, which can be explained by slightly different concentrations (DS:  $w_{TPP} = 0.70$ ). The high temperature behavior of  $W(T)$  ( $250 \text{ K} < T < 280 \text{ K}$ ) for  $w_{TPP} = 0.4$  shows a different trend compared to the measured  $W(T)$ , which can be overcome by taking a shorter cutoff time  $\tau_c = \tau_{\alpha_1}^{DS}/30$  (dashed green line) instead of  $\tau_c = \langle \tau_{\alpha_1}^{DS} \rangle$ . This demonstrates that although the overall effects of the cutoff in the distribution function (area) are rather small, it determines

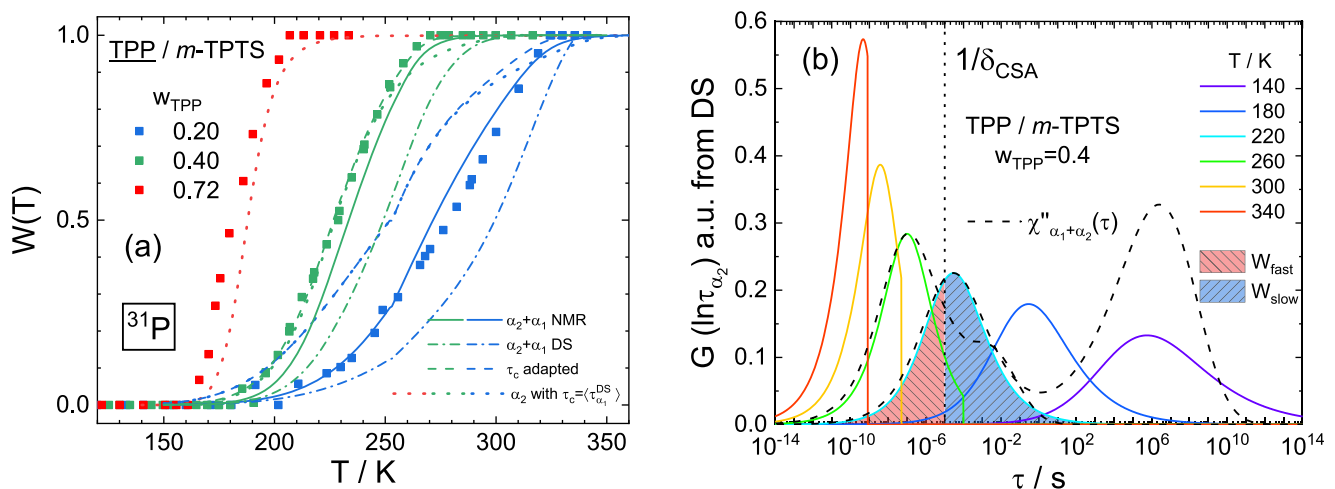


**FIG. 7.** (a) Weighting factor  $W(T)$  representing the Lorentzian part of the <sup>31</sup>P spectra for the different concentrations (squares). Dotted lines:  $W(T)$  calculated according to  $G(\ln \tau_{\alpha_2})$  with a cutoff at the average DS time constant  $\tau_c = \langle \tau_{\alpha_1}^{DS} \rangle$  from Ref. 31. Dashed lines:  $G(\ln \tau_{\alpha_2})$  with shorter  $\tau_c$  (cf. text). Dashed-dotted lines: DS  $\alpha_2$ - and  $\alpha_1$ -relaxation. Solid lines: reduced fraction of the  $\alpha_1$ -relaxation based on the NMR analysis. (b) Distribution of correlation times  $G(\ln \tau_{\alpha_2})$  from DS for the mixture  $w_{TPP} = 0.4$  with a cutoff  $\tau_c = \tau_{\alpha_1}^{DS}/30$  for different temperatures (solid colored lines). Dashed black lines: susceptibilities  $\chi''_{\alpha_1 + \alpha_2}$  considering the DS  $\alpha_2$ - and  $\alpha_1$ -relaxation for 220 K and 260 K. Fast on the NMR time scale ( $1/\delta_{CSA}$ ): red striped area ( $W_{fast}$ ). Slow: blue striped area ( $W_{slow}$ ).

strongly the high temperature behavior of  $W(T)$ . The temperature dependence of the distribution function  $G(\ln \tau_{\alpha_2})$  is shown for this concentration and the shorter cutoff as colored lines in Fig. 7(b). For the lowest evaluable concentration  $w_{TPP} = 0.2$ , the calculated behavior with reduced cutoff  $\tau_c = \tau_{\alpha_1}^{DS}/5$  (dashed blue line) differs strongly from the experimental found one. The minor kink in the temperature dependence results from the strong-to-fragile transition of the corresponding time constants (cf. Part I). Thereby, considering only  $G(\ln \tau_{\alpha_2})$  exaggerates the liquid-like portion of the TPP dynamics over the whole temperature range.

Two explanations can be discussed explaining the discrepancy. (i) The dielectric  $\alpha_1$ -relaxation reflects cross-relaxation contributions<sup>35,58</sup> and (ii) part of the additive molecules take part in the dynamics of the high- $T_g$  component.<sup>11,29</sup> The first idea would correspond to the presented scenario in Fig. 7 (dotted lines), that  $W(T)$  can be explained by the  $\alpha_2$ -relaxation alone, because the NMR

experiments probe solely incoherent dynamics. To account for the second possibility, the dielectric  $\alpha_1$ -relaxation will be additionally considered next. Therefore, we would have to use in addition to  $G(\ln \tau_{\alpha_2})$  the distribution function of the  $\alpha_1$ -relaxation  $G(\ln \tau_{\alpha_1})$ , which is described by the GCD function in the dielectric spectra. Yet, the GCD function has no analytically accessible distribution function. Therefore, we use the total susceptibility function  $\chi''_{\alpha_1+\alpha_2}(T)$  instead, which is a good approximation for such broad distributions. This ansatz is shown for two temperatures as black dashed lines in Fig. 7(b). The relative relaxation contributions  $\Delta\varepsilon_1/(\Delta\varepsilon_1 + \Delta\varepsilon_2)$  can be taken from Fig. 11(b) (lines). This yields the dashed-dotted lines in Fig. 7(a). This approach reveals a  $W(T)$  curve significantly shifted to higher temperatures, as expected, but overestimates the contribution of the  $\alpha_1$ -process for the two investigated samples  $w_{TPP} = 0.2$  and  $0.4$ . Thus, both interpretations of the dielectric spectra fail to reproduce the actual  $W(w_{TPP}, T)$  measured by NMR.

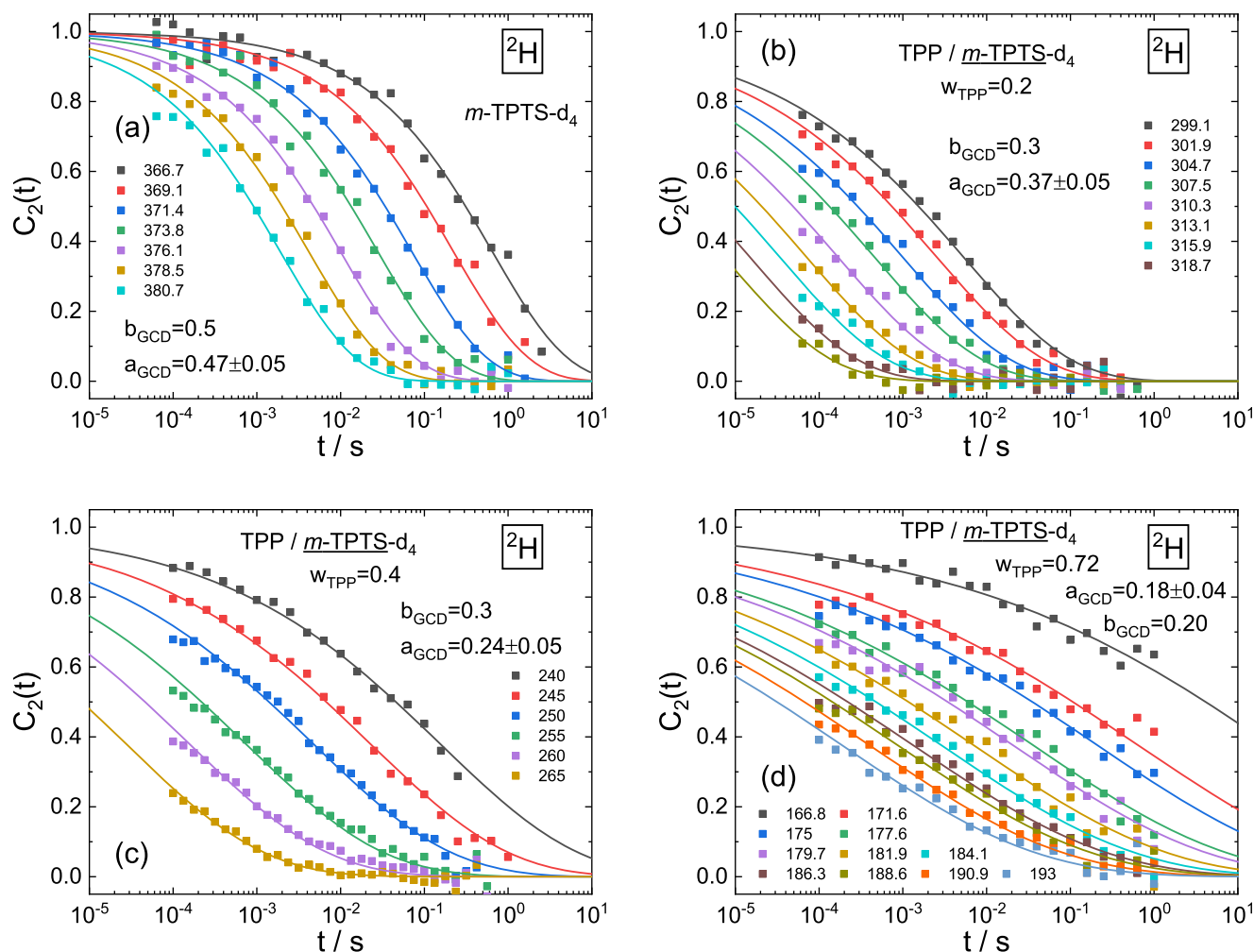


**FIG. 8.**  $^2\text{H}$  NMR correlation function  $C_2(t)$  (squares) of the pure high- $T_g$  component  $m\text{-TPTS-d}_4$  (a) and its mixtures with TPP [ $w_{TPP} = 0.2$  (b),  $0.4$  (c), and  $0.72$  (d)]. The measured decays are corrected for the  $T_{1\rho}$ -decay and for  $F_\infty \approx 0.05$  [cf. Eqs. (7) and (8)]. Temperature in K is color-coded. Lines: GCD fits according to Eq. (1); width parameters indicated.

We shall return to this point after considering the results from the stimulated echo experiments.

### C. Reorientational correlation function of the high- $T_g$ component

Stimulated echo decays were measured by  $^2\text{H}$  and  $^{31}\text{P}$  NMR to probe the dynamics of both components (see Sec. II). Figure 8 displays the decay curves of the high- $T_g$  component for the three mixtures together with that of neat  $m$ -TPTS- $d_4$ . Pure  $m$ -TPTS- $d_4$  [Fig. 8(a)] exhibits a behavior typical of pure glass formers. The GCD interpolation, which was used to describe the dielectric  $\alpha_1$ -spectrum in Part I, yields a Kohlrausch type decay with  $\beta_K = 0.50$  as its special case ( $\beta_K = b_{GCD} \cong a_{GCD}$ ). The corresponding time constants  $\tau_{\alpha_1}(T)$  are included in Fig. 9(b), where they are compared to those of the mixtures (see below). In the mixtures, the decay remains essentially of Kohlrausch character, yet the stretching parameter decreases with the increasing TPP concentration; explicitly,  $b_{GCD}$  decreases from 0.50 to 0.20 temperature-independent for each mixture. Speaking in the notion of an underlying distribution  $G(\ln \tau_{\alpha_1})$ , a strong broadening is observed upon adding the low- $T_g$  component. Remarkably, however, this broadening does not show up in two-phase  $^2\text{H}$  NMR spectra (cf. Fig. 3) being characteristic of pronounced heterogeneities—in contrast to the case of TPP (see Fig. 4).

Quantitatively, the parameters of the fits of the echo decays are compared to those of the dielectric  $\alpha_1$ -relaxation<sup>31</sup> in Fig. 9(a). Therefore, the fits are numerically Fourier transformed into the susceptibility representation, and the FWHM of the peak is determined. Fair agreement between the parameters determined by DS (open circles) and NMR (squares) is given.

Looking at the corresponding time constants of the echo decays, which are presented in Fig. 9(b) in comparison to the peak time constants determined by DS (Part I), shows agreement, too.

Thereby, one has to discriminate between average time constants  $\langle \tau_{\alpha} \rangle$  (open triangles), defined as the integral over the correlation function and the most probable time constant of the peak  $\tau_{peak}$  (crosses), determined from the (dielectric) susceptibility representation ( $\tau_{peak} = 1/(2\pi\nu_{peak})$ ). As long as the peaks are rather narrow and symmetric ( $w_{TPP} \leq 0.2$ ), only negligible differences exist. These differences increase for higher concentrations  $w_{TPP}$  up to almost two decades. Interestingly,  $\langle \tau_{\alpha}^{NMR} \rangle$  coincides for all concentrations almost perfectly with  $\tau_{peak}^{DS}$ . Nevertheless, also  $\tau_{peak}^{NMR}(T)$  is several decades more separated from the corresponding correlation times determined for the  $\alpha_2$ -process (cf. Fig. 11 and Part I), clearly showing the two separated main relaxation processes in the mixtures. The time constants from the stimulated echo experiments are expanded to higher temperatures by those determined from the spin-lattice relaxation rate  $R_1$  and spin-spin relaxation rate  $R_2$  (see Sec. II and the supplementary material). The glass transition temperatures of the high- $T_g$  component in the mixtures [ $T_{g1} = T(\tau_{\alpha_1}^{NMR} = 100 \text{ s})$ ], determined for the NMR analysis, confirm the  $T_{g1}$ 's from DS and DSC [see Fig. 2(b)]. In conclusion, considering the rather limited time-resolution of about five decades, time constants and spectral width of the dielectric  $\alpha_1$ -relaxation correspond well to the time domain response provided by  $^2\text{H}$  NMR of  $m$ -TPTS- $d_4$ .

### D. Reorientational correlation function of the low- $T_g$ component

The dynamics of the low- $T_g$  component TPP is probed by  $^{31}\text{P}$  NMR stimulated echo decays; it shows a more complex behavior (cf. Fig. 10). The shown data is corrected for the  $T_1(T)$ -decay (measured independently) as well as with a temperature independent spin diffusion, different for each concentration (see Sec. II and the Appendix). The total amplitude was chosen in the way that the

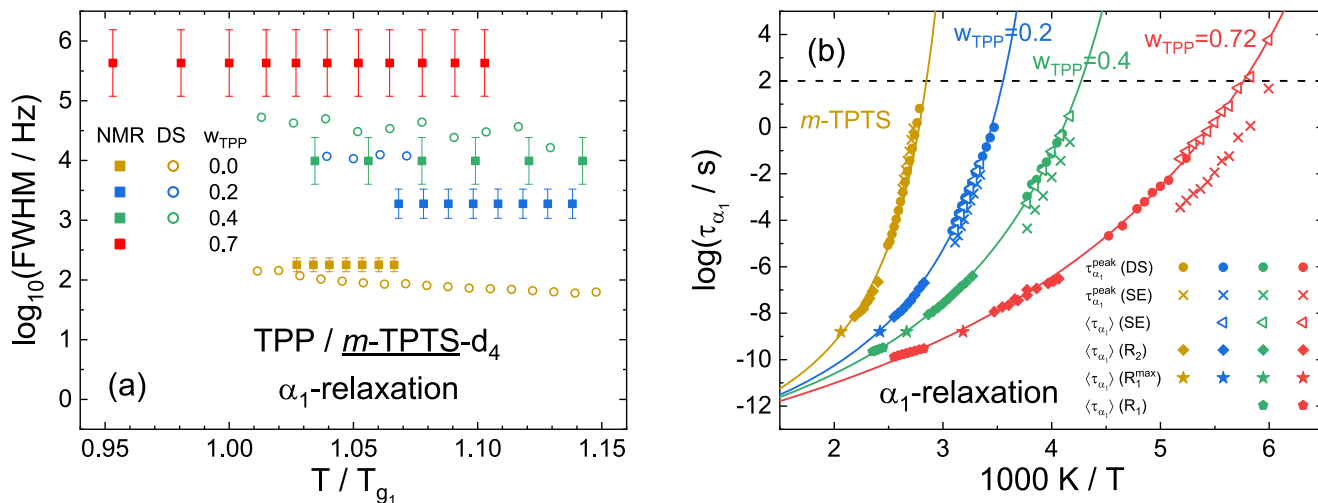


**FIG. 9.** (a) Comparison of the FWHM in decades of the  $\alpha_1$ -relaxation spectrum as a function of reduced temperature  $T/T_{g1}$  (squares:  $^2\text{H}$  stimulated echo; open circles: DS<sup>31</sup>). No DS shape analysis was possible for  $w_{TPP} = 0.7$ .<sup>31</sup> (b) Time constants of the  $\alpha_1$ -relaxation for neat  $m$ -TPTS- $d_4$  and the mixtures from various techniques. Relaxation peak time constants  $\tau_{\alpha_1}^{peak}$  from DS (circles)<sup>31</sup> and  $^2\text{H}$  stimulated echo measurements (crosses). Average time constants  $\langle \tau_{\alpha_1} \rangle$  from  $^2\text{H}$  stimulated echo (SE, open triangles), spin-spin relaxation rates ( $R_2$ , diamonds), spin-lattice relaxation rate maxima ( $R_1^{max}$ , stars), and spin-lattice relaxation rates in the fast motion limit ( $R_1$ , pentagons).

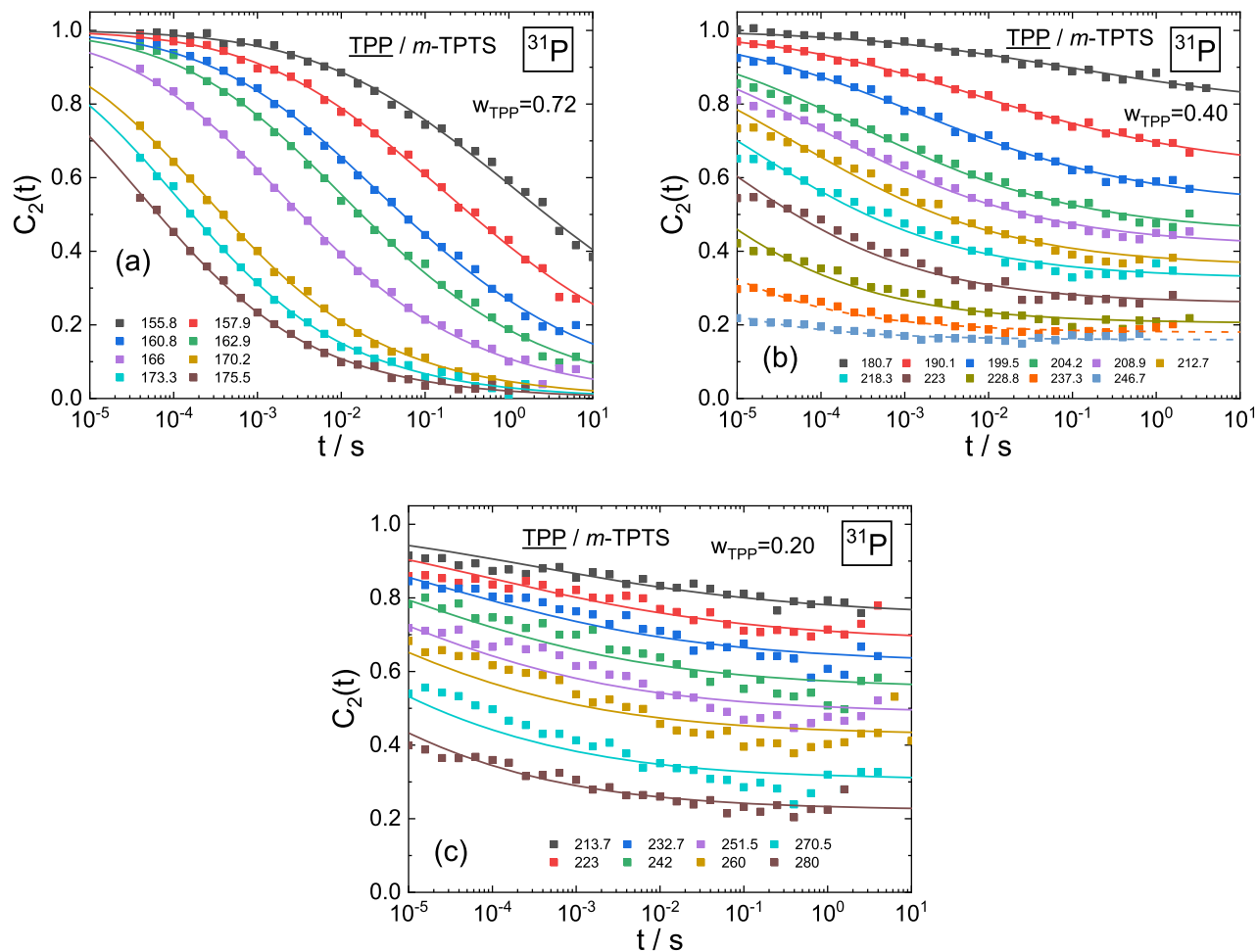


**FIG. 10.**  $^{31}\text{P}$  NMR correlation function  $C_2(t)$  (squares) of the low- $T_1$  component in the mixtures  $w_{\text{TPP}} = 0.72$  (a), 0.4 (b), and 0.2 (c). The measured decays are  $T_1$  and spin diffusion corrected [cf. Eqs. (7) and (8) and Appendix]. Temperature in K is color-coded. Lines: (a) HN fits; (b), and (c) HN fits with a residual plateau value ( $\phi_{\text{HN}} + f_{\alpha_1}$ ). For a detailed explanation, see text. Dashed lines in (b): guide for the eye.

stimulated echo decays at  $10\ \mu\text{s}$  match the weighting factor determined from the 1D spectra ( $C_2(10\ \mu\text{s}) \approx 1 - W(T)$ ). The weighting factor  $W(T)$  measures the fraction of TPP molecules which reorients faster than  $1/\delta_{\text{CSA}} \approx 10\ \mu\text{s}$  and thus has already relaxed before the stimulated echo measurement starts. One recognizes a strong stretching of the decays compared to that of pure TPP ( $\beta_K = 0.58$ ),<sup>36</sup> which becomes even broader with decreasing  $w_{\text{TPP}}$ . In the case of  $w_{\text{TPP}} = 0.20$ , a more or less logarithmic decay is found, which at highest temperatures shows a trend to yield a time-independent plateau  $f_{\alpha_1}$ , i.e., the correlation loss halts at long times. This suggests, that some TPP molecules do not relax on the time scale of most other TPP molecules. We emphasize that the precise estimate of this fraction of non-relaxing molecules depends on the procedure to correct the stimulated echo decays due to spin diffusion, which may lead to some overestimation of this fraction (see the Appendix). Of course, interpreting the plateau value as originating from a sub-population of TPP molecules only relaxing along the slow  $\alpha_1$ -process assumes

that the reorientation remains isotropic also at lower temperatures, i.e., it does not become anisotropic. As said before, numerous 2D exchange experiments identified isotropic reorientation at low temperatures; however, due to the very long correlation decays, one cannot demonstrate this for all molecules.<sup>29,52,53</sup> Still, we think it is fair to assume isotropic reorientation.

The dielectric  $\alpha_2$ -relaxation, which should probe the TPP dynamics in DS, is characterized by an extreme broadening on the low-frequency side in contrast to the high-frequency broadening of the  $\alpha_1$ -relaxation [cf. Fig. 2(a)]. In order to compare DS and NMR, the numerical Fourier transform of a HN function is used to describe the correlation loss in Eq. (8) for the  $^{31}\text{P}$  stimulated echo decays. The truncation of the HN function applied in Part I can be neglected in the time domain representation since the truncation comes into play only at high temperatures and longest (not probed) times. Starting with the highest concentration  $w_{\text{TPP}} = 0.72$ , the decays can be perfectly described with a vanishing  $f_{\alpha_1}$  [cf. Fig. 10(a)]. The parameter

$c_{HN} = 0.65$ , defining the high-frequency power law, is kept constant like in the DS analysis, the corresponding  $a_{HN}(T)$  (open red circles) is compared to the DS parameters (red diamonds) in Fig. 14(b), and the obtained peak time constants (red triangles) are included in Fig. 11(a). Almost perfect agreement is found considering the slight concentration difference (DS:  $w_{TPP} = 0.70$ ), showing that both techniques probe the same dynamics.

The analysis for the lower concentrations becomes more challenging, since the time window is rather small compared to the overall stretching and the correlation function seems to decay only partly in the accessible range. Therefore, we assumed for  $w_{TPP} = 0.4$  that the parameter  $a_{HN}(T)$  and  $c_{HN}$  follow the same temperature dependence as revealed by DS [see Fig. 14(b), Appendix, green dashed line] and account for the non-relaxing plateau  $f_{\alpha_1}$ . Consequently, only the parameter  $\tau_{peak}$  and  $f_{\alpha_1}$  were fitted, producing good results for the decay curves [cf. lines in Fig. 10(b)] as well as the time constants [green open triangles in Fig. 11(a)]. Thereby, a certain temperature dependence is found for  $f_{\alpha_1}(T)$ , demonstrated in Fig. 11(b) as green squares. As shown for the higher additive concentrations  $w_{TPP} \geq 0.4$ , agreement is found for the time constants as well as shape parameters. Therefore, these parameters are adopted completely from the DS analysis for the lowest concentration  $w_{TPP} = 0.2$  to achieve at least some information about  $f_{\alpha_1}(T)$  from these extremely broad decays [blue squares in Fig. 11(b)]. Furthermore, average time constants  $\langle \tau_{\alpha_2} \rangle$  for higher temperatures are included in Fig. 11(a) from  $R_1$  and  $R_2$  measurements (see Sec. II and the supplementary material), indicating a fragile-to-strong transition. The differences of the time constants referring to a given concentration result due to different experiments;  $\langle \tau_{\alpha_2} \rangle$  as integral over the correlation function is not accessible for low temperatures.

The parameter  $f_{\alpha_1}(T)$  is a measure of the portion of TPP molecules keeping up correlation until longest times, presumably up to the  $\alpha_1$ -relaxation time scale. In Fig. 11(b),  $f_{\alpha_1}(T)$  (squares) is

compared to  $\Delta\epsilon_1/\Delta\epsilon(T)$  (open circles), which provides similar information from the DS analysis. At all concentrations,  $f_{\alpha_1}(T)$  is significantly lower than  $\Delta\epsilon_1/\Delta\epsilon(T)$ , indicating that the dielectric relaxation strength is inflated, speaking in the notion of molecular populations. Furthermore,  $f_{\alpha_1}(T)$  starts to grow at lower temperatures (around  $T_{g1}$ ) compared to DS.

With the information about  $f_{\alpha_1}(w_{TPP}, T)$ , we can now attempt to resolve the discrepancies shown in Fig. 7(a) for the weighting factor  $W(T)$ . Using the shown logistic interpolations [dashed lines,  $f_l = a/(1 + \exp(-b/(x - x_0)))$ ] for  $f_{\alpha_1}(T)$ , the solid lines in Fig. 7(a) are obtained for the  $w_{TPP} = 0.2$  and 0.4 samples. Thereby,  $W(T)$  was calculated from the DS susceptibility  $\chi''_{\alpha_1+\alpha_2}$  but with the  $\alpha_1$ -relaxation strength contribution given by  $f_{\alpha_1}(T)$ . Considering the large number of parameters for the determination of  $W(T)$  (interpolations of time constants, shape parameters, relaxation strengths from stimulated echo, etc. We find good agreement, especially for the  $w_{TPP} = 0.2$  mixture where both previous DS estimations failed to describe the measured  $W(T)$  at all. This consistent description of  $W(T)$  and the stimulated echo decays make us confident that indeed a fraction of TPP molecules follows the dynamics of the high- $T_g$  component.

To give a final comparison between the relaxation processes of the high- $T_g$  component (blue open circles) and that of the dynamically decoupled low- $T_g$  component TPP (yellow/red squares), the correlation function  $C_2(t)$  and its fits (dashed vs solid lines) at comparable relaxation times are shown in Fig. 12(a). The difference already seen in the DS spectra [cf. Fig. 2(b)] is clearly visible also in  $C_2(t)$ : whereas the high- $T_g$  component shows a strong broadening at short times (high frequencies), the additive shows a pronounced long-time tail manifesting dielectrically in a low-frequency broadening.

Finally, the overall dynamic picture is presented in Fig. 12(b), where the time constants of both relaxations ( $\alpha_1$ : full symbols,  $\alpha_2$ : open symbols) are shown for the full concentration range from

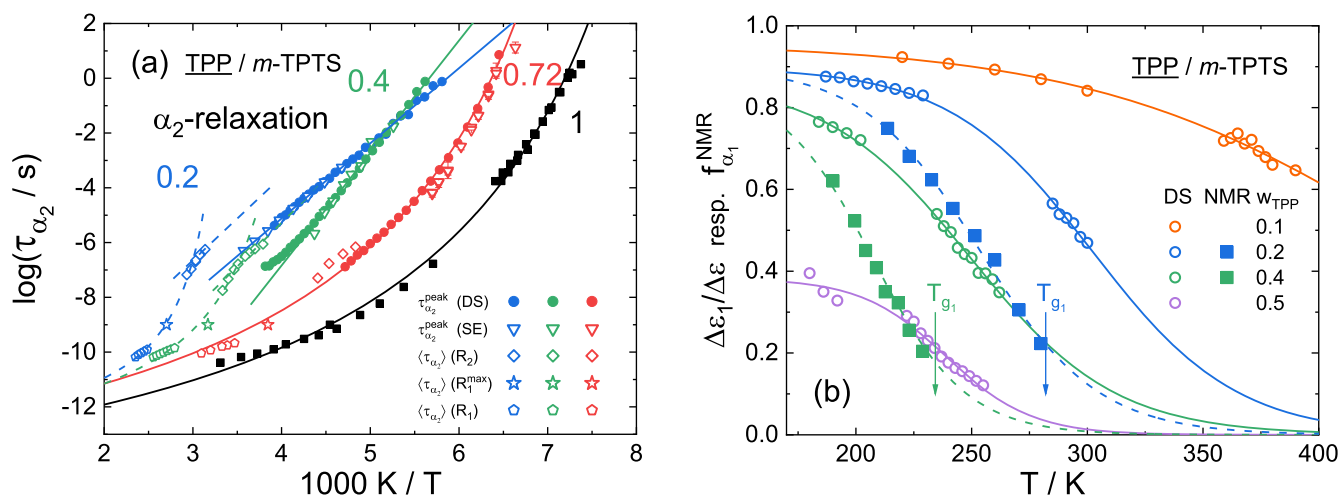


**FIG. 11.** Time constants of the  $\alpha_2$ -relaxation for neat TPP (black squares)<sup>36</sup> and for the mixtures from various techniques and different experiments. Relaxation peak time constants  $\tau_{\alpha_2}^{peak}$  from DS (circles)<sup>31</sup> and  $^2\text{H}$  stimulated echo measurements (SE, open triangles). Average time constants  $\langle \tau_{\alpha_2} \rangle$  from  $^{31}\text{P}$  NMR relaxation measurements (for a detailed explanation, see Fig. 9). Concentration is color coded. (b) Relative relaxation strength of the  $\alpha_1$ -process  $\Delta\epsilon_1/\Delta\epsilon$  (open circles) for several concentrations as a function of temperature from DS.<sup>31</sup> Residual plateau value  $f_{\alpha_1}(T)$  (squares) from  $^{31}\text{P}$  NMR stimulated echos for  $w_{TPP} = 0.2$  and 0.4. Lines: logistic interpolations.

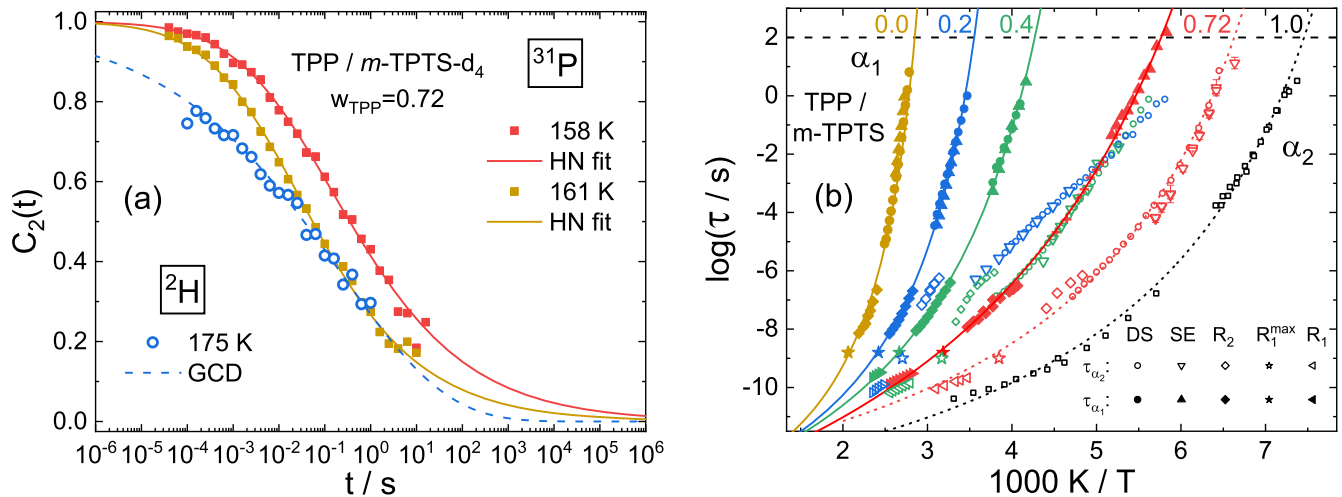


**FIG. 12.** (a) Stimulated echo decays of the high- $T_g$  component  $m$ -TPTS- $d_4$  (open blue circles,  $^2\text{H}$ ) and the additive TPP (red/yellow squares,  $^{31}\text{P}$ ) at comparable time constants in the mixture  $w_{\text{TPP}} = 0.72$ . Dashed blue line: GCD interpolation [FT of Eq. (1)]. Red/yellow line: HN interpolation. (b) Time constants  $\tau_{\alpha_1}(w_{\text{TPP}}, T)$  (closed symbols) and  $\tau_{\alpha_2}(w_{\text{TPP}}, T)$  (open symbols) from all NMR experiments (cf. Fig. 9), DS (circles,  $w_{\text{TPP}} = 0.70$ ), $^{31}$  and the literature (neat TPP, open squares). $^{36}$  Color coded concentration  $w_{\text{TPP}}$  is indicated.

the variety of different NMR experiments performed in this study. A VFT temperature dependence is found for  $\tau_{\alpha_1}(T)$  for all measured concentrations, whereas a fragile-to-strong transition is found for  $\tau_{\alpha_2}(T)$  at intermediate concentrations. Thereby, the activation energy in the Arrhenius temperature region decreases with the decreasing additive concentration, leading to the shown maximum in  $T_{g_2}(w_{\text{TPP}})$  [cf. Fig. 2(a)].

#### IV. DISCUSSION AND CONCLUSIONS

The most prominent result of our NMR study is given by the observation of a highly decoupled liquid-like additive dynamics in the matrix of the high- $T_g$  component. It manifests itself in the appearance of two-phase spectra extending over a very large temperature interval basically from temperatures slightly above  $T_{g_1}^{\text{TPP}}$  to  $T_{g_1}(w_{\text{TPP}})$  of the mixture. A very broad distribution  $G(\ln \tau_{\alpha_2})$  of isotropic reorientation characterizes the dynamics. Moreover, such motional heterogeneities are actually dynamical in the sense that slow and fast molecules mutually exchange their time constants. $^{29,52,53}$  Consequently, we think that the additive dynamics involves rotation as well as translation as already proposed previously. $^{52}$  The corresponding dielectric  $\alpha_2$ -spectra display a pronounced low-frequency broadening, a feature not observed in neat glass formers [cf. Fig. 2(a)]. The  $\alpha_2$ -relaxation becomes extremely wide at concentrations down to  $w_{\text{TPP}} = 0.04$ . $^{31}$  The corresponding time correlation function probed by the stimulated echo method features a quasi-logarithmic decay, $^{18,29,30,53}$  or at least a peculiarly stretched decay. Moreover, it yields a plateau which indicates that a fraction of TPP molecules decays at much longer times, a feature not so clearly recognizable in our previous experiments. $^{18,29,30}$  This suggests that these molecules are associated with the matrix dynamics of the high- $T_g$  component (see below). Comparing different binary systems with high  $T_g$ -contrast, the described phenomena in terms of the weighting factor  $W(T)$ , for example, appear to show a generic behavior (cf. Fig. 6).

Given this especially broad distribution  $G(\ln \tau_{\alpha_2})$ , it is impossible to extract a mean correlation time defined by the spectral density at zero frequency or equivalently by the integral over the correlation function as usually done. Instead, one has to content oneself with taking the most probable time constant as provided by the dielectric peak position, for example. Consequently, one expects deviations when different observables are analyzed in the time or frequency domain. Nevertheless, applying the same model function interpolating both dielectric and NMR observables, we essentially find agreement among the time constants linked to the dynamics of the high- $T_g$  and the low- $T_g$  component, respectively, i.e., to  $\alpha_1$ - and  $\alpha_2$ -relaxation as probed by both techniques. As in other binary systems, $^{18,29}$  the such extracted dielectric time constants  $\tau_{\alpha_2}(T)$  follow an Arrhenius temperature dependence at low concentrations, whereas a VFT behavior is observed at high  $w_{\text{TPP}}$  basically following parallel to  $\tau_{\alpha_1}(T)$ . Extrapolating  $\tau_{\alpha_2}(T)$  to low temperatures, in addition to  $T_{g_1}(w_{\text{TPP}})$ , a second  $T_{g_2}(w_{\text{TPP}})$  value can be defined, which passes through a maximum, while  $T_{g_1}(w_{\text{TPP}})$  displays a plasticizer effect. This maximum of  $T_{g_2}(w_{\text{TPP}})$  directly follows from the fact that the apparent activation energy of  $\tau_{\alpha_2}(T)$  decreases with lowering the additive concentration $^{31}$  accompanied by an increase in the width of the temperature range of two-phase spectra. In other words, the lower the additive concentration, the weaker its dynamics slows down. Even if one refrains from extrapolating  $\tau_{\alpha_2}(T)$  to define a  $T_{g_2}$  value, it is obvious that the additive dynamics is highly decoupled from that of the high- $T_g$  component, in particular, at low  $w_{\text{TPP}}$ .

As demonstrated (see Fig. 4), our preliminary study of a  $w_{\text{TPP}} = 0.04$  sample discloses two-phase spectra as well. However, presently it is not clear whether the two-phase temperature interval follows the trend suggested by the spectra of the other samples with higher concentration, i.e., becoming continuously broader (dashed lines in Fig. 4), or whether it shrinks. We note that the dielectric spectra of the  $w_{\text{TPP}} = 0.04$  sample do not seem to become narrower

compared to that of the  $w_{TPP} = 0.2$  sample [Fig. 2(a)]. It is difficult to imagine that such two-phase spectra reflecting presumably cooperative dynamics of the additive are still observed in the limit of very low concentration, and consequently, one expects that the two-phase character disappears at very low concentrations. For example, many optical experiments are done by adding some dye molecules at very low concentration to probe the main dynamics of a glassy matrix.<sup>59,60</sup> We note, however, that two-phase spectra were also reported for deuterated 3.4% hexamethyl benzene and even for 0.5% benzene in oligo styrene.<sup>52</sup> Hence, such spectra may be just the finger print of molecules diffusing translationally in a random potential created by the amorphous matrix. Quantitative cross polarization may help to push NMR studies toward this limit of infinite dilution.<sup>61</sup>

In contrast to the dynamics of the additive, the high- $T_g$  component displays no two-phase spectra and the corresponding NMR stimulated echo decays exhibit a progressively stronger stretching compared to that of the neat system, yet it remains of Kohlrausch-type. Although at certain concentrations, the stimulated echo decays of additive and high- $T_g$  component seem to look rather similar (in the given experimental time window), the corresponding dielectric NMR spectra are very different [cf. Figs. 2 and 12(a)]. In accordance with the absence of the two-phase character of the NMR spectra, we do not interpret this broadening of the dielectric  $\alpha_1$ -spectra as a consequence of a particular distribution of isotropic reorientations but rather a feature similar to the excess wing phenomenon reported for pure glass formers.<sup>62,63</sup> Of course, detecting such subtle features in the time domain is very difficult, given the dynamic resolution of the stimulated echo technique.

Binary mixtures consisting of particles with large size-disparity were thoroughly investigated by MD simulations. Studies focus mostly on mixtures of hard (HS)<sup>25,28</sup> or soft spheres;<sup>22–24,64</sup> thus, orientational degrees are missing (see, however, Refs. 65 and 66). Analyzing the state space in terms of the volume fractions of the two HS particles, two transitions scenarios from the fluid (F) to the glass (G) are identified:<sup>28</sup> A transition to a “double glass” (DG) observed at a high volume fraction of the small particles characterized by the simultaneous arrest of self and collective dynamics and a “single glass” (SG) induced at a low volume fraction and characterized by the arrest of the large particles only. Thus, in the latter case, a dynamic decoupling of both particle species is reported with the large particles exhibiting an essentially standard glass transition controlled by the cage effect, while the small particles still remain mobile. Small particles move in connected cavities in the slow or arrested matrix particles, which acts as a confining medium, yet they undergo long-range transport displaying an infinite localization length. Furthermore, a separation between self- (coherent) and collective (incoherent) dynamics is observed for the small particles. Self-correlators decay to zero at temperatures where coherent correlations are frozen along the arrest of the large particles. The dynamics of the binary systems was also analyzed by the mode coupling theory.<sup>21,22,25,67</sup> Again, coherent dynamics of the small particles leads to an additional peak at frequencies connected with that of the slow dynamics of the large particles.<sup>20</sup>

The mentioned simulation work did not address the question what happens in the limit of infinite additive dilution, i.e., tracer dynamics in a disordered solid.<sup>68,69</sup> Here, the mean square displacement shows sub-diffusive transport at intermediate time

before turning to long-range diffusion at longest times. Pronounced dynamic heterogeneities were reported<sup>69</sup> depending on the matrix structure—possibly accompanied by the experimental two-phase spectra reported at a concentration down to 0.5%.<sup>52</sup>

The counter-intuitive and challenged behavior of  $T_{g_2}(w_{TPP})$ ,<sup>33,34</sup> leading to  $T_g$  values becoming lower and lower at low  $w_{TPP}$ , may find its explanation by the sketched scenarios reported for asymmetric HS mixtures. Assuming that a mapping from HS systems to molecular systems is permissible, our experiments on molecular systems suggest a crossover from a F–DG scenario at high additive concentrations to a F–SG at low concentrations. This is sketched in Fig. 2(b). The demarcation line (vertical dashed line) between the two regions in the “state diagram” is given by the maximum position of  $T_{g_2}(w_{TPP})$ . At high additive concentrations,  $T_{g_2}(w_{TPP})$  is clearly lower than  $T_{g_1}(w_{TPP})$ , yet it basically follows  $T_{g_1}(w_{TPP})$ ; in contrast, at low concentrations,  $T_{g_2}(w_{TPP})$  strongly diverges from  $T_{g_1}(w_{TPP})$ . In this latter F–SG transition, actually no second  $T_g$  is expected, and the experimentally observed very low  $T_{g_2}(w_{TPP})$  (experimentally defined as an isodynamical point) only signals that additive molecules reflect a trend not to arrest. However, we have to keep in mind that the stimulated echo decays as well as the dielectric spectra clearly display a distribution  $G(\ln \tau_{\alpha_2})$  with a pronounced long-time tail reaching more or less times on the order of  $\tau_{\alpha_1}$ , a feature not so clearly recognized in the simulation.<sup>28</sup> We note that in MD work on soft sphere mixtures, quasi-logarithmic decays were reported for the small particles but more pronounced in the density–density correlation function than in the self-part. In any case, taking into account orientational degrees of freedom may significantly change the picture.<sup>65,66,70,71</sup>

Up to our knowledge, one thing is not reported in the MD studies but suggested by our NMR experiments that solely probe single-particle (incoherent) dynamics: a second population of small-size particles associated with the dynamics of the high- $T_g$  component for temperatures around and below  $T_{g_1}$ . Of course, these temperatures are hardly simulated. However, concerning the dielectric spectral fractions  $\Delta\epsilon_i/\Delta\epsilon$ , they do not appear to reflect the actual populations of the two molecules. Although the relaxation strength of the high- $T_g$  component is by a factor of 260 smaller than that of the low- $T_g$  component, the relaxation strengths of  $\alpha_1$ - and  $\alpha_2$ -relaxation become similar already at intermediate concentrations [cf. Fig. 11(b)]. In our previous publications,<sup>18,29,30</sup> like Blochowicz and co-workers,<sup>11,17</sup> we interpreted this feature in terms of assuming a fraction of additive molecules associated with the dynamics of the high- $T_g$  component. In the present study, we attempt to estimate this fraction by analyzing both the weighting factor  $W(T)$  and the stimulated echo decay, i.e., from NMR experiments alone. Both NMR observables provide consistently population fractions that are significantly lower than those reported by dielectric spectra. Moreover, we find a trend that the population of the TPP molecule linked to the matrix dynamics decreases with temperature, although this decrease is difficult to quantify precisely.

The significance difference between the self (incoherent)-dynamics and the collective dynamics probed by the density–density correlation could be understood by a simple picture:<sup>35</sup> A single additive molecule leaves the matrix sites on the time scale  $\tau_{\alpha_2}$  but other

molecules visit an identical site, thus keeping some correlations up to the time scale  $\tau_{\alpha_1}$  at which the high- $T_g$  matrix relaxes. This scenario may also explain the higher dielectric fraction compared to  $f_{\alpha_1}$  from NMR: Due to cross relaxation being relevant in DS, the enhanced amplitude of the dielectric  $\alpha_1$ -relaxation may reflect contributions of coherent dynamics. Here, we mention that in a recent dielectric study investigating tributyl phosphate (a homologue of TPP), an additional process in the dielectric spectrum slightly slower than the  $\alpha$ -relaxation was identified, which disappears when TBP is diluted with an inert solvent.<sup>58</sup> Possibly, the non-ideal behavior  $\Delta\epsilon(w_{TPP})$  [inset of Fig. 2(a)] may such find its explanation either.

Summarizing the component dynamics revealed by our NMR and dielectric studies of various mixtures with quite different  $T_g$  contrast,<sup>11,12,19,72</sup> it appears that essentially the  $T_g$ -contrast controls the evolution of the relaxation spectrum with concentration. In the case of a large contrast as given in the present low-molecular system and usually in polymer-plasticizer systems, the above described generic relaxation pattern is observed. Reducing the  $T_g$ -contrast, qualitatively similar results are reported.<sup>72</sup> Of course, the extent of decoupling of the component dynamics shrinks as well as does the width of the temperature interval displaying two-phase spectra. Importantly, however, two-phase are now also observed for the high- $T_g$  component.<sup>72</sup> It appears that the extent of dynamic heterogeneities becomes more symmetric as expected when concentration fluctuations play a major role.<sup>73</sup>

The sketched scenario is also observed in polymer blends:<sup>9</sup> Dynamically decoupled component dynamics, spectral broadening with failure of FTS, and a fragile-to-strong transition of the low- $T_g$  polymer around  $T_{gi}$  are observed in asymmetric blends and attributed to confinement effects. The phenomena were discussed in terms of concentrations fluctuation and self-concentration effects due to chain connectivity, respectively. We also note that recently it was argued that “the dynamics of hydrated proteins are the same as the dynamics of highly asymmetric mixtures of glass-formers.”<sup>74</sup>

## SUPPLEMENTARY MATERIAL

Detailed information about the synthesis of  $m$ -TPTS- $d_4$  as well as the relaxation times  $R_1(T)$  and  $R_2(T)$  for the different samples are given as the [supplementary material](#).

## ACKNOWLEDGMENTS

This research was funded by the Deutsche Forschungsgemeinschaft (DFG, German Research Foundation), Grant Nos. Schm 703/9-1, RO 907/19, and SFB 840. T.K., B.P., and E.R. also acknowledge the support of Jürgen Senker.

## APPENDIX: DIELECTRIC SPECTRA OF $m$ -TPTS- $d_4$ , SPIN DIFFUSION EFFECTS, AND SPECTRAL PARAMETERS OF $\alpha_2$ RELAXATION

The dielectric spectra of  $m$ -TPTS were presented in Part I and those of its deuterated counterpart are shown in Fig. 13(a). Fits by a GCD function [cf. FT of Eq. (1)] are applied demonstrating good interpolation of the relaxation peak with  $b_{GCD} = 0.5$  and  $a_{GCD}$  varying only slightly with temperature ( $0.65 \pm 0.1$ ). Regarding the peak time constants in Fig. 14(b), satisfying agreement is found compared to those from different NMR experiments as well as non-deuterated  $m$ -TPTS (DS). The  $T_g$  value [given by  $\tau_{\alpha}(T_g) = 100$  s] is found to be 6 K higher than that of  $m$ -TPTS ( $T_g = 350$  K).

To correctly interpret the  $^{31}\text{P}$  NMR stimulated echo experiments, certain damping factors must be considered. Whereas the  $T_1$  relaxation time was measured independently for each temperature (cf. [supplementary material](#)), the additional damping at even longer times, the spin diffusion, can only be determined at lowest temperatures. In Fig. 14(a), for  $w_{TPP} = 0.4$ , the measured stimulated echo decays are corrected for the  $T_1(T)$ -decay. At the lowest temperatures, one recognizes an additional relaxation showing a less stretched decay. Its shape stays almost temperature independent and

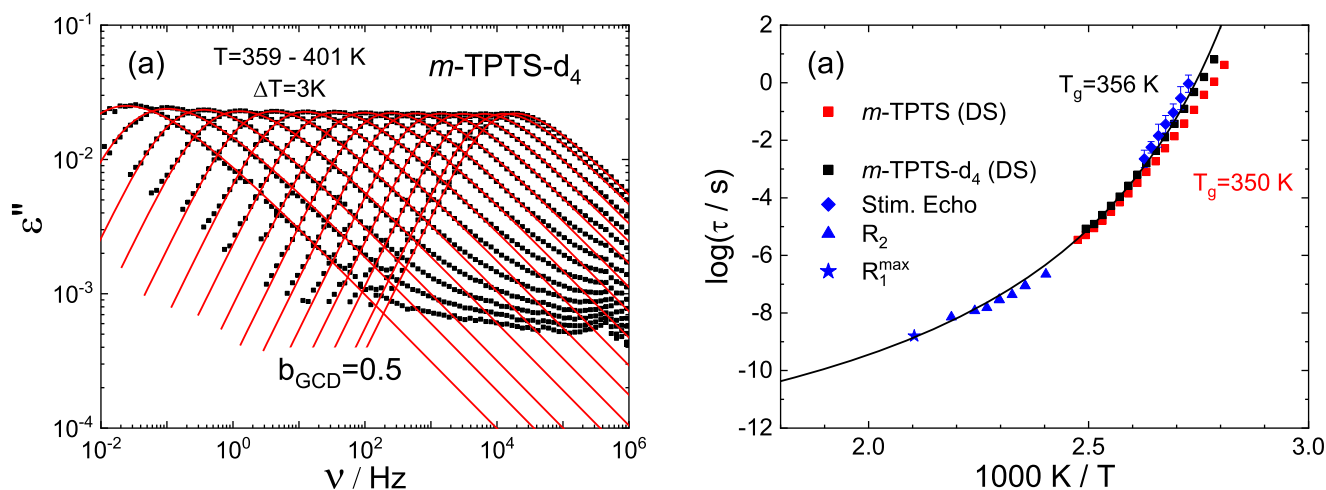


**FIG. 13.** (a) DS relaxation spectra of  $m$ -TPTS- $d_4$ . Red lines: GCD interpolations with  $b_{GCD} = 0.5$ . (b) Peak time constants  $\tau_{\alpha}(T)$  of the neat high- $T_g$  component  $m$ -TPTS- $d_4$  (partly deuterated) from DS (black squares) and NMR [stim. echo (blue diamonds),  $R_1$ -maximum (blue star),  $R_2$  (blue triangles)] as well as  $m$ -TPTS (non-deuterated) from DS (red squares).<sup>31</sup> Black line: VFT interpolation yielding  $T_g = T(\tau_{\alpha} = 100 \text{ s}) = 356$  K.

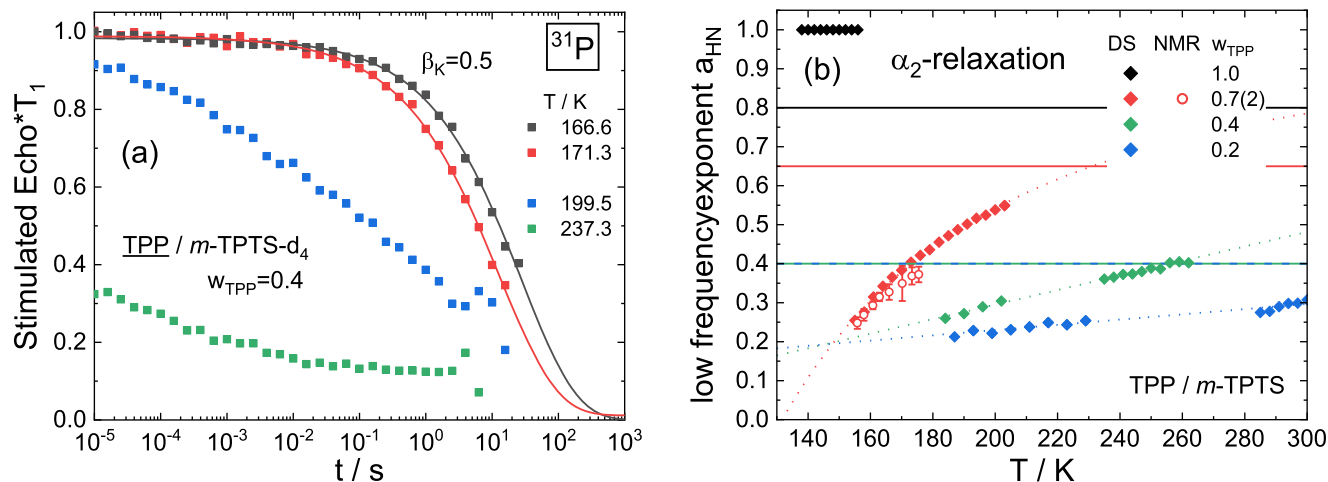


**FIG. 14.** (a)  $^{31}P$  NMR stimulated echo experiments ( $w_{TPP} = 0.4$ ) corrected by the  $T_1$ -decay (squares). Lines: Kohlrausch decays ( $\beta_K = 0.5$ ) determining the spin diffusion time constant. (b) Fitting parameter of the  $\alpha_2$ -relaxation from DS (diamonds:  $a_{HN}$ ; lines:  $c_{HN}$ ).<sup>31</sup> Dotted lines: Extrapolations of  $a_{HN}(T)$ . Red open circles:  $a_{HN}(T)$  from  $^{31}P$  NMR stimulated echo ( $w_{TPP} = 0.72$ ) analysis.

the decay time changes only slightly. The longest time constant and shape parameter were then used to correct all measured stimulated echo decays at higher temperatures. These additional measurements were performed for every concentration separately. Given the experimental situation that the actual extreme broad  $^{31}P$  reorientational correlation functions are superimposed by the two additional damping functions, we reach the limits of the stimulated echo technique in binary glass, leading to some margins for errors.

In Fig. 14(b), the DS  $\alpha_2$ -relaxation fit-parameter are shown as diamonds ( $a_{HN}$ ) and lines ( $c_{HN} = a_{HN} \cdot b_{HN}$ ). The dotted lines give the used extrapolations for the calculation of  $W(T)$  and the  $^{31}P$  NMR stimulated echo fits, whereas for  $w_{TPP} = 0.72$ ,  $a_{HN}$  was a free parameter (red open circles).

## DATA AVAILABILITY

The data that support the findings of this study are available from the corresponding author upon reasonable request.

## REFERENCES

- P. Lunkenheimer, U. Schneider, R. Brand, and A. Loid, "Glassy dynamics," *Contemp. Phys.* **41**, 15 (2000).
- K. Binder and W. Kob, *Glassy Materials and Disordered Solids: An Introduction to Their Statistical Mechanics* (World Scientific, NJ, 2005).
- A. Brodin, C. Gainaru, V. Porokhonsky, and E. A. Rössler, "Evolution of dynamic susceptibility in molecular glass formers—A critical assessment," *J. Phys.: Condens. Matter* **19**, 205104 (2007).
- L. Berthier and G. Biroli, "Theoretical perspective on the glass transition and amorphous materials," *Rev. Mod. Phys.* **83**, 587 (2011).
- M. D. Ediger and P. Harrowell, "Perspective: Supercooled liquids and glasses," *J. Chem. Phys.* **137**, 080901 (2012).
- P. G. Wolynes and V. Lubchenko, *Structural Glasses and Supercooled Liquids: Theory, Experiment, and Applications* (Wiley, Hoboken, NJ, 2012).
- M. Scandola, G. Ceccorulli, and M. Pizzoli, "Composition dependence of the glass transition of polymer-diluent mixtures: 2. Two concomitant glass transition processes as a general feature of plasticized polymers," *Polymer* **28**, 2081 (1987).

<sup>8</sup>M. Nakazawa, O. Urakawa, and K. Adachi, "Effect of local heterogeneity on dielectric relaxation spectra in concentrated solutions of poly(vinyl acetate) and poly(vinyl octanoate)," *Macromolecules* **33**, 7898 (2000).

<sup>9</sup>J. Colmenero and A. Arbe, "Segmental dynamics in miscible polymer blends: Recent results and open questions," *Soft Matter* **3**, 1474 (2007).

<sup>10</sup>K. L. Ngai, *Relaxation and Diffusion in Complex Systems* (Springer, New York, 2011).

<sup>11</sup>T. Blochowicz, S. Schramm, S. Lusceac, M. Vogel, B. Stühn, P. Gutfreund, and B. Frick, "Signature of a type-A glass transition and intrinsic confinement effects in a binary glass-forming system," *Phys. Rev. Lett.* **109**, 035702 (2012).

<sup>12</sup>R. Kahlau, D. Bock, B. Schmidtke, and E. A. Rössler, "Dynamics of asymmetric binary glass formers. I. A dielectric and nuclear magnetic resonance spectroscopy study," *J. Chem. Phys.* **140**, 044509 (2014).

<sup>13</sup>G. Goracci, A. Arbe, A. Alegría, Y. Su, U. Gasser, and J. Colmenero, "Structure and component dynamics in binary mixtures of poly[2-(dimethylamino)ethyl methacrylate] with water and tetrahydrofuran: A diffraction, calorimetric, and dielectric spectroscopy study," *J. Chem. Phys.* **144**, 154903 (2016).

<sup>14</sup>T. Blochowicz, C. Karle, A. Kudlik, P. Medick, I. Roggatz, M. Vogel, C. Tschirwitz, J. Wolber, J. Senker, and E. Rössler, "Molecular dynamics in binary organic glass formers," *J. Phys. Chem. B* **103**, 4032 (1999).

<sup>15</sup>K. Kessairi, S. Capaccioli, D. Prevosto, M. Lucchesi, and P. Rolla, "Relaxation dynamics in *tert*-butylpyridine/tristylene mixture investigated by broadband dielectric spectroscopy," *J. Chem. Phys.* **127**, 174502 (2007).

<sup>16</sup>D. Cangialosi, A. Alegría, and J. Colmenero, "Dielectric relaxation of polychlorinated biphenyl/toluene mixtures: Component dynamics," *J. Chem. Phys.* **128**, 224508 (2008).

<sup>17</sup>T. Blochowicz, S. A. Lusceac, P. Gutfreund, S. Schramm, and B. Stühn, "Two glass transitions and secondary relaxations of methyltetrahydrofuran in a binary mixture," *J. Phys. Chem. B* **115**, 1623 (2011).

<sup>18</sup>B. Pötzschner, F. Mohamed, A. Lichtinger, D. Bock, and E. A. Rössler, "Dynamics of asymmetric non-polymeric binary glass formers—A nuclear magnetic resonance and dielectric spectroscopy study," *J. Chem. Phys.* **143**, 154506 (2015).

<sup>19</sup>X. Jin, Z. Li, Y. Liu, S. Feng, and L.-M. Wang, "Identifying the structural relaxation dynamics in a strongly asymmetric binary glass former," *J. Chem. Phys.* **154**, 144504 (2021).

<sup>20</sup>Y. Kaneko and J. Bosse, "Dynamics of binary liquids near the glass transition: A mode-coupling theory," *J. Non-Cryst. Solids* **205–207**, 472 (1996).

- <sup>21</sup>S.-H. Chong, W. Götze, and A. P. Singh, "Mode-coupling theory for the glassy dynamics of a diatomic probe molecule immersed in a simple liquid," *Phys. Rev. E* **63**, 011206 (2000).
- <sup>22</sup>A. J. Moreno and J. Colmenero, "Anomalous dynamic arrest in a mixture of large and small particles," *Phys. Rev. E* **74**, 021409 (2006).
- <sup>23</sup>A. J. Moreno and J. Colmenero, "Relaxation scenarios in a mixture of large and small spheres: Dependence on the size disparity," *J. Chem. Phys.* **125**, 164507 (2006).
- <sup>24</sup>T. Voigtmann and J. Horbach, "Double transition scenario for anomalous diffusion in glass-forming mixtures," *Phys. Rev. Lett.* **103**, 205901 (2009).
- <sup>25</sup>T. Voigtmann, "Multiple glasses in asymmetric binary hard spheres," *Europhys. Lett.* **96**, 36006 (2011).
- <sup>26</sup>T. Sentjabrskaja, E. Zaccarelli, C. De Michele, F. Sciortino, P. Tartaglia, T. Voigtmann, S. U. Egelhaaf, and M. Laurati, "Anomalous dynamics of intruders in a crowded environment of mobile obstacles," *Nat. Commun.* **7**, 11133 (2016).
- <sup>27</sup>N. Müller and M. Vogel, "Relation between concentration fluctuations and dynamical heterogeneities in binary glass-forming liquids: A molecular dynamics simulation study," *J. Chem. Phys.* **150**, 064502 (2019).
- <sup>28</sup>E. Lázaro-Lázaro, J. A. Perera-Burgos, P. Laermann, T. Sentjabrskaja, G. Pérez-Ángel, M. Laurati, S. U. Egelhaaf, M. Medina-Noyola, T. Voigtmann, R. Castañeda-Priego, and L. F. Elizondo-Aguilera, "Glassy dynamics in asymmetric binary mixtures of hard spheres," *Phys. Rev. E* **99**, 042603 (2019).
- <sup>29</sup>D. Bock, R. Kahlau, B. Pötzschner, T. Körber, E. Wagner, and E. A. Rössler, "Dynamics of asymmetric binary glass formers. II. Results from nuclear magnetic resonance spectroscopy," *J. Chem. Phys.* **140**, 094505 (2014).
- <sup>30</sup>B. Pötzschner, F. Mohamed, C. Bäcker, E. Wagner, A. Lichtinger, R. Minikejew, K. Kreger, H.-W. Schmidt, and E. A. Rössler, "Non-polymeric asymmetric binary glass-formers. I. Main relaxations studied by dielectric, <sup>2</sup>H NMR, and <sup>31</sup>P NMR spectroscopy," *J. Chem. Phys.* **146**, 164503 (2017).
- <sup>31</sup>T. Körber, F. Krohn, C. Neuber, H.-W. Schmidt, and E. A. Rössler, "Reorientational dynamics of highly asymmetric binary non-polymeric mixtures—A dielectric spectroscopy study," *Phys. Chem. Chem. Phys.* **23**, 7200 (2021).
- <sup>32</sup>T. Körber, F. Krohn, C. Neuber, H.-W. Schmidt, and E. A. Rössler, "Main and secondary relaxations of non-polymeric high-*T<sub>g</sub>* glass formers as revealed by dielectric spectroscopy," *Phys. Chem. Chem. Phys.* **22**, 9086 (2020).
- <sup>33</sup>S. Valenti, S. Capaccioli, and K. L. Ngai, "Contrasting two different interpretations of the dynamics in binary glass forming mixtures," *J. Chem. Phys.* **148**, 054504 (2018).
- <sup>34</sup>K. L. Ngai, S. Valenti, and S. Capaccioli, "Molecular dynamic in binary mixtures and polymer blends with large difference in glass transition temperatures of the two components: A critical review," *J. Non-Cryst. Solids* **558**, 119573 (2019).
- <sup>35</sup>T. Böhmer, R. Horstmann, J. P. Gabriel, F. Pabst, M. Vogel, and T. Blochowicz, "The origin of apparent slow solvent dynamics in binary mixtures," PNAS (submitted).
- <sup>36</sup>S. Adishchev, D. Bock, C. Gainaru, R. Kahlau, B. Micko, N. Petzold, B. Pötzschner, and E. A. Rössler, "Reorientational dynamics of organophosphate glass formers—A joint study by <sup>31</sup>P NMR, dielectric spectroscopy and light scattering," *Z. Phys. Chem.* **226**, 1149 (2012).
- <sup>37</sup>R. Kahlau, T. Dörfler, and E. A. Rössler, "Secondary relaxations in a series of organic phosphate glasses revealed by dielectric spectroscopy," *J. Chem. Phys.* **139**, 134504 (2013).
- <sup>38</sup>R. Kahlau, D. Kruk, T. Blochowicz, V. N. Novikov, and E. A. Rössler, "Generalization of the Cole–Davidson and Kohlrausch functions to describe the primary response of glass-forming systems," *J. Phys.: Condens. Matter* **22**, 365101 (2010).
- <sup>39</sup>T. Takahashi, H. Kawashima, H. Sugisawa, and T. Baba, "<sup>207</sup>Pb chemical shift thermometer at high temperature for magic angle spinning experiments," *Solid State Nucl. Magn. Reson.* **15**, 119 (1999).
- <sup>40</sup>A. Abragam, *The Principles of Nuclear Magnetism* (Clarendon Press, Oxford, 1961).
- <sup>41</sup>H. W. Spiess, "Rotation of molecules and nuclear spin relaxation," in *Dynamic NMR Spectroscopy*, edited by P. Diehl, E. Fluck, and R. Kosfeld (Springer, Berlin, Heidelberg, 1978), p. 55.
- <sup>42</sup>B. J. Cauley, C. Cipriani, K. Ellis, A. K. Roy, A. A. Jones, P. T. Inglefield, B. J. McKinley, and R. P. Kambour, "Glass transition and dynamics of phosphate esters dissolved in two glassy polymer matrices," *Macromolecules* **24**, 403 (1991).
- <sup>43</sup>Y. Liu, M. M. Turnbull, A. A. Jones, P. T. Inglefield, and R. P. Kambour, "Concentration and temperature dependence of diluent dynamics studied by line shape experiments on a phosphate ester in polycarbonate," *Solid State Nucl. Magn. Reson.* **2**, 289 (1993).
- <sup>44</sup>R. Böhmer, G. Diezemann, G. Hinze, and E. Rössler, "Dynamics of supercooled liquids and glassy solids," *Prog. Nucl. Magn. Reson. Spectrosc.* **39**, 191 (2001).
- <sup>45</sup>E. Rössler, M. Taupitz, K. Börner, M. Schulz, and H. M. Vieth, "A simple method analyzing <sup>2</sup>H nuclear magnetic resonance line shapes to determine the activation energy distribution of mobile guest molecules in disordered systems," *J. Chem. Phys.* **92**, 5847 (1990).
- <sup>46</sup>S. Havriliak and S. Negami, "A complex plane representation of dielectric and mechanical relaxation processes in some polymers," *Polymer* **8**, 161 (1967).
- <sup>47</sup>C. J. F. Böttcher and P. Bordewijk, *Dielectrics in Time-Dependent Fields*, 2nd ed. (Elsevier, Amsterdam, 1978).
- <sup>48</sup>K. Schmidt-Rohr and H. W. Spiess, *Multidimensional Solid-State NMR and Polymers* (Academic Press, London, 1994).
- <sup>49</sup>F. Fujara, S. Wefing, and H. W. Spiess, "Dynamics of molecular reorientations: Analogies between quasielastic neutron scattering and deuteron NMR spin alignment," *J. Chem. Phys.* **84**, 4579 (1986).
- <sup>50</sup>M. Bloom, J. H. Davis, and M. I. Valic, "Spectral distortion effects due to finite pulse widths in deuterium nuclear magnetic resonance spectroscopy," *Can. J. Phys.* **58**, 1510 (1980).
- <sup>51</sup>J. D. Ferry, *Viscoelastic Properties of Polymers* (John Wiley & Sons, New York, 1980).
- <sup>52</sup>P. Medick, M. Vogel, and E. Rössler, "Large angle jumps of small molecules in amorphous matrices analyzed by 2D exchange NMR," *J. Magn. Reson.* **159**, 126 (2002).
- <sup>53</sup>D. Bingemann, N. Wirth, J. Gmeiner, and E. A. Rössler, "Decoupled dynamics and quasi-logarithmic relaxation in the polymer–plasticizer system poly(methyl methacrylate)/tri-*m*-cresyl phosphate studied with 2D NMR," *Macromolecules* **40**, 5379 (2007).
- <sup>54</sup>H. W. Spiess and H. Sillescu, "Solid echoes in the slow-motion region," *J. Magn. Reson.* **42**, 381 (1981).
- <sup>55</sup>C. Schmidt, K. J. Kuhn, and H. W. Spiess, "Distribution of correlation times in glassy polymers from pulsed deuteron NMR," in *Frontiers in Polymer Science*, edited by W. Wilke (Steinkopff, Darmstadt, 1985), p. 71.
- <sup>56</sup>M. Vogel, "Origins of apparent fragile-to-strong transitions of protein hydration waters," *Phys. Rev. Lett.* **101**, 225701 (2008).
- <sup>57</sup>M. Sattig, S. Reutter, F. Fujara, M. Werner, G. Buntkowsky, and M. Vogel, "NMR studies on the temperature-dependent dynamics of confined water," *Phys. Chem. Chem. Phys.* **16**, 19229 (2014).
- <sup>58</sup>F. Pabst, A. Helbling, J. Gabriel, P. Weigl, and T. Blochowicz, "Dipole–dipole correlations and the Debye process in the dielectric response of nonassociating glass forming liquids," *Phys. Rev. E* **102**, 010606 (2020).
- <sup>59</sup>M. T. Cicerone and M. D. Ediger, "Photobleaching technique for measuring ultraslow reorientation near and below the glass transition: tetracene in *o*-terphenyl," *J. Phys. Chem.* **97**, 10489 (1993).
- <sup>60</sup>G. Heuberger and H. Sillescu, "Size dependence of tracer diffusion in supercooled liquids," *J. Phys. Chem.* **100**, 15255 (1996).
- <sup>61</sup>R. L. Johnson and K. Schmidt-Rohr, "Quantitative solid-state <sup>13</sup>C NMR with signal enhancement by multiple cross polarization," *J. Magn. Reson.* **239**, 44 (2014).
- <sup>62</sup>U. Schneider, R. Brand, P. Lunkenheimer, and A. Loidl, "Excess wing in the dielectric loss of glass formers: A Johari–Goldstein  $\beta$  relaxation?," *Phys. Rev. Lett.* **84**, 5560 (2000).
- <sup>63</sup>N. Petzold, B. Schmidtke, R. Kahlau, D. Bock, R. Meier, B. Micko, D. Kruk, and E. A. Rössler, "Evolution of the dynamic susceptibility in molecular glass formers: Results from light scattering, dielectric spectroscopy, and NMR," *J. Chem. Phys.* **138**, 12A510 (2013).

- <sup>64</sup>F. Sciortino, P. Tartaglia, and E. Zaccarelli, "Evidence of a higher-order singularity in dense short-ranged attractive colloids," *Phys. Rev. Lett.* **91**, 268301 (2003).
- <sup>65</sup>T. Theenhaus, R. Schilling, A. Latz, and M. Letz, "Microscopic dynamics of molecular liquids and glasses: Role of orientations and translation-rotation coupling," *Phys. Rev. E* **64**, 051505 (2001).
- <sup>66</sup>C. De Michele, R. Schilling, and F. Sciortino, "Dynamics of uniaxial hard ellipsoids," *Phys. Rev. Lett.* **98**, 265702 (2007).
- <sup>67</sup>J. Bosse and Y. Kaneko, "Self-diffusion in supercooled binary liquids," *Phys. Rev. Lett.* **74**, 4023 (1995).
- <sup>68</sup>T. Franosch, M. Spanner, T. Bauer, G. E. Schröder-Turk, and F. Höfling, "Space-resolved dynamics of a tracer in a disordered solid," *J. Non-Cryst. Solids* **357**, 472 (2011).
- <sup>69</sup>R. C. Roberts, R. Poling-Skutvik, J. C. Conrad, and J. C. Palmer, "Tracer transport in attractive and repulsive supercooled liquids and glasses," *J. Chem. Phys.* **151**, 194501 (2019).
- <sup>70</sup>K. V. Edmond, M. T. Elsesser, G. L. Hunter, D. J. Pine, and E. R. Weeks, "Decoupling of rotational and translational diffusion in supercooled colloidal fluids," *Proc. Natl. Acad. Sci. U. S. A.* **109**, 17891 (2012).
- <sup>71</sup>L. F. Elizondo-Aguilera, E. C. Cortés-Morales, P. F. Zubieta Rico, M. Medina-Noyola, R. Castañeda-Priego, T. Voigtmann, and G. Pérez-Ángel, "Arrested dynamics of the dipolar hard sphere model," *Soft Matter* **16**, 170 (2020).
- <sup>72</sup>T. Körber, R. Minikejew, B. Pötzschner, D. Bock, and E. A. Rössler, "Dynamically asymmetric binary glass formers studied by dielectric and NMR spectroscopy," *Eur. Phys. J. E* **42**, 143 (2019).
- <sup>73</sup>G. Floudas, W. Steffen, E. W. Fischer, and W. Brown, "Solvent and polymer dynamics in concentrated polystyrene/toluene solutions," *J. Chem. Phys.* **99**, 695 (1993).
- <sup>74</sup>S. Capaccioli, L. Zheng, A. Kyritsis, A. Paciaroni, M. Vogel, and K. L. Ngai, "The dynamics of hydrated proteins are the same as those of highly asymmetric mixtures of two glass-formers," *ACS Omega* **6**, 340 (2021).

## Supporting Information

### Reorientational dynamics in highly asymmetric binary low-molecular mixtures – a quantitative comparison of dielectric and NMR spectroscopy results

Thomas Körber,<sup>1</sup> Björn Pötzschner,<sup>1</sup> Felix Krohn<sup>2</sup>, Ernst A. Rössler<sup>1,a)</sup>

<sup>1</sup>Department of Inorganic Chemistry III and Northern Bavarian NMR Centre, University of Bayreuth, 95440 Bayreuth, Germany

<sup>2</sup>Department of Macromolecular Chemistry and Bavarian Polymer Institute, University of Bayreuth, 95440 Bayreuth, Germany

#### Synthesis of *m*-TPTS-d<sub>4</sub>

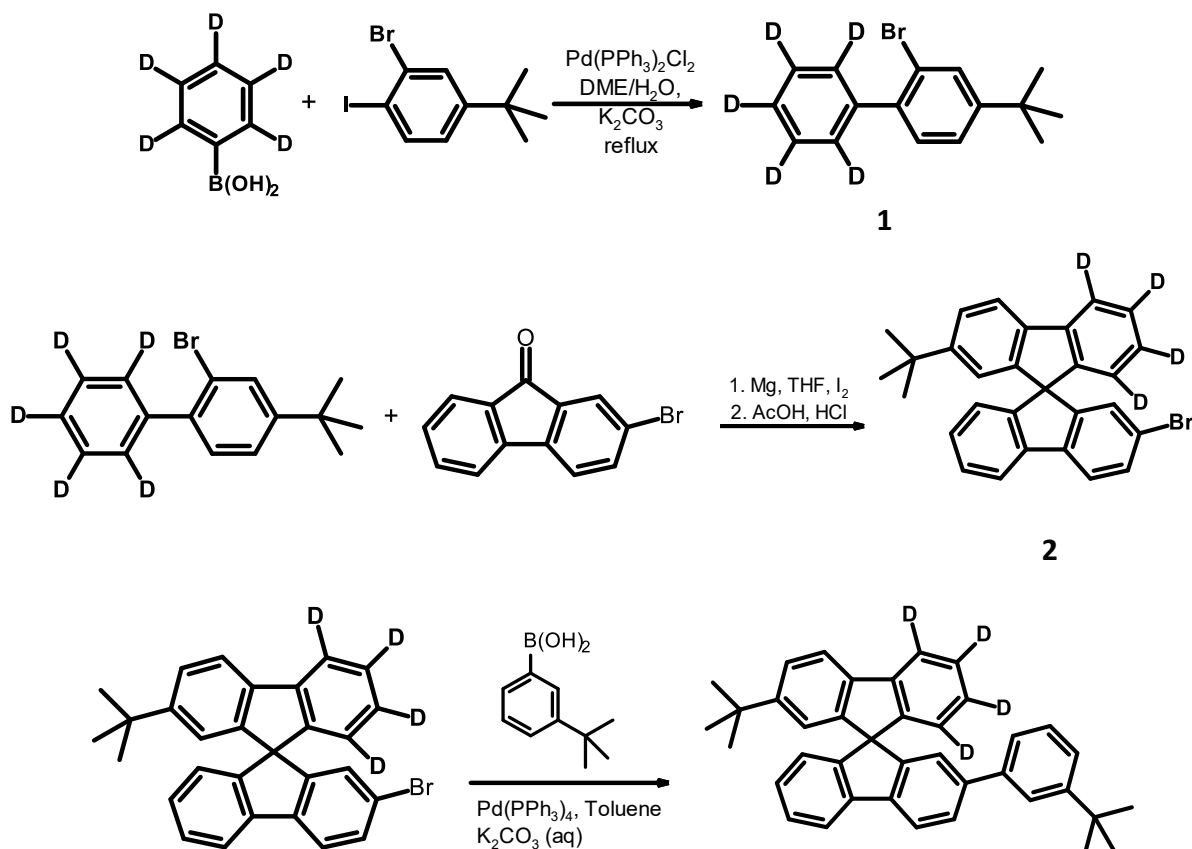


Fig. 1 Synthetic route to *m*-TPTS-d<sub>4</sub>

Synthesis of **1**: 2.00 g (15.75 mmol) Phenyl-*d*<sub>5</sub>-boronic acid and 4.45 g (13.1 mmol) of 3-bromo-4-iodo-*tert*butylphenyl boronic acid are solved in 45 mL of DME and 7.5 mL of H<sub>2</sub>O. 2.55 g of K<sub>2</sub>CO<sub>3</sub> are added, then the mixture is flushed with Argon under stirring for 30 minutes. 110 mg of PdCl<sub>2</sub>(PPh<sub>3</sub>)<sub>2</sub> are added and Argon is flushed for another 30 minutes. Afterwards the mixture is heated to 80 °C for 18 h.

After cooling, DME is removed under reduced pressure, to the residue is given 80 mL of H<sub>2</sub>O and 40 mL of Ether. The phases are separated, the aqueous phase is washed with Ether, the combined organic phases are dried over MgSO<sub>4</sub> and the solvent is removed under reduced pressure. The crude product is further purified by column chromatography with hexane to yield 3.1 g (80 %) of a colourless liquid with a distinct odour.

<sup>1</sup>H NMR (300 MHz, CDCl<sub>3</sub>): δ = 1.36 (s, 9H, *t*-Bu-H), 7.27 (m, 1H, Ar-H), 7.38 (dd, 1H, Ar-H), 7.67 (d, 1H, Ar-H)

Synthesis of **2**: 3.1 g (12.2 mmol) of **1** are mixed with 370 mg of Mg and one spatula tip of I<sub>2</sub> in 30 mL of dry THF and heated under reflux. 3.1 g (12.0 mmol) 2-bromo-fluorenone are dissolved in 10 mL of dry THF. After 5 h, the Grignard reagent is transferred to the fluorenone solution with a syringe and stirred under reflux for further 17 h. Then a few drops of AcOH are given to the solution upon which it clarifies. THF is removed under reduced pressure, the remaining material is dissolved in 30 mL AcOH and 2 mL of 32 % HCl and heated under reflux for 5 h. The product is precipitated with MeOH, filtered, washed with hexane and EtOH, and dried to yield 3.0 g (55 %) of a colourless powder.

<sup>1</sup>H NMR (300 MHz, CDCl<sub>3</sub>): δ = 1.18 (s, 9H, *t*-Bu-H), 6.72 (m, 2H, Ar-H), 6.85 (dd, 1H, Ar-H), 7.12 (dt, 1H, Ar-H), 7.37 (dt, 1H, Ar-H), 7.44 (dd, 1H, Ar-H), 7.48 (dd, 1H, Ar-H), 7.70 (dd, 1H, Ar-H), 7.76 (dd, 1H, Ar-H), 7.82 (m, 1H, Ar-H)

Synthesis of **m-TPTS-d<sub>4</sub>**: 2.97 g of **2** (6.53 mmol) are dissolved in 100 mL dry THF with 1.51 g 3-*tert*butylphenyl boronic acid (8.48 mmol). 60 mL 2M K<sub>2</sub>CO<sub>3</sub>-solution are added and Ar is flushed for 30 minutes. 196 mg Pd(PPh<sub>3</sub>)<sub>4</sub> (0.17 mmol) are added to the mixture and Ar is flushed for another 30 minutes. The mixture is then refluxed for 17 h. After cooling the phases are separated, the organic phase is washed with brine, dried over MgSO<sub>4</sub> and the solvent removed under reduced pressure. The crude product is further purified by column chromatography with cyclohexane / EtAc in a gradient from 100:1 to 20:1 to yield 2.84 g (80 %) of a white solid. After sublimation, a total of 1.73 g remained.

<sup>1</sup>H NMR (300 MHz, CDCl<sub>3</sub>): δ = 1.17 (s, 9H, *t*-Bu-H), 1.30 (s, 9H, *t*-Bu-H), 6.73 (m, 1H, Ar-H), 6.78 (dd, 1H, Ar-H), 6.92 (dd, 1H, Ar-H), 7.10 (td, 1H, Ar-H), 7.15 – 7.30 (m, 3H, Ar-H), 7.34 – 7.46 (m, 3H, Ar-H), 7.61 (dd, 1H, Ar-H), 7.77 (dd, 1H, Ar-H), 7.87 (m, 1H, Ar-H), 7.89 – 7.93 (dd, 1H, Ar-H)

## Correlation times from $R_1$ and $R_2$

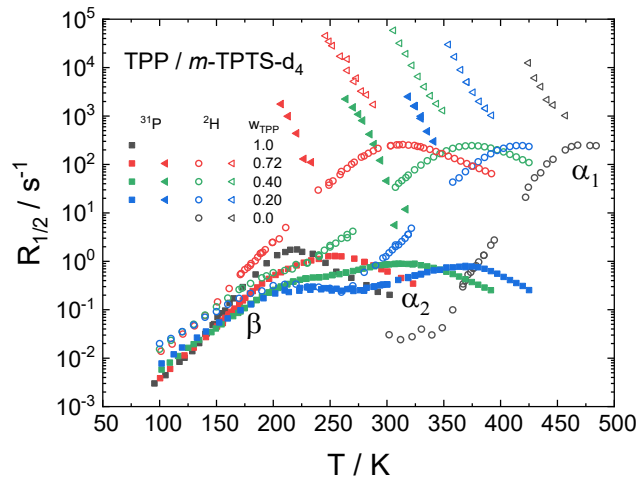


Fig. 2 Spin-lattice relaxation rates  $R_1(w_{TPP})$  ( $^2\text{H}$ : open circles;  $^{31}\text{P}$ : filled squares) and spin-spin relaxation rates  $R_2(w_{TPP})$  ( $^2\text{H}$ : open triangles;  $^{31}\text{P}$ : filled triangles). Concentration  $w_{TPP}$  is colour-coded.

The spin-lattice relaxation rates  $R_1(w_{TPP}, T)$  are measured via the inversion recovery pulse sequence at high temperatures and via the saturation recovery pulse sequence at temperatures below the first  $R_1$  maximum. The rates are defined as inverse of the average spin lattice relaxation time  $R_1 = 1/\langle T_1 \rangle$ . The spin-spin relaxation rates  $R_2(w_{TPP}, T)$  were determined in the limit of magnetic field inhomogeneities not spoiling the free induction decay from the width of the Lorentzian line via  $R_2 = \pi \Delta \nu_{FWHM}$ .

To determine the time constants in a model free manner, the coupling constants at lowest temperatures were required. Therefore,  $\delta_{CSA} = 2\pi * 19 \text{ kHz}$  was used to calculate the  $^{31}\text{P}$  NMR time constants  $\langle \tau_{\alpha_2} \rangle$ , and  $\delta_Q = 2\pi * 137 \text{ kHz}$  for the  $^2\text{H}$  NMR time constants  $\langle \tau_{\alpha_1} \rangle$ . The corresponding equations are explained in the main part (cf. *Section II*).



---

## V References

1. K. Chang, “The Nature of Glass Remains Anything but Clear”, The New York Times (2008).
2. P. W. Anderson, “Through the glass lightly”, Science 267, 1615 (1995).
3. M. Cukierman, J. W. Lane, and D. R. Uhlmann, “High-temperature flow behavior of glass-forming liquids: A free-volume interpretation”, J. Chem. Phys. 59, 3639 (1973).
4. T. Blochowicz, A. Brodin, and E. A. Rössler, “Evolution of the dynamic susceptibility in supercooled liquids and glasses”, in *Advances in chemical physics. Fractals, Diffusion, and Relaxation in Disordered Complex Systems*. Volume 133, edited by W. T. Coffey and Y. P. Kalmykov (John Wiley & Sons, Inc., Hoboken, New Jersey, 2006), p. 127.
5. B. Schmidtke, N. Petzold, R. Kahlau, M. Hofmann, and E. A. Rössler, “From boiling point to glass transition temperature: transport coefficients in molecular liquids follow three-parameter scaling”, Physical Review E 86, 41507 (2012).
6. C. A. Angell, “Formation of glasses from liquids and biopolymers”, Science 267, 1924 (1995).
7. A. Tölle, “Neutron scattering studies of the model glass former *ortho*-terphenyl”, Rep. Prog. Phys. 64, 1473 (2001).
8. G. Floudas, M. Paluch, A. Grzybowski, and K. Ngai, *Molecular dynamics of glass-forming systems. Effects of pressure* (Springer, Berlin, Heidelberg, 2011).
9. H. Z. Cummins, G. Li, Y. H. Hwang, G. Q. Shen, W. M. Du, J. Hernandez, and N. J. Tao, “Dynamics of supercooled liquids and glasses: comparison of experiments with theoretical predictions”, Z. Phys. B 103, 501 (1997).
10. R. Böhmer, G. Diezemann, G. Hinze, and E. Rössler, “Dynamics of supercooled liquids and glassy solids”, Prog. Nucl. Magn. Reson. Spectrosc. 39, 191 (2001).
11. R. Kubo, “The fluctuation-dissipation theorem”, Rep. Prog. Phys. 29, 255 (1966).
12. P. Lunkenheimer, U. Schneider, R. Brand, and A. Loidl, “Glassy dynamics”, Contemp. Phys. 41, 15 (2000).
13. K. Binder and W. Kob, *Glassy materials and disordered solids*. An introduction to their statistical mechanics, Rev. ed. (World Scientific, Singapore, Hackensack, 2011).
14. P. G. Wolynes and V. Lubchenko, *Structural glasses and supercooled liquids. Theory, experiment, and applications* (Wiley, Hoboken, New Jersey, 2012).
15. N. Petzold, B. Schmidtke, R. Kahlau, D. Bock, R. Meier, B. Micko, D. Kruk, and E. A. Rössler, “Evolution of the dynamic susceptibility in molecular glass formers: results from light scattering, dielectric spectroscopy, and NMR”, J. Chem. Phys. 138, 12A510 (2013).
16. H. Vogel, “Das Temperaturabhängigkeitsgesetz der Viskosität von Flüssigkeiten.”, Phys. Z., 645 (1921).

- 
17. G. S. Fulcher, "Analysis of recent measurements of the viscosity of glasses", *J. Am. Ceram. Soc.* 8, 339 (1925).
  18. G. Tammann and W. Hesse, "Die Abhängigkeit der Viscosität von der Temperatur bei unterkühlten Flüssigkeiten", *Z. Anorg. Allg. Chem.* 156, 245 (1926).
  19. Kivelson, Tarjus, and Zhao, "Fitting of viscosity: Distinguishing the temperature dependences predicted by various models of supercooled liquids", *Phys. Rev. E* 53, 751 (1996).
  20. J. C. Mauro, Y. Yue, A. J. Ellison, P. K. Gupta, and D. C. Allan, "Viscosity of glass-forming liquids", *PNAS* 106, 19780 (2009).
  21. C. A. Angell, K. L. Ngai, G. B. McKenna, P. F. McMillan, and S. W. Martin, "Relaxation in glassforming liquids and amorphous solids", *J. Appl. Phys.* 88, 3113 (2000).
  22. R. Kohlrausch, "Theorie des elektrischen Rückstandes in der Leidener Flasche", *Annalen der Physik* 167, 179 (1854).
  23. G. Williams and D. C. Watts, "Non-symmetrical dielectric relaxation behaviour arising from a simple empirical decay function", *Trans. Faraday Soc.* 66, 80 (1970).
  24. K. Duvvuri and R. Richert, "Dynamics of glass-forming liquids. VI. Dielectric relaxation study of neat decahydro-naphthalene", *J. Chem. Phys.* 117, 4414 (2002).
  25. M. Paluch, J. Knapik, Z. Wojnarowska, A. Grzybowski, and K. L. Ngai, "Universal behavior of dielectric responses of glass formers: role of dipole-dipole interactions", *Phys. Rev. Lett.* 116, 25702 (2016).
  26. D. W. Davidson and R. H. Cole, "Dielectric Relaxation in Glycerine", *J. Chem. Phys.* 18, 1417 (1950).
  27. C. J. F. Böttcher and P. Bordewijk, *Dielectrics in time-dependent fields*, 2. completely rev. ed. (Elsevier, Amsterdam, 1978).
  28. S. Havriliak and S. Negami, "A complex plane representation of dielectric and mechanical relaxation processes in some polymers", *Polymer* 8, 161 (1967).
  29. T. Blochowicz, C. Tschirwitz, S. Benkhof, and E. A. Rössler, "Susceptibility functions for slow relaxation processes in supercooled liquids and the search for universal relaxation patterns", *J. Chem. Phys.* 118, 7544 (2003).
  30. U. Schneider, R. Brand, P. Lunkenheimer, and A. Loidl, "Excess wing in the dielectric loss of glass formers: A Johari-Goldstein  $\beta$  relaxation?", *Phys. Rev. Lett.* 84, 5560 (2000).
  31. G. P. Johari and M. Goldstein, "Viscous liquids and the glass transition. II. Secondary relaxations in glasses of rigid molecules", *J. Chem. Phys.* 53, 2372 (1970).
  32. A. K. Hassan, L. Börjesson, and L. M. Torell, "The boson peak in glass formers of increasing fragility", *J. Non-Cryst. Solids* 172-174, 154 (1994).
  33. A. Kudlik, S. Benkhof, T. Blochowicz, C. Tschirwitz, and E. Rössler, "The dielectric response of simple organic glass formers", *J. Mol. Struct.* 479, 201 (1999).
  34. K. L. Ngai, P. Lunkenheimer, C. León, U. Schneider, R. Brand, and A. Loidl, "Nature and properties of the Johari-Goldstein  $\beta$ -relaxation in the equilibrium liquid state of a class of glass-formers", *J. Chem. Phys.* 115, 1405 (2001).

- 
35. A. Döfl, M. Paluch, H. Sillescu, and G. Hinze, “Dynamics in supercooled polyalcohols: Primary and secondary relaxation”, *J. Chem. Phys.* 117, 6582 (2002).
  36. P. Lunkenheimer, R. Wehn, T. Rieger, and A. Loidl, “Excess wing in the dielectric loss of glass formers: further evidence for a  $\beta$ -relaxation”, *J. Non-Cryst. Solids* 307-310, 336 (2002).
  37. Menon and Nagel, “Evidence for a divergent susceptibility at the glass transition”, *Phys. Rev. Lett.* 74, 1230 (1995).
  38. B. Guiselin, C. Scalliet, and L. Berthier, “Microscopic origin of excess wings in relaxation spectra of deeply supercooled liquids”, arXiv:2103.01569v1 (2021).
  39. J. D. Stevenson and P. G. Wolynes, “A universal origin for secondary relaxations in supercooled liquids and structural glasses”, *Nature Phys* 6, 62 (2009).
  40. K. L. Ngai and M. Paluch, “Classification of secondary relaxation in glass-formers based on dynamic properties”, *J. Chem. Phys.* 120, 857 (2004).
  41. V. K. Malinovsky, V. N. Novikov, P. P. Parshin, A. P. Sokolov, and M. G. Zemlyanov, “Universal Form of the Low-Energy (2 to 10 meV) Vibrational Spectrum of Glasses”, *Europhys. Lett.* 11, 43 (1990).
  42. Kiebel, Bartsch, Debus, Fujara, Petry, and Sillescu, “Secondary relaxation in the glass-transition regime of ortho-terphenyl observed by incoherent neutron scattering”, *Physical review. B, Condensed matter* 45, 10301 (1992).
  43. E. Bartsch, F. Fujara, B. Geil, M. Kiebel, W. Petry, W. Schnauss, H. Sillescu, and J. Wuttke, “Signatures of the glass transition in a van der Waals liquid seen by neutrons and NMR”, *Physica A* 201, 223 (1993).
  44. H. Franz, W. Petry, and A. Baron, “Quasielastic scattering: slow dynamics of glasses”, *Hyperfine Interactions* 123/124, 865 (1999).
  45. S. Bauer, M. Storek, C. Gainaru, H. Zimmermann, and R. Böhmer, “Molecular motions in supercooled and glassy ibuprofen: deuteron magnetic resonance and high-resolution rheology study”, *J. Phys. Chem. B* 119, 5087 (2015).
  46. Q. Wang, S. T. Zhang, Y. Yang, Y. D. Dong, C. T. Liu, and J. Lu, “Unusual fast secondary relaxation in metallic glass”, *Nat. Commun.* 6, 7876 (2015).
  47. R. Torre, P. Bartolini, and R. M. Pick, “Time-resolved optical Kerr effect in a fragile glass-forming liquid, salol”, *Phys. Rev. E* 57, 1912 (1998).
  48. A. Aouadi, C. Dreyfus, M. Massot, R. M. Pick, T. Berger, W. Steffen, A. Patkowski, and C. Alba-Simionesco, “Light scattering study of the liquid–glass transition of meta-toluidine”, *J. Chem. Phys.* 112, 9860 (2000).
  49. A. Brodin and E. A. Rössler, “Depolarized light scattering study of glycerol”, *Eur. Phys. J. B* 44, 3 (2005).
  50. J. Gabriel, F. Pabst, and T. Blochowicz, “Debye process and  $\beta$ -relaxation in 1-propanol probed by dielectric spectroscopy and depolarized dynamic light scattering”, *J. Phys. Chem. B* 121, 8847 (2017).
  51. C. Gainaru, O. Lips, A. Troshagina, R. Kahlau, A. Brodin, F. Fujara, and E. A. Rössler, “On the nature of the high-frequency relaxation in a molecular glass former: a joint study of glycerol by field cycling NMR, dielectric spectroscopy, and light scattering”, *J. Chem. Phys.* 128, 174505 (2008).

- 
52. R. Böhmer, K. L. Ngai, C. A. Angell, and D. J. Plazek, “Nonexponential relaxations in strong and fragile glass formers”, *J. Chem. Phys.* 99, 4201 (1993).
  53. A. I. Nielsen, T. Christensen, B. Jakobsen, K. Niss, N. B. Olsen, R. Richert, and J. C. Dyre, “Prevalence of approximate square root( $t$ ) relaxation for the dielectric alpha process in viscous organic liquids”, *J. Chem. Phys.* 130, 154508 (2009).
  54. S. P. Bierwirth, R. Böhmer, and C. Gainaru, “Generic primary mechanical response of viscous liquids”, *Phys. Rev. Lett.* 119, 248001 (2017).
  55. C. Gainaru, “Spectral shape simplicity of viscous materials”, *Phys. Rev. E* 100, 20601 (2019).
  56. P. Ehrenfest, *Phasenumwandlungen im ueblichen und erweiterten Sinn, classifiziert nach den entsprechenden Singularitaeten des thermodynamischen Potentials* (N. V. Noord-Hollandsche Uitgevers Maatschappij, Amsterdam, 1933).
  57. G. Gee, “Some thermodynamic properties of high polymers, and their molecular interpretation”, *Q. Rev., Chem. Soc.* 1, 265 (1947).
  58. I. Prigogine and R. Defay, *Chemical Thermodynamics* (Longmans, Green, 1954).
  59. N. Hirai and H. Eyring, “Bulk viscosity of polymeric systems”, *J. Polym. Sci.* 37, 51 (1959).
  60. M. Goldstein, “Validity of the Ehrenfest equation for a system with more than one ordering parameter: Critique of a paper by DiMarzio”, *J. Appl. Phys.* 46, 4153 (1975).
  61. P. K. Gupta and C. T. Moynihan, “Prigogine–Defay ratio for systems with more than one order parameter”, *J. Chem. Phys.* 65, 4136 (1976).
  62. C. T. Moynihan and A. V. Lesikar, “Comparison and analysis of relaxation processes at the glass transition temperature”, *Ann. NY Acad. Sci.* 371, 151 (1981).
  63. M. D. Ediger, C. A. Angell, and S. R. Nagel, “Supercooled Liquids and Glasses”, *J. Phys. Chem.* 100, 13200 (1996).
  64. P. G. Debenedetti, *Metastable liquids. Concepts and principles* (Princeton Univ. Press, Princeton, N.J, 1996).
  65. J. C. Dyre, “*Colloquium: The glass transition and elastic models of glass-forming liquids*”, *Rev. Mod. Phys.* 78, 953 (2006).
  66. W. Kauzmann, “The nature of the glassy state and the behavior of liquids at low temperatures”, *Chem. Rev.* 43, 219 (1948).
  67. G. Adam and J. H. Gibbs, “On the Temperature Dependence of Cooperative Relaxation Properties in Glass-Forming Liquids”, *J. Chem. Phys.* 43, 139 (1965).
  68. E. Leutheusser, “Dynamical model of the liquid-glass transition”, *Phys. Rev. A* 29, 2765 (1984).
  69. U. Bengtzelius, W. Gotze, and A. Sjolander, “Dynamics of supercooled liquids and the glass transition”, *J. Phys. C: Solid State Phys.* 17, 5915 (1984).
  70. W. Götze, *Complex dynamics of glass-forming liquids. A mode-coupling theory* (Oxford University Press, Oxford, New York, 2009).
  71. W. Götze, “The mode-coupling theory of liquid-to-glass transitions”, *J. Phys.: Condens. Matter* 2, SA201-SA205 (1990).

- 
72. T. R. Kirkpatrick and D. Thirumalai, “Dynamics of the structural glass transition and the p-spin-interaction spin-glass model”, *Phys. Rev. Lett.* 58, 2091 (1987).
  73. T. R. Kirkpatrick and P. G. Wolynes, “Connections between some kinetic and equilibrium theories of the glass transition”, *Phys. Rev. A* 35, 3072 (1987).
  74. T. R. Kirkpatrick and D. Thirumalai, “Random First Order Theory concepts in Biology and Condensed Matter physics”, arXiv:1412.5017 (2014).
  75. P. G. Debenedetti and F. H. Stillinger, “Supercooled liquids and the glass transition”, *Nature* 410, 259 (2001).
  76. A. Heuer, “Exploring the potential energy landscape of glass-forming systems: from inherent structures via metabasins to macroscopic transport”, *J. Phys.: Condens. Matter* 20, 373101 (2008).
  77. F. H. Stillinger and P. G. Debenedetti, “Glass transition thermodynamics and kinetics”, *Annu. Rev. Condens. Matter Phys.* 4, 263 (2013).
  78. J. P. Garrahan and D. Chandler, “Coarse-grained microscopic model of glass formers”, *PNAS* 100, 9710 (2003).
  79. F. Ritort and P. Sollich, “Glassy dynamics of kinetically constrained models”, *Advances in Physics* 52, 219 (2003).
  80. C. Monthus and J.-P. Bouchaud, “Models of traps and glass phenomenology”, *J. Phys. A: Math. Gen.* 29, 3847 (1996).
  81. K. S. Schweizer, “Derivation of a microscopic theory of barriers and activated hopping transport in glassy liquids and suspensions”, *J. Chem. Phys.* 123, 244501 (2005).
  82. S. Mirigian and K. S. Schweizer, “Unified theory of activated relaxation in liquids over 14 decades in time”, *J. Phys. Chem. Lett.* 4, 3648 (2013).
  83. W. Kob and H. C. Andersen, “Testing mode-coupling theory for a supercooled binary Lennard-Jones mixture I: The van Hove correlation function”, *Phys. Rev. E* 51, 4626 (1995).
  84. Kob and Andersen, “Testing mode-coupling theory for a supercooled binary Lennard-Jones mixture. II. Intermediate scattering function and dynamic susceptibility”, *Phys. Rev. E* 52, 4134 (1995).
  85. U. R. Pedersen, T. B. Schröder, and J. C. Dyre, “Phase diagram of Kob-Andersen-type binary Lennard-Jones mixtures”, *Phys. Rev. Lett.* 120, 165501 (2018).
  86. Z. Chen, W. Qi, and R. K. Bowles, “Glass forming phase diagram and local structure of Kob-Andersen binary Lennard-Jones nanoparticles”, *J. Chem. Phys.* 149, 94502 (2018).
  87. M. Becher, T. Wohlfromm, E. A. Rössler, and M. Vogel, “Molecular dynamics simulations vs field-cycling NMR relaxometry: Structural relaxation mechanisms in the glass-former glycerol revisited”, *J. Chem. Phys.* 154, 124503 (2021).
  88. L. Berthier and G. Biroli, “Theoretical perspective on the glass transition and amorphous materials”, *Rev. Mod. Phys.* 83, 587 (2011).
  89. M. M. Hurley and P. Harrowell, “Kinetic structure of a two-dimensional liquid”, *Phys. Rev. E* 52, 1694 (1995).

- 
90. W. Kob, C. Donati, S. J. Plimpton, P. H. Poole, and S. C. Glotzer, “Dynamical heterogeneities in a supercooled Lennard-Jones liquid”, *Phys. Rev. Lett.* 79, 2827 (1997).
  91. E. Flenner and G. Szamel, “Lifetime of dynamic heterogeneities in a binary Lennard-Jones mixture”, *Phys. Rev. E* 70, 52501 (2004).
  92. E. Flenner and G. Szamel, “Dynamic heterogeneities above and below the mode-coupling temperature: evidence of a dynamic crossover”, *J. Chem. Phys.* 138, 12A523 (2013).
  93. K. Schmidt-Rohr and H. W. Spiess, “Nature of nonexponential loss of correlation above the glass transition investigated by multidimensional NMR”, *Phys. Rev. Lett.* 66, 3020 (1991).
  94. R. Böhmer, G. Hinze, G. Diezemann, B. Geil, and H. Sillescu, “Dynamic heterogeneity in supercooled ortho-terphenyl studied by multidimensional deuteron NMR”, *Europhys. Lett. (Europhysics Letters)* 36, 55 (1996).
  95. U. Tracht, M. Wilhelm, A. Heuer, H. Feng, K. Schmidt-Rohr, and H. W. Spiess, “Length Scale of Dynamic Heterogeneities at the Glass Transition Determined by Multidimensional Nuclear Magnetic Resonance”, *Phys. Rev. Lett.* 81, 2727 (1998).
  96. B. Schiener, R. V. Chamberlin, G. Diezemann, and R. Böhmer, “Nonresonant dielectric hole burning spectroscopy of supercooled liquids”, *J. Chem. Phys.* 107, 7746 (1997).
  97. R. Richert, “Heterogeneous dynamics in liquids: fluctuations in space and time”, *J. Phys.: Condens. Matter* 14, R703-R738 (2002).
  98. T. Blochowicz and E. A. Rössler, “Nonresonant dielectric hole burning in neat and binary organic glass formers”, *J. Chem. Phys.* 122, 224511 (2005).
  99. H. Sillescu, “Heterogeneity at the glass transition: a review”, *J. Non-Cryst. Solids* 243, 81 (1999).
  100. L. Berthier, G. Biroli, J.-P. Bouchaud, L. Cipelletti, D. El Masri, D. L'Hôte, F. Ladieu, and M. Pierno, “Direct experimental evidence of a growing length scale accompanying the glass transition”, *Science* 310, 1797 (2005).
  101. C. Dalle-Ferrier, C. Thibierge, C. Alba-Simionesco, L. Berthier, G. Biroli, J.-P. Bouchaud, F. Ladieu, D. L'Hôte, and G. Tarjus, “Spatial correlations in the dynamics of glassforming liquids: Experimental determination of their temperature dependence”, *Phys. Rev. E* 76, 41510 (2007).
  102. A. S. Keys, L. O. Hedges, J. P. Garrahan, S. C. Glotzer, and D. Chandler, “Excitations are localized and relaxation is hierarchical in glass-forming liquids”, *Phys. Rev. X* 1, 21013 (2011).
  103. D. Coslovich, M. Ozawa, and W. Kob, “Dynamic and thermodynamic crossover scenarios in the Kob-Andersen mixture: Insights from multi-CPU and multi-GPU simulations”, *Eur. Phys. J. E* 41, 62 (2018).
  104. L. Berthier, E. Flenner, C. J. Fullerton, C. Scalliet, and M. Singh, “Efficient swap algorithms for molecular dynamics simulations of equilibrium supercooled liquids”, *J. Stat. Mech.* 2019, 64004 (2019).

- 
105. A. D. S. Parmar, B. Guiselin, and L. Berthier, “Stable glassy configurations of the Kob-Andersen model using swap Monte Carlo”, *J. Chem. Phys.* 153, 134505 (2020).
  106. A. Abragam, *The Principles of Nuclear Magnetism* (Clarendon Press, Oxford, 1961).
  107. K. Schmidt-Rohr and H. W. Spiess, *Multidimensional solid-state NMR and polymers* (Academic Press, London, 1994).
  108. F. Kremer and A. Schönhal, *Broadband Dielectric Spectroscopy* (Springer, Berlin, Heidelberg, 2003).
  109. D. Kivelson and P. Madden, “Theory of dielectric relaxation”, *Mol. Phys.* 30, 1749 (1975).
  110. J. P. Gabriel, P. Zourchang, F. Pabst, A. Helbling, P. Weigl, T. Böhmer, and T. Blochowicz, “Intermolecular cross-correlations in the dielectric response of glycerol”, *Phys. Chem. Chem. Phys.* 22, 11644 (2020).
  111. P.-M. Déjardin, S. V. Titov, and Y. Cornaton, “Linear complex susceptibility of long-range interacting dipoles with thermal agitation and weak external ac fields”, *Phys. Rev. B* 99, 24304 (2019).
  112. F. Fujara, S. Wefing, and H. W. Spiess, “Dynamics of molecular reorientations: Analogies between quasielastic neutron scattering and deuteron NMR spin alignment”, *J. Chem. Phys.* 84, 4579 (1986).
  113. A. Patkowski, W. Steffen, H. Nilgens, E. W. Fischer, and R. Pecora, “Depolarized dynamic light scattering from three low molecular weight glass forming liquids: a test of the scattering mechanism”, *J. Chem. Phys.* 106, 8401 (1997).
  114. B. Pötzschner, F. Mohamed, A. Lichtinger, D. Bock, and E. A. Rössler, “Dynamics of asymmetric non-polymeric binary glass formers-A nuclear magnetic resonance and dielectric spectroscopy study”, *J. Chem. Phys.* 143, 154506 (2015).
  115. B. Pötzschner, F. Mohamed, C. Bächer, E. Wagner, A. Lichtinger, R. Minikejew, K. Kreger, H.-W. Schmidt, and E. A. Rössler, “Non-polymeric asymmetric binary glass-formers. I. Main relaxations studied by dielectric,  $^2\text{H}$  NMR, and  $^{31}\text{P}$  NMR spectroscopy”, *J. Chem. Phys.* 146, 164503 (2017).
  116. A. Jedrzejowska, M. Matussek, K. L. Ngai, K. Grzybowska, K. Jurkiewicz, and M. Paluch, “New paradigm of dielectric relaxation of sizable and rigid molecular glass formers”, *Phys. Rev. E* 101, 10603 (2020).
  117. G. Williams and D. C. Watts, “Molecular motion in the glassy state. The effect of temperature and pressure on the dielectric  $\beta$  relaxation of polyvinyl chloride”, *Trans. Faraday Soc.* 67, 1971 (1971).
  118. A. Arbe, D. Richter, J. Colmenero, and B. Farago, “Merging of the  $\alpha$  and  $\beta$  relaxations in polybutadiene: A neutron spin echo and dielectric study”, *Phys. Rev. E* 54, 3853 (1996).
  119. K. L. Ngai and M. Paluch, “Inference of the evolution from caged dynamics to cooperative relaxation in glass-formers from dielectric relaxation data”, *J. Phys. Chem. B* 107, 6865 (2003).

- 
120. T. Körber, F. Mohamed, M. Hofmann, A. Lichtinger, L. Willner, and E. A. Rössler, “The nature of secondary relaxations: the case of poly(ethylene-*alt*-propylene) studied by dielectric and deuteron NMR Spectroscopy”, *Macromolecules* 50, 1554 (2017).
  121. C. Gainaru, R. Böhmer, R. Kahlau, and E. Rössler, “Energy landscape in molecular glasses probed by high-resolution dielectric experiments”, *Phys. Rev. B* 82, 104205 (2010).
  122. M. Vogel and E. Rössler, “Slow  $\beta$  process in simple organic glass formers studied by one- and two-dimensional  $^2\text{H}$  nuclear magnetic resonance. I”, *J. Chem. Phys.* 114, 5802 (2001).
  123. M. Vogel, C. Tschirwitz, G. Schneider, C. Koplin, P. Medick, and E. Rössler, “A  $^2\text{H}$  NMR and dielectric spectroscopy study of the slow  $\beta$ -process in organic glass formers”, *J. Non-Cryst. Solids* 307-310, 326 (2002).
  124. D. Bock, R. Kahlau, B. Micko, B. Pötzschner, G. J. Schneider, and E. A. Rössler, “On the cooperative nature of the  $\beta$ -process in neat and binary glasses: a dielectric and nuclear magnetic resonance spectroscopy study”, *J. Chem. Phys.* 139, 64508 (2013).
  125. L.-M. Wang, Y. Tian, R. Liu, and K. L. Ngai, “Anomalous component dynamics of a binary mixture of associating glass-forming liquids”, *J. Phys. Chem. B* 115, 719 (2011).
  126. D. Bock, T. Körber, F. Mohamed, B. Pötzschner, and E. A. Rössler, “Dynamic Heterogeneities in Binary Glass-Forming Systems”, in *The Scaling of Relaxation Processes*, edited by F. Kremer and A. Loidl (Springer, Cham, Switzerland, 2018), p. 173.
  127. T. Körber, F. Krohn, C. Neuber, H.-W. Schmidt, and E. A. Rössler, “Main and secondary relaxations of non-polymeric high-T<sub>g</sub> glass formers as revealed by dielectric spectroscopy”, *Phys. Chem. Chem. Phys.* 22, 9086 (2020).
  128. E. Rössler and P. Eiermann, “Reorientational dynamics in supercooled *m*-tricresyl phosphate: Its relation to main and secondary relaxation—  $^{31}\text{P}$  nuclear magnetic resonance study of relaxation, line shape, and stimulated echo”, *J. Chem. Phys.* 100, 5237 (1994).
  129. B. Schmidtke, N. Petzold, M. Flämig, and E. A. Rössler, “From boiling point down to the glass transition - dynamics of molecular liquids described by a generalized Angell plot”, in *Fragility of glass-forming liquids*, edited by A. L. Greer (Hindustan Book Agency, New Delhi, 2014), p. 129.
  130. W. Schnauss, F. Fujara, and H. Sillescu, “The molecular dynamics around the glass transition and in the glassy state of molecular organic systems: a  $^2\text{H}$ -nuclear magnetic resonance (NMR) study”, *J. Chem. Phys.* 97, 1378 (1992).
  131. T. Dries, F. Fujara, M. Kiebel, E. Rössler, and H. Sillescu, “ $^2\text{H}$ -NMR study of the glass transition in supercooled ortho-terphenyl”, *J. Chem. Phys.* 88, 2139 (1988).
  132. N. Petzold and E. A. Rössler, “Light scattering study on the glass former *o*-terphenyl”, *J. Chem. Phys.* 133, 124512 (2010).

- 
133. R. Meier, R. Kahlau, D. Kruk, and E. A. Rössler, “Comparative studies of the dynamics in viscous liquids by means of dielectric spectroscopy and field cycling NMR”, *J. Phys. Chem. A* 114, 7847 (2010).
  134. J. Wuttke, W. Petry, and S. Pouget, “Structural relaxation in viscous glycerol: coherent neutron scattering”, *J. Chem. Phys.* 105, 5177 (1996).
  135. W. Kob and H. C. Andersen, “Kinetic lattice-gas model of cage effects in high-density liquids and a test of mode-coupling theory of the ideal-glass transition”, *Phys. Rev. E* 48, 4364 (1993).
  136. L. J. Lewis and G. Wahnström, “Molecular-dynamics study of supercooled ortho-terphenyl”, *Phys. Rev. E* 50, 3865 (1994).
  137. G. Williams, “Molecular motion in glass-forming systems”, *J. Non-Cryst. Solids* 131-133, 1 (1991).
  138. M. Cook, D. C. Watts, and G. Williams, “Correlation function approach to the dielectric behaviour of amorphous polymers”, *Trans. Faraday Soc.* 66, 2503 (1970).
  139. F. Pabst, A. Helbling, J. Gabriel, P. Weigl, and T. Blochowicz, “Dipole-dipole correlations and the Debye process in the dielectric response of nonassociating glass forming liquids”, *Phys. Rev. E* 102, 10606 (2020).
  140. F. Pabst, J. P. Gabriel, T. Böhmer, P. Weigl, A. Helbling, T. Richter, P. Zourchang, T. Walther, and T. Blochowicz, “Generic Structural Relaxation in Supercooled Liquids”, *J. Phys. Chem. Lett.* 12, 3685 (2021).
  141. N. Bloembergen, E. M. Purcell, and R. V. Pound, “Relaxation effects in nuclear magnetic resonance absorption”, *Phys. Rev.* 73, 679 (1948).
  142. E. Rössler and H. Sillescu, “ $^2\text{H}$  NMR study of supercooled toluene”, *Chem. Phys. Lett.* 112, 94 (1984).
  143. M. Becher, T. Körber, A. Döß, G. Hinze, C. Gainaru, M. Vogel, R. Böhmer, and E. A. Rössler, “Nuclear spin relaxation in viscous liquids: relaxation stretching of single-particle probes”, *J. Phys. Chem. B*, 125, 13519 (2021).
  144. P. J. Hains and G. Williams, “Molecular motion in polystyrene-plasticizer systems as studied by dielectric relaxation”, *Polymer* 16, 725 (1975).
  145. J. Colmenero and A. Arbe, “Segmental dynamics in miscible polymer blends: Recent results and open questions”, *Soft Matter* 3, 1474 (2007).
  146. G. Ceccorulli, M. Pizzoli, and M. Scandola, “Composition dependence of the glass transition temperature of polymer-diluent systems: 1. Experimental evidence of a dual behaviour in plasticized PVC”, *Polymer* 28, 2077 (1987).
  147. M. Nakazawa, O. Urakawa, and K. Adachi, “Effect of local heterogeneity on dielectric relaxation spectra in concentrated solutions of poly(vinyl acetate) and poly(vinyl octanoate)”, *Macromolecules* 33, 7898 (2000).
  148. K. L. Ngai, *Relaxation and diffusion in complex systems* (Springer, New York, NY, 2011).
  149. T. Blochowicz, S. Schramm, S. Lusceac, M. Vogel, B. Stühn, P. Gutfreund, and B. Frick, “Signature of a type-A glass transition and intrinsic confinement effects in a binary glass-forming system”, *Phys. Rev. Lett.* 109, 35702 (2012).

- 
150. R. Kahlau, D. Bock, B. Schmidtke, and E. A. Rössler, “Dynamics of asymmetric binary glass formers. I. A dielectric and nuclear magnetic resonance spectroscopy study”, *J. Chem. Phys.* 140, 44509 (2014).
  151. T. Blochowicz, C. Karle, A. Kudlik, P. Medick, I. Roggatz, M. Vogel, C. Tschirwitz, J. Wolber, J. Senker, and E. Rössler, “Molecular dynamics in binary organic glass formers”, *J. Phys. Chem. B* 103, 4032 (1999).
  152. K. Kessairi, S. Capaccioli, D. Prevosto, M. Lucchesi, and P. Rolla, “Relaxation dynamics in tert-butylpyridine/tristyrene mixture investigated by broadband dielectric spectroscopy”, *J. Chem. Phys.* 127, 174502 (2007).
  153. D. Cangialosi, A. Alegría, and J. Colmenero, “Dielectric relaxation of polychlorinated biphenyl/toluene mixtures: Component dynamics”, *J. Chem. Phys.* 128, 224508 (2008).
  154. T. Blochowicz, S. A. Lusceac, P. Gutfreund, S. Schramm, and B. Stühn, “Two glass transitions and secondary relaxations of methyltetrahydrofuran in a binary mixture”, *J. Phys. Chem. B* 115, 1623 (2011).
  155. X. Jin, Z. Li, Y. Liu, S. Feng, and L.-M. Wang, “Identifying the structural relaxation dynamics in a strongly asymmetric binary glass former”, *J. Chem. Phys.* 154, 144504 (2021).
  156. Y. Kaneko and J. Bosse, “Dynamics of binary liquids near the glass transition: A mode-coupling theory”, *J. Non-Cryst. Solids* 205-207, 472 (1996).
  157. S.-H. Chong, W. Götze, and A. P. Singh, “Mode-coupling theory for the glassy dynamics of a diatomic probe molecule immersed in a simple liquid”, *Phys. Rev. E* 63, 11206 (2000).
  158. A. J. Moreno and J. Colmenero, “Anomalous dynamic arrest in a mixture of large and small particles”, *Phys. Rev. E* 74, 21409 (2006).
  159. A. J. Moreno and J. Colmenero, “Relaxation scenarios in a mixture of large and small spheres: Dependence on the size disparity”, *J. Chem. Phys.* 125, 164507 (2006).
  160. T. Voigtmann and J. Horbach, “Double transition scenario for anomalous diffusion in glass-forming mixtures”, *Phys. Rev. Lett.* 103, 205901 (2009).
  161. T. Voigtmann, “Multiple glasses in asymmetric binary hard spheres”, *EPL* 96, 36006 (2011).
  162. T. Sentjabrskaja, E. Zaccarelli, C. D. Michele, F. Sciortino, P. Tartaglia, T. Voigtmann, S. U. Egelhaaf, and M. Laurati, “Anomalous dynamics of intruders in a crowded environment of mobile obstacles”, *Nat. Commun.* 7, 11133 (2016).
  163. N. Müller and M. Vogel, “Relation between concentration fluctuations and dynamical heterogeneities in binary glass-forming liquids: A molecular dynamics simulation study”, *J. Chem. Phys.* 150, 64502 (2019).
  164. E. Lázaro-Lázaro, J. A. Perera-Burgos, P. Laermann, T. Sentjabrskaja, G. Pérez-Ángel, M. Laurati, S. U. Egelhaaf, M. Medina-Noyola, T. Voigtmann, R. Castañeda-Priego, and L. F. Elizondo-Aguilera, “Glassy dynamics in asymmetric binary mixtures of hard spheres”, *Phys. Rev. E* 99, 42603 (2019).

- 
165. L. A. Utracki, *Polymer alloys and blends: Thermodynamics and rheology* (Carl Hanser Verlag, Munich, 1990).
  166. M. Pizzoli, M. Scandola, and G. Ceccorulli, "Molecular motions in polymer-diluent systems: Polystyrene-tritolylphosphate", *Eur. Polym. J.* **23**, 843 (1987).
  167. D. A. Savin, A. M. Larson, and T. P. Lodge, "Effect of composition on the width of the calorimetric glass transition in polymer-solvent and solvent-solvent mixtures", *J. Polym. Sci. B Polym. Phys.* **42**, 1155 (2004).
  168. T. P. Lodge, E. R. Wood, and J. C. Haley, "Two calorimetric glass transitions do not necessarily indicate immiscibility: The case of PEO/PMMA", *J. Polym. Sci. B Polym. Phys.* **44**, 756 (2006).
  169. J. E. G. Lipson and S. T. Milner, "Multiple glass transitions and local composition effects on polymer solvent mixtures", *J. Polym. Sci. B Polym. Phys.* **44**, 3528 (2006).
  170. A. N. Gaikwad, E. R. Wood, T. Ngai, and T. P. Lodge, "Two calorimetric glass transitions in miscible blends containing poly(ethylene oxide)", *Macromolecules* **41**, 2502 (2008).
  171. D. Bock, R. Kahlau, B. Pötzschner, T. Körber, E. Wagner, and E. A. Rössler, "Dynamics of asymmetric binary glass formers. II. Results from nuclear magnetic resonance spectroscopy", *J. Chem. Phys.* **140**, 94505 (2014).
  172. R. Kahlau, T. Dörfler, and E. A. Rössler, "Secondary relaxations in a series of organic phosphate glasses revealed by dielectric spectroscopy", *J. Chem. Phys.* **139**, 134504 (2013).
  173. G. B. McKenna, "Confit III. Summary and perspectives on dynamics in confinement", *Eur. Phys. J. Special Topics* **141**, 291 (2007).
  174. A. Schönhals, H. Goering, C. Schick, B. Frick, M. Mayorova, and R. Zorn, "Segmental dynamics of poly(methyl phenyl siloxane) confined to nanoporous glasses", *Eur. Phys. J. Special Topics* **141**, 255 (2007).
  175. G. Buntkowsky, H. Breitzke, A. Adamczyk, F. Roelofs, T. Emmeler, E. Gedat, B. Grünberg, Y. Xu, H.-H. Limbach, I. Shenderovich, A. Vyalikh, and G. Findenegg, "Structural and dynamical properties of guest molecules confined in mesoporous silica materials revealed by NMR", *Phys. Chem. Chem. Phys.* **9**, 4843 (2007).
  176. S. Gradmann, P. Medick, and E. A. Rössler, "Glassy dynamics in nanoconfinement as revealed by  $^{31}\text{P}$  NMR", *J. Phys. Chem. B* **113**, 8443 (2009).
  177. D. Bock, N. Petzold, R. Kahlau, S. Gradmann, B. Schmidtke, N. Benoit, and E. A. Rössler, "Dynamic heterogeneities in glass-forming systems", *J. Non-Cryst. Solids* **407**, 88 (2015).
  178. D. Demuth, M. Sattig, E. Steinrücken, M. Weigler, and M. Vogel, " $^2\text{H}$  NMR studies on the dynamics of pure and mixed hydrogen-bonded liquids in confinement", *Z. Phys. Chem.* **232**, 1059 (2018).
  179. J. D. Ferry, *Viscoelastic properties of polymers* (John Wiley & Sons, New York, 1980).

- 
180. S. Valenti, S. Capaccioli, and K. L. Ngai, “Contrasting two different interpretations of the dynamics in binary glass forming mixtures”, *J. Chem. Phys.* 148, 54504 (2018).
  181. K. L. Ngai, S. Valenti, and S. Capaccioli, “Molecular dynamic in binary mixtures and polymer blends with large difference in glass transition temperatures of the two components: A critical review”, *J. Non-Cryst. Solids*, 119573 (2021).
  182. E. Rössler, M. Taupitz, K. Börner, M. Schulz, and H.-M. Vieth, “A simple method analyzing  $^2\text{H}$  nuclear magnetic resonance line shapes to determine the activation energy distribution of mobile guest molecules in disordered systems”, *J. Chem. Phys.* 92, 5847 (1990).
  183. P. Medick, M. Vogel, and E. Rössler, “Large angle jumps of small molecules in amorphous matrices analyzed by 2D exchange NMR”, *J. Magn. Reson.* 159, 126 (2002).
  184. D. Bingemann, N. Wirth, J. Gmeiner, and E. A. Rössler, “Decoupled dynamics and quasi-logarithmic relaxation in the polymer–plasticizer system poly(methyl methacrylate)/tri-*m*-cresyl phosphate studied with 2D NMR”, *Macromolecules* 40, 5379 (2007).
  185. S. Adishchev, D. Bock, C. Gainaru, R. Kahlau, B. Micko, N. Petzold, B. Pötzschner, and E. A. Rössler, “Reorientational dynamics of organophosphate glass formers – a joint study by  $^{31}\text{P}$  NMR, dielectric spectroscopy and light scattering”, *Z. Phys. Chem.* 226, 1149 (2012).
  186. F. Sciortino, P. Tartaglia, and E. Zaccarelli, “Evidence of a Higher-Order Singularity in Dense Short-Ranged Attractive Colloids”, *Phys. Rev. Lett.* 91, 268301 (2003).
  187. A. Zetsche and E. W. Fischer, “Dielectric studies of the  $\alpha$ -relaxation in miscible polymer blends and its relation to concentration fluctuations”, *Acta Polymer.* 45, 168 (1994).
  188. S. K. Kumar, R. H. Colby, S. H. Anastasiadis, and G. Fytas, “Concentration fluctuation induced dynamic heterogeneities in polymer blends”, *J. Chem. Phys.* 105, 3777 (1996).
  189. R. Kant, S. K. Kumar, and R. H. Colby, “What length scales control the dynamics of miscible polymer blends?”, *Macromolecules* 36, 10087 (2003).
  190. G.-C. Chung, J. A. Kornfield, and S. D. Smith, “Compositional dependence of segmental dynamics in a miscible polymer blend”, *Macromolecules* 27, 5729 (1994).
  191. T. P. Lodge and T. C. B. McLeish, “Self-concentrations and effective glass transition temperatures in polymer blends”, *Macromolecules* 33, 5278 (2000).
  192. E. Leroy, A. Alegría, and J. Colmenero, “Segmental dynamics in miscible polymer blends: modeling the combined effects of chain connectivity and concentration fluctuations”, *Macromolecules* 36, 7280 (2003).
  193. S. Shenogin, R. Kant, R. H. Colby, and S. K. Kumar, “Dynamics of miscible polymer blends: predicting the dielectric response”, *Macromolecules* 40, 5767 (2007).

- 
194. J. Bosse and Y. Kaneko, “Self-diffusion in supercooled binary liquids”, *Phys. Rev. Lett.* 74, 4023 (1995).
  195. V. Krakoviack, “Liquid-glass transition of a fluid confined in a disordered porous matrix: A mode-coupling theory”, *Phys. Rev. Lett.* 94, 65703 (2005).
  196. J. Kurzidim, D. Coslovich, and G. Kahl, “Dynamic arrest of colloids in porous environments: disentangling crowding and confinement”, *J. Phys.: Condens. Matter* 23, 234122 (2011).
  197. F. Höfling, T. Franosch, and E. Frey, “Localization transition of the three-dimensional lorentz model and continuum percolation”, *Phys. Rev. Lett.* 96, 165901 (2006).
  198. K. Dawson, G. Foffi, M. Fuchs, W. Götze, F. Sciortino, M. Sperl, P. Tartaglia, T. Voigtmann, and E. Zaccarelli, “Higher-order glass-transition singularities in colloidal systems with attractive interactions”, *Phys. Rev. E* 63, 11401 (2000).
  199. M. Sperl, “Logarithmic relaxation in a colloidal system”, *Phys. Rev. E* 68, 31405 (2003).
  200. W. Götze and T. Voigtmann, “Effect of composition changes on the structural relaxation of a binary mixture”, *Phys. Rev. E* 67, 21502 (2003).
  201. E. Martinez-Sotelo, M. A. Escobedo-Sánchez, and M. Laurati, “Effect of size disparity on the structure and dynamics of the small component in concentrated binary colloidal mixtures”, *J. Chem. Phys.* 151, 164504 (2019).
  202. E. M. Zirdehi, T. Voigtmann, and F. Varnik, “Multiple character of non-monotonic size-dependence for relaxation dynamics in polymer-particle and binary mixtures”, *J. Phys.: Condens. Matter* 32, 275104 (2020).
  203. T. Körber, R. Minikejew, B. Pötzschner, D. Bock, and E. A. Rössler, “Dynamically asymmetric binary glass formers studied by dielectric and NMR spectroscopy”, *Eur. Phys. J. E* 42, 143 (2019).
  204. R. Kahlau, D. Kruk, T. Blochowicz, V. N. Novikov, and E. A. Rössler, “Generalization of the Cole–Davidson and Kohlrausch functions to describe the primary response of glass-forming systems”, *J. Phys.: Condens. Matter* 22, 365101 (2010).
  205. G. Hinze and H. Sillescu, “ $^2\text{H}$  nuclear magnetic resonance study of supercooled toluene: Slow and fast processes above and below the glass transition”, *J. Chem. Phys.* 104, 314 (1996).
  206. M. Vogel, P. Medick, and E. A. Rössler, “Secondary relaxation processes in molecular glasses studied by nuclear magnetic resonance spectroscopy”, in *Annual Reports on NMR Spectroscopy*, edited by G. A. Webb (Academic Press, 2005), Vol. 56, p. 231.
  207. T. Körber, F. Krohn, C. Neuber, H.-W. Schmidt, and E. A. Rössler, “Reorientational dynamics of highly asymmetric binary non-polymeric mixtures - a dielectric spectroscopy study”, *Phys. Chem. Chem. Phys.* 23, 7200 (2021).
  208. M. Wübbenhorst and J. van Turnhout, “Analysis of complex dielectric spectra. I. One-dimensional derivative techniques and three-dimensional modelling”, *J. Non-Cryst. Solids* 305, 40 (2002).

- 
209. T. Blochowicz, *Broadband Dielectric Spectroscopy in Neat and Binary Molecular Glass Formers. Frequency and Time Domain Spectroscopy, Non-Resonant Spectral Hole Burning*, Dissertation, Universität Bayreuth, 2003.
210. B. Schmidtke, N. Petzold, R. Kahlau, and E. A. Rössler, "Reorientational dynamics in molecular liquids as revealed by dynamic light scattering: from boiling point to glass transition temperature", *J. Chem. Phys.* 139, 84504 (2013).
211. B. Pötzschner, F. Mohamed, C. Bächer, E. Wagner, A. Lichtinger, D. Bock, K. Kreger, H.-W. Schmidt, and E. A. Rössler, "Non-polymeric asymmetric binary glass-formers. II. Secondary relaxation studied by dielectric,  $^2\text{H}$  NMR, and  $^{31}\text{P}$  NMR spectroscopy", *J. Chem. Phys.* 146, 164504 (2017).
212. B. Micko, C. Tschirwitz, and E. A. Rössler, "Secondary relaxation processes in binary glass formers: emergence of "islands of rigidity"", *J. Chem. Phys.* 138, 154501 (2013).
213. Ernst A. Rössler,  *$^2\text{H}$ -NMR-Untersuchungen am system Polystyrol/Toluol*, Dissertation, 1984.
214. M. Gordon and J. S. Taylor, "Ideal copolymers and the second-order transitions of synthetic rubbers. I. Non-crystalline copolymers", *J. Appl. Chem.* 2, 493 (1952).
215. T. Theenhaus, R. Schilling, A. Latz, and M. Letz, "Microscopic dynamics of molecular liquids and glasses: role of orientations and translation-rotation coupling", *Phys. Rev. E* 64, 51505 (2001).
216. C. D. Michele, R. Schilling, and F. Sciortino, "Dynamics of uniaxial hard ellipsoids", *Phys. Rev. Lett.* 98, 265702 (2007).
217. K. V. Edmond, M. T. Elsesser, G. L. Hunter, D. J. Pine, and E. R. Weeks, "Decoupling of rotational and translational diffusion in supercooled colloidal fluids", *PNAS* 109, 17891 (2012).
218. L. F. Elizondo-Aguilera, E. C. Cortés-Morales, P. F. Zubieta Rico, M. Medina-Noyola, R. Castañeda-Priego, T. Voigtmann, and G. Pérez-Ángel, "Arrested dynamics of the dipolar hard sphere model", *Soft Matter* 16, 170 (2020).
219. M. T. Cicerone and M. D. Ediger, "Photobleaching technique for measuring ultraslow reorientation near and below the glass transition: tetracene in o-terphenyl", *J. Phys. Chem.* 97, 10489 (1993).
220. G. Heuberger and H. Sillescu, "Size dependence of tracer diffusion in supercooled liquids", *J. Phys. Chem.* 100, 15255 (1996).
221. R. L. Johnson and K. Schmidt-Rohr, "Quantitative solid-state  $^{13}\text{C}$  NMR with signal enhancement by multiple cross polarization", *J. Magn. Reson.* 239, 44 (2014).
222. T. Böhmer, R. Horstmann, J. P. Gabriel, F. Pabst, M. Vogel, and T. Blochowicz, "Origin of apparent slow solvent dynamics in concentrated polymer solutions", *Macromolecules* 54, 10340 (2021).
223. G. Floudas, W. Steffen, E. W. Fischer, and W. Brown, "Solvent and polymer dynamics in concentrated polystyrene/toluene solutions", *J. Chem. Phys.* 99, 695 (1993).

- 
224. S. Capaccioli, L. Zheng, A. Kyritsis, A. Paciaroni, M. Vogel, and K. L. Ngai, “The dynamics of hydrated proteins are the same as those of highly asymmetric mixtures of two glass-formers”, ACS Omega 6, 340 (2021).



---

## Acknowledgement

Hereby, I want to thank all the people who supported me during this thesis.

Most importantly, I want to thank my “Doktorvater” Ernst Rössler, for the possibility to do my PhD studies in his group. Especially his attitude, to give the freedom which is needed for successful new research combined with his support and assistance no matter what kind of problem came up, made the last almost five years a particular pleasure. I really appreciated the intense personal collaboration in the university but also especially the discussions about non-scientific content.

An important factor for the good atmosphere in the group, were of course my former colleagues and friends Max Flämig and Björn Pötzschner, providing guidance and support in and outside of university life. I want to thank all my coworkers during the various projects and especially Felix Krohn for the successful cooperation.

Furthermore, I want to specially thank Jürgen Senker and his whole group (AC III), who included me as a matter of course, after we had to leave our own laboratories, for the last two years, and where I found numerous new colleagues and friends as well as a lot of fun besides work.

Last but not least, I want to thank from the bottom of my heart my partner Sanja Bláha, who supported me the whole time the best way possible, and my parents Gertrud and Karl as well as my sisters Anja and Katja Körber, who gave me the support and opportunity to become the man I am right now.

Sincerely yours

Thomas

---

## Eidesstattliche Versicherung

Hiermit versichere ich an Eides statt, dass ich die vorliegende Arbeit selbstständig verfasst und keine anderen als die von mir angegebenen Quellen und Hilfsmittel verwendet habe.

Weiterhin erkläre ich, dass ich die Hilfe von gewerblichen Promotionsberatern bzw. –vermittlern oder ähnlichen Dienstleistern weder bisher in Anspruch genommen habe, noch künftig in Anspruch nehmen werde.

Zusätzlich erkläre ich hiermit, dass ich keinerlei frühere Promotionsversuche unternommen habe.

Bayreuth,

-----  
Thomas Körber